PREDICTION OF CHILLING RATES FOR FOOD PRODUCT PACKAGES

A thesis presented in partial fulfilment of the requirements for the degree of Doctor of Philosophy in Food Engineering at Massey University, Palmerston North, New Zealand.

Michael Francis North

2000

ABSTRACT

Many food product packages contain significant air void fractions in which natural convection and radiation heat transfer occurs. This may significantly affect the cooling rate of the package as a whole. Voids tend to be either rectangular (at the top of the package), approximately triangular (e.g. in corners of the package), or can be represented as a combination of both shapes. For widely used meat cartons containing voids the bulk of the heat transfer can be modelled two-dimensionally, ignoring end effects.

Empirical *Nu* vs. *Ra* correlations for horizontal rectangular air voids were available from the technical literature. Since corresponding published data were not obtainable for right-angled isosceles triangular air voids cooled from above with a hypotenuse-down orientation, temperature-time data were collected from twenty-eight transient chilling trials using analogue food packages that contained different sized voids (up to 50mm high) with this shape and orientation. A reliable finite element package was used to model the heat transfer as a conduction process throughout the entire analogue package. The effective thermal conductivities that best-fitted modelled and measured temperature-time profiles within each of five sequential time intervals during cooling were determined. The results were then curve-fitted to generate *Nu* vs. *Ra* correlations.

New two-dimensional finite element models were developed for predicting chilling rates of food packages that contained combinations of isosceles triangular and/or horizontal rectangular air voids. The models were solved by using a customised heat conduction program called FINELX, in which the effective thermal conductivity in the voids was re-calculated at the start of every time-step from the *Nu* vs. *Ra* correlations, but the heat transfer was otherwise modelled as conduction.

The finite element model was tested against twenty independent transient chilling trials using an analogue food package that contained rectangular and triangular voids of various heights. Predictions from the finite element model agreed to within ±7% and ±12% (at the 95% level of confidence) of the measured data for packages containing rectangular voids and packages containing combined rectangular and triangular voids respectively. This indicated that the model was an accurate simulator of the overall heat transfer occurring in packages that contained significant air void fractions.

Previously available simple methods for the prediction of chilling rates of such packages assumed that the contents were homogeneous solids with 'effective' thermal properties based upon the packaging arrangement and the relative amounts of solid and air. These methods were shown to be inaccurate.

A simple model based on the semi-infinite slab shape was developed for predicting chilling rates of food packages that contained combinations of isosceles triangular and/or horizontal rectangular void shapes. The simple model accounted for the presence of air voids by the use of effective heat transfer coefficients. Several types of solution method were possible: from analytical methods to simple numerical methods with a run-time of only a few seconds on a 350MHz Pentium II computer, which was significantly less than the 3 hours preparation and 5 hours run-time for the finite element model. Testing of the simple model against measured data from forty-eight transient chilling trials yielded 95% confidence intervals of (-6, +12)%, (-15, +11)%, and (-9, +17)% for packages containing rectangular voids, triangular voids, and combined voids respectively. The quality of prediction indicated that the assumptions employed during the development of the simple model did not worsen its accuracy beyond a level that was likely to be acceptable in industry.

Although the simple model gave relatively accurate results for much less computational effort, the customised finite element approach would allow researchers to extend the applicability of the model to any void shape, provided that natural convection and radiation heat transfer data within that particular void shape were available.

ACKNOWLEDGEMENTS

Firstly, I would like to sincerely thank my excellent and dedicated supervisors for their continued advice, assistance, guidance and support during this project:

- Dr. Andrew Cleland, Chief Executive Officer, The Institution of Professional Engineers New Zealand Inc. (Chief Supervisor).

- Dr. Simon Lovatt, Team Leader, Processing and Preservation Technology, AgResearch Food Systems and Technology, Hamilton.

A big thank you to the Processing and Preservation Technology team at AgResearch Food Systems and Technology for all their advice and technical support. Craig Lawson, Robert Kemp and Jim Willix for their invaluable experience and assistance, particularly in the experimental phases of this work. Dr. Mark Harris and Dr. Inge Merts for their advice and inspiration. Keith Hill for keeping my car running and my stereo humming. And to the entire team for running all those simulations!

Thank you to my friends and to my fellow postgraduate students who kept me sane (and *almost* sober) throughout this 'ordeal' – Clint & Emily, Dave, Jules, JB (Guru Sansui), Julz, Karen & Graham, Claire, Jen & Chris, Layton & Julie, Ayn, Katie, Zippy, Amy, Kristen, Rochelle, Michelle, and James.

Thanks to the boys of AFFLUVIUM - Kane 'Lightning' Thomas, Aaron 'Overcast' O'Donnell, 'Kermit' Williams, and Art Davey - for always being there (even if it was an hour late!). And for putting up with my organisational skills, my oversized vocal chords and my love of the word 'No!!!'. We're going to the moon baby!

Finally I would like to thank my family:

- My parents, Jeanette and John, for all your love, and emotional and financial support. I couldn't have done this without knowing you were there.

- Louise & Tyrone, Graeme & Sharon, and all the 'rellys'. Thanks for your well wishes and encouragement.

- Michelle, thank you for your love, support, patience and understanding.

This work is dedicated to the loving memory of Adele & Bill Wilson ('Nana & Poppa'), and Janina Barycza ('Nana-in-Australia').

Thank you to the New Zealand Public Good Science Fund for funding this work under project FRST MRI 501.

"If you don't eat yer meat, you can't have any pudding."

Roger Waters, The Wall (Part II), PINK FLOYD

Table of Contents

Abstract ii

Acknowledgements iv

Table of Contents vi

List of Figures xiii

List of Tables xix

Chapter *Page No.*

1. Introduction **1.1**

2. Literature Review **2.1**

2.1 Scope of the Review 2.1

2.2 Unsteady State Heat Transfer by Conduction in Solids 2.1

2.2.1 Physical Models for Chilling of Solid Biological Materials 2.1

2.2.2 Model Formulation 2.2

2.2.3 Boundary Conditions 2.2

2.2.4 Initial Conditions 2.4

2.2.5 Numerical Solutions 2.4

2.2.5.1 The Finite Difference Method 2.4

2.2.5.2 The Finite Element Method 2.7

2.2.5.3 The Boundary Element Method 2.10

2.2.5.4 The Control Volume Method 2.10

2.2.6 Analytical Solutions 2.10

2.2.7 Empirically-adapted Solutions 2.12

2.2.8 Composite Solids - Effective Thermal Properties Theory 2.16

2.3 Natural Convection 2.19

2.3.1 Numerical Solutions (Computational Fluid Dynamics) 2.19

2.3.1.1 Existing Commercial CFD Solvers 2.22

2.3.2 Analytical Solutions 2.23

2.3.3 Empirical Solutions 2.26

2.4 Summary 2.27

3. Preliminary Considerations 3.1

4. Preliminary Collection and Analysis of Data for Packages Containing Triangular Voids 4.1

4.1 Objectives 4.1

4.2 Experimental Methodology 4.1

4.3 Evaluation of Input Data 4.7

4.3.1 Thermal Properties of Test Materials 4.7

4.3.2 Sample Dimensions 4.7

4.3.3 Cooling Medium Temperature 4.8

4.3.4 Surface Heat Transfer Coefficients 4.8

4.3.5 Edge Effects 4.11

4.4 Measured Time-Temperature Data in the Test Samples 4.13

4.5 Development and Testing of a Finite Element Model 4.16

4.5.1 The Preliminary FINEL Model - No edge effect included 4.16

4.5.2 Testing the Preliminary FINEL Grid 4.18

4.5.3 Comparison of the preliminary model with data from blocks containing no voids 4.19

4.5.4 The Second FINEL Model - Edge effect included 4.19

4.5.5 Testing the Second FINEL Grid 4.22

4.5.6 Comparison of second model with data from blocks containing no voids 4.22

4.6 Comparison of Measured and Predicted Data 4.24

4.7 Conclusions 4.28

5. Improved Data Collection and Model Development for Packages Containing Triangular Voids 5.1

5.1 Experimental Methodology 5.2

5.2 Evaluation of Input Data 5.6

5.2.1 Sample Dimensions 5.6

5.2.2 Thermal Property Data 5.7

5.2.3 Initial and Boundary Conditions 5.7

5.3 Measured Time-Temperature Data in the Test Samples 5.10

5.4 Development of a New Numerical Model 5.14

5.4.1 Effect of varying *errlim* in PDEase2D 5.14

5.4.2 Accounting for the third dimension edge effect 5.16

5.4.3 Re-estimating the surface heat transfer coefficients 5.19

5.5 Prediction of Cooling Rates for Packages Containing Triangular Filled Voids 5.21

5.6 Prediction of Cooling Rates for Packages Containing Triangular Air Voids 5.25

5.7 Estimating the Effective Thermal Conductivity of Triangular Air Voids 5.27

5.8 Finding a Relationship Between *Ra* and *Nu* for Triangular Air Voids 5.29

6. Development and Testing of a Model for Predicting Heat Transfer During Chilling of Packages Containing Horizontal Rectangular Voids 6.1

6.1 Introduction 6.1

6.2 Selection and Development of Numerical Method 6.2

6.2.1 Increasing the Capacity of FINELX 6.3

6.2.2 Including Natural Convection in Air Voids based upon the Rayleigh Number 6.3

6.2.3 Including Radiation Heat Transfer in Rectangular Voids 6.4

6.2.4 Constructing Spatial Grids for FINELX 6.6

6.2.5 Testing the Natural Convection and Radiation Calculations within FINELX 6.6

6.3 Experimental Methodology for Model Testing 6.7

6.3.1 Accounting for Radiation Heat Transfer in Rectangular Voids 6.9

6.3.2 Experimental Apparatus and Design 6.9

6.4 Evaluation of Input Data 6.12

6.4.1 Sample Dimensions 6.12

6.4.2 Thermal Property Data 6.12

6.4.3 Initial and Boundary Conditions 6.12

6.4.3.1 Cooling Medium Temperatures 6.12

6.4.3.2 Heat Transfer Coefficients 6.13

6.4.3.3 View Factors for Radiation Heat Transfer in Rectangular Voids 6.14

6.5 Comparison of Measured and Predicted Data for Other Runs 6.16

6.6 Conclusions 6.18

7. Development and Testing of a Model for Predicting Heat Transfer During Chilling of Packages Containing Combined Rectangular and Triangular Voids **7.1**

7.1 Development of the Physical Model 7.1

7.2 Incorporating the Physical Model into FINELX 7.3

7.3 Experimental Methodology for Model Testing 7.4

7.4 Evaluation of Input Data 7.7

7.4.1 Sample Dimensions 7.7

7.4.2 Thermal Property Data 7.7

7.4.3 Initial and Boundary Conditions 7.7

7.4.3.1 Cooling Medium Temperatures 7.7

7.4.3.2 Heat Transfer Coefficients 7.7

7.4.3.3 View Factors for Radiation Heat Transfer in Rectangular Voids 7.8

7.5 Comparison of Measured and Predicted Data 7.8

7.6 Conclusions 7.12

8. Development of a Simple Method for Predicting Heat Transfer During Chilling of Packages Containing Rectangular and Triangular Voids **8.1**

8.1 Simplification of the Prediction Method 8.1

8.2 Dealing With Asymmetric Heat Transfer Coefficients 8.3

8.3 Food Packages Containing Rectangular Voids 8.4

8.3.1 Development of a Simple Physical Model 8.4

8.3.2 Calculation Method and Relevant Equations 8.5

8.3.3 Averaging Temporal Variations – One Step Calculations 8.7

8.4 Food Packages Containing Triangular Voids 8.7

8.4.1 Development of a Simple Physical Model 8.7

8.4.2 Averaging Temporal Variations 8.9

8.4.3 Averaging Spatial Variations 8.9

8.5 Food Packages Containing Combined Void Spaces 8.13

8.6 Accuracy of Predictions by the Simple Models 8.15

8.6.1 Food Packages Containing Rectangular Voids 8.16

8.6.2 Food Packages Containing Triangular Voids 8.21

8.6.3 Food Packages Containing Combined Voids 8.30

8.6.4 Cooling Times vs. Cooling Rates 8.33

8.7 Comparison Against Other Existing Prediction Methods 8.35

8.8 Commercial Applications of the New Models 8.41

8.9 Discussion and Conclusions 8.41

9. Conclusions **9.1**

Notation Not.1

References Ref.1

Appendices:

A1. Determination of Thermal Conductivity for Test Materials A1-1

A1.1 Polycarbonate Sheeting A1-1

A1.2 'Styrodur' Polystyrene Insulation A1-4

A2. User's Guide to FINELX Program A2-1

A3. Worked Examples Using The Simpler Prediction Method A3-1

A4. Published Work: A4-1

Prediction of Chilling and Freezing Rates of Cartoned Meat A4-2

Methods for Evaluating the Effect of Large Voids on Food Package Cooling Times A4-4

The Effect of Void Space on Chilling Times for Food Product Packages A4-13

List of Figures

2.1 A banded matrix 2.8

2.2 Boundary conditions on a horizontal infinite cylinder 2.24

3.1 Photographs showing cross sections of four types of boneless primal cut packages 3.2

3.2 Diagram of the thermal resistances within a full meat carton undergoing three-dimensional cooling 3.3

3.3 Diagram of simplified physical model 3.4

4.1 Diagram of simplified physical model with and without a headspace void 4.1

4.2 Photograph of test sample holder 4.2

4.3 Diagram of test sample holder 4.4

4.4 Diagram of plate cooler 4.4

4.5 Diagram of the heat transfer pathways of edge effects 4.12

4.6 Plot of centre temperature vs. time for Tylose blocks containing no voids, and blocks containing 50mm high air voids and 50mm high filled voids 4.13

4.7 Plot of log unaccomplished temperature change ($\ln Y_c$) vs. time for same data in Figure 4.5 4.14

4.8 FINEL grid with no edge effect (data taken from Run 6) 4.17

4.9 Plot of measured and predicted $\ln Y_{LS}$ vs. time (Run 4) 4.20

4.10 Plot of measured and predicted $\ln Y_C$ vs. time (Run 4) 4.20

4.11 Plot of measured and predicted $\ln Y_{US}$ vs. time (Run 4) 4.20

4.12 FINEL grid with edge effect included (data taken from Run 6) 4.21

4.13 Plot of measured and predicted $\ln Y_{LS}$ vs. time (Run 4) 4.23

4.14 Plot of measured and predicted $\ln Y_C$ vs. time (Run 4) 4.23

4.15 Plot of measured and predicted $\ln Y_{US}$ vs. time (Run 4) 4.23

4.16 Diagram of three treatments used to determine the third dimension edge effect 4.27

5.1 Side elevation of polycarbonate sample holder containing two Tylose blocks 5.2

5.2 Photograph of a sample holder 5.3

5.3 Diagram of two sample holders within the plate cooler 5.4

5.4 Plot of centre temperature vs. time for Tylose blocks containing no voids, and for blocks containing 50mm high filled voids and 50mm high air voids 5.10

5.5 Plot of $\ln Y_c$ vs. time for the same samples shown in Figure 5.4 5.11

5.6 Plot of $[d(\ln Y_c)/dt]$ vs. time for the same samples shown in Figure 5.4 5.11

5.7 (Cooling time)/(Solid block cooling time) at higher HTC 5.13

5.8 (Cooling time)/(Solid block cooling time) at lower HTC 5.13

5.9 Example data file from PDEase2D 5.15

5.10 Example of the grid created by PDEase2D 5.22

5.11 Plot of $\ln Y_c$ vs. time for measured and predicted data from blocks with filled voids – 20mm voids, high HTC (Run 2) 5.23

5.12 Plot of $\ln Y_c$ vs. time for measured and predicted data from blocks with filled voids – 20mm voids, low HTC (Run 1) 5.23

5.13 Plot of $\ln Y_c$ vs. time for measured and predicted data from blocks with filled voids – 30mm voids, high HTC (Run 9) 5.23

5.14 Plot of $\ln Y_c$ vs. time for measured and predicted data from blocks with filled voids – 30mm voids, low HTC (Run 6) 5.23

5.15 Plot of $\ln Y_c$ vs. time for measured and predicted data from blocks with filled voids – 40mm voids, high HTC (Run 15) 5.23

5.16 Plot of $\ln Y_c$ vs. time for measured and predicted data from blocks with filled voids – 40mm voids, low HTC (Run 11) 5.23

5.17 Plot of $\ln Y_c$ vs. time for measured and predicted data from blocks with filled voids – 50mm voids, high HTC (Run 5) 5.23

5.18 Plot of $\ln Y_c$ vs. time for measured and predicted data from blocks with filled voids – 50mm voids, low HTC (Run 6) 5.23

5.19 Plot of percentage difference between measured and predicted times vs. void height 5.25

5.20 Comparison of predicted $\ln Y_c$ vs. time plots for a Tylose block containing filled voids and still-air voids (HTC = 12.7 $Wm^{-2}K^{-1}$) 5.26

5.21 Diagram of transverse void positions for triangular voids cooled from above and below 5.29

5.22 Plot of *Ra* vs. *Nu* for triangular voids cooled from below (conduction and radiation only) 5.31

5.23 Plot of *Ra* vs. *Nu* for triangular voids cooled from above (conduction, radiation and natural convection) 5.33

6.1 Diagram of a sample holder containing rectangular horizontal voids 6.8

6.2 Side elevation of a sample holder containing rectangular horizontal voids 6.9

6.3 Diagram of a sample holder arrangement within the plate cooler 6.10

6.4 Plot showing an increase in the cooling rate of a block due to radiation heat transfer occurring in rectangular horizontal voids (data taken from Run 6) 6.15

6.5 Plot of $\ln Y_c$ vs. time for measured and predicted data from blocks containing horizontal rectangular voids with transparent walls – 10mm void, high HTC (Run 7) 6.17

6.6 Plot of $\ln Y_c$ vs. time for measured and predicted data from blocks containing horizontal rectangular voids with transparent walls – 10mm void, low HTC (Run 8) 6.17

6.7 Plot of $\ln Y_c$ vs. time for measured and predicted data from blocks containing horizontal rectangular voids with transparent walls – 30mm void, high HTC (Run 9) 6.17

6.8 Plot of $\ln Y_c$ vs. time for measured and predicted data from blocks containing horizontal rectangular voids with transparent walls – 30mm void, low HTC (Run 10) 6.17

7.1 Two-dimensional roll-like flow in a rectangular void 7.1

7.2 Expected two-dimensional roll-like flow in a combined void 7.2

7.3 Simplified physical model for combined voids 7.2

7.4 Areas of overlap in a combined void 7.3

7.5 Side elevation of a sample holder containing combined rectangular and triangular voids 7.4

7.6 Plot showing an increase in the cooling rate of a block due to the presence of triangular voids (data taken from Runs 2A & 2B) 7.8

7.7 Plot of $\ln Y_c$ vs. time for measured and predicted data from blocks containing combination of voids – 25mm rectangular and 50mm triangular voids, high HTC (Run 1B) 7.10

7.8 Plot of $\ln Y_c$ vs. time for measured and predicted data from blocks containing combination of voids – 25mm rectangular and 50mm triangular voids, high HTC (Run 2B) 7.10

7.9 Plot of $\ln Y_c$ vs. time for measured and predicted data from blocks containing combination of voids – 25mm rectangular and 50mm triangular voids, low HTC (Run 3B) 7.10

7.10 Plot of $\ln Y_c$ vs. time for measured and predicted data from blocks containing combination of voids – 25mm rectangular and 50mm triangular voids, low HTC (Run 4B) 7.10

7.11 Plot of $\ln Y_c$ vs. time for measured and predicted data from blocks containing combination of voids – 10mm rectangular and 30mm triangular voids, high HTC (Run 5A) 7.10

7.12 Plot of $\ln Y_c$ vs. time for measured and predicted data from blocks containing combination of voids – 10mm rectangular and 50mm triangular voids, high HTC (Run 5B) 7.10

7.13 Plot of $\ln Y_c$ vs. time for measured and predicted data from blocks containing combination of voids – 10mm rectangular and 30mm triangular voids, low HTC (Run 6A) 7.11

7.14 Plot of $\ln Y_c$ vs. time for measured and predicted data from blocks containing combination of voids – 10mm rectangular and 50mm triangular voids, low HTC (Run 6B) 7.11

7.15 Plot of $\ln Y_c$ vs. time for measured and predicted data from blocks containing combination of voids – 10mm rectangular and 30mm triangular voids, low HTC (Run 7A) 7.11

7.16 Plot of $\ln Y_c$ vs. time for measured and predicted data from blocks containing combination of voids – 10mm rectangular and 50mm triangular voids, low HTC (Run 7B) 7.11

8.1 Simple physical model for food packages containing rectangular air voids 8.4

8.2 Simple physical model for food packages containing triangular air voids 8.8

8.3 A physical model treating the triangular air void as an effective heat transfer coefficient 8.9

8.4 A physical model treating the triangular air void as part of the solid material with an effective heat transfer coefficient 8.11

8.5 A physical model showing averaging of spatially varying heat transfer coefficients 8.12

8.6 Simple physical model for food packages containing combined air spaces 8.14

8.7 Plot of percentage differences from the measured data for prediction method A and prediction method B (with one step) 8.20

8.8 Plot of percentage differences from the measured data for prediction methods D and F 8.25

8.9 Sideways heat flow in the polycarbonate packaging layer 8.26

8.10 Diagram of the steady-state FINELX simulation to determine the effect of sideways heat flow 8.26

8.11 Plot of percentage differences from the measured data for prediction method A and prediction method F (with effective area adjustment included) 8.30

8.12 Plot of percentage differences from the measured data for prediction methods G and H 8.32

List of Tables

2.1 Models for effective thermal conductivity of composite solids 2.18

2.2 Solutions to CFD of natural convection within various enclosure types 2.21

2.3 Analytical solutions of steady state natural convection within horizontal layers (adapted from Goldstein *et al.*, 1990) 2.25

2.4 Empirical solutions of steady state natural convection within various enclosure types 2.27

4.1 Treatment table for preliminary data collection 4.6

4.2 Thermal properties of test materials used in preliminary data collection 4.7

4.3 Individual estimates of lower surface (LS) and upper surface (US) HTC 4.11

4.4 Measured times for one $\ln Y_c$ reduction of blocks with filled voids or air voids 4.15

4.5 Comparison of prediction methods – centre temperatures 4.18

4.6 Comparison of prediction methods – centre temperatures 4.22

4.7 Comparison of measured and predicted times for one $\ln Y_c$ reduction 4.25

5.1 Treatment table for improved data collection 5.6

5.2 Thermal properties of test substances 5.7

5.3 Times for one $\ln Y_c$ reduction for blocks with triangular voids of various heights 5.12

5.4 Percentage difference between measured and predicted times for one $\ln Y_c$ reduction for runs with no voids 5.20

5.5 Measured and predicted times for one $\ln Y_c$ reduction for blocks with triangular filled voids 5.24

5.6 Thermal and physical properties of air 5.26

5.7 *Nu* values for triangular air voids estimated by matching the measured and predicted data 5.28

6.1 Comparison of predicted cooling times of blocks containing rectangular voids with and without natural convection and radiation heat transfer 6.7

6.2 Treatment for trials with horizontal rectangular voids 6.11

6.3 Percentage difference between measured and predicted times for one $\ln Y_c$ reduction of blocks containing no voids 6.14

6.4 Comparison of predicted times for one $\ln Y_c$ reduction of blocks containing rectangular voids with and without natural convection and radiation heat transfer 6.15

6.5 Comparison of measured and predicted times for one $\ln Y_c$ reduction of blocks containing voids that had transparent or blackened walls 6.17

7.1 Treatment table for trials with combined voids 7.6

7.2 Comparison of measured and predicted times for one $\ln Y_c$ reduction of blocks containing 25mm high rectangular voids 7.9

7.3 Comparison of measured and predicted times for one $\ln Y_c$ reduction of blocks containing combined voids of various heights 7.11

8.1 Description of prediction methods used in section 8.6 8.16

8.2 Results from prediction method B (with 5 steps) 8.17

8.3 Comparison of measured data and results from prediction methods A and B (with 5 steps) - Times for one $\ln Y_c$ reduction 8.18

8.4 Comparison of times for one $\ln Y_c$ reduction predicted by method B with a different number of steps 8.19

8.5 Results from prediction method C 8.19

8.6 Comparison of measured data and results from prediction methods B (with one step) and C - Times for one $\ln Y_c$ reduction 8.20

8.7 Comparison of measured data and results from prediction methods D and E - Times for one $\ln Y_c$ reduction 8.22

8.8 Results from prediction method F 8.23

8.9 Percentage differences between prediction method F, the measured data, and prediction methods D and E 8.24

8.10 Combinations of boundary conditions for Figure 8.10 8.27

8.11 Estimated total heat flow values (with and without sideways heat flow) 8.27

8.12 Results from prediction method F with effective area adjustment included 8.28

8.13 Percentage differences between prediction method F (with effective area adjustment), the measured data, and prediction methods D and F 8.29

8.14 Results from prediction method H 8.31

8.15 Comparison of measured data and results from prediction methods G and H - Times for one $\ln Y_c$ reduction 8.32

8.16 Comparison of measured data and results from prediction methods A and B (with one step) - Times for 1.5 $\ln Y_c$ reductions 8.33

8.17 Comparison of measured data and results from prediction methods D and F (with effective area adjustment included) - Times for 1.5 $\ln Y_c$ reductions 8.34

8.18 Comparison of measured data and results from prediction methods G and H - Times for 1.5 $\ln Y_c$ reductions 8.35

8.19 Comparison of times for one $\ln Y_c$ reduction predicted by new and existing prediction methods for packages containing rectangular air voids 8.37

8.20 Percentage differences from measured data for new and existing prediction methods of packages containing rectangular air voids 8.38

8.21 Comparison of times for one $\ln Y_c$ reduction predicted by new and existing prediction methods for packages containing triangular air voids 8.38

8.22 Percentage differences from measured data for new and existing prediction methods of packages containing triangular air voids 8.39

8.23 Comparison of times for one $\ln Y_c$ reduction predicted by new and existing prediction methods for packages containing combined air voids 8.40

8.24 Percentage differences from measured data for new and existing prediction methods of packages containing combined air voids 8.40

1. INTRODUCTION

The international market for New Zealand's primary sector exports is extensive and competitive. In particular, there is increasing demand for fresh, chilled meat. These large boneless meat cuts are distributed as a number of individual items (wrapped or unwrapped) enclosed in an overall package that is typically of nominal dimensions 520 x 360 x 180mm. Air fills the gaps between the meat cuts.

Accurate prediction of the heat transfer from these packages is important because the quality and tenderness of the meat cuts is highly dependent upon the rate at which it is chilled (Chrystall, 1989). If chilling is too rapid, meat can undergo 'cold shortening', where the muscle fibres contract and cause a direct increase in toughness and a reduction in the product quality (Locker and Hagyard, 1963). However, if chilling is too slow excessive microbial growth can occur on the product, also leading to unacceptable product quality. Keeping the temperature-time profile of meat cuts within a satisfactory operating range during chilling will ensure that the potential product tenderness and microbial quality is realised.

Existing methods for prediction of chilling rates in packages that contain significant air voids assume the contents are an homogeneous solid with 'effective' thermal properties based upon the packaging arrangement and relative amounts of solid and air. The air voids are usually assumed to be small and evenly distributed, thus heat is conducted along unbroken pathways that are defined by straight lines or curves perpendicular to isothermals in the solid. However, the air voids contained in chilled meat cartons and similar packages may not be evenly distributed and a significant amount of heat transfer may be attributable to mechanisms such as natural convection and radiation within the voids. In such cases effective thermal property methods may not be accurate.

A new prediction method that accounts for the effects of significant air voidage within enclosed packages will assist in the design of optimal chilling processes, and benefit food engineers and the international food industry with whom they work.

2. LITERATURE REVIEW

2.1 Scope of the Review

The literature covered in this review is categorised into two major areas of relevant research: modelling of unsteady state heat transfer by conduction in solids (including composites modelled with no gas movement in the voids), and modelling of natural convection within enclosures.

2.2 Unsteady State Heat Transfer by Conduction in Solids

2.2.1 Physical Models for Chilling of Solid Biological Materials

Although solid biological materials contain a liquid phase component, unsteady state heat transfer through solid biological materials is usually considered to be solely by conduction. Thus the biological material is treated as an homogeneous solid in which the liquid water is immobilised.

Solutions to the equations describing the heat transfer differ widely in both complexity and accuracy. This review classifies solutions for unsteady state heat conduction models into three groups but it is acknowledged that due to the overlap between types of solutions, the correct classification of some solutions is not clear-cut:

1. Numerical solutions, which discretise the object volume and evaluate transient characteristics (such as temperature and thermal properties) at set points within the volume in discrete time steps. The solutions are not mathematically exact but the underlying models attempt to represent most of the important physical processes.

2. Analytical solutions, which give exact mathematical solutions to a model but the model itself may not include all important physical processes.

3. Empirically-adapted solutions, which are based on observation or experiment (e.g. adjustment of predictions by analytical solutions through the use of multiplicative factors, curve-fitting of parameters in a model to fit the results to experimental data or heuristics for data selection). Note that the underlying mathematical techniques used in these solutions can be either numerical or analytical. In such cases it is often not possible to define the model and solution method separately.

2.2.2 Model Formulation

Modelling of unsteady state heat conduction encompasses prediction of temperature with respect to four independent variables: time and displacement in three dimensions (x, y and z). Expressed mathematically, the phenomenon is described by the well-known Fourier equation for heat conduction:

$$C(T)\frac{\partial T}{\partial t} = \frac{\partial}{\partial x}\left[k(T)\frac{\partial T}{\partial x}\right] + \frac{\partial}{\partial y}\left[k(T)\frac{\partial T}{\partial y}\right] + \frac{\partial}{\partial z}\left[k(T)\frac{\partial T}{\partial z}\right] \qquad (2.1)$$

where C is volumetric heat capacity (J m^{-3} K^{-1})
T is temperature (K or °C)
t is time (s)
k is the thermal conductivity of the object (W m^{-1} K^{-1})
x is displacement in first dimension (m)
y is displacement in second dimension (m)
z is displacement in third dimension (m)

Solution of this parabolic partial differential equation with appropriate boundary and initial conditions will yield a physically realistic model of the heating or cooling process provided the real process is always one of heat conduction. Due to the complexity of solutions for practical problems in which $C(T)$ and $k(T)$ may be complex functions, simplified models have also been developed.

2.2.3 Boundary Conditions

Traditionally, boundary conditions for unsteady state heat transfer have been categorised into five types, referred to as the first, second, third and fourth kinds, and the symmetry boundary condition. The first kind (also known as a Dirichlet condition) is a prescribed surface temperature:

$$T_s = T_a \qquad (2.2)$$

where T_s is the surface temperature of the object (K or °C)
T_a is the ambient temperature surrounding the object (K or °C)

The second kind of boundary condition (also known as a Neumann condition) covers the case of a fixed rate of heat flow to the surface: e.g.

$$\phi = -kA\left[\frac{\partial T}{\partial x}\right]_{x=0} \tag{2.3}$$

for a planar boundary at x = 0

where ϕ is the heat flow to the surface (W)

A is the surface area of the object (m^2)

The third kind (also known as a Fourier, mixed boundary condition, or Newton's law of cooling) covers convection at the objects surface e.g. for a planar surface at $x = 0$:

$$h_e\left(T_a - T_s\right) = -k\left[\frac{\partial T}{\partial x}\right]_{x=0} \tag{2.4}$$

where h_e is the surface heat transfer coefficient (W m^{-2} K^{-1})

The fourth kind of boundary condition (also a Dirichlet condition) defines surface temperature as a function of time:

$$T_s = f(t) \tag{2.5}$$

The fifth and final case applies to an axis of symmetry or an insulated surface (also a Neumann condition):

$$\left[\frac{\partial T}{\partial x}\right]_{x=0} = 0 \tag{2.6}$$

The second and fourth kinds of boundary conditions occur very rarely in industrial situations and the first and fifth kinds can be considered particular cases of the third kind with $h_e = \infty$ and $h_e = 0$ respectively. This, coupled with the option of being able to include additional modes of heat transfer (eg. radiation and/or evaporation albeit approximately) in an equation of the same form as equation (2.4), makes the third kind of boundary condition the most important.

2.2.4 Initial Conditions

The initial condition, i.e. an object's temperature distribution with respect to all three dimensions, must be defined:

$$T_i = f(x, y, z) \tag{2.7}$$

where T_i is temperature at $t = 0$ (K or °C)

2.2.5 Numerical Solutions

Numerical solutions are likely to be relevant to the meat carton problem because of their ability to handle irregular shapes, non-homogeneous materials and non-constant external conditions. All numerical solutions predict values at discrete points for a set of independent parameters, and the solution procedure must be repeated each time these parameters change. The two most commonly used numerical methods are finite differences and finite elements. Other techniques such as the boundary element method and the control volume method will be briefly discussed.

2.2.5.1 The Finite Difference Method

The finite difference method is implemented by dividing an object into even space steps with centrally located nodes at which the temperature is evaluated for each time step. Several schemes exist and these are derived by approximations to the Fourier equation through truncation of a Taylor series.

Finite differences are applicable for one-, two- and three-dimensional heat conduction but it is convenient to discuss and compare schemes for one-dimensional heat conduction. The so-called 'explicit finite differences scheme' is given by:

$$C_j^i \frac{T_j^{i+1} - T_j^i}{\Delta t} = \frac{1}{\Delta x^2}\left[k_{j+1/2}^i\left(T_{j+1}^i - T_j^i\right) - k_{j-1/2}^i\left(T_j^i - T_{j-1}^i\right)\right] \tag{2.8}$$

where Δt is the time step (s)

Δx is the space step (m)

i is the current time step

$i+1$ is one time step into the future

j is the nodal position within a space step

$k^{i}_{j+1/2}$ is evaluated at $\left(T^{i}_{j+1} + T^{i}_{j}\right)/2$

$k^{i}_{j-1/2}$ is evaluated at $\left(T^{i}_{j-1} + T^{i}_{j}\right)/2$

Note that the left hand side of equation (2.8) is not 'centrally located', i.e. C is evaluated at time level i, not at the midpoint time level ($i+\frac{1}{2}$) and the same holds true for the whole right hand side.

Crank & Nicolson (1947) proposed the 'Crank-Nicolson scheme':

$$C^{i}_{j}\frac{T^{i+1}_{j} - T^{i}_{j}}{\Delta t} = \frac{1}{2\Delta x^{2}}\left[k^{i}_{j+1/2}\left(T^{i}_{j+1} - T^{i}_{j} + T^{i+1}_{j+1} - T^{i+1}_{j}\right) - k^{i}_{j-1/2}\left(T^{i}_{j} - T^{i}_{j-1} + T^{i+1}_{j} - T^{i+1}_{j-1}\right)\right] \quad (2.9)$$

The problem is partially overcome, but $k_{j+1/2}$, $k_{j-1/2}$ and C can only be evaluated at the midpoint time level ($i+\frac{1}{2}$) by iteration. Implicit solution is required by solving a set of simultaneous equations.

Lees (1966) developed the 'Lees scheme', both reducing Taylor series truncation error on the left-hand side and centrally locating the scheme by using three time levels:

$$\begin{aligned} C^{i}_{j}\frac{T^{i+1}_{j} - T^{i-1}_{j}}{2\Delta t} = \frac{1}{3\Delta x^{2}}\Big[&k^{i}_{j+1/2}\left(T^{i+1}_{j+1} - T^{i+1}_{j} + T^{i}_{j+1} - T^{i}_{j} + T^{i-1}_{j+1} - T^{i-1}_{j}\right) \\ &- k^{i}_{j-1/2}\left(T^{i+1}_{j} - T^{i+1}_{j-1} + T^{i}_{j} - T^{i}_{j-1} + T^{i-1}_{j} - T^{i-1}_{j-1}\right)\Big] \end{aligned} \quad (2.10)$$

Cleland & Earle (1977) reported one practical shortcoming of such schemes in freezing calculations. If the temperature change per time step is too large, the temperatures at which $C(T)$ is evaluated can miss or 'jump' the latent heat peak in the $C(T)$ curve. A continuous heat (energy) balance that will indicate if the time steps are too large to prevent jumping of the latent heat peak can avoid this. Although phase change within a meat carton will not be investigated in this work, Cleland & Earle (1984) suggest that a heat balance check is obligatory when using finite difference or finite element methods as a check on calculation validity. Cleland (1990) states that truncation errors can be minimised by using at least 10 space steps (11 nodes) from product surface to thermal centre of objects.

The third kind of boundary condition, at $j = 0$, is easily incorporated into all these schemes because it can effectively be handled as a Dirichlet condition. Specifically, it is implemented by setting $T_{-1} = T_e$, $k_{-1/2} = h_e.\Delta x$ and dividing the left hand side of equation 2.10 by two to account for the fact that a surface node has only half the volume of material compared to an internal node.

As previously mentioned, the implicit finite difference methods can be extended to higher space dimensions. However, a set of simultaneous equations of size (M x N x O) must be solved at each time step, where M is the number of nodes in the x-direction, N is the number of nodes in the y-direction and O is the number of nodes in the z-direction. Furthermore the coefficient matrix is no longer tri-diagonal and computer resource requirements are much higher.

The Alternating Direction Implicit (A.D.I) method is an extension to the finite difference method that allows evaluation of unsteady state heat transfer in two- and three-dimensions but still ensures retention of a tri-diagonal coefficient matrix. The two-dimensional unsteady state heat transfer case is more convenient to present. A node (T_0) is surrounded by four other nodes, two in each dimension (say T_L , T_R , T_T and T_B denoting nodes to the left, right, top and bottom respectively). Then alternate traverses are made in each direction. For example, in a simple scheme horizontally:

$$C_0^i \frac{T_0^{i+1} - T_0^i}{\Delta t} = \frac{1}{\Delta x^2}\left[(T_L^i - 2T_0^i + T_R^i) + (T_T^{i+1} - 2T_0^{i+1} + T_B^{i+1})\right] \qquad (2.11)$$

The bias in this formula is balanced by reversing the order of the second derivative approximations in the vertical traverse:

$$C_0^{i+1} \frac{T_0^{i+2} - T_0^{i+1}}{\Delta t} = \frac{1}{\Delta x^2}\left[(T_L^{i+2} - 2T_0^{i+2} + T_R^{i+2}) + (T_T^{i+1} - 2T_0^{i+1} + T_B^{i+1})\right] \qquad (2.12)$$

Note that on a horizontal traverse new values are computed for the row of nodes (T_T and T_B are fixed) and on a vertical traverse new values are computed for the column of nodes (T_L and T_R are fixed).

Comprehensive testing of the Lees scheme against experimental results for freezing of water-based solids was reported in the papers of Cleland & Earle (1977a, 1979a, b).

Various regularly shaped test materials were used and the predicted results were in agreement with the experimental data across 180 trials.

2.2.5.2 The Finite Element Method

The finite element method divides the space of interest into non-overlapping elements which need not be of uniform size or shape, and thus it is more suitable for irregular shapes because it allows them to be more easily described. The nodes at which temperatures are calculated are positioned on the vertices or the boundaries of each element. The method uses variational calculus to state an integral equivalent to the Fourier equation. Minimising this integral at each node and for every time step by the Rayleigh-Ritz or Galerkin Method creates an approximate solution.

For solution of the Fourier equation with one-dimensional heat conduction in an infinite slab the integral is stated by Cleland (1990) as:

$$I = 0.5 \int_{x=0}^{R} \left[k \left(\frac{\partial T}{\partial x} \right)^2 + 2CT \frac{\partial T}{\partial t} \right] dx \tag{2.13}$$

which can be rewritten as:

$$I = I_k + I_C \tag{2.14}$$

where $I_k = 0.5 \int_{x=0}^{R} k \left(\frac{\partial T}{\partial x} \right)^2 dx$

$$I_C = 0.5 \int_{x=0}^{R} 2CT \frac{\partial T}{\partial t} dx$$

I can then be minimised by setting the first derivative to zero:

$$\frac{dI}{d\mathbf{T}} = \frac{dI_k}{d\mathbf{T}} + \frac{dI_C}{d\mathbf{T}} = \mathbf{0} \tag{2.15}$$

where $\mathbf{T}$ is the vector of nodal temperatures

$\mathbf{0}$ is a vector containing all zeroes

The general form of the solution is:

$$\mathbf{C}\dot{\mathbf{T}} = -\mathbf{K}\,\mathbf{T} \tag{2.16}$$

where $\mathbf{C}$ is the capacitance matrix

$\mathbf{K}$ is the global conductance matrix

Equation 2.16 represents a set of simultaneous ordinary differential equations, with one equation per nodal variable. The global conductance matrix is *banded* (Figure 2.1), which means that all of the non-zero coefficients (labelled C) are located relatively close to the main diagonal and all of the coefficients beyond the bandwidth are zero.

$$\begin{array}{c} \left|\leftarrow \text{bandwidth} \rightarrow\right| \\ \begin{bmatrix} C & C & C & C & 0 & 0 & 0 & 0 \\ C & C & C & C & C & 0 & 0 & 0 \\ C & C & C & C & C & C & 0 & 0 \\ C & C & C & C & C & C & C & 0 \\ 0 & C & C & C & C & C & C & C \\ 0 & 0 & C & C & C & C & C & C \\ 0 & 0 & 0 & C & C & C & C & C \\ 0 & 0 & 0 & 0 & C & C & C & C \end{bmatrix} \end{array}$$

Figure 2.1 A banded matrix

The efficiency of solution typically decreases as the bandwidth increases. Norrie & de Vries (1978) summarise the most common solution methods as either *direct* (including Gauss elimination, Cholesky decomposition, LDL^T factorisation, and frontal solution) or *iterative* (including the Jacobi method, the Gauss-Seidel method, Successive Over-Relaxation, and Richardson's method).

There is great flexibility in using the finite element method, particularly when constructing the space grid. Segerlind (1984) gives a comprehensive introduction to gridding and general application of the method. The elements can be one, two or three-dimensional. A one-dimensional element has only a finite length (which can vary between adjacent elements) and no other measure of shape. Two-dimensional elements are usually triangular or quadrilateral and three-dimensional elements are usually cuboid. Segerlind also discusses shape functions, which are used to describe either the element

geometry or the behaviour of the nodal variable along the element boundaries. There are two commonly used shape functions - linear and quadratic. A linear shape function corresponds to a linear temperature profile along the boundaries of straight-sided elements. Since a linear function only requires two points for definition, the temperature profile along the boundary of an element with a linear shape function requires only two nodes (one at the end of each boundary). Thus a two-dimensional linear triangular element has three boundaries and three nodes, and a linear quadrilateral element has four boundaries and four nodes. A quadratic shape function can either be used to define a linear temperature profile along curved element boundaries, or a quadratic temperature profile along straight-sided element boundaries. The quadratic shape function requires three nodes per boundary (one at each end and one other node along the boundary that need not be centrally positioned). A two-dimensional quadratic triangular element would have six nodes, and a quadratic quadrilateral element would have eight nodes.

A regular mesh (with all elements the same size) is not necessary when using the finite element method. In areas where a comparatively steep (with respect to position) temperature profile occurs in the solid being modelled, the mesh can be refined with smaller elements to enable the numerical approximations of the rapidly changing nodal variable to be more accurate. Likewise if temperature is relatively uniform over a given mesh area, larger elements can be used.

Although there is much flexibility within the finite element method (with a choice of different mesh types, different element sizes and node positions), certain guidelines must be followed in order to ensure a stable solution. Just like the finite difference method, there should be more than 10 nodes between the object surface and thermal centre (this is more important than the number of elements between surface and centre), time steps should be small enough to give a good heat balance, the numerical integrations must be accurate, and adjacent elements should not differ greatly in size (Cleland, 1990).

Cleland *et al.* (1984 & 1987a) compared the predictions from a finite element method to large bodies of data for freezing of regular and multi-dimensional shapes. They concluded that with sensible discretisation, prediction method inaccuracy was negligible for this method. Prediction of chilling rates is also likely to be accurate because the case of chilling does not involve complications such as thermophysical properties changing rapidly with temperature or a change in object density due to phase change.

2.2.5.3 The Boundary Element Method

The boundary element method is similar to the finite element method. However discretisation is restricted to the boundary region of the object, thereby reducing the required amount of data preparation and computing resources. The method is only considered accurate for objects of large surface area to volume ratios (Wrobel & Brebbia, 1979), and widespread use in prediction of food cooling is not foreseen (Cleland, 1990). Banerjee & Wilson (1989) indicated that commercial finite element computer programs have a clear advantage over those that use the boundary element method, primarily due to the relative amount of development that has gone into each method.

2.2.5.4 The Control Volume Method

In the control volume method, the object is discretised into a number of non-overlapping 'volumes' (or 'areas' in a two-dimensional case) often referred to as 'zones'. In a single component system each of the volumes is assumed to be internally perfectly mixed and therefore at uniform temperature. An ordinary differential equation (ODE) is required for each volume to account for the heat transfer occurring by interaction with adjacent volumes.

In multi-component systems, where inter-mixing of the components is on such a fine scale that separation of the components into different zones each containing one component is not practical, the heat transfer is usually modelled by using a separate ODE for each component within each volume. Although each individual component within a volume is at a uniform temperature the entire volume is not considered to be perfectly mixed. Cleland *et al.* (1982) and Cleland (1985) developed such models where intra-volume interactions between components were allowed, but inter-volume interactions could only occur through the continuous-phase component of the system (usually air). Models developed by Amos (1995) and Tanner (1998), for predicting heat transfer through apple cartons cooled by forced convection, were more physically realistic. Amos also included the inter-volume interaction between the packaging and the solid food, and Tanner considered all possible intra- and inter-volume interactions.

2.2.6 Analytical Solutions

Analytical methods have yielded exact solutions for unsteady state heat conduction in so-called 'regularly shaped' objects (the infinite slab, infinite cylinder, sphere, infinite rectangular rod, rectangular brick, finite cylinder, cone and rectangular parallelepiped)

provided the object is of homogenous composition, with a uniform initial condition and exposed to constant external conditions. At temperatures above a biological material's initial freezing temperature, its thermal properties vary only slightly with temperature. Hence for cooling of regularly shaped objects with no phase change, analytical solutions with constant thermal properties are useful.

The solutions for temperature are in the form of a converging infinite series. Carslaw & Jaeger (1959) report the solutions for several regularly shaped objects. Only the infinite cylinder with the third kind of boundary condition is described here, by way of example.

Four dimensionless numbers are used:

1. The Biot number (*Bi*):

$$Bi = \frac{h_e \cdot R}{k} \tag{2.17}$$

where R is the characteristic dimension or minimum half-thickness of the object (m)

2. The Fourier number (*Fo*):

$$Fo = \frac{k\,t}{C\,R^2} \tag{2.18}$$

3. The fractional unaccomplished temperature change (Y) for some point within the object:

$$Y = \frac{\left(T - T_a\right)}{\left(T_i - T_a\right)} \tag{2.19}$$

and,

4. the fractional unaccomplished temperature change (Y_{av}) at the mass average point in the object:

$$Y_{av} = \frac{\left(T_{av} - T_a\right)}{\left(T_i - T_a\right)} \tag{2.20}$$

For the case of the infinite cylinder:

$$Y = \sum_{i=1}^{\infty} \frac{2Bi\,J_0(\beta_i\, r/R)}{(\beta_i^2 + Bi^2)J_0(\beta_i)} \exp\left(-\beta_i^2 Fo\right) \tag{2.21}$$

$$Y_{av} = \sum_{i=1}^{\infty} \frac{4Bi^2}{\beta_i^2(\beta_i^2 + Bi^2)} \exp\left(-\beta_i^2 Fo\right) \tag{2.22}$$

the values of β are the roots of the equation:

$$\beta J_1(\beta) - Bi\,J_0(\beta) = 0 \tag{2.23}$$

where J_0 and J_1 are zero- and first-order Bessel's functions, respectively.

In cases of asymmetrical heat transfer, or where the external cooling medium temperature or the external heat transfer coefficient changes continuously with time, Duhamel's theorem (Carslaw and Jaeger, 1959) can lead to exact analytical solutions. Simple approximate methods have been developed by Cleland & Davey (1995) and by Tanner *et al.* (1995) for cases when a step change in the external cooling medium temperature or the external heat transfer coefficient occurs, respectively.

2.2.7 Empirically-adapted Solutions

Analytical methods are limited in their ability to deal with complex models (especially for irregularly shaped objects). Empirical adaptation has been used to address this problem. Due to the irregular meat cut shapes in a meat carton empirical adaptation methods are considered relevant. Some of the assumptions inherent when using analytical methods (homogenous composition, uniform initial condition and constant external conditions) are retained by empirical solutions.

Chilling processes are characterised by an exponentially decreasing centre temperature after an initial lag period. For the infinite slab and cylinder and the sphere, the

exponential fall is approximated by only one significant term in the analytical series solution. The general form of the solution is then:

$$Y_c = \frac{(T_c - T_a)}{(T_i - T_a)} = j_c \exp(-2.303\, t / f) \tag{2.24}$$

$$Y_{av} = \frac{(T_{av} - T_a)}{(T_i - T_a)} = j_{av} \exp(-2.303\, t / f) \tag{2.25}$$

where j_c is the lag factor for the centre position

j_{av} is the lag factor for the mass average temperature

f is the time for a 90% reduction in Y (s)

Alternatively f can be replaced with the half-life time $t_{0.5}$, where $t_{0.5} = 0.3010\, f$ (s).

Equation (2.24) or (2.25) can be used to predict chilling rates of irregularly shaped objects. The values of f, $t_{0.5}$, j_c and j_{av} are functions of object shape and Biot number. These can be calculated for regular shapes by analytical methods. However for irregular shapes it is necessary to determine shape factors for specific geometric and Biot number combinations by other methods.

Eight different methods for determining shape factors have been used:

1. Determination by experiment. From equations (2.24) and (2.25) a plot of $\ln(Y_c)$ or $\ln(Y_{av})$ versus time will yield f or $t_{0.5}$ (from the slope) and j_c or j_{av} (from the intercept). The values are specific to the object (size, shape and composition) and the surface heat transfer coefficient used in the experiments.

2. Several researchers (e.g. Earle & Fleming, 1967, Wade, 1984) have simply chosen the closest of the regular shapes and used analytical methods to calculate chilling time. Experiments must first be conducted to relate the size and shape of the object to an 'equivalent' R value for use with the analytical methods.

3. Cleland (1990) showed how attempts to determine universal shape factors have used limiting cases, such as the example of when the heat transfer is assumed to be totally externally controlled ($h_e \rightarrow 0$ and hence $Bi \rightarrow 0$). In this case the analytical solutions for regular shapes all yield the equation:

$$Y = \exp\left[-\left(h_c t / RC\right)\left(AR / V\right)\right] \tag{2.26}$$

where V is the volume of the object (m^3)
A is the surface area of the object (m^2)

AR / V is the dimensionless shape factor. As $Bi \rightarrow 0$, j_c and $j_{av} \rightarrow 1$, $f = 2.303\ V\ C / (h_e\ A)$ and $t_{0.5} = 0.693\ V\ C / (h_e\ A)$, this shape factor gives exact solutions for all shapes at $Bi = 0$, however as Bi increases it becomes increasingly inaccurate.

4. Smith *et al.* (1967, 1968), Clary *et al.* (1968, 1971) and Smith & Nelson (1969) used a geometry index (G). When $Bi \rightarrow \infty$, the exponential decrease in T_c gives a slope of $-\beta^2$ on a plot of $\ln(Y_c)$ versus Fo (from analytical solutions, e.g. equations (2.17)-(2.23)). For a sphere the same plot yields a slope of $-\pi^2$. G is then defined as the ratio of the slopes of these two plots, and elliptical shapes are approximated by the equation:

$$G = \frac{1}{4} + \frac{3}{8\beta_1} + \frac{3}{8\beta_2} \tag{2.27}$$

where G is the geometry index
β_1 is the ratio L_y/L_x
β_2 is the ratio L_z/L_x
L_x is the length of the objects shortest dimension or $2R$ (m)
L_y is the length of the first dimension orthogonal to L_x (m)
L_z is the length of the second dimension orthogonal to L_x (m)

Irregular shapes can then be related to the nearest equivalent ellipsoidal shape with equal orthogonal cross-sectional areas. A system of charts relates G to the exact analytical solution for a sphere and predictions can then be made. However the geometry index method is not dependent on Biot number and further attempts to account for this by use of a pseudo-Biot number introduced large interpretive errors at $Bi > 5$ (Lin, 1994).

5. Cleland & Earle (1982) developed the concept of a shape factor with Biot number dependency called E (equivalent heat transfer dimensionality). E is a multiplicative factor for irregularly shaped objects that shortens or lengthens the chilling time of the closest regularly shaped object to account for heat transfer occurring in other dimensions. Predictions for ellipsoidal, cylindrical and rectangular shapes are based on

the analytical solutions for the sphere, cylinder and slab respectively. The method is restricted to prediction of chilling time for the thermal centre of an object. Testing over a wide range of shapes and cooling conditions gave 95% confidence bounds of ±12%.

Lin (1994) further developed the use of the shape factor (E), based on the first term of the series analytical solution for a sphere, by considering its values at the two limiting conditions, $Bi = 0$ and $Bi \rightarrow \infty$ (denoted E_0 and E_∞ respectively). A weighting function dependent on the Biot number was then used to estimate E at other values of Bi. Empirical formulae were developed to calculate the lag factor, j, in a similar way to the estimation of E. Testing of predictions was done on a wide range of irregularly shaped objects under varying cooling conditions. The method predicted chilling times to within -7.6 to +5.6% for the thermal centre position and ±9.4% for the mass average case.

6. Fikiin & Fikiina (1971) used curve-fitted analytical solutions to establish the following mathematical expression for chilling time prediction:

$$t = \frac{V}{AR}\frac{CR^2}{k}\left[(2.3/Bi + 0.8)\ln\frac{T_i - T_a}{T - T_a} + 0.12\right] \qquad (2.28)$$

The shape factor is given by the ratio V/AR irrespective of Biot number, although this is only exact at $Bi = 0$ for slab, cylinder and sphere shapes. Testing of the method in 256 trials yielded an accuracy of ±9.1%. Baehr (1953) and Rutov (1958) proposed methods of the same type with prediction accuracies of 10.3% and 12.8% respectively. Cleland (1990) states that such methods are likely to lose accuracy at high Biot numbers.

7. Sanz *et al.* (1986) used a z-transfer function method - a form of 'dynamic curve fitting' to scale results from one chilling trial to a different temperature/time regime providing other conditions (particularly the heat transfer coefficient) remained constant.

8. Cuesta *et al.* (1990) proposed a graphical method to predict centre and mass average temperatures. The exponential half-chilling times for slab, cylinder and sphere shapes were used to construct diagrams of dimensionless times. The method had some shortcomings - irregular shapes had to be handled in conjunction with other methods

(such as methods 5 and 6 given above) and it could only predict for $Y_{av}<0.25$ but still with significant error of about ±10% within that range of Y_{av}.

2.2.8 Composite Solids - Effective Thermal Properties Theory

Researchers have proposed a large number of methods for calculating effective thermal properties. Pham (1989) recognised two different classes - empirical curve fitting of measured data, and equations derived from physical models. Pham (1989) and Lin (1994) stated that the latter is the most commonly used calculation method because of its more general applicability. Lin explained in detail how different ratios of the constituent thermal properties are used according to the structure of the components. Two assumptions were made for most of the physical models where air is the dispersed phase:

1. The voids are evenly distributed, and
2. They are of uniform size and too small for any natural convection to occur.

In a carton of primal meat cuts the first assumption does not hold, and the second assumption may also not be true. However this type of simplified model may still give useful insights so the theory was reviewed.

Effective Volumetric Heat Capacity

The mass of the air within the voids is assumed to be negligible compared to the mass of the solid material, hence:

$$\rho_e \approx (1-\varepsilon)\rho_s \tag{2.29}$$

where ρ_e is effective density of the composite solid (kg m^{-3})
ρ_s is density of the solid component without voids (kg m^{-3})
ε is porosity - the relative volume taken up by air voids

and thence:

$$C_e \approx (1-\varepsilon)C_s \tag{2.30}$$

where C_e is the effective volumetric heat capacity of a composite object (J m^{-3} K^{-1})

C_s is the volumetric heat capacity of the solid component of a composite object ($Jm^{-3}K^{-1}$)

Effective Thermal Conductivity

The thermal conductivity of a composite object is dependent on the types of material it is made up of, and the way the components are structured to make up the object. A number of models for calculating effective thermal conductivity have been proposed in the literature. Lin (1994) identified eight of the most commonly used methods for evaluation. Table 2.1 summarises these methods.

Lin *et al.* (1997) compared the thermal conductivities predicted by the eight methods against measured values from the chilling of rectangular bricks of Cheddar cheese with known porosity. They found that the method of Krischer (1963) gave the most accurate predictions of thermal conductivity (with a standard error of approximately 10%), similar to the findings of Murakami & Okos (1989). However Murakami & Okos expressed the distribution factor (f) in terms of porosity and moisture content, whereas the Lin *et al.* did not consider moisture content and f was curve-fitted dependent upon porosity only. Lin *et al.* also noted an apparent dependence of f on Biot number. The cause was attributed to either uncertainty in the thermal conductivity data of the Cheddar cheese (the effect of the uncertainties will be more significant at higher *Bi*) or natural convection in the air voids (causing the effective thermal conductivity to be under-predicted).

Table 2.1 Models for effective thermal conductivity of composite solids

Method or Author(s)	Model for effective thermal conductivity
Parallel component heat conduction model	$k_e = (1-\varepsilon)k_s + \varepsilon k_g$
Series component heat conduction model	$\frac{1}{k_e} = \frac{1-\varepsilon}{k_s} + \frac{\varepsilon}{k_g}$
Maxwell-Eucken model (Eucken, 1940)	$k_e = k_s\left(\frac{1-2U_1\varepsilon}{1+U_1\varepsilon}\right)$ where $U_1 = \frac{k_s - k_g}{2k_s + k_g}$
Levy (1981)	Uses the Maxwell-Eucken model and replaces ε with F where $2F = \frac{2}{U_2} - 1 + 2\varepsilon - \left[\left(\frac{2}{U_2} - 1 + 2\varepsilon\right)^2 - \frac{8\varepsilon}{U_2}\right]^{1/2}$ and $U_2 = \frac{(k_g - k_s)^2}{(k_s - k_g)^2 + \frac{k_s k_g}{2}}$
Kopelman (1966)	$k_e = \frac{k_s(1-U_3)}{1-U_3(1-\varepsilon^{1/3})}$ where $U_3 = \frac{\varepsilon^{2/3}}{1-k_g/k_s}$
Hill *et al.* (1967)	$k_e = (2U_4 - U_4^2)k_g + (1-4U_4+3U_4^2)k_s + \frac{8(U_4 - U_4^2)k_s k_g}{U_4 k_s + (4-U_4)k_g}$ where $U_4 = 2 - \sqrt{4-2\varepsilon}$
Krischer (1963)	$\frac{1}{k_e} = \frac{1-f}{(1-\varepsilon)k_s + \varepsilon k_g} + f\left(\frac{1-\varepsilon}{k_s} + \frac{\varepsilon}{k_g}\right)$ where f is a distribution factor $0 < f < 0.25$
Effective Medium Theory (Mattea *et al.*, 1986)	$(1-\varepsilon)\frac{k_e - k_s}{k_s + 2k_e} + \varepsilon\frac{k_e - k_g}{k_g + 2k_e} = 0$

where k_e is the effective thermal conductivity of the composite object ($Wm^{-1}K^{-1}$)
k_s is the thermal conductivity of the solid ($Wm^{-1}K^{-1}$)
k_g is the thermal conductivity of the gas component ($Wm^{-1}K^{-1}$)

2.3 Natural Convection

Buoyancy-induced flow is fluid motion that occurs due to external forces acting upon density gradients within the fluid. The external force is usually gravity and the density gradients usually arise from localised heating or cooling near a heat transfer surface. Historically, problems are classified as external flow (free convection) or internal flow (natural convection). External flow problems are considerably simpler to analyse than internal ones (Ostrach, 1968), because the bulk of the fluid is unaffected by the boundary layer. However, for enclosed internal flows the bulk of the fluid (called the 'core') is partially or fully surrounded by the boundary layers at the enclosure walls. Hence the core flow depends on the surrounding boundary layers, which in turn, are influenced by the core.

Ostrach (1964) points out that internal flows consist of two basic modes. The first, usually referred to as conventional convection, occurs whenever a density gradient is normal to the gravity vector. In such a case flow immediately ensues. The second mode, called unstable convection, occurs when the density gradient is parallel to but opposed to the gravity vector. In this situation the fluid remains in a state of unstable equilibrium (due to heavier fluid being above lighter) until a critical density gradient is exceeded. A spontaneous flow then results that eventually becomes steady and cellular-like. Both conventional and unstable modes can interact in a given configuration.

The extent of natural convection within enclosures due to thermal gradients depends on the enclosure size and shape, the temperature difference across the enclosure walls and the fluid properties. The literature reviewed is classified into numerical, analytical and empirical solutions.

2.3.1 Numerical Solutions (Computational Fluid Dynamics)

The physical aspects of any fluid are governed by three fundamental principles: conservation of mass, momentum and energy. Computational fluid dynamics (CFD) is the science of determining a numerical solution to the governing equations of all three. Formulation of the equations is accomplished by consideration of the laws of conservation. The system is discretised in time (for unsteady state flow only) and space, and mass and momentum balances are constructed for each of the spatial elements. A mass balance gives *the equation of continuity* and a momentum balance leads to the *Navier-Stokes equations*. The equations have been known for more than 150 years,

however only recently have improvements in computing speed and memory allowed realistically priced solutions of the equations to be possible and hence have seen CFD emerge as a viable method for calculation of fluid flow.

The *energy equation* is:

$$\rho\left(\frac{\partial h}{\partial t}+v_x\frac{\partial h}{\partial x}+v_y\frac{\partial h}{\partial y}+v_z\frac{\partial h}{\partial z}\right)=\frac{\partial}{\partial x}\left(\alpha\frac{\partial h}{\partial x}\right)+\frac{\partial}{\partial y}\left(\alpha\frac{\partial h}{\partial y}\right)+\frac{\partial}{\partial z}\left(\alpha\frac{\partial h}{\partial z}\right) \tag{2.31}$$

The *equation of continuity* is:

$$\frac{\partial\rho}{\partial t}+\frac{\partial}{\partial x}(v_x\rho)+\frac{\partial}{\partial y}(v_y\rho)+\frac{\partial}{\partial z}(v_z\rho)=0 \tag{2.32}$$

and the *Navier-Stokes equations* (under laminar flow conditions) are represented by:

Rate of change of momentum = Torque from body forces + Thermodynamic pressure + Viscous stress tensor (2.33)

The expression is conserved in three dimensions-

x-dimension: $$\rho\left(\frac{\partial v_x}{\partial t}+v_x\frac{\partial v_x}{\partial x}+v_y\frac{\partial v_x}{\partial y}+v_z\frac{\partial v_x}{\partial z}\right)=\rho g_x-\frac{\partial P}{\partial x}+\left(\frac{\partial\tau_{xx}}{\partial x}+\frac{\partial\tau_{yx}}{\partial y}+\frac{\partial\tau_{zx}}{\partial z}\right) \tag{2.34}$$

y-dimension: $$\rho\left(\frac{\partial v_y}{\partial t}+v_x\frac{\partial v_y}{\partial x}+v_y\frac{\partial v_y}{\partial y}+v_z\frac{\partial v_y}{\partial z}\right)=\rho g_y-\frac{\partial P}{\partial y}+\left(\frac{\partial\tau_{xy}}{\partial x}+\frac{\partial\tau_{yy}}{\partial y}+\frac{\partial\tau_{zy}}{\partial z}\right) \tag{2.35}$$

z-dimension: $$\rho\left(\frac{\partial v_z}{\partial t}+v_x\frac{\partial v_z}{\partial x}+v_y\frac{\partial v_z}{\partial y}+v_z\frac{\partial v_z}{\partial z}\right)=\rho g_z-\frac{\partial P}{\partial z}+\left(\frac{\partial\tau_{xz}}{\partial x}+\frac{\partial\tau_{yz}}{\partial y}+\frac{\partial\tau_{zz}}{\partial z}\right) \tag{2.36}$$

where v is the fluid velocity in the respective dimension (m s^{-1})
h is the fluid enthalpy (J kg^{-1})
α is the fluid thermal diffusivity (s^{-1})
ρ is the density of the fluid (kg m^{-3})
g is the gravity force in the respective dimension (N)
P is the fluid pressure (Pa)
μ is the fluid viscosity (Pa s)

and $$\tau_{ij} = \mu\left(\frac{\partial v_i}{\partial x_j} + \frac{\partial v_j}{\partial x_i}\right) + \delta_{ij}\left(\kappa - \tfrac{2}{3}\mu\right)\frac{\partial v_k}{\partial x_k} \qquad (2.37)$$

where τ is the viscous stress tensor (Pa)

δ_{ij} is the Kroneker delta (when $i = j$, $\delta_{ij} = 1$ and when $i \neq j$, $\delta_{ij} = 0$)

κ is the bulk viscosity of the fluid (Pa s)

Table 2.2 Solutions to CFD of natural convection within various enclosure types

Enclosure Type	**Author(s)**	**Solution Method**
1. Horizontal infinite cylinder enclosures	Hellums & Churchill (1962)[S,U]	FD
2. Horizontal rectangular enclosures	Drummond & Korpela (1987)[S,U]	FD
3. Inclined rectangular enclosures	Catton *et al.* (1974)[S]	FE
	Ozoe *et al.* (1974a[S] & 1974b[S])	FD
4. Triangular enclosures with horizontal bases	Akinsete & Coleman (1982)[S]	FD
	Poulikakos & Bejan (1983a)[S,U]	FD
	del Campo *et al.* (1988)[S]	FE
	Salmun (1995)[U]	FD
5. Annulus between two horizontal concentric cylinders	Kuehn & Goldstein (1976)[S]	FD
	Castrejon & Spalding (1988)[S,U]	FV
6. Annulus between two vertical concentric cylinders	Charmchi & Sparrow (1982)[S]	FD
7. Irregularly shaped enclosures	Coulter & Guceri (1987)[S]	FD with BFC
	Nithiarasu *et al.* (1998)[U]	FE

where [S] or [U] refer to whether the study investigated steady or unsteady state fluid flow

FD refers to finite difference methods

FE refers to finite element methods

FV refers to finite volume methods

BFC refers to body-fitted coordinates

Although many CFD studies that provide solutions to natural convection within enclosures have been conducted, Ostrach (1988) reviewed both the successful and unsuccessful numerical solutions in an extensive review of the literature. Ostrach stressed that simplification of the problem or the use of results from "similar" problems can be risky due to the high sensitivity of the convection to enclosure type and the imposed boundary conditions. The use of experiments to guide and validate numerical solutions to natural convection was highly recommended. A list of numerical solutions of natural convection (validated by experiment) is categorised by enclosure type in Table 2.2.

2.3.1.1 Existing Commercial CFD Solvers

The recent advancements in computing power have allowed several CFD computer packages to become commercially available. Some of these types of software make it unnecessary for the user to tackle the numerical analysis of the equations themselves. Usually the user need only define the necessary boundary conditions for their specific situation. However due to the generality of such packages, construction of complex geometric models, even by an experienced user, can take up to a few months (Nguyen & Pham, 1999). Often a certain amount of custom-written code must be added to the CFD package to enable problem specificity to be achieved.

One of the most commonly used CFD packages is PHOENICS, developed by CHAM Ltd., UK. PHOENICS is a general numerical solution code that employs the control volume method (Castrejon & Spalding, 1988), which also makes it able to model unsteady state heat conduction in solids (see section 2.2.5.4). Therefore modelling heat transfer in composite solids with natural convection in the air voids could be possible.

Nguyen & Pham (1999) modelled simultaneous forced convection and conduction in a meat carcass undergoing transient cooling using a CFD package called FLUENT. They found that the computations for a 20-hour carcass chilling run (in a simplified situation) took about one week on a 350MHz Pentium II computer. The long computation time was attributed to the irregular object shape and the required re-evaluation of the velocity fields as the thermal fields changed. Prediction of natural convection occurring in voids that are contained within otherwise solid objects undergoing transient cooling may be expected to have a similar computation time.

2.3.2 Analytical Solutions

The primary dimensionless parameter influencing the flow field is the Rayleigh number (*Ra*) - the product of the Prandtl number (*Pr*, the ratio of hydrodynamic and thermal boundary layer thicknesses) and the Grashof number (*Gr*, the ratio of buoyancy to viscous forces).

$$Pr = \frac{v}{\alpha} \tag{2.38}$$

where v is the kinematic viscosity ($m^2\ s^{-1}$)
α is the thermal diffusivity ($m^2\ s^{-1}$)

$$Gr = \frac{\xi g (T_{hot} - T_{cold}) x^3}{v^2} \tag{2.39}$$

where ξ is the volumetric expansion coefficient (K^{-1})
T_{hot} is the hot wall temperature (°C)
T_{cold} is the cold wall temperature (°C)
x is the characteristic dimension of the enclosure (m)

The characteristic dimension used in the calculation of Grashof number differs for each enclosure type, e.g. for a horizontal cylinder it is the diameter, for a vertical rectangle it is height. At low Rayleigh numbers, there are very few natural convection currents and heat transfer through the enclosure occurs mainly by conduction and/or radiation. As the Rayleigh number increases, more flow occurs and the amount of heat transfer from convection increases. For enclosures, the Nusselt number expresses the ratio of the mechanisms involved in heat transfer:

$$Nu = \frac{h.x}{k} \tag{2.40}$$

where h is the film heat transfer coefficient acting upon the enclosure walls ($W\ m^{-2}\ K^{-1}$)

The increase in heat transfer due to natural convection is often expressed as an *effective* or *apparent thermal conductivity* (k_{eff}) where:

$$k_{eff} = kNu \tag{2.41}$$

Solutions therefore define Nu as a function of all appropriate influencing variables.

Analytical solutions to natural convection are limited to enclosures of regular shape. Although the solutions are mathematically exact, Ostrach (1988) points out that the models used often are not truly physically representative of the flow field. He also states that analytical solutions have given "important insights", but experimental studies were usually critical in revealing the true nature of flow - "The experiments also indicated the folly of ad hoc physical assumptions for such complex problems". Hence analytical solutions to natural convection within irregular shapes were considered to be generally of low practical importance.

Horizontal Cylinders

Ostrach (1988) gives an overview of research on the analytical solution of natural convection within horizontal infinite cylinder enclosures. In the model, the cylinder enclosure has imposed boundary conditions of constant temperature with the temperature extrema on opposite ends of the cylinder on an angle designated ϕ (see Figure 2.2) and a cosine temperature distribution around the cylinder wall. There are no corner effects and heating from above or below can be achieved by changing the angle ϕ (Weinbaum, 1964).

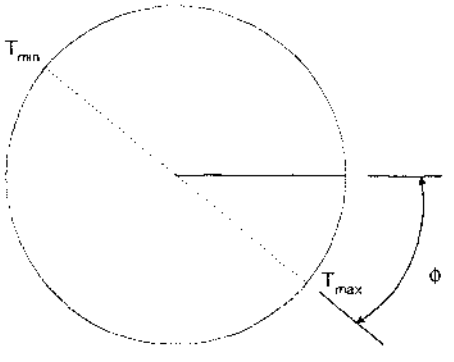

Figure 2.2 Boundary conditions on a horizontal infinite cylinder

In early research the enclosed fluid was treated as having a flowing boundary layer adjacent to the cylinder wall, surrounding a central core (Ostrach, 1950, and Weinbaum, 1964). The core was assumed to be isothermal with solid body rotation, regardless of the imposed thermal boundary conditions. However experimental work carried out by several researchers - Martini & Churchill (1960), Eckert & Carlson (1961), and Elder (1965) - instead showed that most of the flow occurred in the narrow ring adjacent to the cylinder

wall. The interior core region appeared to be stagnant but consisted of thermally stratified horizontal isotherms with temperature increasing vertically upward. Later, Van Dyke (1964) used the method of matched asymptotic expansions to solve the problem and correctly predicted that the flow characteristics were a circumferentially orientated boundary layer joining the horizontal cross-flow in the core. The upper and lower halves of the core flow in opposite directions.

Table 2.3 Analytical solutions of steady state natural convection within horizontal layers (adapted from Goldstein *et al.*, 1990)

Authors	Models	Pr range	Equation
Priestly (1959)	Mixing length	-	$Nu = K\,Ra^{1/3}$
Kraichnan (1962)	Mixing length	$Pr < 0.1$	$Nu = 0.17(Pr\,Ra)^{1/3}$
		$Pr > 0.1$	$Nu = 0.089\,Ra^{1/3}$
Howard (1963)	Optimum theory	-	$Nu_{max} = (Ra/248)^{1/3}$
Herring (1964)	Mean field equation	$Pr \rightarrow \infty$	$Nu = 0.115\,Ra^{1/3}$
Howard (1966)	Model of thermals	-	$Nu \propto Ra^{1/3}$
Roberts (1966)	Asymptotic expansion	-	$Nu \leq 0.278(Ra^2 \log Ra^2)^{1/5}$
Busse (1969)	Optimum theory	-	$Nu_{max} = (Ra/1035)^{1/2}$
Chan (1971)	Optimum theory	$Pr \rightarrow \infty$	$Nu_{max} = 0.152\,Ra^{1/3}$
Long (1976)	Buoyancy defect law	$Pr = 0.8$	$Nu = \dfrac{0.0524\,Ra^{1/3}}{\left[1 - 1.021(RaNu)^{-\frac{1}{12}}\right]^{4/3}}$
		$Pr = 6.8$	$Nu = \dfrac{0.04356\,Ra^{1/3}}{\left[1 - 1.402(RaNu)^{-\frac{1}{12}}\right]^{4/3}}$
Canuto & Goldman (1985)	Turbulence model	$Pr = 6.8$	$Nu = 0.044\,Ra^{1/3}$
		$Pr = 1000$	$Nu = 0.061\,Ra^{1/3}$
Arpaci (1986)	Thermal micro-scale	-	$Nu = \left[PrRa/(1+Pr)\right]^{1/3}$

Horizontal Layers

Edwards & Catton (1969) showed that for horizontal rectangular enclosures with height-to-width ratios less than 0.2 the lateral walls (whether insulated or conducting) have little influence on the natural convection within the enclosure. Such enclosures can be considered to have natural convection characteristics identical to that of an infinite horizontal layer of air. Natural convection within horizontal layers heated from below and with isothermal boundaries is often termed Rayleigh-Bénard convection, because the flow field and the heat transfer through the layer (given by the Nusselt number, *Nu*) are highly dependent upon the value of the Rayleigh number (*Ra*). Table 2.3 (first presented by Goldstein *et al.*, 1990) is a list of the notable analytical solutions to natural convection within horizontal layers, the models that were used and their range of applicability.

2.3.3 Empirical Solutions

The difficulty in accurately predicting the influence of the boundary layer upon the flow field means that experimental verification of numerical and analytical solutions are common-place in studies of natural convection. This large pool of data can be used to test new numerical and analytical solutions or directly used to develop empirical correlations to predict natural convection heat transfer through enclosures of the same shape. Empirical correlations for natural convection heat transfer are expressed using the same dimensionless parameters as for analytical solutions (usually *Ra* and *Nu*). Although published data can be beneficial to researchers those available are limited to mostly regular enclosure shapes (Iyican *et al.*, 1980). The user must also take careful note of the experimental methods used. In particular, the study should account for the effects of radiation heat transfer and unwanted heat transfer through the edges of the test apparatus (Goldstein *et al.*, 1990). Table 2.4 summarises empirical solutions to steady state natural convection, listed by enclosure type.

Table 2.4 Empirical solutions of steady state natural convection within various enclosure types

Enclosure Type	**Author(s)**
1. Horizontal finite cylinder enclosures	Martini & Churchill (1960)
2. Vertical finite cylinder enclosures	Garon & Goldstein (1973)
3. Horizontal infinite layers	Mull & Reiher (1930), Goldstein & Chu (1969), Hollands *et al.* (1975), Hollands (1984)
4. Inclined rectangular layers	Hollands & Konicek (1973)
5. Triangular enclosures with hypotenuse-down orientation	Flack (1980), Akinsete & Coleman (1982), Poulikakos & Bejan (1983b)
6. Annulus between two horizontal concentric cylinders	Kuehn & Goldstein (1976), Van de Sande & Hamer (1979), Boyd (1983)

2.4 Summary

Solution techniques for heat transfer by conduction in solids have been well developed by researchers. Numerical, analytical and empirical solutions have been shown to be specifically applicable to different types of chilling situations. Proper use of the correct method has been shown to give accurate solutions to heat transfer in regularly or irregularly shaped solids (including composite solids containing small and evenly dispersed air voids) that are undergoing chilling where the boundary and initial conditions may or may not be uniform and constant.

Analytical and empirical solutions to natural convection within regularly shaped air-filled enclosures have been well developed by researchers, although most studies have concentrated upon high Rayleigh number situations (where the size or temperature difference across the void is large). Many numerical solutions have been developed for regularly and irregularly shaped air-filled enclosures, but few have been adequately validated by reliable experimental data. Irregularly shaped enclosures and enclosures with low Rayleigh numbers have not been intensively studied.

3. PRELIMINARY CONSIDERATIONS

The main objective of this work was to develop an accurate model to predict chilling rates of meat cartons for export by the New Zealand Meat Industry. Predicting the heat transfer properties of composite and packaged foods with significant air voids and without ventilation encompasses a vast number of diversified food types, their different packaging systems and their different possible arrangements within the package.

The New Zealand Meat Industry exports two main types of meat packages: bulk pack and primal cut packages - both usually contain approximately 27kg of meat. The bulk pack type is usually a fibreboard carton, inner-lined with a polyethylene bag and filled with small off-cuts of meat. Due to the small size of the meat cuts, the air voids are small and evenly distributed through the package apart from the rectangular headspace void above the meat. This void may or may not be partially filled by excess polyethylene bag as it is folded over the top of the meat. The primal cut meat carton can be of solid fibreboard or corrugated fibreboard but the carton is instead filled with much larger, individually vacuum-wrapped, whole muscle, boneless meat cuts. Bulk pack meat is generally of less economic value than primal cut meat and is more often frozen whereas primal cuts are generally only chilled. A numerical model for predicting freezing of bulk pack meat cartons with natural convection in the headspace has been developed by Wee & Pham (1990). The current study will concentrate upon prime cut meat cartons undergoing chilling, a separate problem. There were no other models found in the international literature that were designed to predict heat transfer through food packages that contained large, irregularly shaped air voids.

The typical prime cut carton is 520mm long, 360mm wide and 180mm high. The four main types of meat cuts placed into primal cut packages (striploins, tenderloins, cube rolls, and rumps) are packed into the carton by hand to give minimum wasted carton volume. Hence the position, size and shape of the cuts is different for every carton.

Striploins, tenderloins, cube rolls, and rumps are approximately elliptical in shape and are usually arranged in a single layer across or along the length of the carton, which creates voids across or along the top of the carton (Figure 3.1). The extent of natural convection and radiation within an air-filled enclosure is dependent on the size and shape of the enclosure, the temperature driving force across the enclosure walls, the physical and thermal properties of the air and the emissivity of the enclosure walls. The physical and thermal properties of air and the emissivity of the enclosure walls are expected to be

approximately constant over the small temperature range encountered when chilling meat cartons. Hence the size and shape of, and temperature driving force across the voids are the most important variables to be considered.

a) Striploins

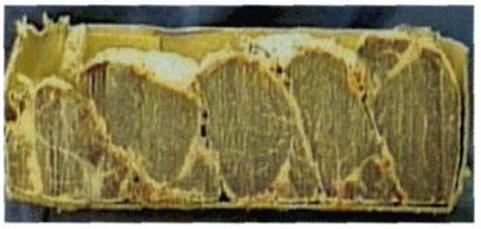

b) Tenderloins

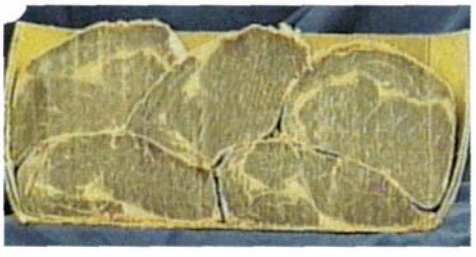

c) Cube rolls

d) Rumps

Figure 3.1 Photographs showing cross sections of four types of boneless primal cut packages (note: these packages have been frozen to allow ban sawing to be carried out)

Due to the infinite number of different packaging configurations that could occur in the real situation it was considered necessary to develop a simplified physical model. This simplified physical model represents the typical real situation, but allows a mathematical model to be developed.

The largest voids occur where the sculpted muscle shapes of the meat cuts do not fit the rectangular shape of the carton and primarily across the top of the carton. These *surface voids* (voids contacting the inner surface of the carton) will also have the greatest initial temperature driving force across them, because one or more of the enclosure walls is in contact with the cooling medium. *Surface voids* are expected to maximise natural convection and radiation effects, and hence the simplified model system considers them specifically.

Commercial chilling of primal cut meat cartons is carried out in an air blast cooler or plate cooler. In a blast cooling operation the cartons are usually arranged in layers of one carton thickness and air is blown across the top and bottom surfaces of the carton. Although the carton sides make up 46% of the external heat transfer area, the lengths of the second and third dimensions (Figure 3.2) make the internal resistance to heat transfer (x/k) high in these directions. The equivalent heat transfer dimensionality (E) calculated by the method of Lin (1994) that includes the effects of cooling from all three dimensions is typically 1.18 (i.e. edge heat transfer decreases the cooling time by only about 18% assuming a Biot number of approximately 3.0, similar rates of heat transfer from all surfaces, and that the carton is solidly packed with meat). However the single layer blast cooling arrangement also limits the circulation of air around the sides of the cartons, making the heat transfer coefficient on the sides of the carton low compared to that experienced on the top and bottom surfaces, and thus further reducing the E value.

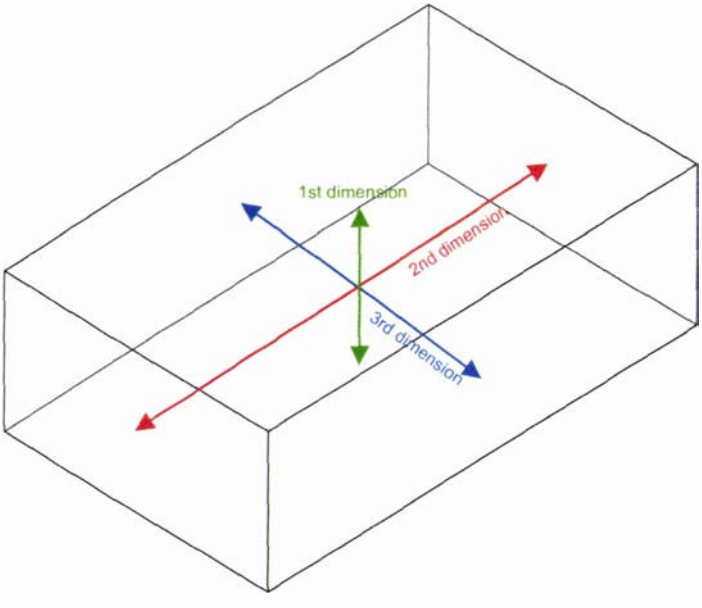

Figure 3.2 Diagram of the thermal resistances within a full meat carton undergoing three dimensional cooling

The situation is similar for cartons that are plate cooled. The cooler plates only contact the top and bottom carton surfaces. Hence cooling from the sides can only occur through the cold air that may be present within gaps between cartons. This mode of heat removal is also at a lower rate compared to that experienced on the top and bottom surfaces, and the E value calculated above will be much closer to unity. As heat transfer through the sides of the carton makes up only a small proportion of the total heat transfer it enables the system to be treated realistically by assuming that cooling only occurs through the top

and bottom surfaces. Given that the pieces are laid along a carton, a two-dimensional model with neither side nor end heat transfer effects was considered valid (Figure 3.3a).

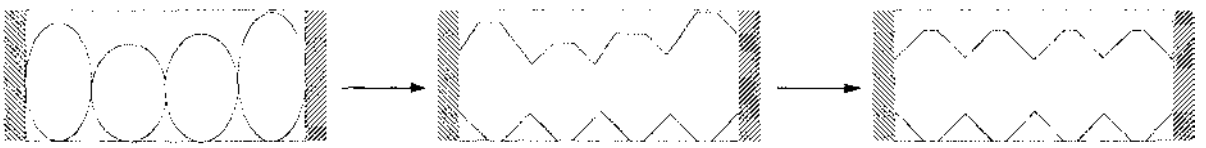

a) Reality **b) Ideal Model** **c) Simplified Model**

Figure 3.3 Diagram of simplified physical model

The ideal physical model shown in Figure 3.3b simplifies the real situation from rounded and irregularly shaped solid meat cuts of varying size surrounded by irregular air void shapes, to a solid block with combinations of different sized rectangular and right-angled isosceles triangular shaped air voids cut into it. Characterising the two-dimensional shape of the ideal model requires only the carton dimensions, the height of the rectangular voids and the height and position of each of the triangular voids. Even the model in Figure 3.3b may be unduly complex for analysis. Hence the simplified version of Figure 3.3c was adopted. This latter model was considered the most physically realistic that could be used, whilst being practical within the physical resources available. It is also acknowledged that the simplified physical model system in Figure 3.3c would better mimic commercial reality if any mathematical model developed could allow for the inclusion of irregularly shaped fat layers within the solid block, but the extra complexity was beyond what could be tackled in a practical sense.

In chapter 2, numerical, analytical and empirical research on natural convection within enclosures was reviewed. The review showed that natural convection-induced fluid movement was highly dependent upon the shape of the enclosure and its boundary conditions. As a consequence it was decided to initially investigate the effects of rectangular and triangular void shapes separately. Extensive research has already been carried out to investigate heat transfer within horizontal rectangular enclosures [Mull & Reiher (1930), Goldstein & Chu (1969), Hollands *et al.* (1975), Ahlers (1980), Hollands (1984), and Drummond & Korpela (1987)]. However very little research has looked at triangular enclosures and the majority of these studies have focused on attic spaces (a hypotenuse-down orientation) and usually where the enclosure is cooled from above [Poulikakos & Bejan (1983 a & b), del Campo *et al.* (1988)] with the exception of Flack (1980) who studied hypotenuse-down orientation but included cooling from below. Flack's study showed that little natural convection occurred within hypotenuse-down

triangular voids cooled from below, and that radiation made up more than 80% of the total heat transfer. Triangular voids cooled from above with a hypotenuse-up orientation (the reverse shape to that in found in the above mentioned studies) will also involve radiation heat transfer and are more likely to have a significant proportion of heat transfer attributable to natural convection.

Taking all these factors into account, the step by step objectives for this research were to:

1. Investigate the effect that voids of a typical size and shape have upon the chilling rate of primal cut meat cartons. This would be accomplished by collecting experimental data using the simplified physical model system (described above) cooled within a closely controlled measurement environment. This would extend the existing pool of measured data for coupled natural convection and radiation heat transfer through triangular enclosures with hypotenuse-up or hypotenuse-down orientations, and also combined triangular/headspace voids.

2. Use the experimental data to test existing empirical prediction methods for natural convection heat transfer through horizontal rectangular enclosures.

3. Develop and validate a numerical model that accurately predicts the heat transfer through the simplified physical model system.

4. Develop a simple method that accurately predicts conduction heat transfer rates in the simplified physical model developed above (to test the accuracy of the simple method, predictions will be compared to those from the numerical model and the experimental data).

5. The results of the research were expected to be a generally applicable numerical model that accurately predicts conduction heat transfer rates in packages of known size and configuration, and a simple model that can be quickly and easily applied by engineers to estimate temperature-time profiles within meat cartons with diversified packaging arrangements.

4. PRELIMINARY COLLECTION AND ANALYSIS OF DATA FOR PACKAGES CONTAINING TRIANGULAR VOIDS

4.1 Objectives

Leading on from the project objectives stated in Chapter 3, the objectives of the first stage of data collection and analysis were:

1) To develop accurate and reproducible data collection methods,

2) To investigate the extent to which natural convection and radiation heat transfer occurring typically sized voids affects the cooling rate of the cartoned product, and

3) To provide experimental data for preliminary selection of a suitable numerical model of the heat transfer.

In order to investigate triangular voids separately from rectangular voids the limiting case of the simplified physical model developed in Chapter 3 (shown in Figure 4.1, where the headspace above the product did not exist) was investigated first.

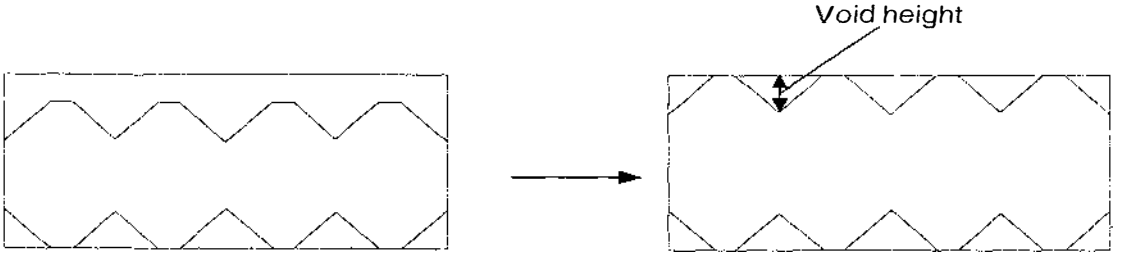

a) With Rectangular Headspace Void b) Without Rectangular Headspace Void

Figure 4.1 Diagram of simplified physical model with and without a headspace void

4.2 Experimental Methodology

A range of chilling experiments was planned in which temperatures were measured whilst simultaneously cooling a block containing air voids and an identical test block with insulating foam in the voids (to prevent radiation heat transfer and effectively immobilise the air in the voids).

Tylose MH1000 was chosen as the test material because of its homogeneous composition, easily moulded nature and well-known thermal properties. It was prepared using the hot water method (Riedel, 1960) which sets slower than when made with cold water and allows more time for thorough mixing and careful arrangement into the sample holders. A standard calculation technique used by MIRINZ Food Technology and Research Ltd. accounted for the loss of hot water due to evaporation. Using duplicate measurements, the mean moisture content of the Tylose gel was found to be 76.4%.

By using the vertical axis of symmetry of the simplified model (Figure 4.1b) the length of the test blocks could be halved (from 0.52m to 0.26m). Two identical rectangular sample holders with 40mm thick expanded polystyrene walls were constructed (Figures 4.2 and 4.3).

Figure 4.2 Photograph of test sample holder

Each holder contained two identically shaped 0.26m x 0.36m x 0.18m Tylose blocks, placed side-by-side to be cooled simultaneously. The sides of the Tylose blocks were held in shape by the polystyrene walls of the sample holder. Various sized right angled

isosceles triangular voids were produced by cutting out or adding pieces of Tylose from the originally solid blocks so that the top and bottom surfaces of each block had two side located 'half' and one centrally located 'full' right angled isosceles triangular voids. Within each sample holder the voids of one of the blocks were filled with polystyrene. To hold the shape of the air voids on the bottom surface of the second block, a 360mm long, 1mm thick L-shaped section of solid acrylic plastic was placed under the Tylose block and pointed upwards to create an attic-shaped space. Several different plastic sections were constructed to enable voids of different heights to be supported.

Sixteen copper-constantan T-type thermocouple pairs were calibrated at 0°C in an ice/water reference. The temperatures measured using these thermocouples were inferred by adjusting each thermoelectric voltage reading with respect to the voltage offset measured at 0°C. The adjusted readings would be expected to be more inaccurate as they move away from 0°C, but since temperature data was mostly only used after a ln$Y$ value of -0.5 had been reached, the maximum expected temperature reading that was used was about +18°C. This was not expected to significantly affect the accuracy of the temperature measurements. Furthermore, since the thermoelectric voltage per °C increases with temperature, the voltage offset measured at 0°C becomes less critical at higher temperatures. The thermocouples were positioned within each block as shown in Figure 4.3. Four were positioned at the centre, four on the surfaces, and eight midway between centre and surface. The centre and midway thermocouples were attached along PVC plastic rods (2mm diameter, 180mm long). Whilst taking care to ensure they stood vertical, the rods were inserted into the top surface of the Tylose blocks (at appropriate positions) until the tip of the rod reached the bottom surface of the block. The manufacturer of the rods (Cadillac Plastics Pacific Group Pty. Ltd.) stated the thermal conductivity of PVC as ~0.2 $Wm^{-1}K^{-1}$. Comparison with the thermal conductivity of Tylose (~0.5 $Wm^{-1}K^{-1}$) suggested that there would be no more heat transfer out of the block along the PVC rods than if they weren't in the block but that the rods may have influenced the heat transfer in some unquantified manner is acknowledged. Each surface thermocouple was positioned as close to the surface as possible by hand.

Surface heat transfer coefficients were varied using different numbers of layers of approximately 2mm thick fibreboard (the same type used in 27kg meat cartons) outside the top and bottom surfaces of the test boxes.

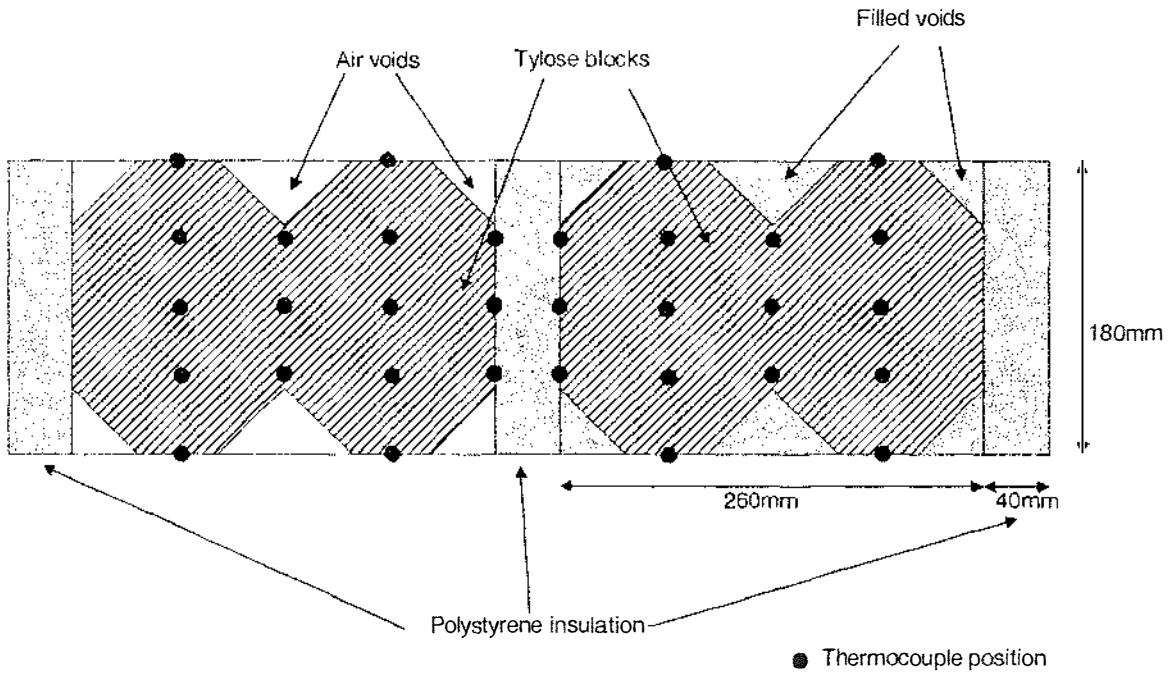

Figure 4.3 Diagram of test sample holder

A custom-built plate cooler consisting of two hollow aluminium plates contained within an insulated box was used. Alcohol at approximately 0°C was circulated through the plates from a Julabo FP-65 low temperature bath set to external temperature control with the external temperature sensor connected to the top plate of the cooler. Any part of the sensor that was not in contact with the cooler plate was insulated. Five previously calibrated T-type copper-constantan thermocouple pairs were placed in various positions on the plates.

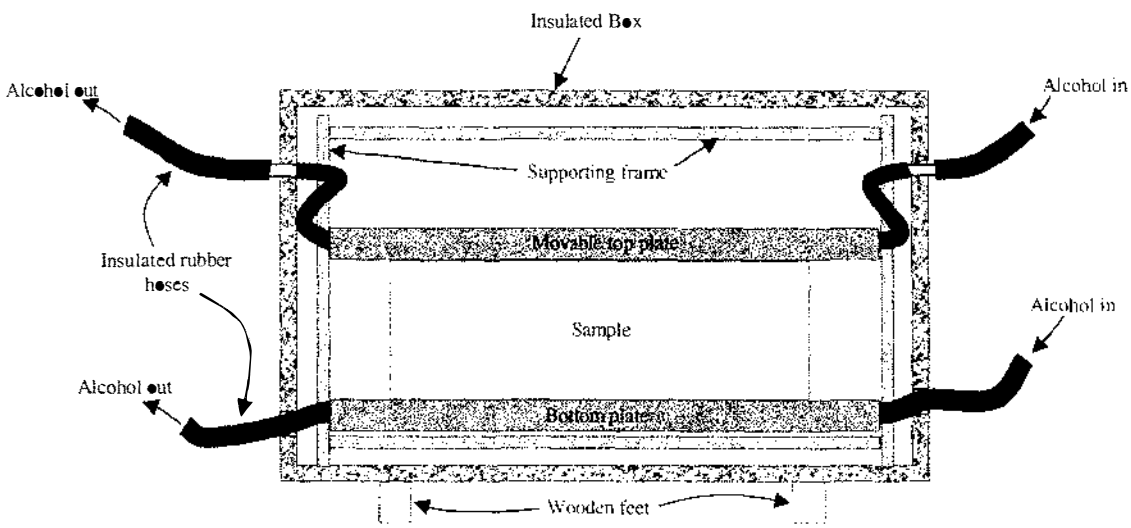

Figure 4.4 Diagram of plate cooler

All thermocouples were attached to a Hewlett-Packard HP3497A data logging system connected to an IBM-compatible personal computer running MS-DOS and a logging and analysis program named MIRLOG developed at MIRINZ Food Technology and Research Ltd.

Before each run, the controlled-temperature bath was operated until the plates of the cooler equilibrated to the desired working temperature. The sample holder and surrounding fibreboard sheets (previously equilibrated to a uniform temperature in a warm room set to 30°C) were insulated during transport to the plate cooler. The 32 thermocouple pairs from the two Tylose blocks were promptly connected to the data recording system by two 16-pin connectors. The sample holder was then placed between the plates of the cooler and the start time noted. The blocks were cooled until the slowest cooling thermocouple reading was below 2°C. This ensured that a minimum $\ln Y_c$ value (equation 4.1) of at least -2.5 had been reached. Below this value the uncertainty in temperature measurement of approximately ±0.2°C was significant compared to the remaining possible temperature change of less than 2°C.

$$Y_c = \frac{(T_c - T_a)}{(T_i - T_a)} \tag{4.1}$$

where Y_c is fractional unaccomplished temperature change at the centre of the sample
T_c centre temperature of the sample (°C)
T_a ambient (plate) temperature (°C)
T_i initial temperature of the sample (°C)

The effect of five different void sizes at two different surface heat transfer coefficients were investigated (Table 4.1). The experiments were started before construction of all samples was complete so the order in which the entire set of runs was performed could not be randomised. However randomisation of runs within the samples available at any time was carried out.

Table 4.1 Treatment table for preliminary data collection

Void height (mm)	Fibreboard sheets	Order
0	1	1
0	1	2
0	3	3
0	3	4
10	1	15
10	3	17
20	1	12
20	3	14
30	1	13
30	3	11
40	1	6
40	1	7
40	1	10
40	3	5
40	3	8
40	3	9
50	1	18
50	3	16

4.3 Evaluation of Input Data

4.3.1 Thermal Properties of Test Materials

The thermal properties of the materials used in the preliminary data collection and analysis are shown in Table 4.2. During the experimental trials, the temperature of the test materials did not fall outside the range given in the table (-0.63°C to +39.37°C), so all temperature dependent thermal property data were linearly interpolated within this temperature range and the volumetric specific heat capacity was assumed to be constant.

Amos *et al.* (2000) conducted baseline tests with water in their measurement of Tylose enthalpy and achieved an error of -0.1%, at worst. They also reported the thermal conductivity of Tylose from the measurements of Willix *et al.* (1998) who stated an accuracy of ±0.9% for the procedures used. Although uncertainty values were not available for the thermal properties of expanded polystyrene foam and still air, the values in Table 4.2 were expected to be within about ±10% of their true values.

Table 4.2 Thermal properties of test materials used in preliminary data collection

Material	H at -0.63°C	H at +39.37°C	k at -0.63°C	k at +39.37°C
Tylose [a]	0.000	152.4	0.459	0.494
Polystyrene [b]	0.000	0.960	0.030	0.036
Still Air [c]	0.000	0.052	0.024	0.027

where H is volumetric enthalpy (MJm^{-3})
[a] from Amos *et al.* (2000)
[b] In "Comparison of Materials" (1976)
[c] from Perry & Green (1984)

4.3.2 Sample Dimensions

Sample dimensions were measured before each run using vernier calipers. Three replicate measurements of the sample length, width and height were taken. Void position and size was determined by measurement of the void vertices in relation to the closest end of the sample (also using vernier calipers). Thermocouple positions were also measured in this manner. The readings were considered to accurately represent mean values to ± 1mm.

4.3.3 Cooling Medium Temperature

An investigation into individual thermocouples on the plates showed that at the start of the runs three of the thermocouples rose in temperature and then dropped again. These were the thermocouples that were in direct contact with the cooler plates as well as the cardboard sheets around the Tylose sample. The temperature rise measured by these thermocouples was due to sensible heat removal from the cardboard sheets, which did not result in a change in the actual cooling medium temperature. Hence these three thermocouples were eliminated from use in calculating the mean plate temperature and for each run the remaining two thermocouples were averaged to estimate the plate temperature. The estimated mean cooling medium temperature was considered to accurately represent the true mean to $\pm$ 0.2°C.

4.3.4 Surface Heat Transfer Coefficients

In spite of the expectation of top to bottom symmetry in runs without voids, upper and lower surface temperature profiles in early runs were different from each other - with the upper surface always cooling more slowly. It was suspected that this phenomenon was due to slumping of the Tylose block, causing the upper surface of the block to lose contact with the upper plate. Therefore the upper and lower surface heat transfer coefficients (HTC's) were estimated separately.

The Goodman integral profile method for a semi-infinite slab (Goodman, 1964) gives analytical solutions to an approximate heat-balance integral assuming that the temperature profile in the surface 'boundary layer' is represented by a cubic function. The method has been applied in work by Srinivasa Murthy *et al.* (1974) and Cleland & Earle (1976). In the current work it was used to estimate each surface HTC because sufficient surface temperature/time data could be collected over a time where the surface of interest was not affected by the cooling of the opposing surface or by edge effects. For the case with the third kind of boundary condition, the following approximation holds true:

$$\tfrac{1}{3}\left(\frac{h}{k}\right)^2 \alpha t = \left(2Y_s^2\right)^{-1} - \tfrac{1}{2} + \ln Y_s \qquad (4.2)$$

where Y_s is fractional unaccomplished temperature change at the surface of the sample

If the surface temperature profile of the product is measured then the surface HTC (h in equation 4.2) can be calculated from the slope of a Goodman plot: $[(2Y_s^2)^{-1} - ½ + \ln(Y_s)]$ vs. time.

In practice, the surface temperature profiles for the first 30 minutes were used to construct Goodman plots. Slopes were calculated by regression, with most plots yielding R^2 values of 0.999 and with worst cases of 0.996 (lower surface) and 0.992 (upper surface). The Y values at the geometric centre were calculated after 30 minutes using equation 4.1, and none were found to be below 0.998, indicating little or no change in the thermal centre temperature. However it is acknowledged that this method may be subject to inaccuracies from the assumption that the block is a homogeneous solid, when it actually contains filled voids or air voids that may affect the surface temperature profiles by lateral conduction. Further the block is assumed to undergo only one-dimensional heat transfer whereas in reality it is affected by second and third dimension edge effects to some extent. The use of short times (<30 minutes) minimised these errors.

Lower Surface HTC

Earlier runs had four lower surface thermocouples in place - two on the lower surface of the block with air voids and two on the lower surface of the block with filled voids. The thermocouples that cooled fastest were assumed to be the best placed and thus were used as the best estimates of temperature on the lower surface. The two fastest cooling thermocouples agreed with each other yet were within different blocks, which indicated likely consistency of placement.

Fewer surface temperature measurements were available in later runs because thermocouple fragility had resulted in some breakages that were not detected and fixed until several runs had taken place, and sometimes both thermocouples that had cooled fastest in earlier runs broke. As a result, for some of the later runs there were no reliable surface temperature measurements available to estimate HTC's. In total, five estimates of lower surface HTC were gathered for the runs with one fibreboard sheet and six estimates were gathered for the runs with three fibreboard sheets (Table 4.3).

The mean lower surface HTC's were (to 95% confidence) 39.4 ± 2.3 $Wm^{-2}K^{-1}$ for one fibreboard sheet and 14.8 ± 0.7 $Wm^{-2}K^{-1}$ for three fibreboard sheets.

Several paired t-tests showed with 95% confidence that the lower surface HTC did not differ significantly between runs throughout the investigation, did not differ significantly

between the two Tylose blocks within each sample holder, and did not display any trend with void size or contact area. This suggests good contact was achieved on the lower surface of the samples.

The value of the Biot number (*Bi*) could not be accurately determined because the Tylose blocks experienced asymmetrical cooling and because the effective thermal conductivity of the composite Tylose blocks was unknown. However, as an approximate indication of the ratio of internal to external heat transfer, a 90mm thick infinite slab of Tylose cooled from one surface only with a heat transfer coefficient of 39.4 $Wm^{-2}K^{-1}$ or 14.8 $Wm^{-2}K^{-1}$ would have experienced a *Bi* value of 7.5 or 2.8 respectively.

Upper Surface HTC

Due to the postulated slumping phenomenon the upper surface HTC's could have varied significantly within and between runs and could follow more subtle trend effects (e.g. HTC values may be lower for blocks containing air voids because there may be more chance of sagging within the voids along the bottom surface, which would cause the top surface of the Tylose block to slump away from the cooler plate). It was not possible to eliminate thermocouples from the HTC estimation procedure on the basis that relative cooling rate was a function of quality of placement because any slower cooling thermocouples may have been at a position where the sample had slumped away from the cooler plate more. Therefore separate upper surface HTC's were calculated for each run. Goodman plots of all upper surface thermocouples were prepared and the replicate estimates of upper surface HTC were averaged separate to give mean values within each run (shown in Table 4.3). The true upper surface HTC's may be higher than those estimated because it is likely the averaging procedure used some data from slightly ill-positioned thermocouples that did not give a good representation of the true surface temperature.

As previously mentioned, due to asymmetrical cooling and the unknown effective thermal conductivity of the composite Tylose blocks, the *Bi* value could not be accurately determined. However, an approximate indication of the ratio of internal to external heat transfer is given in parentheses next to each individual value of upper surface heat transfer coefficient in Table 4.3. The approximation assumed a 90mm thick infinite slab of Tylose cooled from one surface only using the appropriate heat transfer coefficient.

Table 4.3 Individual estimates of lower surface (LS) and upper surface (US) HTC

Order	Void height (mm)	Fibreboard sheets	Measured LS HTC ($Wm^{-2}K^{-1}$)	Mean LS HTC ($Wm^{-2}K^{-1}$) [*Bi* in parentheses]	Measured US HTC ($Wm^{-2}K^{-1}$) [*Bi* in parentheses]
1	0	1	42.8	39.4 [*7.5*]	36.2 [*6.9*]
2	0	1	41.2	39.4 [*7.5*]	30.5 [*5.8*]
6	40	1	no estimate	39.4 [*7.5*]	15.7 [*3.0*]
7	40	1	36.9	39.4 [*7.5*]	10.9 [*2.1*]
10	40	1	no estimate	39.4 [*7.5*]	9.7 [*1.9*]
12	20	1	39.8	39.4 [*7.5*]	no estimate
13	30	1	38.5	39.4 [*7.5*]	9.5 [*1.8*]
15	10	1	37.3	39.4 [*7.5*]	11.3 [*2.2*]
18	50	1	no estimate	39.4 [*7.5*]	no estimate
3	0	3	15.6	14.8 [*2.8*]	12.0 [*2.3*]
4	0	3	15.2	14.8 [*2.8*]	7.3 [*1.4*]
5	40	3	14.1	14.8 [*2.8*]	10.0 [*1.9*]
8	40	3	no estimate	14.8 [*2.8*]	7.7 [*1.5*]
9	40	3	no estimate	14.8 [*2.8*]	7.8 [*1.5*]
11	30	3	14.2	14.8 [*2.8*]	5.1 [*1.0*]
14	20	3	14.7	14.8 [*2.8*]	no estimate
16	50	3	no estimate	14.8 [*2.8*]	no estimate
17	10	3	no estimate	14.8 [*2.8*]	no estimate

4.3.5 Edge Effects

Heat loss or gain through the sides or ends of the Tylose blocks was minimised by the use of polystyrene insulation. Any heat transfer occurring through these pathways was referred to as an 'edge effect'. Heat transferring through the sides of the sample holder shown in Figure 4.3 is referred as the second dimension edge effect, and heat transferred through the ends of the same figure is the third dimension edge effect.

Both the second and third dimension edge effects would initially enhance cooling via two different heat transfer pathways shown in Figure 4.5. Pathway A is through the insulation to the cooler plates and pathway B is through the insulation to the surrounding air. As the block temperature dropped below the surrounding air temperature, the second pathway would reverse to slow the net cooling rate of the block.

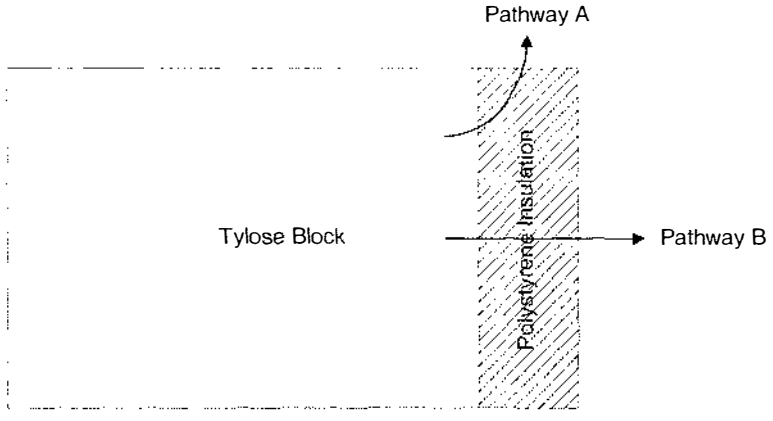

Figure 4.5 Diagram of the heat transfer pathways of edge effects

The boundary conditions occurring on the outer edges of the polystyrene were of the third kind but were not directly measured. The HTC's estimated for the lower surface of the Tylose blocks were assumed to also apply along the top and bottom surfaces of the polystyrene because they were likely to be in good contact with the fibreboard sheets and the cooler plates. However the side surface of the polystyrene was exposed to the air within the insulated box of the plate cooler. Cleland *et al.* (1987b) estimated the heat transfer coefficient of still air upon a vertical surface to be approximately 5 $Wm^{-2}K^{-1}$.

In the absence of measurements, a steady state heat balance was used to estimate the mean temperature of the air within the plate cooler. The air inside the plate cooler box was assumed to be perfectly mixed and at a uniform temperature. The plates of the cooler and the warm outside air were assumed to be the only pathways for heat transfer to and from the air inside the box. The heat transfer coefficient (h_1) between the internal air and the inside walls of the box, and the internal air and the cooler plates was assumed to be 5 W m^{-2} K^{-1}. The cooler plates were 670 x 440 x 22mm but the exposed plate area (A_1) was calculated to be only 0.64m^2 because the sample holder containing the Tylose blocks covered some of the plate surface. The cooler plates were at approximately -1°C. The external air conditions outside the box were assumed to be represented by an HTC of 10 W m^{-2} K^{-1} and a temperature of 25°C (typical local summer conditions). The box was constructed of aluminium with glass wool insulation and the mean inner and outer dimensions of the box were measured as 950 x 550 x 668mm, giving a heat transfer area (A_2) of 3.05m^2. The thickness of the glass wool insulation was 50mm (measured using vernier calipers) and the thermal conductivity was estimated to be 0.037 W m^{-1} K^{-1} from Perry & Green (1984). This gave an overall heat transfer coefficient (h_2) between the internal air and the external air of 0.61 W m^{-2} K^{-1}. Under steady state conditions and with

no heat flowing from the sample between the plates, the heat flowing in from the outside air (ϕ_{in}) must be equal to the heat flowing out through the cooler plates (ϕ_{out}):

$$\phi_{in} = \phi_{out} \tag{4.3}$$

so,

$$h_1 A_1 (T_{\text{inside air}} - T_{\text{cooler plates}}) = h_2 A_2 (T_{\text{outside air}} - T_{\text{inside air}}) \tag{4.4}$$

and,

$$T_{\text{inside air}} = \frac{h_2 A_2 T_{\text{outside air}} + h_1 A_1 T_{\text{cooler plates}}}{h_2 A_2 + h_1 A_1} = 8.5°\text{C} \tag{4.5}$$

4.4 Measured Time-Temperature Data in the Test Samples

Due to thermocouple breakages, measured temperature data were not obtained from all positions along the centre axis. Therefore the term 'centre' refers to the slowest cooling of any of the four thermocouple positions along the centre axis.

Figure 4.6 shows typical centre temperature-time profiles from three different blocks (one with no voids, one with 50mm high air voids and one with 50mm high filled voids) under similar cooling conditions. The profiles show the block with no voids cooling fastest even though it has more mass (and therefore more thermal mass) than blocks with voids. The results also show the block with air voids cooling faster than the block with filled voids, presumably due to natural convection and radiation effects (and in spite of the foam thermal conductivity being higher than that of still air).

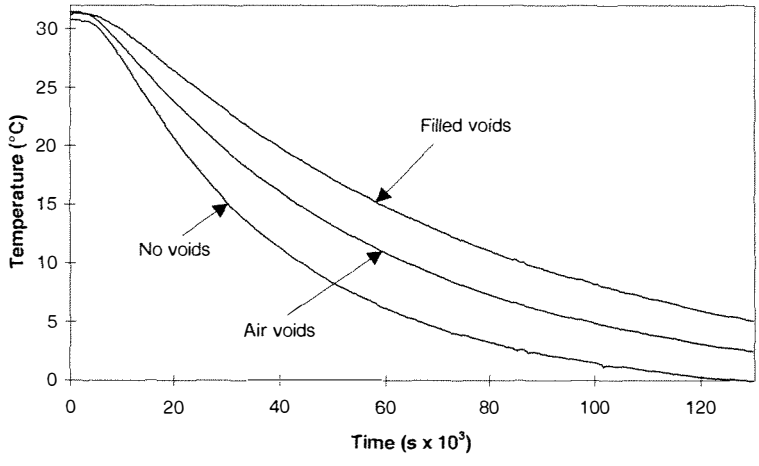

Figure 4.6 Plot of centre temperature vs. time for Tylose blocks containing no voids (Run 2), and blocks containing 50mm high air voids and 50mm high filled voids (Run 18)

Figure 4.7 shows a plot of log fractional unaccomplished temperature change ($\ln Y_c$) vs. time from the same data as Figure 4.6. The slope of the straight-line section of a $\ln Y_c$ vs. time plot is a commonly used measure of cooling rate. Between $\ln Y_c$ of -0.5 and -1.5 the $\ln Y_c$ vs. time plots for all runs yielded essentially straight lines so the time taken for this $\ln Y_c$ reduction was used as a measure of cooling rate. These plots are often subject to small 'peaks' and/or 'valleys' along the otherwise smooth cooling line. The imperfections were most likely due to small variations in the actual ambient temperature (when a mean value was used to calculate Y_c). They may have also been due to electrical interference caused by power surges, or the use of certain electrical appliances, in the vicinity of the thermocouples and the data logging equipment. These small 'peaks' and 'valleys' were ignored in the analysis of similar measured data throughout this thesis. The measured times for one $\ln Y_c$ reduction ($\ln Y_c$ = -0.5 to $\ln Y_c$ = -1.5) from all eighteen runs are summarised in Table 4.4.

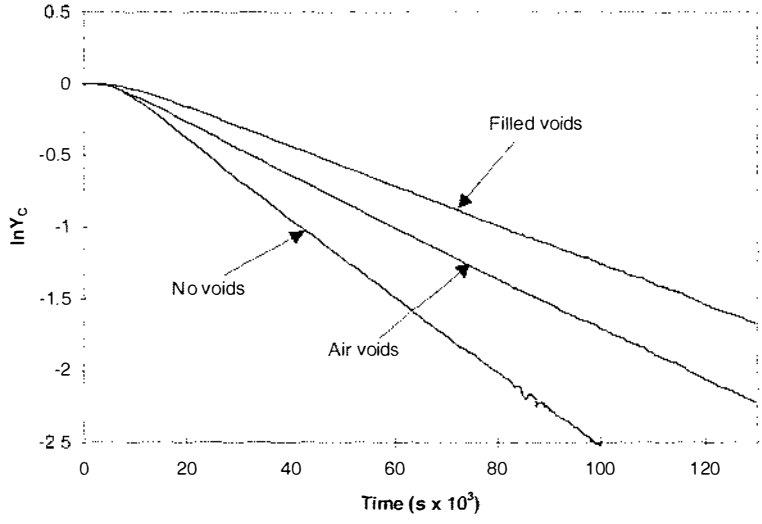

Figure 4.7 Plot of log unaccomplished temperature change ($\ln Y_c$) vs. time for same data in Figure 4.6

Three replicate measurements were carried out for four different run conditions (samples containing either 40mm high filled voids or 40mm high air voids, and with either one or three layers of fibreboard sheeting). These data were used to estimate the experimental uncertainty. There was a 95% certainty that each individual measurement lay within ± 8% of the mean value.

Even within the same heat transfer situation, cooling times that were measured using thermocouples at different positions along the centre axis may be different from each other if the second dimension edge effect is important. The greatest effect would be on

the slowest cooling block (with 50mm high filled voids and HTC = 14.8 $Wm^{-2}K^{-1}$) and for thermocouples nearest the block ends. The maximum observed percentage difference for one $\ln Y_c$ reduction between thermocouples along the centre axis of this sample was 2%, and this was within total experimental uncertainty.

Table 4.4 shows that all packages containing air voids cooled faster than those with filled voids of the same size. However it was only at a void size of 40mm or greater that the percentage difference between air and filled void packages was greater than the experimental uncertainty of 13%. It is probable that these differences arose from a combination of natural convection and radiation effects occurring within the void.

Table 4.4 Measured times for one $\ln Y_c$ reduction of blocks with filled voids or air voids (seconds x 10^3)

No. of Fibreboard Sheets	Void height (mm)	Filled voids	Air voids	% Difference
1	0	37[a]	37[a]	-0
	10	45	43	-4
	20	49	46	-6
	30	53	51	-4
	40	58, 61, 60	51, 53, 49	-15
	50	74	57	-23
3	0	54[a]	51[a]	-6
	10	50	45	-10
	20	65	63	-3
	30	73	68	-7
	40	74, 74, 74	61, 64, 63	-15
	50	85	62	-15

[a] solid block (no void space)

Although the collected data followed trends that were consistent with fundamental heat transfer theories and the results suggested that natural convection and radiation effects were likely to be significant in the cooling of packages with significant air voids, the collected data could not be used as the basis of a model because it did not consider separate effects of half-size and full-size triangular voids nor the effects of voids cooled

from above and below. The results were also affected by asymmetric cooling (i.e. different upper and lower surface HTC's), and subject to some patchiness of data due to the high frequency of thermocouple breakages. However, the data were considered suitable for the development of a preliminary numerical model. The finite element method was chosen as the prediction method because of the ease with which it can describe multi-dimensional shapes and handle the asymmetric heat transfer coefficients present in the measured data.

4.5 Development and Testing of a Finite Element Model

The software used to develop the model was called FINEL. It was originally developed by Pham at MIRINZ Food Technology and Research Ltd. in 1989. It is a FORTRAN encoded program that uses the finite element method (with triangular elements) to solve two-dimensional heat conduction problems. The grid geometry must be fully described by the user in the form of coordinates for nodes and element positions. FINEL allows temperature dependent thermal properties to be modelled with up to 5 different constituent materials and 5 boundaries (of first, second or third kind) with a time variable environment at each boundary. The program was compiled and run on a UNIX operating system.

4.5.1 The Preliminary FINEL Model - No edge effect included

A two-dimensional grid of the smallest possible representative problem space was constructed in FINEL (Figure 4.8). The grid had a higher resolution at material boundaries where there was a significant difference between the thermal properties of the two materials (e.g. boundaries between the Tylose and the voids) and care was taken to ensure that adjacent elements did not differ significantly in size. To ensure that the grid remained below the upper limit on the number of nodes and the number of elements in FINEL, a vertical axis of symmetry was used (due to asymmetrical surface heat transfer coefficients a horizontal axis of symmetry could not be used). The preliminary model did not account for edge effects (i.e. the left and right sides of the grid were assumed to be perfectly insulated).

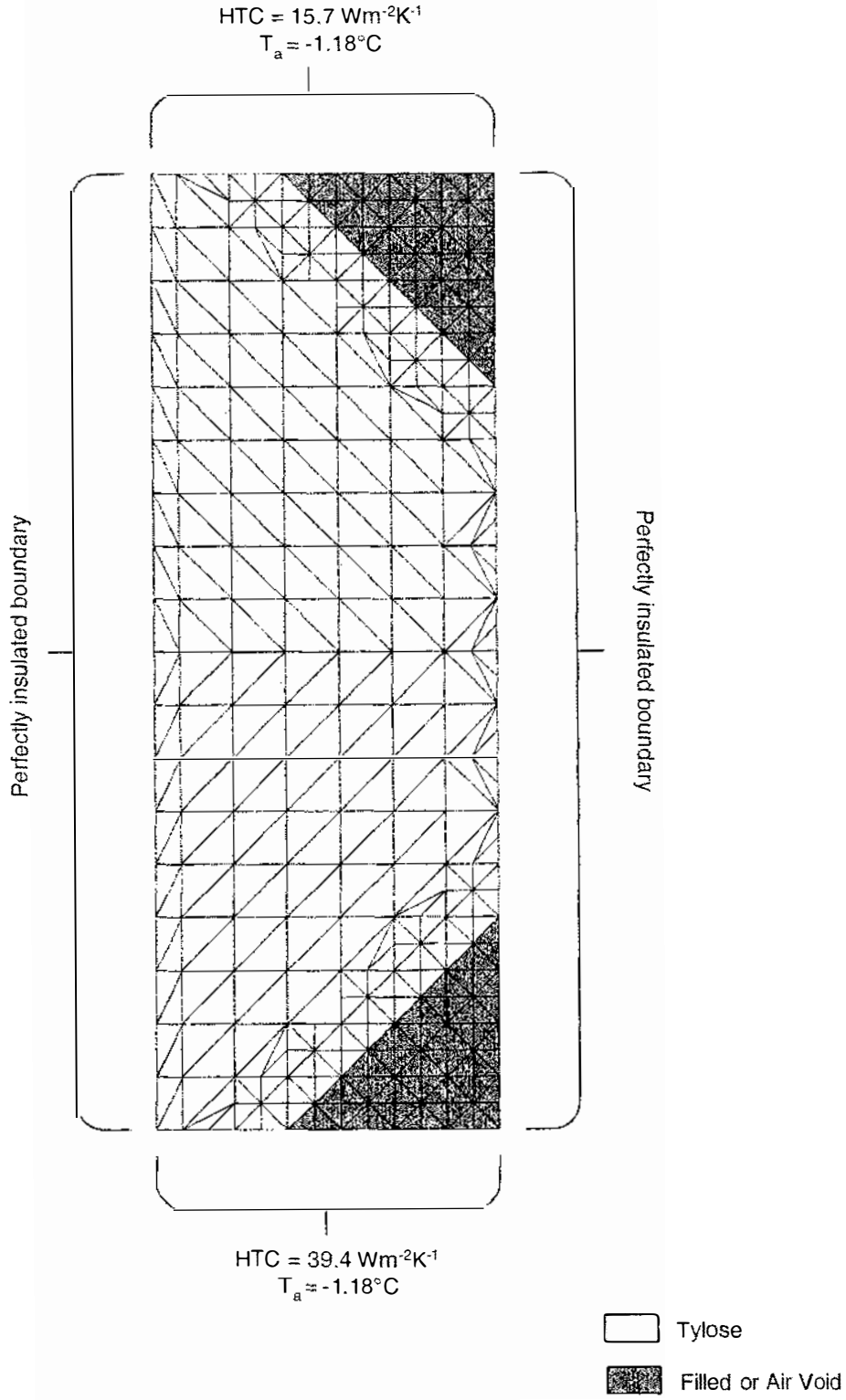

Figure 4.8 FINEL grid with no edge effect (data taken from Run 6)

4.5.2 Testing the Preliminary FINEL Grid

To test the grid a simulation was run with all elements containing Tylose-like material (with constant thermal properties) initially at 30°C. Third kind boundary conditions were imposed on the top and bottom surfaces of 20 $Wm^{-2}K^{-1}$ (midway between the lower surface HTC's estimated from the measured data) at 0°C, and the left and right sides of the block were assumed to be perfectly insulated. Temperatures at eight positions along the centre axis of the FINEL grid were compared to temperatures predicted by two other methods (the analytical solution for an infinite slab and a one-dimensional grid solved by a different heat conduction finite element program - FEM by Cleland, 1985). Comparisons were carried out at two times - 36000 and 75600 seconds. Table 4.5 summarises the results.

Table 4.5 Comparison of prediction methods - centre temperatures (°C)

Prediction Method	36000 sec.	75600 sec.
FINEL (average of eight nodes)	15.87	6.32
FINEL (left edge where n=10)	15.83	6.30
FINEL (right edge where n=16)	15.92	6.34
Analytical solution	15.87	6.32
1-D 'FEM' (n=10)	15.89	6.32
1-D 'FEM' (n=16)	15.88	6.32

where n = number of nodes between centre and surface axes.

The results show that the FINEL grid predicted the average centre temperature well. However there was a stable temperature oscillation along the centre axis, which should be an isothermal line. The difference between the centre temperatures on the left and right edge of the FINEL grid (in Table 4.5) was not due to a difference in the number of nodes from centre to surface - otherwise the right edge, with more nodes (n=16 c.f. n=10), would have given closer agreement to the other solution methods.

The small temperature oscillations that were apparent in the results from the two finite element programs FINEL and FEM were assumed to be a consequence of the numerical approximations. The oscillations were accepted because they were small compared to the accuracy of measured temperatures (±0.05°C c.f. ±0.2°C).

4.5.3 Comparison of the preliminary model with data from blocks containing no voids

Data files for use with the FINEL grid were developed using the input data estimated in section 4.3. Four simulations were run for comparison with the measured data from blocks containing no voids. Heat balances of all simulations were found to be satisfactory (less than 0.1% discrepancy) and transient temperature data from the same positions as in the experimental blocks were collected. Care was taken to ensure no abnormal nodal temperature predictions resulted from the stable oscillations (e.g. no nodes within the Tylose block were below the cooling medium temperature, along a vertical axis node temperatures decreased monotonically toward the surface, etc.).

Typical plots of measured and predicted data for blocks with no voids are shown in Figures 4.9 - 4.11. Agreement between the measured and predicted cooling rate of the upper surface (US) was good, but the cooling rate of the lower surface (LS) and centre (C) was underestimated. It was postulated that this disagreement might be at least in part attributable to the second and third dimension edge effects that occur in the measured data, but were not accounted for in the predicted data.

4.5.4 The Second FINEL Model - Edge effect included

Although the third dimension edge effect could not be included in FINEL because it was only a two-dimensional finite element scheme, the second dimension edge effect was added to the improved second model. To include the second dimension edge effect, the FINEL grid in Figure 4.8 was adjusted to include 40mm of polystyrene attached to the right hand side of the Tylose and a boundary condition beyond it. The new grid is shown in Figure 4.12. The FINEL source code was adjusted to increase the upper limit on the number of nodes and the number of elements to allow the grid for the second model to run. The same system input data as the preliminary FINEL model was used but with data describing the second dimension edge effect included.

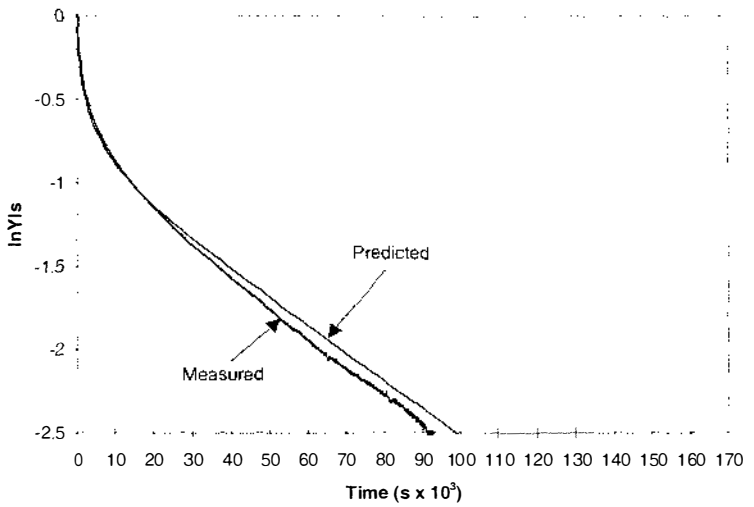

Figure 4.9 Plot of measured and predicted $\ln Y_{LS}$ vs. time (run 4)

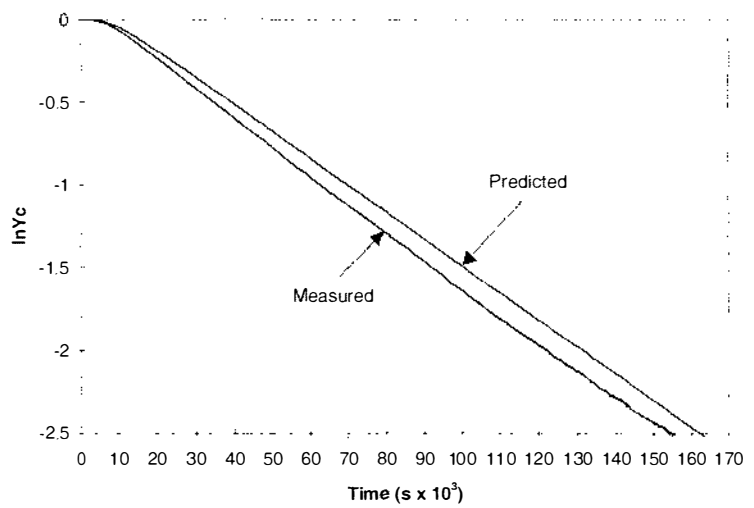

Figure 4.10 Plot of measured and predicted $\ln Y_{C}$ vs. time (run 4)

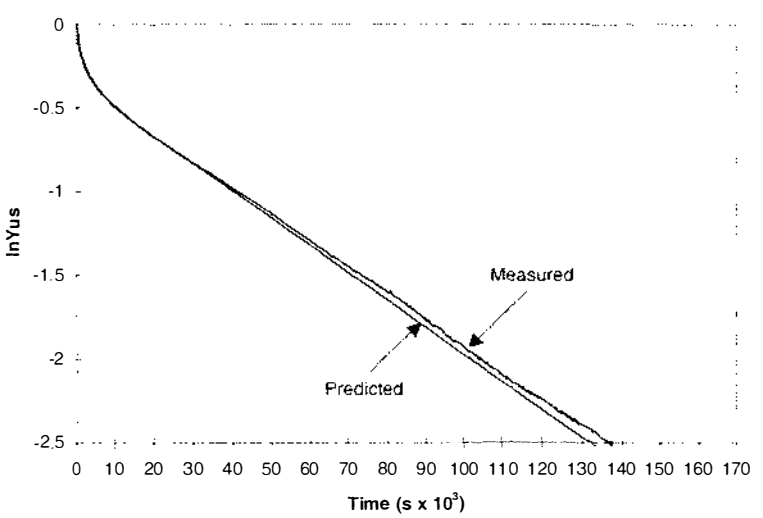

Figure 4.11 Plot of measured and predicted $\ln Y_{US}$ vs. time (run 4)

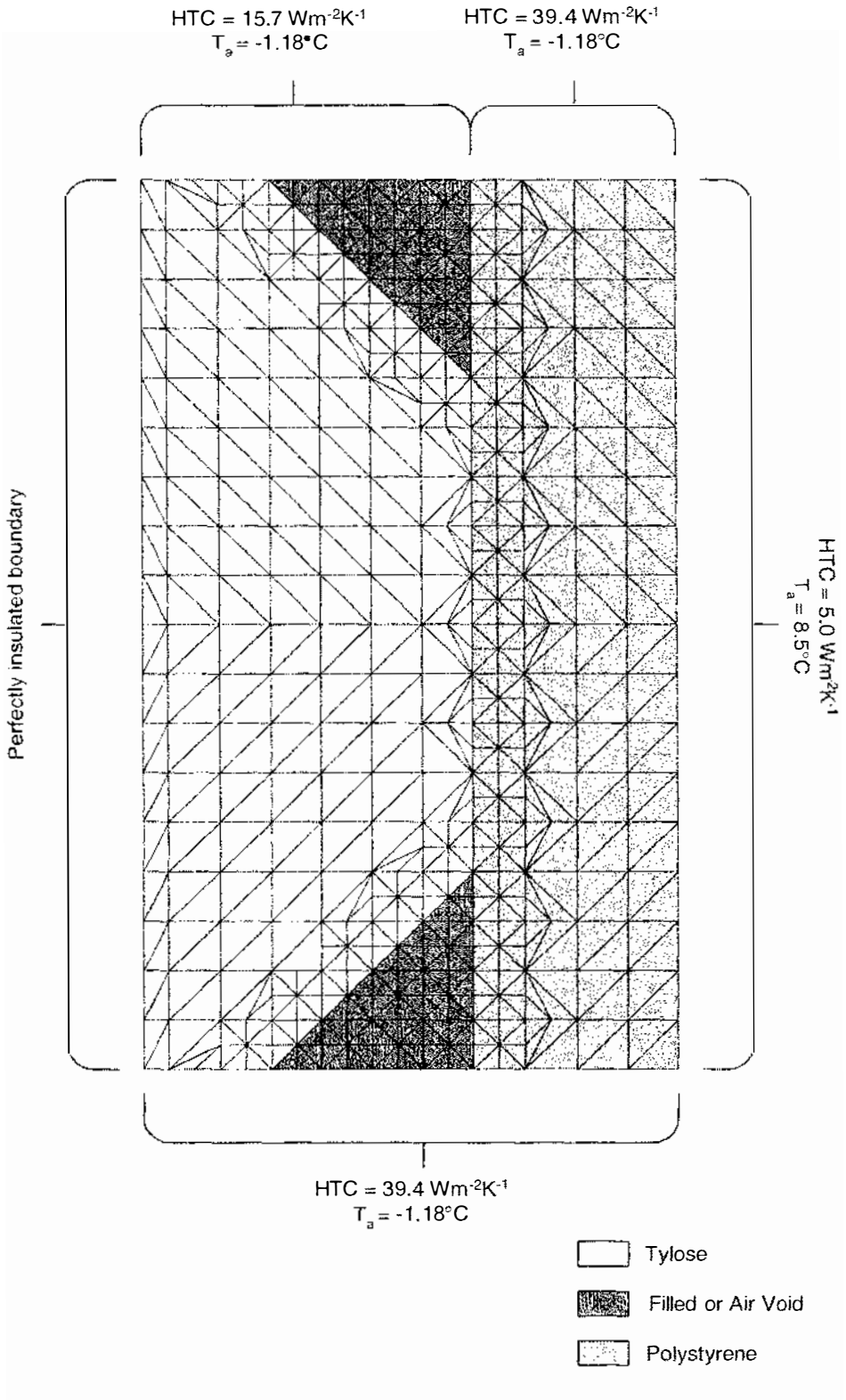

Figure 4.12 FINEL grid with edge effect included (data taken from Run 6)

The HTC estimate from Cleland *et al.* (1987) and the estimated mean air temperature from the heat balance in section 4.3.5 were used. A sensitivity analysis on the heat transfer coefficient used on the far right side beyond the insulation was carried out using

duplicate FINEL simulations. The first simulations used the side boundary condition of 5 $Wm^{-2}K^{-1}$ at 10°C and the second simulations used 7 $Wm^{-2}K^{-1}$ at 10°C (a 40% change in HTC). There was no perceivable difference between the two sets of predictions for Tylose temperatures.

4.5.5 Testing the Second FINEL Grid

Comparison of the model predictions with two other reliable prediction methods of one-dimensional heat transfer was carried out in the same way as in section 4.5.2. The results are given in Table 4.6. The temperature oscillation along isothermal lines was again present, but was tolerated.

Table 4.6 Comparison of prediction methods - centre temperatures (°C)

Prediction Method	36000 sec.	75600 sec.
FINEL (average of eight nodes)	15.86	6.31
FINEL (left edge where n=10)	15.70	6.25
FINEL (right edge where n=16)	15.92	6.34
Analytical solution	15.87	6.32
1-D 'FEM' (n=10)	15.89	6.32
1-D 'FEM' (n=16)	15.88	6.32

4.5.6 Comparison of second model with data from blocks containing no voids

Data files for use with the second FINEL grid were developed using the input data estimated in section 4.3. Four simulations were run for comparison with measured data from blocks containing no voids. Heat balances of all simulations were again found to be satisfactory (less than 0.1% discrepancy) and transient temperature data was collected in the same positions as in the experimental blocks. Again, care was taken to ensure no abnormal nodal temperature predictions had occurred through oscillatory behaviour.

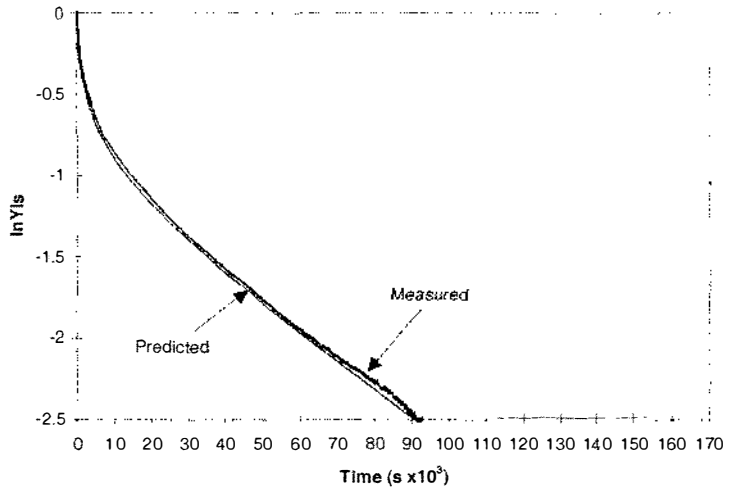

Figure 4.13 Plot of measured and predicted $\ln Y_{LS}$ vs. time (run 4)

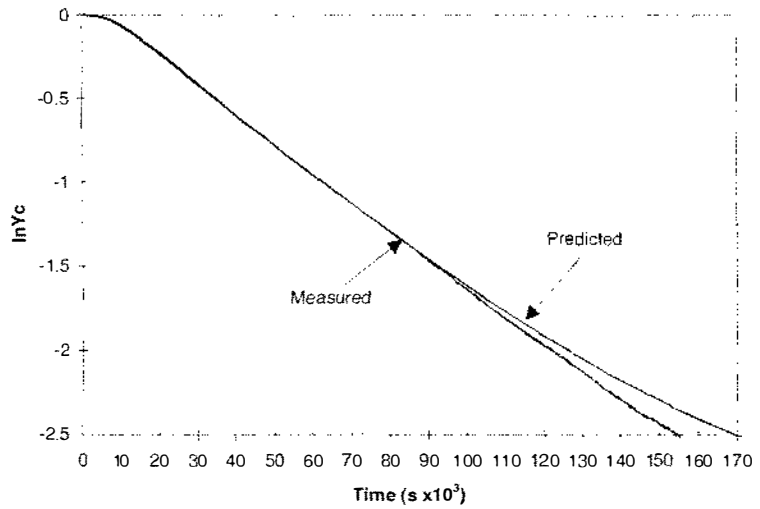

Figure 4.14 Plot of measured and predicted $\ln Y_{C}$ vs. time (run 4)

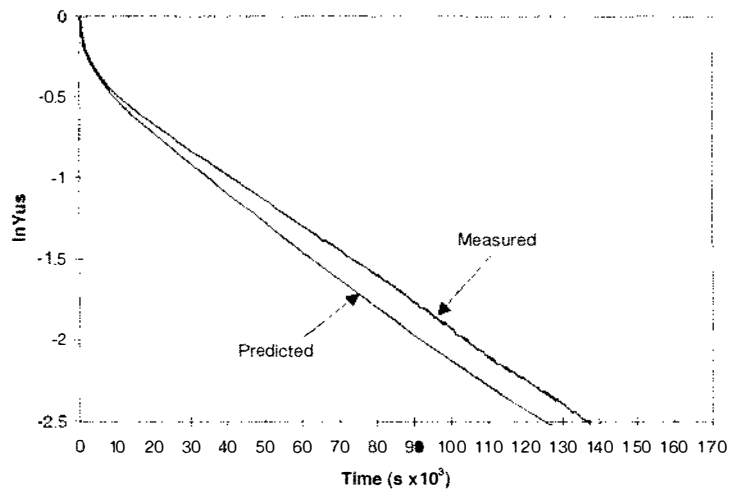

Figure 4.15 Plot of measured and predicted $\ln Y_{US}$ vs. time (run 4)

Graphical comparison of experimental and simulated results for the first infinite slab run are given in Figures 4.13 - 4.15. The second model showed a marked improvement in the prediction of the cooling rate at the lower surface (LS) and the centre (C). The cooling rate of the upper surface (US) was not as good. However, it was recognised that slumping of the Tylose during the run could have caused the upper surface heat transfer coefficient to change and so this position was the one for which poorest predictions were expected.

Overall, the second model gave much better agreement with measured data than the preliminary model. It was concluded that the inclusion of the third dimension edge effect would likely improve predictions further. However the third dimension edge effect could not be explicitly accounted for in a two-dimensional finite element program.

4.6 Comparison of Measured and Predicted Data

The input data estimated in section 4.3 were used to develop data files for as many runs as possible. The availability of upper surface HTC estimates for individual runs was limited due to thermocouple breakages during the course of the measurement trials and so not all runs could be simulated. Table 4.7 shows measured and predicted times for one $\ln Y_c$ reduction.

Cleland (1990) as gives factors limiting the accuracy of chilling time predictions as:

a) imprecise knowledge about conditions in the chiller,
b) imprecise thermal data for the product,
c) use of a prediction method outside its range of applicability, and
d) shortcomings in the prediction method.

A sensitivity analysis on the effect of the input data (factors a and b above) was carried out. From replicate measurements the likely uncertainty in the lower surface HTC was ±6% and the uncertainty in the individual estimates of upper surface HTC was expected to be about ±10%. The uncertainties in the estimates of Tylose thermal conductivity and specific heat capacity were ±4% (Willix *et al.*, 1998) and ±5% (Lindsay & Lovatt, 1994) respectively. The uncertainties in the estimates of thermal conductivity and specific heat capacity for expanded polystyrene were expected to be about ±10% respectively. By using the extreme case combinations of likely maximum and minimum values of input data the estimated maximum percentage change in predicted times for one $\ln Y_c$ reduction was ±9%.

Table 4.7 Comparison of measured and predicted times for one $\ln Y_c$ reduction (s x 10^3)

Void Type	No. of Fibreboard Sheets	Void height (mm)	Measured	Predicted	% Difference
Filled	1	0	37[a]	36	-3
		10	45	45	0
		20	49	-	-
		30	53	57	+8
		40	58, 61, 60	62, 64, 65	+7, +5, +8
		50	74	-	-
	3	0	54[a]	58	+7
		10	50	-	-
		20	65	-	-
		30	73	78	+7
		40	74, 74, 74	79, 82, 82	+7, +11, +11
		50	85	-	-
Air	1	0	37[a]	36	-3
		10	43	45	+5
		20	46	-	-
		30	51	59	+16
		40	51, 53, 49	64, 67, 68	+25, +26, +39
		50	57	-	-
	3	0	51[a]	52	+2
		10	45	-	-
		20	63	-	-
		30	68	81	+19
		40	61, 64, 63	82, 86, 85	+34, +34, +35
		50	62	-	-

[a] solid block (no void space)

A prediction method used outside its range of applicability (factor c from above) implies the neglect of some parts of the physical system within the model. The finite element program FINEL was designed for use in heat conduction problems, it copes with asymmetric HTC's, multiple component, and irregularly shaped physical systems. However it is only two-dimensional and neglecting the third dimension edge effect in the finite element model was considered an aspect of significance. This effect should have been most prominent for the slowest cooling Tylose blocks. This was confirmed by the data in Table 4.7 - percentage differences between measured and predicted cooling times were larger for blocks that had longer cooling times.

The extent of the third dimension edge effect was estimated by comparing two predicted cooling times: one for a block with a third dimension edge effect and one for a block without.

The predicted cooling times and mass average temperature-time profiles of blocks without a third dimension edge effect were already known (from Table 4.7). The slowest cooling block (with 40mm high filled voids and three fibreboard sheets) was chosen for analysis because it was likely to have the most significant third dimension edge effect (Figure 4.16a). Iterative simulations using FINEL found the equivalent top and bottom surface HTC for the Tylose block in Figure 4.16b (a solid 0.36m x 0.18m Tylose block with perfectly insulated sides) that gave the closest match to the mass average temperature-time profile of the block in Figure 4.16a by minimising the sum of squared differences between the $\ln Y_{av}$ vs. time profiles at ten evenly spaced time intervals. The equivalent HTC's for block *b* were found to be 7.4 $Wm^{-2}K^{-1}$ (to one decimal place) if one assumed symmetrical cooling of the solid block, and the same cooling medium temperature as block *a*. In this way block *b* cooled at the same rate as block *a* but only underwent one-dimensional heat transfer - the second dimension edge effect was implicitly accounted for the by the equivalent HTC. Block *b* did not include any third dimension edge effect.

The block in Figure 4.16c represented the same situation as block *b* (i.e. the top and bottom surfaces of the Tylose block are cooled with the implicit second dimension edge effect), but included a third dimension edge effect. The third dimension edge effect was represented by placing 40mm thick layers of polystyrene on the left and right sides of the Tylose block. The conditions external to the polystyrene layers were assumed to be the same as those for the second dimension edge effect (as determined in section 4.3.5). The difference in times for one $\ln Y_c$ reduction between block *b* and *c* was solely due to the third dimension edge effect. The third dimension edge effect was estimated to have decreased the time for one $\ln Y_c$ reduction by 11% in the worst case.

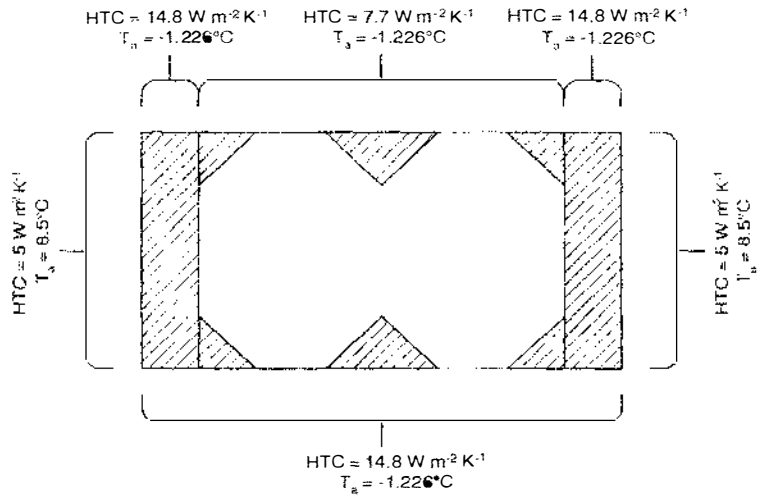

a) 0.26m x 0.18m Tylose block containing 40mm high filled voids

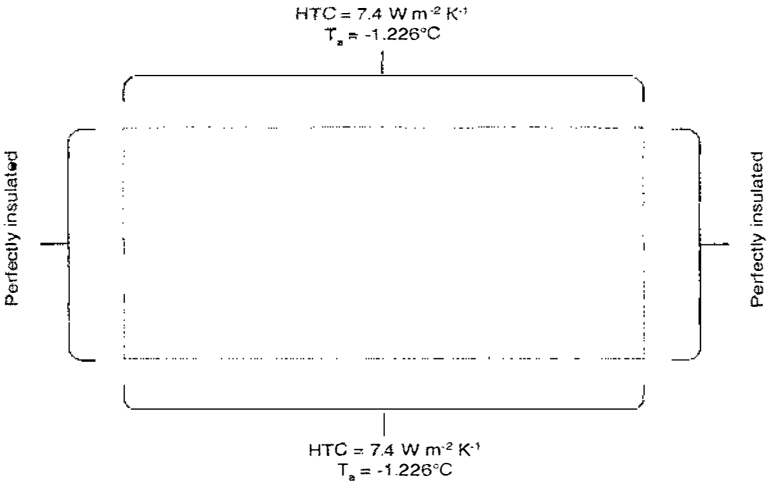

b) 0.36m x 0.18m Tylose block with same mass average temperature-time profile as block a

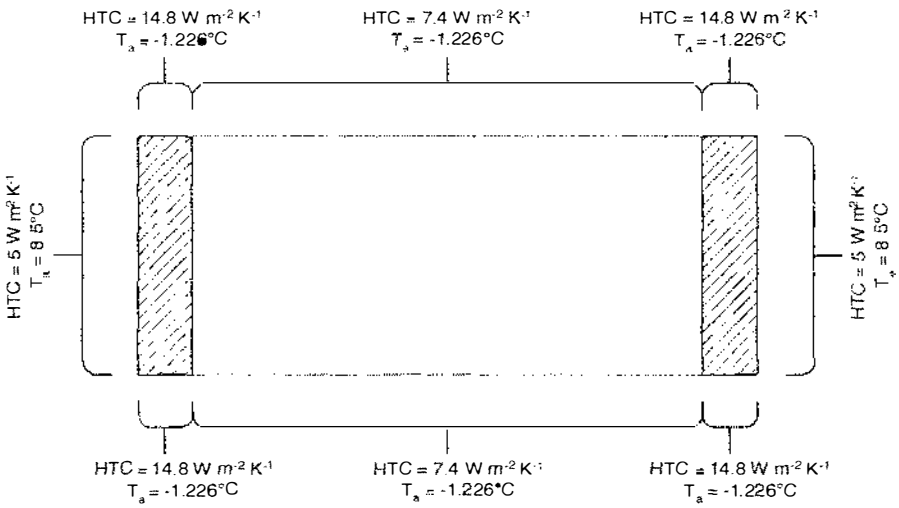

c) Same as block b, but with third dimension edge effect included

Figure 4.16 Diagram of three treatments used to determine the third dimension edge effect

The uncertainty arising from imprecise input data and the effect of ignoring cooling from the third dimension edge of the sample were combined in order to estimate the maximum prediction uncertainty (numerical errors within the finite element model were considered negligible - factor d from above). The maximum prediction uncertainty was (+9,-20)%.

The experimental uncertainty was estimated to be about ±8% in section 4.4 so the combined experimental and prediction uncertainty was (+17,-28)%. For the data in Table 4.7, measured and predicted cooling times for blocks with filled voids agreed to within the experimental and prediction uncertainty limits at all void sizes. However the percentage difference between measured and predicted data for blocks with air voids was outside this range at void heights greater than 30mm. This disagreement outside the combined experimental and prediction uncertainty limits was presumably due to cooling enhancement from natural convection and radiation effects occurring within the air voids. Thus the data supports heat transfer theory which suggested that natural convection and radiation effects would be more significant within larger air voids.

The third dimension edge effect was more significant for blocks with longer cooling times. Hence the larger percentage difference observed between measured and predicted cooling times for air void blocks with more fibreboard sheets (3 c.f. 1) did not necessarily provide evidence to suggest a difference between the natural convection and radiation effects occurring in voids with different surface heat transfer coefficients.

4.7 Conclusions

The preliminary data collection was carried out to investigate whether natural convection and radiation effects occurring in typically sized voids have a significant effect on the cooling rate of cartoned meat. The data were also used to identify key factors in the development of a numerical model.

A major problem of Tylose block 'slumping' occurred through the trials. The upper surface of the blocks fell away from the top cooler plate causing a reduction in the upper surface heat transfer coefficient and subsequent asymmetrical cooling of the sample block. This, coupled with a high number of thermocouple breakages during the trials, made estimation of surface heat transfer coefficients difficult and insufficiently accurate.

The measured data showed that all packages containing air voids cooled faster than those with filled voids. However, only at void heights greater than 30mm did the percentage difference between air and filled void packages become greater than the estimated

experimental error of ±8%. It was postulated that this cooling enhancement arose from a combination of natural convection and radiation effects occurring within the void.

A two-dimensional finite element model was developed using a heat conduction program called FINEL. The model allowed asymmetrical heat transfer coefficients on upper and lower surfaces and accounted for the second dimension edge effect. Predicted and measured data were compared. The measured and predicted data for blocks with no voids and blocks with filled voids at all void sizes agreed to within the combined experimental and prediction uncertainty limits of (+17,-28)%. However the percentage difference between measured and predicted data for blocks with air voids was outside the combined experimental and prediction uncertainty limits at void heights greater than 30mm. This was presumably due to cooling enhancement from natural convection and radiation effects. The data supported heat transfer theory that suggests natural convection and radiation effects are more significant within larger voids.

Although the measured data followed trends consistent with fundamental natural convection theory, further experimental work was necessary. The further work required improved methods to eliminate asymmetric cooling and would allow independent comparison of voids cooled from above and below.

Limitations on the number of elements and nodes allowable in FINEL, and the amount of time required to manually construct FINEL grids and data files, highlighted the need for a better finite element program. The improved program would have to be able to accurately represent the test space without approaching element and node limits, and preferably include an automated mesh generator to save time on data file construction.

5. IMPROVED DATA COLLECTION AND MODEL DEVELOPMENT FOR PACKAGES CONTAINING TRIANGULAR VOIDS

The data collection methods in chapter 4 required refinement so that the influence on cooling rate of heat transfer modes such as natural convection and radiation in voids could be more accurately determined. Features that an ideal experimental system should have and how the system was changed to approach them included:

1. *Independent measurement of the effect of voids of different orientation should be allowed.*
    - blocks would contain only one type of void shape so any difference in cooling rate can be entirely attributed to natural convection and radiation effects in that orientation only (i.e. samples should contain only 'single' or 'double' right angled isosceles triangular voids and the voids should only be on their base (Δ) or on their apex (∇)).

2. *The surface heat transfer coefficients should be constant within and between associated runs.*
    - good contact between plates and sample surface was required:
    - slumping of the Tylose blocks was avoided by enclosing them in a solid box.
    - good contact was ensured by pressing the upper plate down onto the sample.

3. *Evaporative cooling within voids should be eliminated.*
    - Tylose blocks were well sealed to eliminate moisture loss.

4. *Unwanted heat transfer should be eliminated or at least accounted for.*
    - edge effects were minimised by utilising an axis of symmetry.
    - data for edge effects were accurately measured.
    - edge effects were quantified by simulation.

5. *The system should be sturdy and easy to repair.*
    - thicker thermocouple wire was used.
    - Tylose blocks were enclosed within a solid box.
    - the apparatus was designed to enable easy repair or replacement of thermocouples.

5.1 Experimental Methodology

Taking the same approach as in chapter 4, the vertical axis of symmetry was used to reduce the analogue meat carton size to 260mm x 360mm. To allow independent measurement of the effect of voids cooled from above and below, the horizontal axis of symmetry was utilised. Tylose blocks were made up to half the normal meat carton height (90mm c.f. 180mm) with voids cut into one surface only. Two of these Tylose blocks were placed side by side within a sample holder (one block containing air voids and one with filled voids - see Figure 5.1). This effectively created identical conditions of external heat transfer and enabled direct comparison of cooling rates between the blocks.

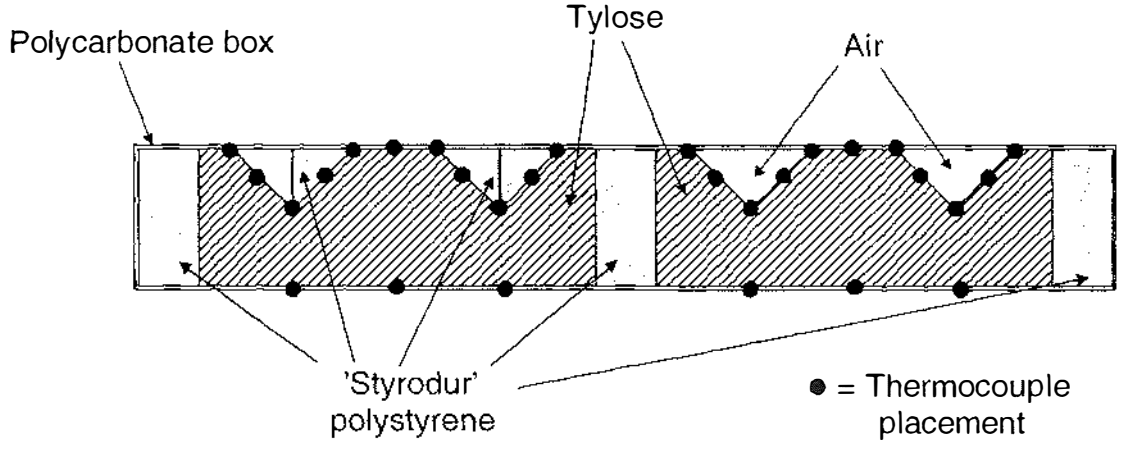

Figure 5.1 Side elevation of polycarbonate sample holder containing two Tylose blocks

Polycarbonate boxes were used as sample holders. In this way, slumping was eliminated, the pliable Tylose gel was kept in the desired geometric shape, and sample deterioration due to moisture loss was avoided. A 360mm long, 1mm thick L-shaped section of solid acrylic plastic lined the surface of each void (top and bottom) to ensure they held their shape. Several different sizes of these plastic sections were constructed to enable voids of different heights to be supported.

Within the Tylose blocks, two-dimensional heat flow was desired so the sides and ends were insulated. The expanded polystyrene insulation used in the preliminary data collection was replaced by *Styrodur*, a rigid commercial polystyrene insulation manufactured by BASF New Zealand Ltd. *Styrodur* has a similar thermal conductivity to that of still air (and lower than that of expanded polystyrene), but a higher specific heat capacity. However the extra heat to be removed from the *Styrodur* made up only 0.2% (in

the worst case) of the total heat to be removed from the whole sample holder. A 40mm thick layer of *Styrodur* was placed between the two blocks in each sample holder to reduce the heat flow between them. The measured temperature data that will described in section 5.3 and standard quasi-steady state heat transfer equations were used to estimate the mean sideways heat flow. In the worst case, where the cooling rates of the two blocks were most different, the mean sideways heat flow between them was only 0.4% of the mean vertical heat flow from the block containing filled voids.

Figure 5.2 Photograph of a sample holder

In order to halve the total number of trials, two different sample holders were cooled at the same time (one with voids contacting the bottom cooler plate and one with voids contacting the top cooler plate - see Figure 5.3). A 40mm thick layer of *Styrodur* was placed between the top and bottom sample holders to reduce the heat flow between them. Given that the samples have similar temperatures at any time only a small heat flow between them is likely. The measured temperature data from section 5.3 and standard quasi-steady state heat transfer equations were used to estimate the mean heat flow between the top and bottom sample holders. In the worst case, where the difference in centre temperature between the top and bottom blocks was at a maximum, the mean heat flow from the centre of the bottom sample to the centre of the top sample was 0.3% the total heat flow from the centre of the bottom sample.

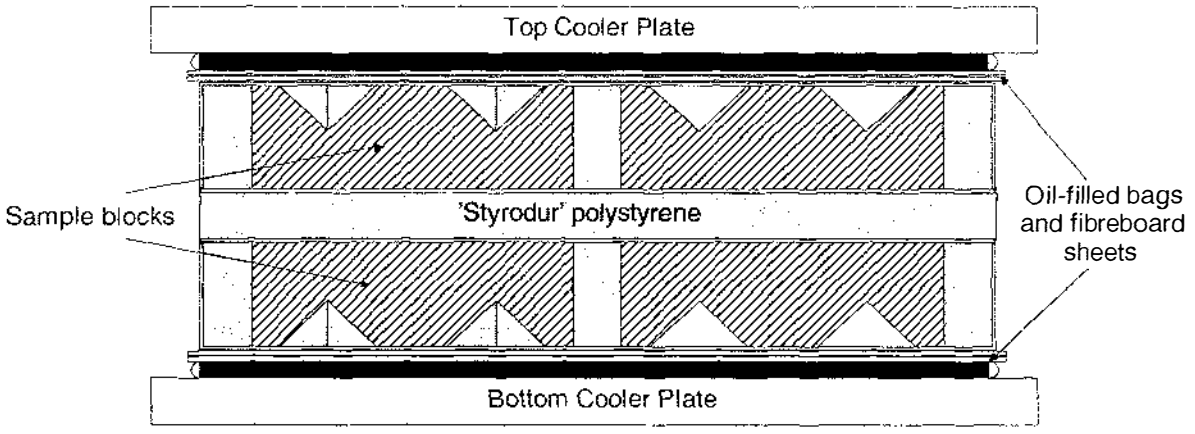

Figure 5.3 Diagram of two sample holders within the plate cooler

The same plate cooler used in the preliminary data collection was used to cool the blocks. The plates contained alcohol at approximately 0°C which was circulated and cooled by a Julabo FPW65-MS low temperature bath on an internal set point. The cooler plates were slightly warped due to the loads that had been applied in previous work. Planing the plates flat would have only made them weaker, adding extra aluminium plating would have been a temporary solution, and an attempt to use a layer of conductive grease was unsuccessful due to the entrainment of air pockets between the sample surface and the grease. Therefore another technique to make the external heat transfer coefficient to the sample uniform was devised. Strong vegetable oil-filled plastic bags were placed between the plates and the sample. The oil ensured good contact with the warped cooler plates and the flat sample surface. Each oil bag (0.68m x 0.44m in area) was filled with approximately 3.0 litres of oil, which yielded an average oil layer thickness between the sample and the cooler plates of approximately 10mm.

The oil was regarded as the external cooling medium and given that it was not considered to be within the system boundary, the thermal mass of the oil could be ignored.

To ensure good contact between the sample and the plates it was necessary to apply pressure to the movable top plate. An evenly distributed load of 100kg was used. The extent of contact between the oil bag and the sample was investigated by using 'Bearing Blue' machining ink by Power Plus, Kelray Australia Pty Ltd. A thin layer of this blue ink was smeared onto the top surface of a sample holder and a sheet of paper was placed between the sample holder and the oil bag. Any areas of contact left a residue of blue ink on the sheet of paper. Contact between the oil bag and the holder was found to be very good with almost all of the paper covered in blue ink and the areas of non-contact small and evenly dispersed over the surface.

The inlet and outlet temperatures of the top and bottom plates, the temperature of the air inside the plate cooler, and the temperatures at various positions within the Tylose blocks were measured with copper/constantan thermocouples, calibrated at 0°C using an ice/water slurry. The readings of the three thermocouples positioned on the surface of each Tylose block were recorded every 10 seconds by a Grant 1200 series Squirrel meter/logger. All other thermocouple readings were collected every 30 seconds by a Hewlett Packard HP 3497A data logger and recorded onto an IBM-compatible PC.

Five sample holders (with two Tylose blocks in each) were constructed with right angle isosceles triangular voids of differing heights (0, 20, 30, 40 and 50mm) and one replicate of the sample holder with 50mm high voids was also constructed. One of the sample holders with 50mm high voids was eventually converted to a block containing 50mm high 'half' voids by placing a vertical strip of corrugated cardboard down the centre of the air void. Trials were carried out at two different rates of heat transfer by placing different heat transfer resistances between the oil bags and the samples. The first heat transfer resistance was comprised of the polycarbonate box only and the second included the addition of two sheets of 1.65mm thick fibreboard. Each of the seven sample holders was tested under four treatments (cooled from above or below at a high or low HTC) giving 28 sets of data. A further two replicates of the sample holder with 50mm voids cooled from above with a high HTC, and two extra replicates of the sample holder with 30mm voids cooled from below with a high HTC were also carried out. With these extra four, a total of 32 data sets were collected over sixteen runs (with two sample holders per run). The runs were started before construction of all sample holders was complete so the order in which the runs were performed could not be randomised. However random selection of runs within the samples available at any time was carried out. A treatment table is given in Table 5.1.

Before each run was started, two sample holders were equilibrated to approximately 30°C in a warm room. The two oil bags and any sheets of fibreboard to be used in the experiment were placed between the plates of the cooler. The Julabo FPW65-MS low temperature bath was switched on. After the coolant outlet temperature of the top and bottom plates had reached the desired operating temperature (0°C), the apparatus was left for at least 30 minutes to allow the aluminium plates, the oil bags and the fibreboard sheets to reach an equilibrium temperature.

All exposed surfaces of the sample holders were insulated during transport to the cooler. Male/female thermocouple connectors were joined and data logging was started. The

temporary insulation was removed and the sample holders were immediately placed between the plates of the cooler, the oil bags and the fibreboard sheets. Ten 10kg weights were then distributed evenly over the surface of the top plate. Each run was stopped after the slowest cooling thermocouple reading was below 2.0°C.

Table 5.1 Treatment table for improved data collection

Run No.	Cooled from above	Cooled from below	Fibreboard sheets	Order
1	20mm voids	no voids	2	1
2	20mm voids	no voids	0	4
3	no voids	20mm voids	2	5
4	no voids	20mm voids	0	8
5	30mm voids	50mm voids	0	2
6	30mm voids	50mm voids	2	3
7	50mm voids	30mm voids	0	7
8	50mm voids	30mm voids	2	6
9	50mm voids	30mm voids	0	9
10	50mm voids	50mm voids	0	10
11	50mm voids	40mm voids	2	12
12	40mm voids	50mm voids	2	13
13	50mm 'half' voids	50mm 'half' voids	0	16
14	50mm 'half' voids	50mm 'half' voids	2	15
15	50mm voids	40mm voids	0	11
16	40mm voids	30mm voids	0	14

5.2 Evaluation of Input Data

5.2.1 Sample Dimensions

Sample dimensions were measured using vernier calipers. Three measurements of each of the sample length, width and height were taken. Void position and size was measured by two readings of the coordinates of the void's vertices in relation to the closest end of the sample. Thermocouple positions were also measured in this manner. The estimates of mean values were considered accurate to ± 1mm.

5.2.2 Thermal Property Data

The thermal property data of the materials used in this chapter are given in Table 5.2.

Table 5.2 Thermal properties of test substances

Property/Substance	Tylose*	Polycarbonate	'Styrodur' Polystyrene
k (W/mK)	$0.468 + 0.00154T$	$0.245^{\ddagger}$	$0.031^{\ddagger}$
c (J/kg K)	-	$1255^{\dagger\dagger}$	$1255^{\dagger\dagger}$
ρ (kg/m^3)	-	$1170^{\ddagger}$	$30.8^{\ddagger}$
C (J/m^{3}K)	4.065×10^6	1.468×10^6	3.87×10^4

where T = temperature (°C)

* Amos *et al.* (2000)

†† In "Comparison of Materials" (1976)

‡ Measured by author

For Tylose, Amos *et al.* (2000) reported the specific heat capacity (from Lindsay & Lovatt, 1994) and the thermal conductivity (from Willix *et al.*, 1998). The respective uncertainties in these measured data were ±5% and ±4% respectively. Although uncertainty values were not available for the specific heat capacity of polycarbonate and Styrodur, the values in Table 5.2 were expected to be within about ±10% of their true values, and the true mean thermal conductivities were estimated to be within ±20% and ±15% of the respective values measured by the author (detail of measurement methods and uncertainty calculations are given in Appendix A1).

5.2.3 Initial and Boundary Conditions

The blocks were assumed to be initially at a uniform temperature equal to the measured centre temperature at the start of each run, which was measured to ±0.2°C.

Boundary conditions were of the third kind, and thus estimates of the mean cooling medium temperature and the surface heat transfer coefficients were required.

Cooling Medium Temperatures

The cooling medium temperature at the inlet and outlet of the cooler plates was measured. The cooling medium flow rate was sufficiently high that the difference between the inlet and outlet temperatures was always within the estimated accuracy of the thermocouples

(±0.2°C). However these temperatures did not give a true indication of the cooling medium temperature represented by the oil temperature in the oil bags.

Heat transfer from the sides or ends of the sample was ignored and the thermal capacities of the polycarbonate box and oil bags were neglected. An approximate energy balance was therefore:

$$h_{overall} A\int_{t_1}^{t_2} (T_s - T_a)dt \approx \left[\int_0^R H\,dx\right]_{t_2} - \left[\int_0^R H\,dx\right]_{t_1} \qquad (5.1)$$

where $h_{overall}$ is the overall heat transfer coefficient representing the polycarbonate wall, the oil bag and oil, and any contact resistance ($Wm^{-2}K^{-1}$)
A is the sample surface area undergoing cooling (m^2)
T_s is the surface temperature of the sample (°C or K)
T_a is the plate temperature (°C or K)
H is the enthalpy of the sample (J)

In seeking to use equation 5.1, because only the centre and surface temperatures of the Tylose block were measured, a linear temperature profile through the Tylose block was assumed.

The overall heat transfer coefficients estimated by back-calculation were 7.0 and 10.8 $Wm^{-2}K^{-1}$ for the cases with and without fibreboard. If the thermal capacity effect of the oil continues to be ignored then quasi-steady state heat transfer analysis suggests that at any time:

$$T_{oilbag} \approx T_a + \left[\frac{h_{overall}\, x_{oilbag}}{k_{oil}}\right](T_s - T_a) \qquad (5.2)$$

where $T_{oil\,bag}$ is the temperature of the oil bag surface nearest the sample (°C or K)
Q is the heat flux through the top surface of the Tylose block ($W\,m^{-2}$)
$x_{oil\,bag}$ is the thickness of the oil bag (m)
k_{oil} is the thermal conductivity of oil = 0.15 $Wm^{-1}K^{-1}$ (Perry & Green, 1984)

Equation 5.2 assumed that no natural convection was occurring within the oil layer. This was considered to be a reasonable assumption since the sum of resistances (including the oil bag with no natural convection) was lower than the overall values estimated by back-

calculation above, which suggested no significant natural convection occurred within the oil bags.

The estimated temperature of the oil (the external cooling medium temperature) decreased slowly in an approximately exponential fashion as the sample cooled so the ambient temperature was estimated by a logarithmically weighted average. The estimated mean cooling medium temperatures were 0.4°C and 0.3°C for high and low heat transfer coefficient runs respectively. This is only slightly above the plate temperature (~0°C), indicating that the bulk of the heat transfer resistance external to the sample was in the polycarbonate box and the cardboard sheets.

The air temperature within the plate cooler cabinet was directly measured. Since this also decreased over the course of the run in an exponential fashion, a logarithmically weighted mean value was used in data analysis.

Heat Transfer Coefficients

Approximate overall heat transfer coefficients had been estimated by the heat balance method given above, but these estimates included the heat transfer resistance of the oil bag. By using the sum of resistances method (equation 5.3) the heat transfer resistance of the oil bag was excluded from the heat transfer coefficient value. The high and low HTC's were estimated to be 38.5 and 13.1 $Wm^{-2}K^{-1}$ respectively.

$$\frac{1}{h_{new}} = \frac{1}{h_{overall}} - \frac{x_{oil\,bag}}{k_{oil}} \tag{5.3}$$

where h_{new} is the heat transfer coefficient value excluding the heat transfer resistance of the oil bag ($Wm^{-2}K^{-1}$)

It should be noted that these HTC's were subject to any edge effects and any effect of the thermal capacity of the oil bag, the fibreboard sheets, and the polycarbonate layer being ignored. It was acknowledged that more accurate estimation of the heat transfer coefficients would be necessary before measured and predicted data were compared. However the initial estimates of HTC were considered acceptable for analyses to estimate edge effects.

The value of Biot number (*Bi*) could not be accurately determined because the effective thermal conductivity of the composite samples was unknown. However, as an

approximate indication of the ratio of internal to external heat transfer, a 90mm thick infinite slab of Tylose cooled from one surface only with a heat transfer coefficient of 38.5 $Wm^{-2}K^{-1}$ or 13.1 $Wm^{-2}K^{-1}$ would have experienced a *Bi* value of 7.1 or 2.4 respectively.

5.3 Measured Time-Temperature Data in the Test Samples

Figure 5.4 shows typical centre temperature-time profiles from three different samples (a block with no voids, one with air and one with filled 50mm high voids) under similar cooling conditions. As was observed in the preliminary experiments the block with no voids cooled most quickly even though it had more thermal mass. The block with air voids cooled faster than the block with filled voids, presumably due to natural convection and radiation effects (and in spite of the foam thermal conductivity being slightly higher than that of still air).

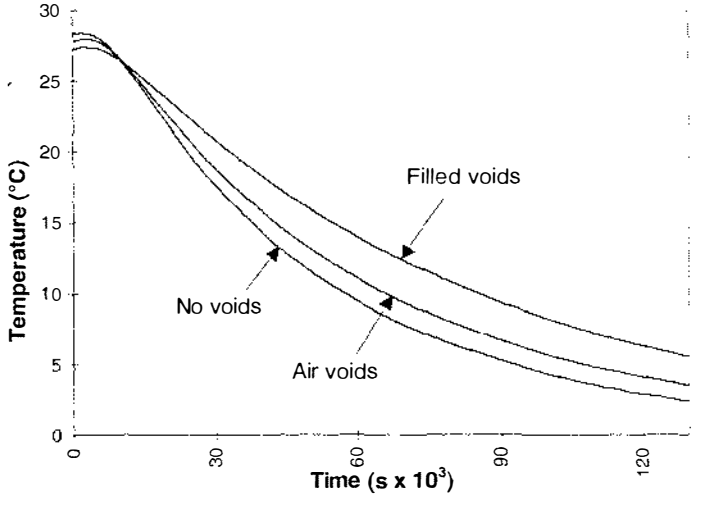

Figure 5.4 Plot of centre temperature vs. time for Tylose blocks containing no voids (Run 4), and for blocks containing 50mm high filled voids and 50mm high air voids (Run 7)

Figure 5.5 is a plot of $\ln Y_c$ vs. time and Figure 5.6 is a plot of the [slope of $\ln Y_c$ vs. time] vs. time, both from the same data as Figure 5.4 (note that at low $\ln Y_c$ values the uncertainty in temperature measurement affects the derivative values). From Figure 5.6 any change in the normalised cooling rate at each stage of the experiment can be observed directly. The normalised cooling rates of the block containing no voids and the block containing filled voids are constant throughout the experiment within experimental uncertainty, but the block with air voids cooled faster near the start of the experiment and slowed to about the same rate as the 'filled voids' block towards the end. This is

consistent with natural convection and radiation effects being more prominent at the start of the experiment when temperature differences across voids are at their highest.

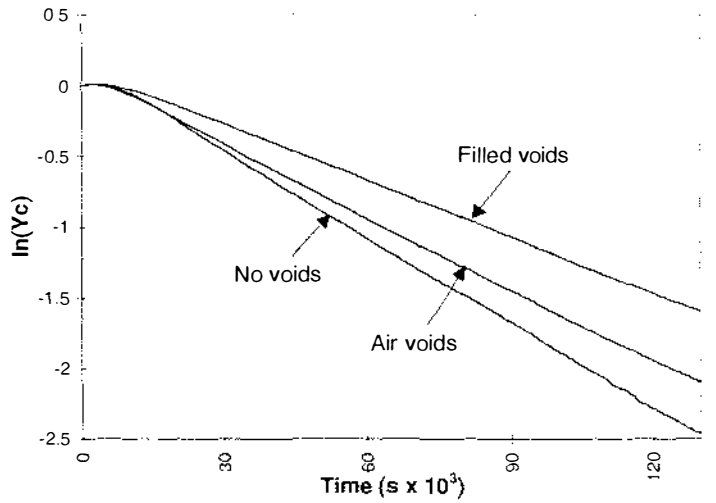

Figure 5.5 Plot of $\ln Y_c$ vs. time for the same samples shown in Figure 5.4

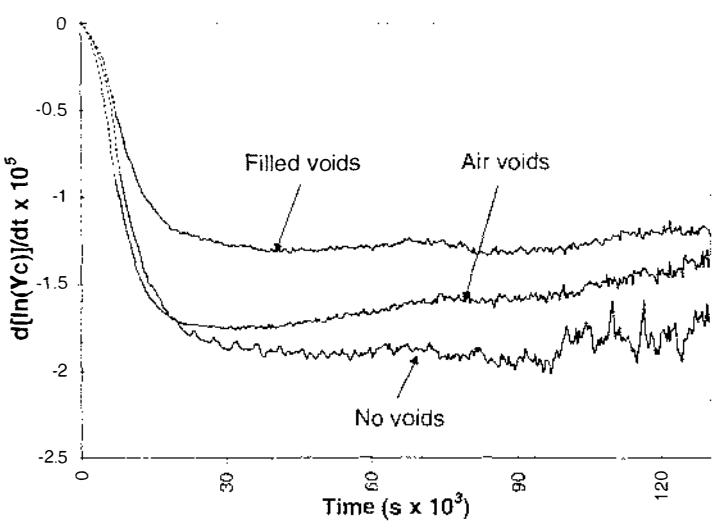

Figure 5.6 Plot of [d($\ln Y_c$)/dt] vs. time for the same samples shown in Figure 5.4

Table 5.3 shows measured times for one $\ln Y_c$ reduction from -0.5 to -1.5. The replicate times for one $\ln Y_c$ reduction from ten runs with Tylose blocks containing 50mm high filled voids cooled with no fibreboard sheets (six runs with one block, and the other four with an independently constructed block) were used to estimate the experimental uncertainty. There was 95% certainty that any measured value was within ±5% of the mean.

All blocks with no voids cooled faster than blocks with voids. Most blocks with air voids cooled as fast or faster than the corresponding blocks with filled voids. However for trials with 30mm high voids, the blocks with air voids cooled at the same rate or slower than

the blocks with filled voids. The failure of these data to match the general trend suggested a possible fault in the construction of the Tylose block used for the runs with 30mm high air voids. All the runs with this block cooled at a much slower rate than expected. By the time these were analysed the Tylose block had significantly deteriorated making proper investigation into the suspected fault impossible, however the cause was suspected to be a large air pocket just under the top surface of the block that would slow the cooling rate of the block considerably. The data from runs using this block (5, 6, 7, 8, 9 and 16 with air voids only) were therefore considered suspicious, and were not used in subsequent analyses.

Blocks with 50mm high 'half' voids showed no difference in cooling rate from corresponding blocks with normal 50mm high voids. This suggested that physically dividing the 50mm high 'half' voids gave natural convection and radiation effects that were similar to those within normal 50mm high voids. Salmun (1995) states that the occurrence of bifurcation (multi-cellular natural convective flow within enclosures) increases as *Ra* increases. Therefore it is possible that the *Ra* in the normal 50mm high voids was large enough to allow bifurcation to occur and that this multi-cellular flow was largely uninterrupted by the divider used in the 50mm high 'half' voids.

Table 5.3 Times for one $\ln Y_c$ reduction for blocks with triangular voids of various heights (seconds x 10^3)

Estimate of HTC ($Wm^{-2}K^{-1}$)	Void height (mm)	Filled voids cooled from above	Air voids cooled from above	Filled voids cooled from below	Air voids cooled from below
38.5	0	49[a]	-	51[a]	-
	20	50	53	53	54
	30	58	64[b]	58, 58, 58	64, 67, 64[b]
	40	66	58	66	68
	50	76, 77, 77, 77	59, 59, 61, 60	74, 77	66, 69
13.1	0	64[a]	-	65[a]	-
	20	66	66	66	66
	30	76	75[b]	70	77[b]
	40	77	72	81	75
	50	90, 87	70, 72	88, 88	76, 79

[a] solid block (no void space), [b] apparently anomalous results

Figures 5.7 and 5.8 show the relative times for one $\ln Y_c$ reduction of blocks with varying void size compared to a block with no voids. Solid lines are drawn between mean values of relative cooling time, dashed lines are given where data was missing or an anomalous

result was encountered. Data for filled voids cooled from above and below are treated as one data set (a paired t-test indicated no difference to a confidence level of 90%). The apparent natural convection and radiation effects were more pronounced in blocks with larger air voids and particularly in blocks that were cooled from above and with a higher HTC, presumably due to the higher temperature differences that would occur around the air voids.

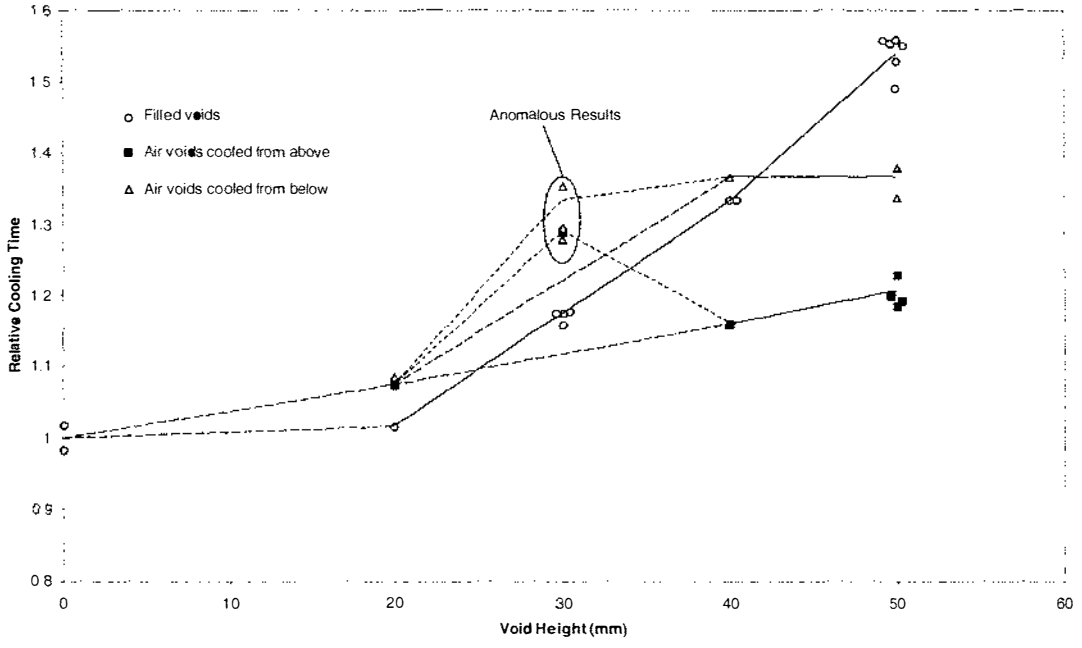

Figure 5.7 (Cooling time)/(Solid block cooling time) at higher HTC

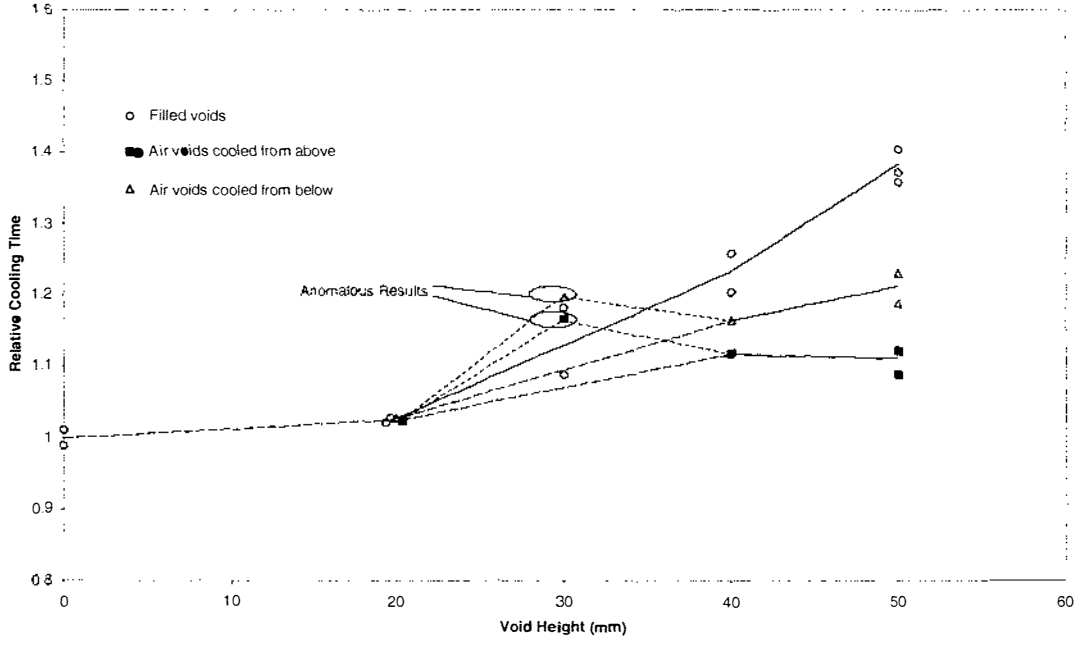

Figure 5.8 (Cooling time)/(Solid block cooling time) at lower HTC

5.4 Development of a New Numerical Model

The preliminary data collection and analysis in chapter 4 highlighted the importance of including the edge effects in the numerical model. The limit on the number of nodes and elements allowed within FINEL made it difficult to accurately model the entire physical system with edge effects included. However, of the numerical modelling frameworks available to the author, finite elements was still considered to be the best so a new commercially available finite element package was obtained and used to construct an improved model. A computational fluid dynamics solver called PHOENICS was also considered, however relevant literature suggested that computation times could be prohibitively long (Nguyen & Pham, 1999).

The finite element package used was PDEase2D version 2.6.1c by Macsyma, Inc. It requires the user to state the partial differential equations to be solved, and to define all appropriate properties, and the initial and boundary conditions. PDEase2D creates a two-dimensional triangular grid within the problem space to an initial level of refinement chosen by the user (eliminating the need for the user to construct the entire grid by hand). The problem is then solved numerically by the Galerkin method using grid and time step refinement algorithms that satisfy error limits set by the user. The simulations can be stopped automatically or manually. The choice of results to present must be made before the simulation has been run. An example data file is given in Figure 5.9 for a two-dimensional 0.36m x 0.09m block of Tylose at a uniform initial temperature of 30°C, and with a third kind of boundary condition on the top surface of 10 $Wm^{-2}K^{-1}$ at 0°C. The block will be cooled for 400000 seconds and the temperature at coordinates (0.16m, 0m) will be recorded in an output file at every time step.

5.4.1 Effect of varying *errlim* in PDEase2D

errlim is a user-selected function in PDEase2D which sets the accuracy goal for automatic adaptive grid refinement. At each time step the root mean square error across all the elements and the individual element errors are tested against the *errlim* value. If either test fails, PDEase2D subdivides all elements whose error is greater than *errlim* and repeats the solution phase. The ideal *errlim* value is one that enables fast solution but gives a simulation accuracy for the problem space that is well within the uncertainty range of temperature measurement for the experiments.

```
Title
"Transient Heat Conduction in 2D"
Select
 errlim= 1e-3
 ngrid=20
Variables
 temp
Definitions
 kx
 ky
 cp
 source= 0
 { conductivity and heat capacity along x and y }
 kxtyl= 0.468 + (0.00154*temp)
 kytyl= 0.468 + (0.00154*temp)
 cptyl= 4.065e6
 tempi= 30  Ta= 0  B1= 10
Initial values
 temp= tempi
Equations
 cp* dt(temp)+ dx(-kx*dx(temp))+ dy(-ky*dy(temp)) = source
Boundaries
 region 1
  cp= cptyl  kx= kxtyl  ky= kytyl
  start (0.32,0.09)
  natural (temp) = 0
  line to (0.32,0) to (0,0) to (0,0.09)
  natural (temp) = B1*(temp-Ta)
  line to finish
Time
 0 to 400000
Histories
 history(temp) at (0.16,0) dv file
End
```

Figure 5.9 Example data file from PDEase2D

The default *errlim* value of 0.001 was used for simulation of a two-dimensional 260 x 90mm Tylose block at a uniform initial temperature of 30°C, perfectly insulated bottom and sides, and a third kind of boundary condition on the top surface with a HTC of 10 $Wm^{-2}K^{-1}$ and an ambient temperature of 0°C. Constant thermal properties (calculated for

Tylose at 15°C) were used to enable the solution to be compared to the analytical solution.

At an *errlim* of 0.001 the simulation took 30 seconds to run and gave a half-cooling time of 51700 seconds. The analytical solution was 51357 seconds (a percentage difference of 0.7%) - more error than was desirable. The test was repeated with an *errlim* value of 0.0001. This simulation took 150 seconds to run and gave a half-cooling time of 51540 seconds (percentage difference of 0.35%) which was regarded as acceptable.

The error had been reduced by 50% with the simulation taking five times longer to run. An *errlim* of 0.0001 was used for all subsequent PDEase2D simulations.

5.4.2 Accounting for the third dimension edge effect

In chapter 4, edge effects were shown to significantly affect the cooling times of the blocks. Modelling the physical system within a two-dimensional finite element program meant the second dimension edge effect could be accounted for explicitly, but the third dimension edge effect could not. Hence an approximate method to include the effect of the third dimension was sought.

In chapter 2 the review of literature showed that prediction of chilling in which there is multi-dimensional heat transfer through homogeneous objects was possible by using a model of one dimensional heat transfer and applying empirical shape factors (assuming the characteristic dimension and chilling conditions are the same). The equivalent heat transfer dimensionality (E) is a commonly used shape factor (Cleland & Earle, 1982), whereby the E value is a multiplication factor. For example, a value of 1.20 implies that the cooling rate is 20% faster than if only one dimensional heat transfer occurred. The 0.20 factor is the influence of the second and/or third dimensions. Thus the chilling time of an homogeneous one dimensional object can be related to the chilling time of an homogeneous multi-dimensional object.

$$t_{MD} = \frac{t_{1D}}{E} \tag{5.4}$$

where E is the equivalent heat transfer dimensionality factor
t_{MD} is the chilling time of a multi-dimensional object (s)
t_{1D} is the chilling time of a one dimensional object (s)

An advantage of E is that the effects of the second and third dimensions can be seen as additive, e.g. the 1.20 might be made up of 1.0 from the primary dimension, 0.14 from the secondary, and 0.06 from the third. This example suggests the effect of the third dimension relative to the first was 6%, and the relativity of the second to the third is 0.14:0.06.

The concept of E was applied to the numerical model in an empirical manner to account for the third dimension edge effect. The approach taken was to look at the relativity of the second and third dimensions. The equivalent heat transfer dimensionality was calculated using the weighting function described by Lin *et al.* (1996):

$$E = \frac{Bi^{4/3} + 1.85}{\frac{Bi^{4/3}}{E_\infty} + \frac{1.85}{E_0}} \tag{5.5}$$

Taking a view of only the second and third dimensions, for a rectangular two-dimensional object (composed of the second and third dimensions of the real shape) the definitions of Lin *et al.* were translated to:

$$E_\infty = 0.75 + \frac{0.75}{\beta_1^{\,2}} \quad \text{and} \quad E_0 = 1 + \frac{1}{\beta_1} \tag{5.6}$$

where β_1 is the ratio L_2/L_3

$$Bi = \frac{h_2 L_2}{k}$$

L_2 is the half-thickness of the second dimension (m)

L_3 is the half-thickness of the third dimension (m)

h_2 is the external heat transfer coefficient of the second dimension ($W\,m^{-2}K^{-1}$)

k is the thermal conductivity of the material in the second dimension ($W\,m^{-1}K^{-1}$)

The complication of dealing with a non-homogeneous object is that calculation of the correct Biot number based on the second dimension is difficult because k is not constant over the length of the second dimension. An 'equivalent' Biot number was defined as the value of Bi that made an homogeneous Tylose block cool at the same rate as the non-homogeneous block subject to the real heat transfer conditions. This led to the necessary implication that a constant 'equivalent' heat transfer coefficient must act upon the external surface of the homogeneous Tylose block.

At this stage it is useful to introduce further heat conduction theory. Heat conduction through multi-dimensional objects can be calculated by superposition of the Y_c values for each dimension (equation 5.7). Hence at any given time the proportion of Y_c for a block with edge effects to Y_c for a block without edge effects can be regarded as the Y_c value arising from the edge effects themselves (equation 5.8).

$$Y_{with\,edge\,effects} = Y_{without\,edge\,effects} \times Y_{edge\,effects} \tag{5.7}$$

and hence,

$$Y_{edge\,effects} = \frac{Y_{with\,edge\,effects}}{Y_{without\,edge\,effects}} \tag{5.8}$$

Transient Y values for the one dimensional heat transfer in the first dimension only ($Y_{without\ edge\ effects}$) were found using PDEase2D. Specifically a 0.26 x 0.09m Tylose block with 6mm layers of polycarbonate on the top and bottom surfaces, cooled from above with a HTC of 25.8 $Wm^{-2}K^{-1}$ (the average value of top surface HTC's used in the experiments and estimated in section 5.2.3) and a cooling medium temperature of 0°C was simulated.

Secondly, the transient Y values for the two dimensional object with heat transfer in the first and second dimensions ($Y_{with\ edge\ effects}$) were found using PDEase2D. A 0.26 x 0.09m Tylose block with 20mm and 40mm thick layers of Styrodur on the left and right sides respectively, and 6mm thick layers of polycarbonate on the top and bottom surfaces, cooled from above with a HTC of 25.8 $Wm^{-2}K^{-1}$ and a cooling medium temperature of 0°C, and cooled from the sides with a HTC of 5 $Wm^{-2}K^{-1}$ and a cooling medium temperature of 6°C (the mean external temperature of the sides) was simulated.

Using equation 5.8 the transient Y values for the second dimension only ($Y_{edge\ effects}$) were found. A $\ln Y_{edge\ effects}$ vs. time plot was constructed. The 'equivalent' second dimension HTC was then found by an iterative method in which calculations by the analytical solution for a homogeneous 0.26m thick Tylose slab undergoing one dimensional cooling at a cooling medium temperature of 6°C were carried out. Different HTC's were tried until the slope of a $\ln Y_c$ vs. time plot matched the slope of the $\ln Y_{edge\ effects}$ vs. time plot.

This 'equivalent' second dimension HTC then yielded an 'equivalent' Biot number for the second dimension of 0.16. Using equation 5.5 the equivalent heat transfer effect of the

third dimension was then estimated to be equivalent to 0.72 (72%) of the heat transfer through the second dimension.

The next requirement was to account for the 72% equivalent extra edge effects in a two-dimensional finite element calculation. The rationale selected was that if the second dimension edge effects were increased by about 72% there would be approximately the right effect added to the two dimensional model. All edge effects were through the Styrodur foam insulation so it was decided to increase its effective thermal conductivity by 72% in further calculations.

A possible problem with this approach was that it would alter heat transfer occurring in locations other than where the edge effects are important. However, since the Styrodur insulation made up more than 85% of the resistance to heat transfer in the second dimension, it seemed probable that most of the third dimension edge effect could be approximately accounted for by multiplying the thermal conductivity of the Styrodur insulation by the factor of 1.72 to give a new value of 0.0534 W m^{-1} K^{-1}. This approach was considered to be better than ignoring third dimension edge effects altogether.

5.4.3 Re-estimating the surface heat transfer coefficients

In section 5.2.3 the surface heat transfer coefficients were estimated by a heat balance and sum of resistances method. These estimates were regarded as only approximate for reasons already stated. A new method was applied to more accurately estimate the surface heat transfer coefficients. An inverse method, first proposed by Bonacina & Comini (1972), was selected. This involved conducting several numerical simulations with varying surface heat transfer coefficients and comparing simulated to measured centre temperature-time profiles, seeking the HTC value that minimised the lack of fit. This inverse method could now include compensation for edge effects and for the thermal capacity of the polycarbonate layer. It also allowed the estimation process to be carried out over the course of the whole experiment, accounting for any temporal variation. Further, the use of centre temperatures forced positional variations in surface heat transfer coefficient to be averaged. This method was considered more accurate than the initial approach.

PDEase2D simulations were carried out for a 260mm x 91mm thick block of Tylose with the left and right sides insulated by a 20mm and 40mm layer of Styrodur respectively (but the thermal conductivity of the Styrodur was multiplied by a factor of 1.72 to account for the third dimension edge effect). A 6mm sheet of polycarbonate was modelled as being

in place on the top and bottom surfaces thereby matching the box construction. The right side convective heat transfer coefficient was set to 5 $Wm^{-2}K^{-1}$ as in chapter 4, and the top surface heat transfer coefficient to the oil bag was varied.

The predicted data were compared to four sets of measured data for blocks with no voids (duplicate sets at high and low surface HTC's). The sum of the squared differences between the measured and predicted $\ln Y_c$ values at eighteen evenly spaced time intervals over the course of the experiment were minimised to find the estimate of surface heat transfer coefficient. The low and high heat transfer coefficients were estimated to be (11.2 and 14.2) and (26.2 and 33.0) $Wm^{-2}K^{-1}$ respectively.

Although the values for each HTC appear quite different, the measured temperature profiles for these runs actually matched each other closely meaning the temperature-time predictions were not particularly sensitive to uncertainty in the external HTC's. The mean low and high heat transfer coefficients were calculated to be 12.7 and 29.6 $Wm^{-2}K^{-1}$.

The validity of these mean values was checked by re-simulation of the measured data using the mean HTC. The percentage difference in times for one $\ln Y_c$ reduction are given in Table 5.4. All four simulations showed good agreement (within ±0.8°C at all times) between measured and predicted temperatures. The mean HTC estimates were used in all subsequent predictions of the blocks containing triangular voids.

Table 5.4 Percentage difference between measured and predicted times for one $\ln Y_c$ reduction for runs with no voids

Run No.	Surface Heat Transfer Coefficient (W/m^2K)	% Difference
1	12.7	-4.6
3	12.7	-1.2
2	29.6	+4.2
4	29.6	+1.7

The approximate values of *Bi* from the new estimates of high and low HTC were 5.4 and 2.3 respectively (assuming a 90mm thick infinite slab of Tylose cooled from one surface only using the appropriate heat transfer coefficient value).

5.5 Prediction of Cooling Rates for Packages Containing Triangular Filled Voids

Twenty-eight simulations were carried out using PDEase2D, and the simulation conditions and system input data from sections 5.2 and 5.4. Exact measurements for each box and void size were used in each run, not the nominal sizes. An example of the grid created by PDEase2D is given in Figure 5.10. The black lines represent x and y coordinates, the blue lines are material boundaries, the green lines are element boundaries (nodes occur at all element vertices) and the red lines indicate where further refinement of the grid is occurring (note the finer mesh near the edges of the top and right-hand surfaces where temperature changes are occurring much faster than the rest of the sample). The temperature vs. time profiles at position A and position B were collected because these positions corresponded to two thermocouple positions used in the experiments. Measured and predicted data were compared at position A where possible, however in runs with samples containing 20mm high voids data were compared at position B due to a defective thermocouple at position A.

Typical measured and predicted $\ln Y_c$ vs. time plots for samples with each different void size and with high and low heat transfer coefficients are shown in Figures 5.11-5.18. Table 5.5 gives a summary of the measured and predicted times for one $\ln Y_c$ reduction. The mean absolute percentage difference is 4.7% with a standard deviation of 4.4%. This indicates good agreement within the expected experimental error. However, the plot of percentage difference vs. void size (Figure 5.19) shows a trend in the difference between measured and predicted data as void size increases. There were several reasons why this was likely to happen. Firstly, any errors in the estimated boundary edge heat transfer would have more effect on blocks that take longer to cool. The measured data showed that increasing void height lengthened cooling time, making errors arising from the approximations in representation of boundary edge heat transfer effects more significant. This hypothesis was supported by the fact that the percentage difference between measured and predicted times for 50mm high voids was consistently larger at low heat transfer coefficients (where the sample took longer to cool). Secondly, as void height increased the proportion of top surface area made up by Tylose decreased significantly and any error in the measurement of this surface area (which was an input variable to the simulations) would severely affect the predicted time in a systematic fashion.

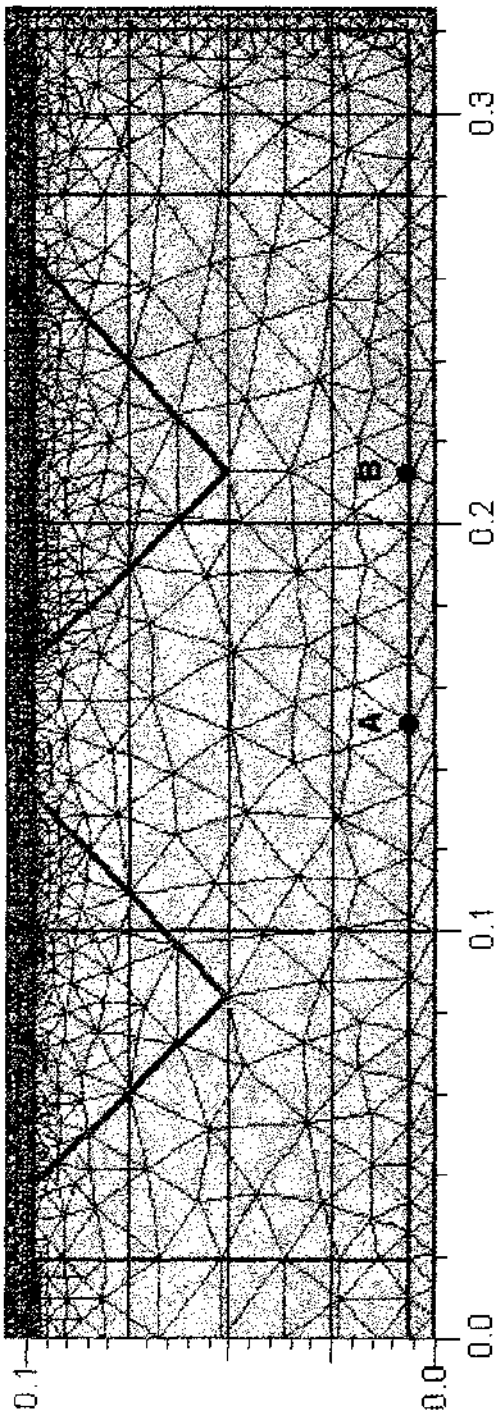

Figure 5.10 Example of the grid created by PDEase2D

Figures 5.11-5.18 Plots of $\ln Y_c$ vs. time for measured and predicted data from blocks with filled voids *(measured = blue, predicted = pink)*:

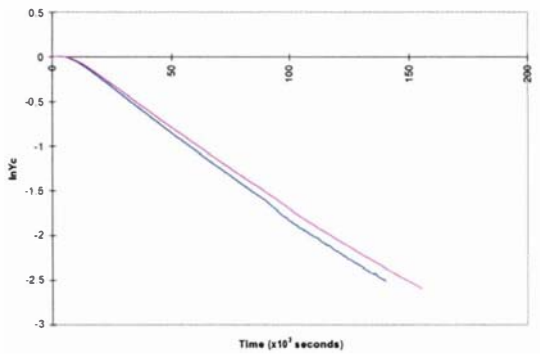

Figure 5.11 - 20mm voids, high HTC (Run 2)

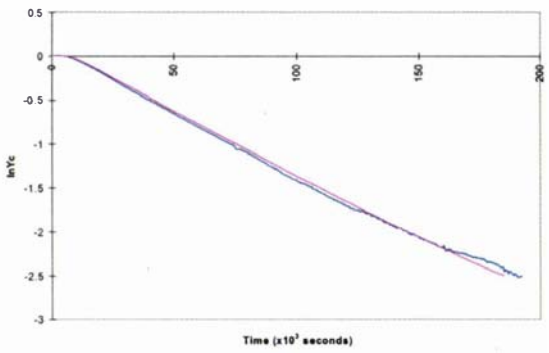

Figure 5.12 - 20mm voids, low HTC (Run 1)

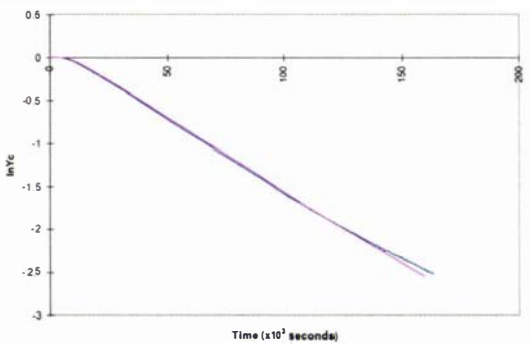

Figure 5.13 - 30mm voids, high HTC (Run 9)

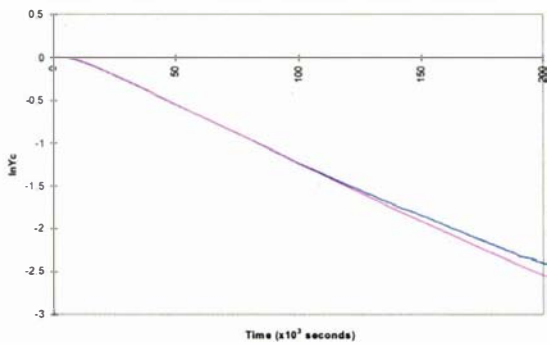

Figure 5.14 - 30mm voids, low HTC (Run 6)

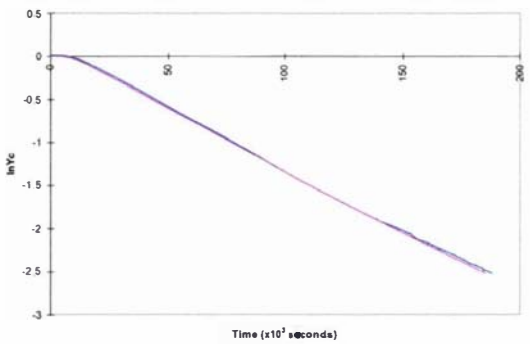

Figure 5.15 - 40mm voids, high HTC (Run 15)

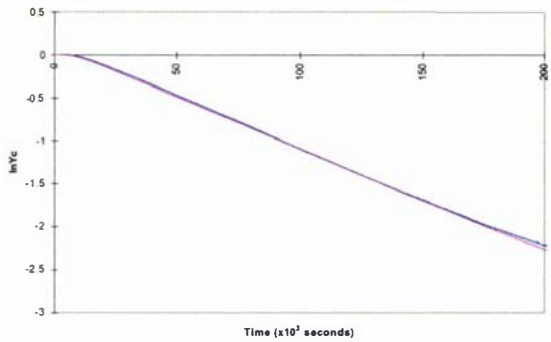

Figure 5.16 - 40mm voids, low HTC (Run 11)

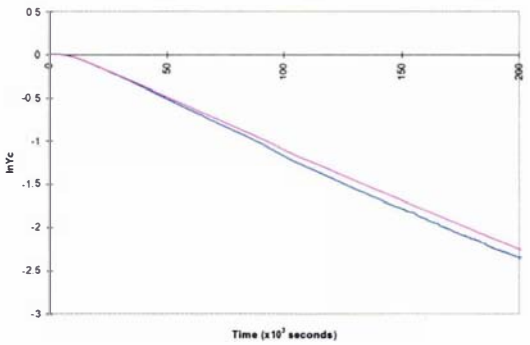

Figure 5.17 - 50mm voids, high HTC (Run 5)

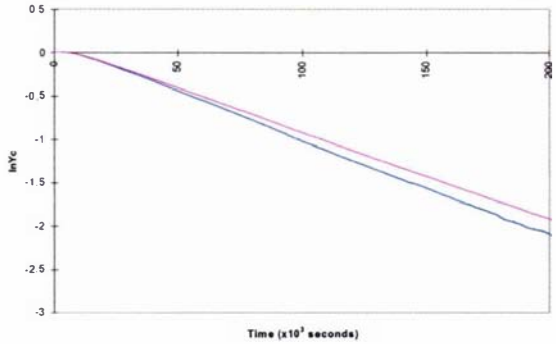

Figure 5.18 - 50mm voids, low HTC (Run 6)

Table 5.5 Measured and predicted times of one $\ln Y_c$ reduction for blocks with triangular filled voids

Run No.	Void Height (mm)	HTC	Measured time (x 10^3 seconds)	Predicted time (x 10^3 seconds)	% difference
2	20	High	50.4	53.7	6.5
4	20	High	54.4	53.4	-1.8
1	20	Low	66.1	67.5	2.1
3	20	Low	65.7	68.2	3.8
5	30	High	58.4	57.9	-0.9
7	30	High	58.3	57.7	-1.0
9	30	High	57.5	57.7	0.3
16	30	High	58.3	57.4	-1.5
6	30	Low	75.8	72.5	-4.4
8	30	Low	69.7	72.3	3.7
15	40	High	66.2	67.8	2.4
16	40	High	66.2	67	1.2
11	40	Low	80.9	82.3	1.7
12	40	Low	77.4	82.4	6.5
5	50	High	77.1	81.5	5.7
7	50	High	75.9	82.9	9.2
9	50	High	77.3	82.9	7.2
10	50	High	77.4	82.6	6.7
10	50	High	74	79.5	7.4
13	50	High	74.8	79.5	6.3
13	50	High	75.5	82.6	9.4
15	50	High	77	80.1	4.0
6	50	Low	88.2	98.2	11.3
8	50	Low	90.2	98	8.6
11	50	Low	87.3	94.4	8.1
12	50	Low	88.2	94.5	7.1
14	50	Low	85.4	97.1	13.7
14	50	Low	86.8	94.2	8.5

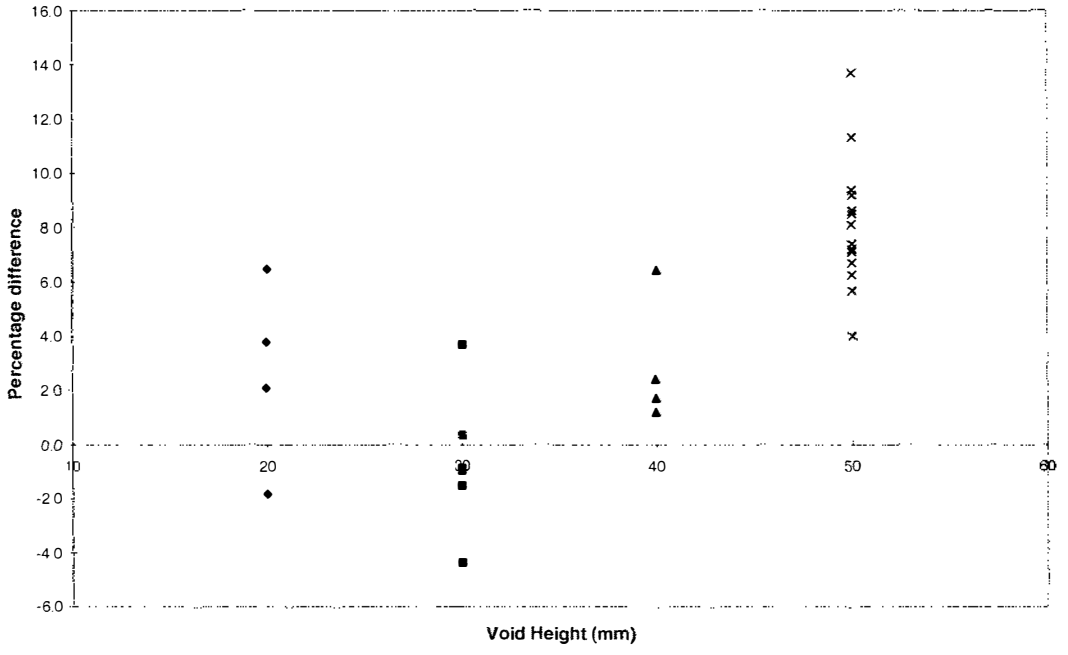

Figure 5.19 Plot of percentage difference between measured and predicted times vs. void height

5.6 Prediction of Cooling Rates for Packages Containing Triangular Air Voids

The finite element model was used to predict the cooling rates of Tylose blocks containing triangular voids filled with air but assuming the air was still. In the simulations, the thermal conductivity and specific heat capacity of the void was changed to that of still air (the properties of still air are given in Table 5.6), and radiation heat transfer between the walls of the void was not included in the model. Twenty-eight runs were carried out using PDEase2D with the system input data that were estimated in sections 5.2 and 5.4. Changing the voids from the thermal properties of Styrodur to those of still air made little change in the predicted cooling rate of the blocks. The largest difference in predicted times for one $\ln Y_c$ reduction between blocks with Styrodur-filled voids and blocks with still air voids was -3.5 % (Figure 5.20 is a $\ln Y_c$ vs. time plot for these two data sets). The initial purpose of filling the voids with Styrodur was to simulate an enclosure containing still air with no radiative heat transfer. The fact that little difference was predicted between these two treatments means that the methodology now allowed the effect of natural convection and radiation to be quantified. The predicted times for one $\ln Y_c$ reduction of blocks containing triangular still air voids are not

presented here as results were close to the same as those predicted for blocks containing triangular filled voids (to within an uncertainty of -3.5 %), already given in Table 5.5.

Table 5.6 Thermal and physical properties of air (from Perry & Green, 1984)

T (K)	ρ (kg m^{-3})	c (J kg^{-1} K^{-1})	k x 10^{2} (W m^{-1} K^{-1})	μ (μPa s)	ν x 10^{5} (m^{2} s^{-1})	α x 10^{5} (m^{2} s^{-1})
250	1.4133	1005.4	2.2269	15.991	1.1315	1.5672
260	1.3587	1005.4	2.3080	16.503	1.2146	1.6896
280	1.2614	1005.7	2.4671	17.503	1.3876	1.9448
300	1.1769	1006.3	2.6240	18.464	1.5689	2.2156
320	1.1032	1007.3	2.7785	19.391	1.7577	2.5003

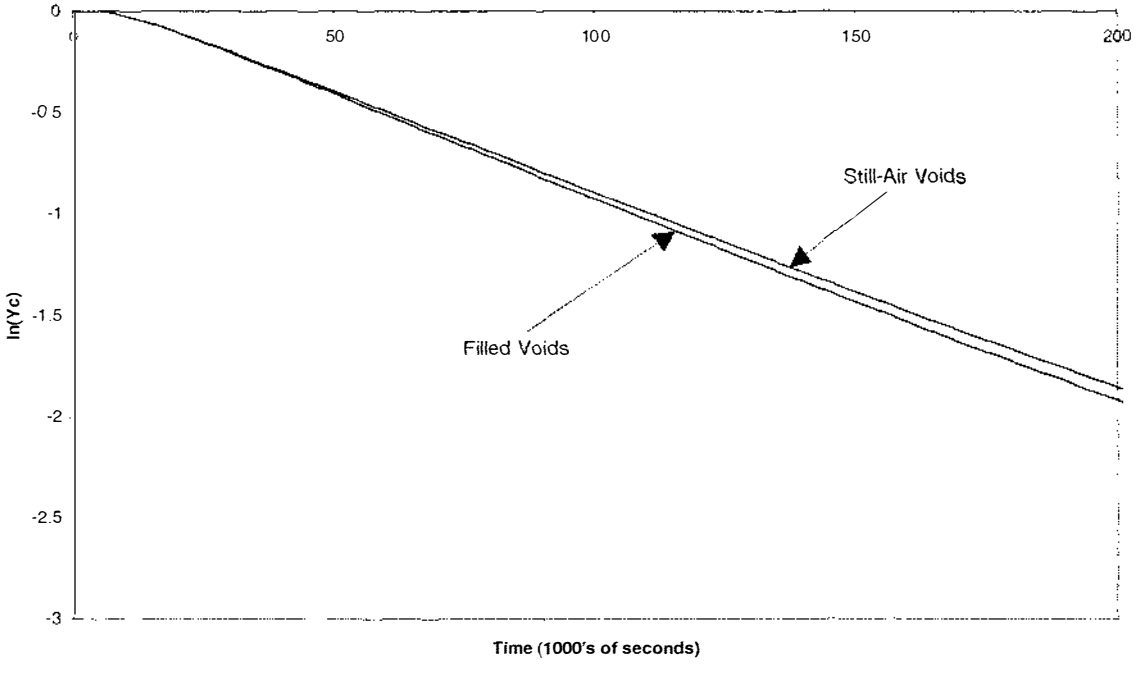

Figure 5.20 Comparison of predicted lnY_c vs. time plots for a Tylose block containing filled voids and still-air voids (HTC = 12.7 W m^{-2} K^{-1})

Most of the predicted times for one lnY_c reduction in blocks containing still air and excluding radiation heat transfer were significantly greater than the measured values. This was expected, and the difference could now be attributed to the combined effects of natural convection and radiation as all other heat transfer effects had been accounted for.

5.7 Estimating the Effective Thermal Conductivity of Triangular Air Voids

Having demonstrated that the greater rate of heat transfer would be attributed to natural convection and radiation, the combined effect could be quantified as an 'effective' thermal conductivity for the void. This was the thermal conductivity that immobilised air in the void would have to have if the cooling rate of the block was to be the same as the experimental values. The effective thermal conductivity would be an indicator of the extent of radiation and natural convection effects. The thermal conductivity of the air within the voids was altered on a trial and error basis until the predicted and measured data matched.

The effective thermal conductivity of the triangular air voids was to be evaluated for various void sizes exhibiting a range of temperature differences across the voids. It was known that the walls of different void enclosures cooled at different rates, which gave different wall temperature distributions at different time ranges over the course of the trials and by inference effective thermal conductivity would vary with time. Thus the mean effective thermal conductivities were evaluated over six different time ranges which approximately corresponded to five equal step changes in the mean Tylose void wall temperature. The time ranges used were: 0-18000 seconds, 18000-43200 seconds, 43200-72000 seconds, 72000-129600 seconds and 129600-180000 seconds.

The mean effective thermal conductivity of different sized air voids for each time range was obtained by multiplying the thermal conductivity of still air by a factor that was equivalent to the Nusselt number, *Nu* (given by equation 5.9).

$$Nu = \frac{k_{eff}}{k_{air}} \tag{5.9}$$

where k_{eff} is the effective thermal conductivity of the air within the void (W m^{-1} K^{-1})
k_{air} is the thermal conductivity of still air (W m^{-1} K^{-1})

Iterative estimations using the same PDEase2D data files as in section 5.6 were performed. For each time range above, the value of *Nu* (to one significant figure) that gave the lowest sum of squared differences between measured and predicted centre temperature at ten evenly spaced time intervals was found. Table 5.7 shows the *Nu* values found for triangular air voids. Given the substantial amount of computation required to

refine the estimates, these are reported to the nearest whole number. The *Nu* values for 20mm high voids are not shown in Table 5.7 because there was no difference between the measured cooling rates for blocks with filled voids and blocks with air voids. All runs with 30mm high air voids were discarded from the analysis as they were considered suspicious in section 5.3, and the measured cooling rates of blocks with air voids were much lower than for blocks with filled voids.

The *Nu* value was expected to be larger toward the beginning of the trials (because of the high temperature differences across the void) and to decrease as the Tylose block cooled. Also larger *Nu* values were expected at larger void sizes, for voids cooled from above and for voids cooled with a high heat transfer coefficient.

Table 5.7 *Nu* values for triangular air voids estimated by matching the measured and predicted data

Run No.	**Void Type**	**HTC**	**⇒ 18000s**	**⇒ 43200s**	**⇒ 72000s**	**⇒ 129600s**	**⇒ 180000s**
16	40 a	high	11	6	5	4	2
15	40 b	high	3	2	2	2	2
7	50 a	high	12	6	7	6	3
5	50 b	high	4	4	4	4	2
12	40 a	low	11	7	5	4	2
11	40 b	low	6	4	4	3	2
8	50 a	low	11	7	7	7	3
6	50 b	low	6	5	5	5	2

where 'void type' refers to the height of the void in mm, and whether the block is cooled from above (a) or below (b) e.g. 40a is a block with 40mm high voids, cooled from above.

5.8 Finding a Relationship Between *Ra* and *Nu* for Triangular Air Voids

The mean void wall temperatures during each time range were estimated from the difference in thermocouple readings at the centre of the cold wall and at the vertex between the two hot walls of the enclosure (shown in Figure 5.21). These mean wall temperatures were then used as estimates of the mean air temperature in the void using equation 5.10, for each void type and during each time range. The mean void air temperature (T_{mv}) in each time range was then used to estimate the volumetric expansion coefficient (β) using equation 5.11, and to linearly interpolate values of kinematic viscosity (v) and thermal diffusivity (α) from Table 5.6 (Perry & Green, 1984).

$$T_{mv} = \frac{T_1 + T_2}{2} \tag{5.10}$$

where T_{mv} is the estimated mean air temperature in the void (°C)
T_1 is the mean hot wall temperature over a given time range (°C)
T_2 is the mean cold wall temperature over a given time range (°C)

$$\xi = \frac{1}{T_{mv}} \tag{5.11}$$

where ξ is the volumetric expansion coefficient (K^{-1})

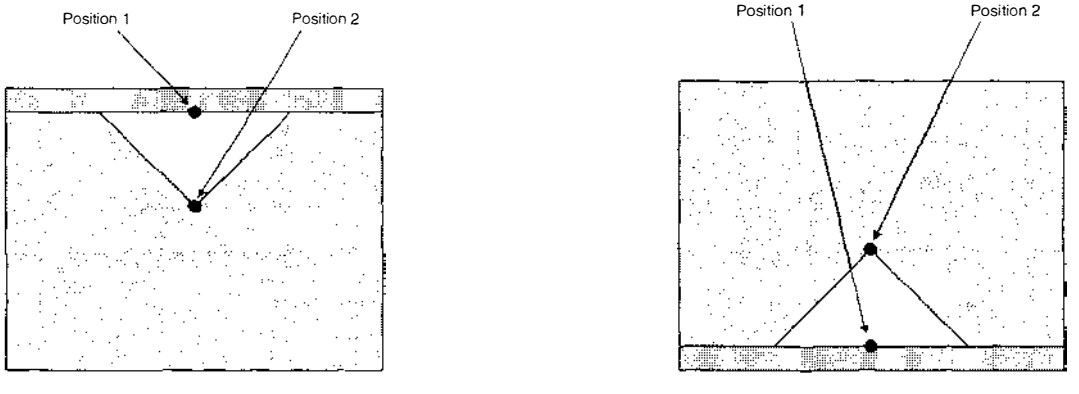

a) Cooled from above b) Cooled from below

Figure 5.21 Diagram of transverse void positions for triangular voids cooled from above and below

The mean Rayleigh number (*Ra*) for each void type during each time range could then be estimated using equation 5.12 or 5.13.

$$Ra = Gr \times Pr = \frac{\xi g(T_1 - T_2)x^3}{v\alpha} \tag{5.12}$$

where x is the characteristic dimension of the enclosure (m)

v is the kinematic viscosity ($m^2\ s^{-1}$)

α is the thermal diffusivity ($m^2\ s^{-1}$)

The thermal property values from Table 5.6 were substituted into equation 5.12 and a regression analysis was carried out, which yielded an R^2 value of 0.999. For air voids where the mean air temperature is between –13°C and 47°C:

$$Ra = 10^6 \times \exp\left(5 - 0.016\frac{T_1 + T_2}{2}\right) \times (T_1 - T_2) \times x^3 \tag{5.13}$$

Ostrach (1988) describes the two basic forms of internal natural convection that are generated by buoyancy - conventional and unstable convection (previously discussed in section 2.3 of the literature review). The density gradients of air within voids that were cooled from below were expected to be parallel to but in the same direction as gravity, and thus conventional or unstable natural convection were unlikely to occur. Therefore, heat transfer in the voids cooled from below occurred through conduction and radiation.

When radiation is expressed as pseudo-convection the heat transfer coefficient that represents its effect is included in *Nu*. This heat transfer coefficient is dependent on the absolute temperature of the void walls rather than on the temperature difference between the void walls. At the beginning of the cooling period all the void walls are hot, and they progressively cool over the course of the process. However, the maximum possible change in temperature was about 30K at an absolute temperature of about 300K, which would give a maximum change in the pseudo-convection heat transfer coefficient of about 25%. Thus, a weak relationship would be expected. Ideally, the relationship fitted to the experimental data would be between *Nu* and mean temperature in the void, but given the varying void wall temperatures it is not clear how the appropriate mean temperature should be determined. It was noted that the temperature difference across the void and the mean temperature in the void are related – high temperature differences occur only early

in the cooling process when the mean void temperature will be higher, and lower temperature differences occur when the mean temperature is lower. Hence, indexing *Nu* to temperature difference (part of *Ra*) rather than mean temperature might still lead to an adequate fit, especially when the considerable experimental uncertainty in the data of Table 5.7 are considered in relation to the small change in the pseudo-convection heat transfer coefficient. Although it had a lower physical basis, an approach relating *Nu* to *Ra* rather than mean void temperature was adopted so that the *Nu* vs. *Ra* relationships could be applied for voids cooled from above and below.

The mean *Ra* was plotted against the corresponding mean estimated *Nu* for each time range for voids that were cooled from below (Figure 5.22). The weak relationship that was expected between *Ra* and *Nu* was observed. This relationship could be modelled using any of several functional forms but the uncertainty in *Nu* justified only the use of linear regression for this case. The linear regression equation that gave the best fit to the measured data (shown as a solid black line in Figure 5.22) was:

$$Nu = 1.12\times10^{-5}\,Ra + 2.31 \qquad [R^2 = 0.31] \qquad (5.14)$$

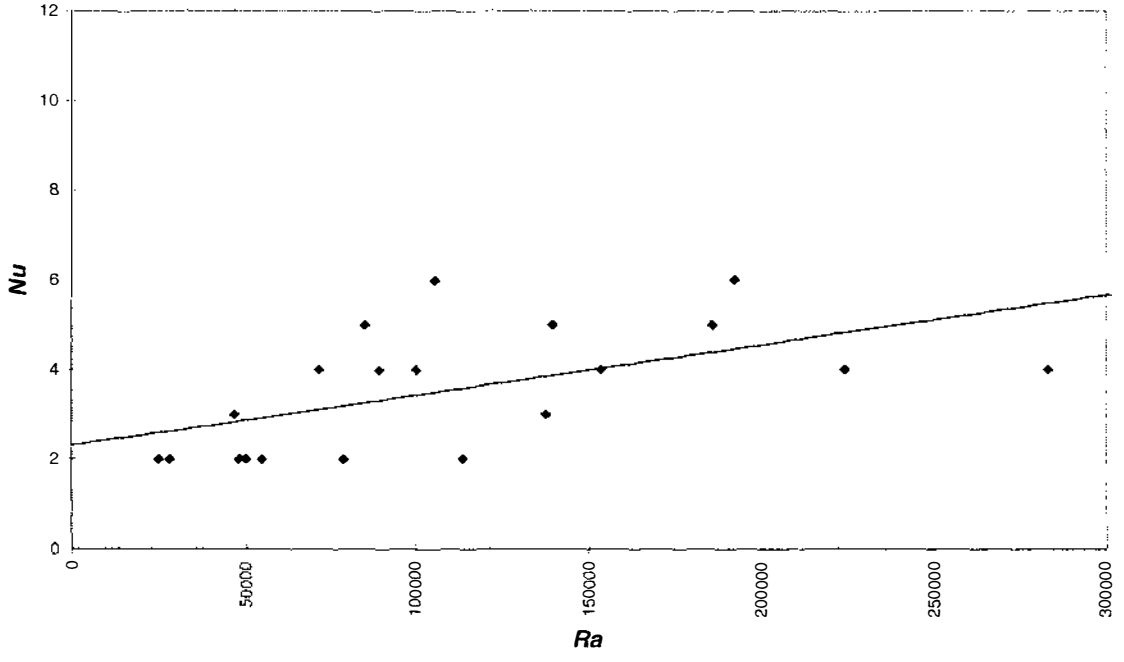

Figure 5.22 Plot of *Ra* vs. *Nu* for triangular voids cooled from below (conduction and radiation only)

The t-statistics on the constant and on the coefficient of the *Ra* term were 4.52 and 2.85 respectively (with corresponding P-values of 0.00026 and 0.011), which suggested that

both terms in equation 5.14 were significant. Equation 5.14 will be used in future models to account for heat transfer due to radiation in triangular-shaped air voids cooled from below.

The mean *Ra* was plotted against the corresponding mean estimated *Nu* for each time range for voids that were cooled from above (Figure 5.23). The air within voids cooled from above was expected to undergo natural convection. Natural convection theory (Hollands *et al.*, 1975) suggests a relationship between *Nu* and *Ra* given by:

$$Nu = aRa^n + b \tag{5.15}$$

where a is the effect of natural convection
b is the effect of conduction and radiation
n is a variable

The effect of conduction and radiation in triangular voids had already been estimated in equation 5.14. Thus substituting equation 5.14 as b in equation 5.15 gave:

$$Nu = aRa^n + 1.12\times10^{-5}Ra + 2.31 \tag{5.16}$$

A regression equation was then estimated by varying the values of a and n from equation 5.16 until the sum of squares difference from the measured data was minimised. The best-fit regression equation (shown as a solid black line in Figure 5.23) was:

$$Nu = 6.30\times10^{-4}Ra^{0.75} + 1.12\times10^{-5}Ra + 2.31 \qquad [R^2 = 0.42] \tag{5.17}$$

Arpaci (1986) showed that for horizontal flat plates the exponent on the *Ra* term in equation 5.17 would be expected to be close to but less than $^1/_3$. Other data for triangular enclosure shapes, either non-right-angled isosceles triangular voids heated or cooled from below with a hypotenuse-down orientation (del Campo *et al.*, 1988) or right-angled non-isosceles triangular voids heated from above with an opposite- or adjacent-down orientation (Akinsete & Coleman, 1982), showed that the exponent for a *Ra* vs. *Nu* correlation for natural convection may also be expected to be close to $^1/_3$ (for voids heated from below) or significantly lower than $^1/_3$ (for voids cooled from below). In order to test whether an n value of $^1/_3$ was statistically justifiable, n was set to $^1/_3$ and the best-fit equation was determined by changing the value of a in equation 5.16. The resulting regression equation (shown as a dotted black line in Figure 5.23) was:

$$Nu = 7.61\times10^{-2}\,Ra^{1/3} + 1.12\times10^{-5}\,Ra + 2.31 \qquad [R^2 = 0.30] \qquad (5.18)$$

By eye, regression equation 5.18 does not fit the measured data as well as equation 5.17 and the sum of squares difference from the measured data is worse. Therefore, equation 5.17 will be used in future models to account for heat transfer due to natural convection and radiation in triangular shaped air voids cooled from above.

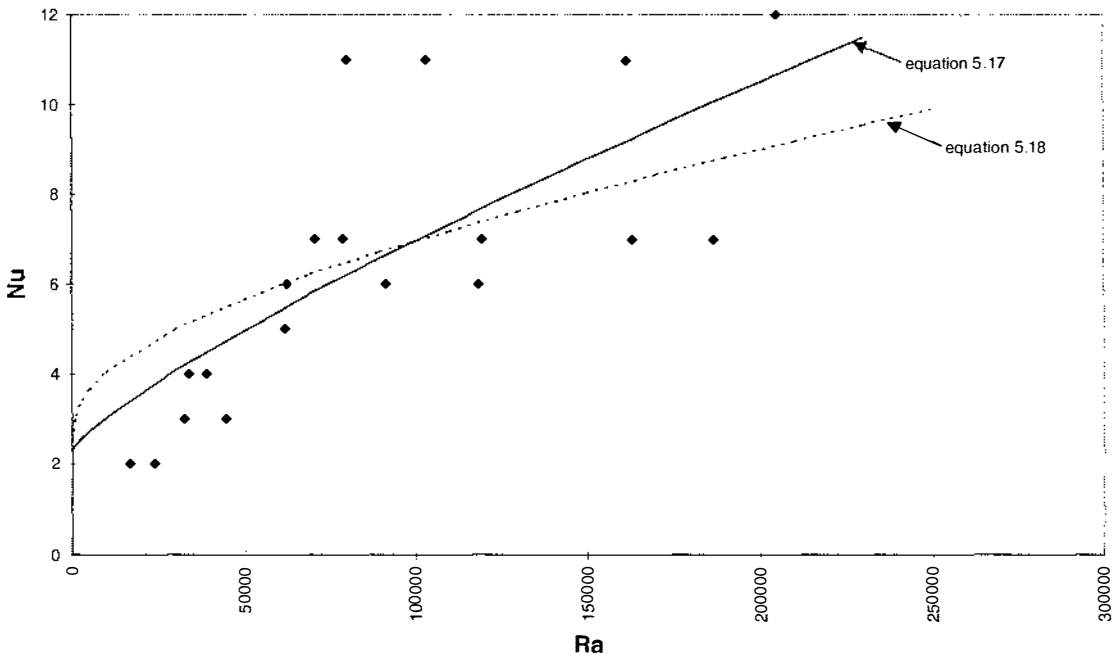

Figure 5.23 Plot of *Ra* vs. *Nu* for triangular voids cooled from above (conduction, radiation and natural convection)

As already discussed, the exponent on the *Ra* term in equation 5.17 was much higher than theoretical expectations. Thus it was recognised that the correlation for triangular air voids developed in this work may not be applicable to other general situations for three main reasons. Firstly, a mean value of *Nu* was used to account for conduction and radiation in a collective manner. Secondly, the non-traditional manner in which *Ra* was calculated was expected to have a significant effect. The value of *Ra* for a triangular void is conventionally calculated using the temperature difference between the hot and cold walls, where each wall is isothermal. However, in this work the void walls were not isothermal. An assumption was made to calculate effective values of *Ra* using the transverse void temperature differences. Therefore the values of *Ra* do not reflect the conventional *Ra* values found in the literature. Thirdly, the mean values of both *Ra* and

Nu were estimated over fairly long time ranges, which reduced the accuracy of each individual data point on Figures 5.22 and 5.23. These departures from convention limit the use of the correlation to predicting radiation and natural convection heat transfer within right-angled isosceles triangular shaped air voids that exist within food product packages. The correlation should not be used in other applications, nor is it recommended to be used outside the *Ra* range in which the empirical data was collected (i.e. do not use for Ra values greater than about $2x10^5$).

6. DEVELOPMENT AND TESTING OF A MODEL FOR PREDICTING HEAT TRANSFER DURING CHILLING OF PACKAGES CONTAINING HORIZONTAL RECTANGULAR VOIDS

6.1 Introduction

The simplified physical model, developed in chapter 3, was a two-dimensional rectangular food product package that may or may not have contained right-angle isosceles triangular shaped voids, or horizontal rectangular headspace voids, or some combination of these two shapes of void. Triangular voids have been investigated in chapters 4 and 5. Chapter 6 examines the effect that horizontal rectangular headspace voids have on the chilling rates of food product packages.

Edwards & Catton (1969) showed that for horizontal rectangular enclosures with height-to-width ratios less than 0.2, the lateral walls (whether insulated or conducting) have little influence on the natural convection within the enclosure. Such enclosures can be considered to have natural convection characteristics identical to that of an infinite horizontal layer of air. The smallest lateral dimension in a meat carton is 360mm, therefore a horizontal rectangular void would have to be 72mm high in order for the lateral walls to influence the amount of natural convection. It is highly unlikely that a horizontal rectangular void of this height would be found in a meat carton, thus the horizontal rectangular voids in this model were considered to behave in the same way as a horizontal layer of air.

Due to the large amount of published empirical data (e.g. Mull & Reiher (1930), Goldstein & Chu (1969), Hollands *et al.* (1975)) that has been collected to quantify the extent of steady state natural convection that occurs in horizontal layers of air, it was considered unnecessary to collect further data to aid empirical natural convection model development for voids of rectangular shape. Instead, an unsteady state finite element conduction model was adapted by using a published steady state empirical correlation to account for the natural convection within the horizontal rectangular enclosures. The correlation given by Hollands *et al.* (1975) for horizontal air layers cooled from above was chosen over others found in the literature because it covered the largest range of Ra and was the most accurate when compared with the measured data collected by Mull & Reiher (1930), Goldstein & Chu (1969), and Hollands *et al.* (1975). The correlation was:

$$Nu = 1 + 1.44\left[1 - \frac{1708}{Ra}\right]^{\bullet} + \left[\left(\frac{Ra}{5830}\right)^{1/3} - 1\right]^{\bullet} \qquad (6.1)$$

where a bracket $[\ ]^{\bullet}$ indicates that if the argument inside the bracket was negative, the quantity was to be taken as zero.

The modelling approach taken assumed a pseudo-steady state natural convection flow within the voids at each time step of the finite element method, i.e. the extent of natural convection was considered constant over the period of the time step, but re-evaluated at the start of each step. An effective thermal conductivity that gave the same total heat transfer resistance across the void, assuming only conduction occurred, was estimated. Thus the void could be modelled as having only conduction heat transfer across it. Wee & Pham (1990), in order to reduce computation effort in their numerical model of freezing a meat carton that contained a horizontal rectangular headspace void, also made this type of pseudo-steady state assumption. They decided that re-calculation of the entire flow field within a given time step was only necessary if a significant change occurred in the heat transfer coefficient between steps. Otherwise a quasi-steady state situation was assumed within the void until the next time step.

The effect of radiation heat transfer between the walls of the void was not included in the empirical correlations of Hollands *et al.* (1975). However the experiences reported in chapter 5 suggested that it was likely to be an important mode of heat transfer in the horizontal rectangular voids found within meat cartons. Thus the numerical model needed to explicitly account for it.

The numerical model incorporating these features was tested against measured data.

6.2 Selection and Development of Numerical Method

Making changes to PDEase2D (the program used in chapter 5) was not easily achievable because it was a commercial package, and the source code and calculation routines were inaccessible to the user. However FINEL, the finite element program used in chapter 4, did not have this problem. The source code was available and changes could be made. The altered version of FINEL is called FINELX hereafter.

6.2.1 Increasing the Capacity of FINELX

FINEL was an MS-DOS based program. The restricted memory available in MS-DOS limited the number of elements and nodes available in FINEL to 600 and 400 respectively. In order to increase the array sizes to better match those available in PDEase2D, FINELX was converted to C++ using Bell Labs' "f2c" conversion program, and ported to a Windows 95 32-bit system. This allowed much larger array sizes, as the number of elements and nodes were only (practically) limited by the increase in simulation time that large arrays would bring. The array sizes were therefore increased by a factor of ten, allowing 6000 elements and 4000 nodes.

6.2.2 Including Natural Convection in Air Voids based upon the Rayleigh Number

FINEL allowed simulation of heat conduction through objects that contained up to five different material types. The thermal properties of these materials could be dependent upon temperature, and they were calculated for each element at every time step. In FINELX the possible number of materials was increased to 20, where material numbers one to five were reserved for normal conducting solids, numbers six to fifteen represented properties for isosceles triangular air voids, and sixteen to twenty represented properties for horizontal rectangular air voids.

If the material number was less than or equal to five then FINELX treated the normal conducting solid material as FINEL would, where the properties depended upon the material type and the temperature of the nodes at the element vertices. However if the material number was greater than five the thermal properties of the void were calculated as a whole rather than for each element. The user was required to provide FINELX with the identities of the two nodes that best represented the two transverse points in the void. For a rectangular void these were the nodes where the largest temperature difference across the void occurred when assessed perpendicular to the product surface at the centre of the object. The positions and temperatures of the two selected nodes were then used to calculate the characteristic dimension, transverse void temperature difference, and mean void temperature at each time step. Since FINELX only dealt with voids that contained air, the mean void temperature (T_{mv}) and the transverse void temperature difference at each time step were all that were required to calculate the Rayleigh number (Ra) of the void (using equations 5.10 to 5.12). The Nusselt number (Nu) for a rectangular void was found by using equation 6.1.

To ensure that the value of *Ra* was never zero (causing equation 6.1 to become undefined) FINELX never allowed the transverse void temperature difference to be less than 0.01°C. For typical air void sizes this temperature difference was small enough to ensure that a negligible amount of heat transfer due to natural convection was predicted in that case.

The effective thermal conductivity of the air, representing the effects of natural convection, was then calculated by equation 6.2. Since the effective thermal conductivity was treated as constant over a whole void, the thermal conductivity of all elements within a void was the same.

$$k_{nat\ conv} = Nu \times k_{air} \tag{6.2}$$

where $k_{nat\ conv}$ is the thermal conductivity of air including natural convection ($Wm^{-1}K^{-1}$)
k_{air} is the thermal conductivity of still air ($Wm^{-1}K^{-1}$)

6.2.3 Including Radiation Heat Transfer in Rectangular Voids

FINELX did not allow boundaries internal to the object. Therefore, radiation heat transfer internal to the object was modelled by defining an equivalent heat conduction process that transferred heat at the same rate. Foust *et al.* (1960) state the equation for the net rate of radiative heat flow from a surface (equation 6.3) where the surface was assumed to be a grey body and isothermal.

$$(\phi_r)_{net} = \varepsilon\sigma A_1 (T_1^4 - T_2^4) \tag{6.3}$$

where $(\phi_r)_{net}$ is the net rate of radiant-energy transfer from a surface (W)
ε is the emissivity of the surface
σ is the Stefan-Boltzmann constant (5.67×10^{-8} W m^{-2} K^{-4})
A_1 is the area of the surface (m^2)
T_1 is the temperature of surface (K)
T_2 is the temperature of the surrounding surfaces (K)

Equation 6.3 holds true if none of the emitted radiation returns to the surface and if the surrounding surfaces are all at the same temperature (T_2). However this is not always the case so view factors, relating the net fraction of radiant energy intercepted by each surrounding surface to the total radiant energy emitted by the surface, are often used instead of a surface emissivity value.

For reasons of simplicity, radiation heat transfer within a rectangular void was assumed to occur only between the top and bottom surfaces (i.e. radiation heat transfer to the sides and ends of the void was ignored). For the case of two parallel plates with large surface areas compared to the clearance between them, Perry & Green (1997) state the equation to estimate the view factor:

$$F_{1\to 2} = \frac{1}{\frac{1}{\varepsilon_1} + \frac{1}{\varepsilon_2} - 1} \tag{6.4}$$

where $F_{1\to 2}$ is the view factor between surfaces 1 and 2

ε_1 is the emissivity of surface 1

ε_2 is the emissivity of surface 2

The net rate of radiant-energy transfer between surfaces 1 and 2 is now given by:

$$(\phi_r)_{net\ 1\to 2} = F_{1\to 2}\sigma A_1 (T_1^4 - T_2^4) \tag{6.5}$$

Since the user had already specified the transverse void nodes within the FINELX data file (to account for natural convection effects) the values of T_1 and T_2 could be recalled by the program. In order to model the radiation heat transfer as pseudo-conduction (in the same way as natural convection), the expression for steady state heat transfer by conduction through an infinite slab of thickness x was used:

$$\phi_r = \frac{k_{rad} A_1}{x}(T_1 - T_2) \tag{6.6}$$

where k_{rad} is the effective air thermal conductivity to include radiation (W m^{-1} K^{-1})

Equations 6.5 and 6.6 were solved for k_{rad} giving:

$$k_{rad} = F_{1\to 2}\sigma x\left(T_1^2 + T_2^2\right)\left(T_1 + T_2\right) \tag{6.7}$$

Hence, the overall effective thermal conductivity of air ($k_{overall}$) that accounted for natural convection and radiation effects within a rectangular void was:

$$k_{overall} = k_{rad} + k_{nat\ conv} \tag{6.8}$$

$k_{overall}$ was applied to all elements with a material number between 16 and 20.

6.2.4 Constructing Spatial Grids for FINELX

Manual grid construction for FINEL was described in chapter 4. This experience showed that for the required fineness of spatial grids, and the large number of elements and nodes necessary to accurately model voids within packages, manual grid construction was an uneconomical use of time. Instead, an independently developed piece of software was used to construct all further grids. This program was called BAMG (Bi-dimensional Anisotropic Mesh Generator) version 0.58. It was developed by Frederic Hocht, INRIA, France in October 1998 and was free to download from the Internet. This software created a triangular mesh within an outline geometry specified by the user. The user could vary the fineness of the mesh around the vertices of the object, and could also specify the identity number of any sub-region within the object. The mesh size control feature was used to allow finer meshing in areas where temperature change was likely to be more rapid, and the sub-region definition feature was used to identify the different material types within the object.

The fully meshed output files from BAMG were in a similar format to the node and element arrays within the input data files used by FINELX. After only minor format adjustments, the input data files for FINELX could be completed by the addition of thermal property data, initial and boundary conditions, and time step information.

6.2.5 Testing the Natural Convection and Radiation Calculations within FINELX

In order to test whether FINELX was plausibly accounting for natural convection and radiation within rectangular voids two qualitative tests were carried out.

The first test compared the temperature-time predictions of two FINELX data files - *file A*, a 260mm x 90mm block of Tylose with a 30mm high rectangular headspace air void and a 6mm thick top layer of polycarbonate initially at 30°C, cooled from the top only, with a surface heat transfer coefficient of 30 $W\ m^{-2}\ K^{-1}$ at an ambient temperature of 0°C. Natural convection within the void was allowed but the view factor was set to a value of zero to prevent radiation heat transfer. *File B* was identical to *file A* except that the headspace void was considered to be filled with a solid that had the same thermal

properties as still air, i.e. no natural convection was accounted for in *file B*. The times for one $\ln Y_c$ reduction for the two treatments are given in Table 6.1. The difference in cooling time was due to the presence of natural convection.

The second test also compared the temperature-time predictions of two FINELX data files - *file B* (as above), and *file C* (identical to *file B* except the view factor of the void was set to a value of one instead of zero). The times for one $\ln Y_c$ reduction for the two treatments are also given in Table 6.1. The difference in cooling time between these two simulations was that arising from radiation.

In order to achieve a satisfactory ongoing energy balance during simulations using the test files given above, i.e. a discrepancy of less than 1% over the course of the 200000 second simulation, a time step of 10 seconds was required. This time step size was used in all further simulations using FINELX, and all results presented by the author in this work were confirmed to have achieved a satisfactory energy balance.

Table 6.1 Comparison of predicted times for one $\ln Y_c$ reduction of blocks containing rectangular voids with and without natural convection and radiation heat transfer (x 10^3 seconds)

Treatment	Times for one $\ln Y_c$ reduction
File A (natural convection only)	94.8
File B (no natural convection or radiation)	490.7
File C (radiation only)	46.4

The data in Table 6.1 indicated that natural convection and radiation effects were being accounted for, and that testing could proceed to establish whether the modelled rates of radiation and natural convection accurately represented reality.

6.3 Experimental Methodology for Model Testing

An experimental methodology similar to that in chapter 5 was used to test the model for packages containing only horizontal rectangular headspace voids. Once again Tylose MH1000 was chosen to be the test substance because its thermal properties were well-known and similar to that of lean beef.

In the review of literature (chapter 2), the numerical simulations of Wee & Pham (1990) indicated significant natural convection occurred within horizontal rectangular headspaces that were as little as 1.0mm deep. Therefore it was considered necessary to be able to accurately construct even and level headspaces of only a few millimeters in height.

Two identical Tylose blocks (approximately 260 x 360 x 90mm) were made up within a polycarbonate box sample holder (Figures 6.1 and 6.2). All edges of the Tylose blocks were insulated with 40mm thick Styrodur polystyrene in order to reduce the heat transfer through the sides, ends, and between the blocks. For the runs with no voids the polycarbonate lid of the box was in direct contact with the top surface of the Tylose. In other runs, the samples contained a horizontal rectangular headspace between the polycarbonate lid and the Tylose block, created by using Styrodur walls of a known height.

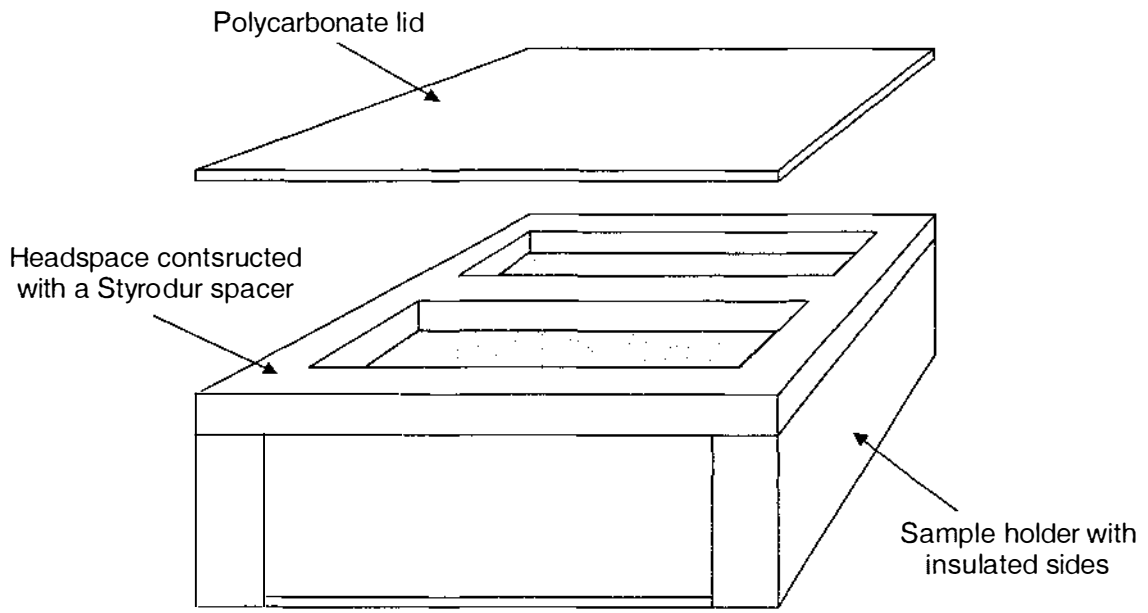

Figure 6.1 Diagram of a sample holder containing rectangular horizontal voids

Care was taken to ensure that a flat even surface on the top of the Tylose block was obtained. The flatness of the surface was examined before each run and restored to level, if necessary, by the placement of a flat block of Styrodur upon the Tylose surface with an evenly dispersed 20kg of weight on top of the Styrodur block for several hours. A layer of polyethylene approximately 0.03mm thick was placed over the Tylose blocks to stop any moisture loss from the samples. Thermocouple positions are shown as dots in Figure 6.2.

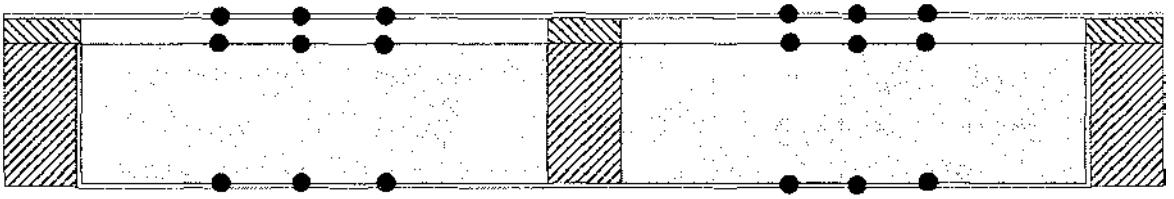

Figure 6.2 Side elevation of a sample holder containing rectangular horizontal voids

6.3.1 Accounting for Radiation Heat Transfer in Rectangular Voids

For a horizontal rectangular void with a Rayleigh number less than 1708 (typical of an air filled void less than 5mm high with a transverse void temperature difference of 30°C), there is no heat transfer attributable to natural convection (Hollands, 1984). Therefore all heat transfer occurs through conduction and radiation only. For a 90mm thick semi-infinite slab of Tylose with a 5mm high horizontal rectangular void above it, initially at a uniform temperature of 30°C and cooled with a HTC of 20 $Wm^{-2}K^{-1}$ and a cooling medium temperature of 0°C, a series of steady state calculations using analytical solutions suggested that up to 60% of the total heat transfer could be due to radiation (assuming a view factor of 1 between the opposing surfaces of the rectangular void). This was considered to be significant enough to suggest that experimental estimation of the view factor of the void surfaces was required for accurate modelling of packages containing horizontal rectangular voids.

Figure 6.2 shows that the top surface of the horizontal rectangular voids was made of polycarbonate. Polycarbonate is transparent and thus a certain amount of transmittance of radiation was expected. To investigate the extent of this effect each run was repeated with the top and bottom surfaces of the void painted black (in order to eliminate any transmittance). For some of the runs only the voids above one of the two blocks within a sample holder were blackened. This meant that both treatments (one block with, and one without, transmittance) could be run simultaneously within the same sample holder.

6.3.2 Experimental Apparatus and Design

Four different rectangular void heights were used for the trials (nominally 0, 5, 10, and 30mm, but each height was confirmed by measurement on a run by run basis). Runs with blocks containing no voids (i.e. 0mm high) were carried out in order to determine the surface heat transfer coefficient. The blocks with nominal 5mm high voids were to be used to determine the extent of radiation heat transfer (explained above). The 10mm and

30mm void heights were chosen to align with those used by Wee and Pham (1990) and with those typically found in bulk-pack and primal cut meat cartons (as assessed from video footage of carton cross-sections from an unrelated study by MIRINZ Food Technology and Research, Ltd.). Two separate sample holders were constructed to allow one to re-equilibrate to the initial temperature while the other was used for an experiment.

The sample holders were cooled from the top surface only using the same custom plate cooler as in chapters 4 and 5. Rather than use oil bags, an extra layer of aluminium plating was placed on top of the slightly warped cooler plates in order to ensure they were flatter for the trials. This method was chosen because during the work described in chapter 5 accurate measurement of the oil bag temperature had proved more difficult than expected. The top plate contained alcohol at approximately 0°C which was circulated and cooled by a Julabo FPW65-MS low temperature bath that was operating on an internal set point. The bottom cooler plate was covered with Styrodur insulation to reduce any heat loss from the bottom of the sample holder. The bottom plate also contained alcohol and was connected to a separate Julabo Ultra-temp FP40 controlled temperature bath system. A Hewlett-Packard HP3497A externally controlled the temperature of this bath so that the readings of two thermocouples within the insulation on the bottom plate stayed within 0.1°C of the mean temperature at the bottom of the sample. This effectively created a zero heat flow or symmetry condition at the bottom of the sample holder (Figure 6.3), and thus allowed the bottom of the sample to be considered the thermal centre. The initial temperature of the sample was approximately 30°C. The runs were started before construction of all sample holders was complete so the order in which the runs were performed could not be randomised. However random selection of runs within the available samples at any time was carried out.

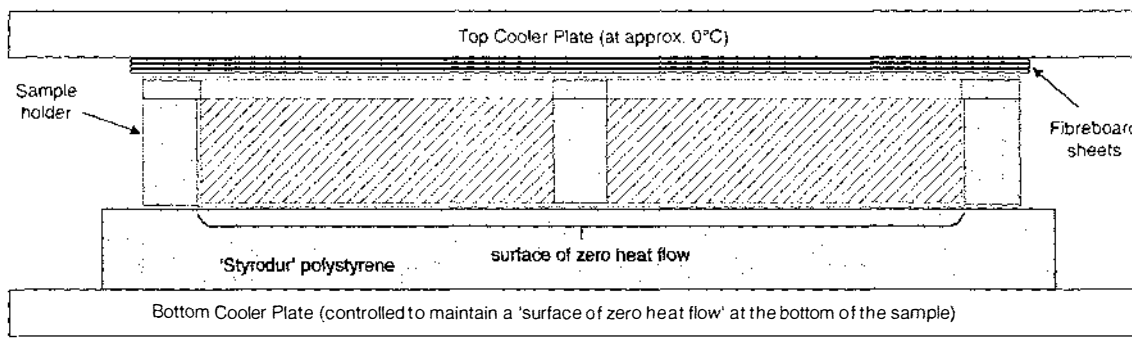

Figure 6.3 Diagram of sample holder arrangement within the plate cooler

All temperatures were measured with T-type copper/constantan thermocouples that had been calibrated to 0°C using an ice bath and a RT200 reference thermometer (200 Ohm

platinum resistor). Figure 6.2 shows that for each Tylose block, three thermocouples were positioned on the interface of the bottom layer of polycarbonate and Tylose - close to the thermal centre. Six thermocouples were also positioned on the opposing surfaces of the horizontal rectangular void - three on the top surface of the Tylose block, and three on the underside of the polycarbonate lid. The readings of the thermocouples on the void surfaces may have been slightly differently influenced by radiation than the Tylose surface itself, so they were not compared to predicted Tylose surface temperature data. Another two thermocouples measured the top plate temperature directly where the plate surface was in contact with the sample. The temperature of the insulation on the bottom plate, and the internal air temperature of the cooler were also measured in duplicate. All fifteen thermocouples were attached to the Hewlett-Packard HP3497A data logging system, which was connected to an IBM-compatible personal computer running MS-DOS and a logging and analysis program, called MIRLOG (developed at MIRINZ Food Technology and Research Ltd.).

Sample holders were cooled at one of two different top surface heat transfer coefficients. The difference in HTC was achieved by placing either one or three sheets of fibreboard between the sample holder and the top cooler plate. Contact integrity between the plate and the sample holder was maintained by placing an even load of 100 kg on top of the movable top plate. A total of 10 runs were carried out for the trials as shown in Table 6.2.

Table 6.2 Treatment table for trials with horizontal rectangular voids

Run No.	Void height (mm)	Left side of holder	Right side of holder	Fibreboard sheets	Run Order
1	0	no void	no void	1	3
2	0	no void	no void	1	1
3	0	no void	no void	3	2
4	0	no void	no void	3	5
5	5	transparent walls	filled void	3	4
6	5	blackened walls	filled void	3	6
7	10	blackened walls	transparent walls	1	7
8	10	blackened walls	transparent walls	3	9
9	30	blackened walls	transparent walls	1	10
10	30	blackened walls	transparent walls	3	8

6.4 Evaluation of Input Data

6.4.1 Sample Dimensions

Sample dimensions were measured using vernier calipers. Three measurements of the sample length, width and height were taken. Void height was measured by six readings of the height of the Styrodur walls. The coordinates of the thermocouple positions were measured in relation to the closest end of the sample. These measurements were considered to represent mean values to an accuracy of ± 1mm.

6.4.2 Thermal Property Data

The thermal properties of all materials used in this chapter are given in Tables 5.2 and 5.6.

6.4.3 Initial and Boundary Conditions

The Tylose blocks were assumed to be initially at a uniform temperature equal to the measured centre temperature at the start of each run. Boundary conditions were of the third kind, and thus estimates of the mean cooling medium temperature and the surface heat transfer coefficients were required.

6.4.3.1 Cooling Medium Temperatures

The cooling medium temperature was measured by two thermocouples positioned on the outer surface of the underside of the top cooler plate. Each thermocouple was laid within a small groove carved into the plate surface and held into position with a strip of aluminium adhesive tape. At any given time, the mean of the two thermocouple temperature readings was considered to give the best representation of the cooling medium temperature. At the start of each run the top cooler plate was warmed slightly by the sample (to about 1 to 1.5°C). The plate temperature decreased rapidly (by 1.5°C in the first two hours), and continued to decrease at a slower rate for the rest of the experiment (the rate was closer to about 0.1°C per 10 to 15 hours). In order to calculate Y values a constant cooling medium temperature is required. A logarithmically weighted mean was taken over the length of each experiment because the change in temperature was approximately exponential.

The air temperature inside the plate cooler was measured every 30 seconds at two different positions. The mean air temperature was calculated for each 30-second period.

Due to the approximately exponential decline of mean air temperature over time, a logarithmically weighted mean was taken over the length of each experiment.

6.4.3.2 Heat Transfer Coefficients

In chapter 5 the surface heat transfer coefficients were estimated by an inverse method that was first proposed by Bonacina & Comini (1972). The method matched predicted centre temperature profiles from numerical simulations to the measured profiles for blocks containing no voids, to estimate the surface heat transfer coefficients that gave the best fit. This method was considered more accurate than other estimation methods because it accounted for any temporal and/or positional variation in surface heat transfer coefficient, so it was used again for this trial.

Two-dimensional FINELX simulations were carried out on a 260mm x 90mm thick block of Tylose with the left and right sides insulated by a 20mm and 40mm layer of Styrodur respectively (the thermal conductivity of the Styrodur was increased by a factor of 1.72 to approximately account for the third dimension edge effect, as in chapter 5). The 6mm thick box of polycarbonate placed around the Tylose and insulation was included in the simulation. The right side convective heat transfer coefficient was set to 5 $Wm^{-2}K^{-1}$ (as in chapters 4 and 5), and the top surface heat transfer coefficient was varied from simulation to simulation.

The predicted temperature data were compared to measured data from four runs with blocks containing no voids (two duplicate sets - one set at high HTC and the other at low HTC). The sum of the squared differences between the measured and predicted $\ln Y_c$ values at eighteen evenly spaced time intervals over the course of the experiment was minimised to find the estimate of surface heat transfer coefficient. The high and low heat transfer coefficients were estimated to be (36.1 and 26.7) and (13.9 and 13.3) $W\ m^{-2}\ K^{-1}$ respectively.

Although the values for each HTC differed between runs, the measured temperature profiles for these runs matched closely with each other. The validity of the mean high and low heat transfer coefficients of 31.4 and 13.6 $W\ m^{-2}\ K^{-1}$ was checked by re-simulation of the no-void runs using FINELX. The percentage differences in times for one $\ln Y_c$ reduction are given in Table 6.3. All four simulations showed good agreement (within $\pm 0.6°C$) between measured and predicted temperatures at any time. The mean HTC estimates were used in all subsequent predictions of the blocks containing horizontal rectangular voids.

Table 6.3 Percentage difference between measured and predicted times for one $\ln Y_c$ reduction of blocks containing no voids

Run No.	Top Surface Heat Transfer Coefficient ($W\ m^{-2}K^{-1}$)	% Difference
1	13.6	-6.9
2	31.4	-0.6
3	13.6	-5.6
4	31.4	-2.0

The value of Biot number (*Bi*) could not be accurately determined because the effective thermal conductivity of the composite samples was unknown. However, as an approximate indication of the ratio of internal to external heat transfer, a 90mm thick infinite slab of Tylose cooled from one surface only with a heat transfer coefficient of 31.4 $Wm^{-2}K^{-1}$ or 13.6 $Wm^{-2}K^{-1}$ would have experienced a *Bi* value of 5.7 or 2.5 respectively.

6.4.3.3 View Factors for Radiation Heat Transfer in Rectangular Voids

The view factors within the rectangular voids were estimated using equation 6.4. Perry and Green (1997) state the emissivity of flat black paint as 0.96, so for rectangular voids where both the top and bottom surfaces were painted black the view factor was estimated to be 0.9 (to one decimal place). For rectangular voids that were unpainted the two radiating surfaces were Tylose and paper fibreboard. No emissivity data were available in the literature for Tylose, however since it is also translucent and is made up of ~75% water, the emissivity of water (0.95) was used (Perry and Green, 1997). Emissivity data for paper fibreboard was also unavailable in the literature; therefore the emissivity of thin paper (0.93) was considered to be the best existing estimate (Perry and Green, 1997). The view factor was calculated to be 0.9 (to one decimal place). The estimated view factors were calculated to an accuracy of one decimal place only due to the approximations required by the lack of comprehensive emissivity data in the literature.

No significant difference was observed between the measured cooling times for blocks containing air voids with transparent (unpainted) walls and the measured cooling times for blocks containing air voids with blackened (painted) walls (Table 6.4). This agreement adds support to the similar values of view factor estimated above. In further analysis of the data, the two treatments (voids with blackened walls, and voids with

transparent walls) were considered to be replicate data. Based on these replicates there was 95% certainty that any measured value was within ±5% of the mean.

Table 6.4 Comparison of measured times for one $\ln Y_c$ reduction of blocks containing air voids that had transparent or blackened walls

Run No.	Cooling time with transparent walls (x 10^3 seconds)	Cooling time with blackened walls (x 10^3 seconds)	% difference
7	97.7	99.3	+1.6
8	109.2	108.5	-0.6
9	96.6	98.6	+2.1
10	117.2	116.9	-0.3

The significance of radiation heat transfer within rectangular voids was observed by comparing the $\ln Y_c$ vs. time profiles of two identical Tylose blocks - one with an actual 6mm high rectangular air void and the other with a 6mm high rectangular filled void (Figure 6.4). The block containing the air void cooled much faster than the block containing the filled void, even though the thermal conductivity of still air is lower than that of Styrodur. The significant increase in cooling rate was almost certainly entirely due to radiation effects because the void was too small to allow natural convection to occur (ie. the *Ra* was less than the value of 1708 suggested by Hollands *et al.* (1975)).

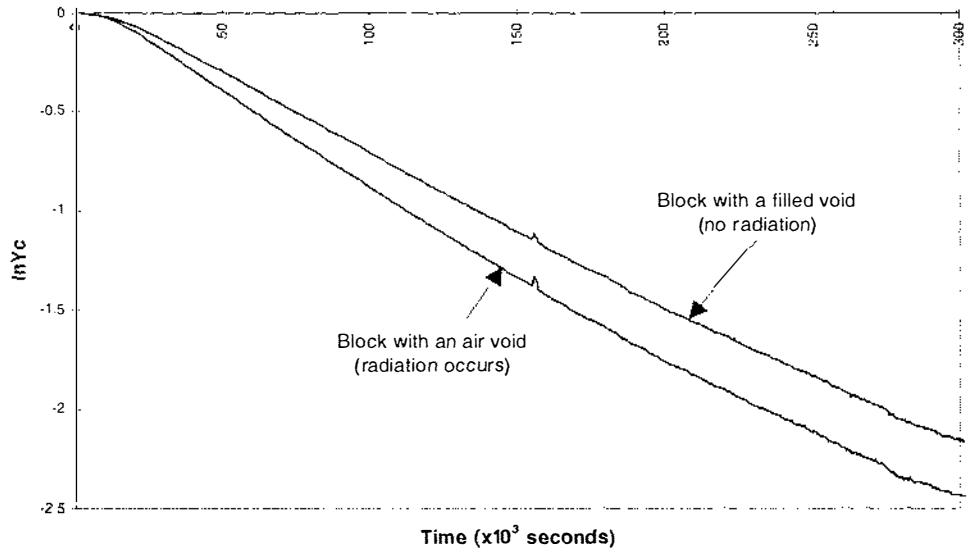

Figure 6.4 Plot showing an increase in the cooling rate of a block due to radiation heat transfer occurring in rectangular horizontal voids (data taken from Run 6)

In order to check whether the estimated view factor for rectangular voids (i.e. 0.9) was realistic, simulations were run in FINELX to predict the times for one $\ln Y_c$ reduction for runs 5 and 6 using this view factor (these blocks contained 6mm high rectangular air voids in which no significant natural convection was expected to occur). The simulations using the estimated view factors predicted the times for one $\ln Y_c$ reduction for runs 5 and 6 to within +3.2% and -4.7% of the measured times respectively. This level of agreement increased the confidence in the estimated values of view factor.

Since most foods and packaging materials would be expected to have emissivity values in the range 0.85 to 0.99, it is likely that a view factor of approximately 0.9 would be widely applicable for flat rectangular enclosures within food product packages.

6.5 Comparison of Measured and Predicted Data for Other Runs

Data files were constructed for FINELX using the input data collected in section 6.4. The predicted temperature-time profiles were compared to those measured in the four experimental runs where natural convection was significant. Figures 6.5-6.8 show the $\ln Y_c$ vs. time plots for the predicted data and data measured for runs with blocks containing voids that had transparent walls (note that the measured cooling rates of blocks containing voids that had blackened walls were negligibly different). The mean measured time and the predicted time for one $\ln Y_c$ reduction are given in Table 6.5. The absolute percentage differences between measured and predicted times were within the limits of experimental uncertainty (±5% from section 6.4.3.3). The small systematic over-estimation of cooling time observed in Table 6.5 was consistent with the results reported in chapter 5, where it was postulated that the two-dimensional model did not fully account for third dimension edge effects, resulting in an under-predicted cooling rate, and subsequently an over-estimated cooling time. The mean percentage difference between measured and predicted data was +1.5% with a standard deviation of 1.8%.

Figures 6.5-6.8 Plots of $\ln Y_c$ vs. time for measured and predicted data from blocks containing horizontal rectangular voids with transparent walls *(measured = blue, predicted = pink)*:

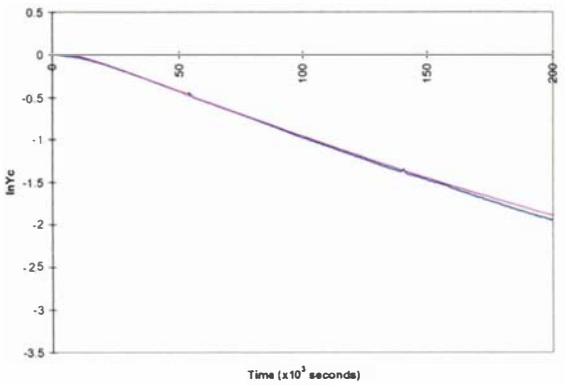

Figure 6.5 – 10mm void, high HTC (Run7)

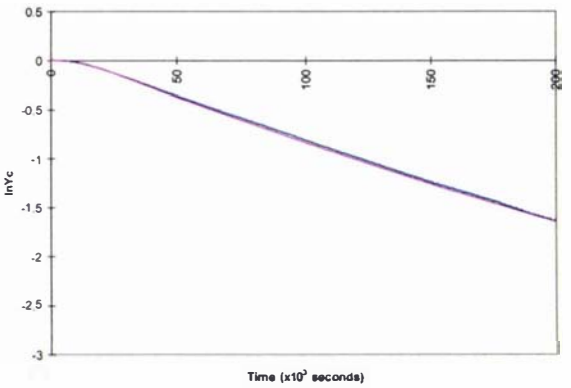

Figure 6.6 – 10mm void, low HTC (Run 8)

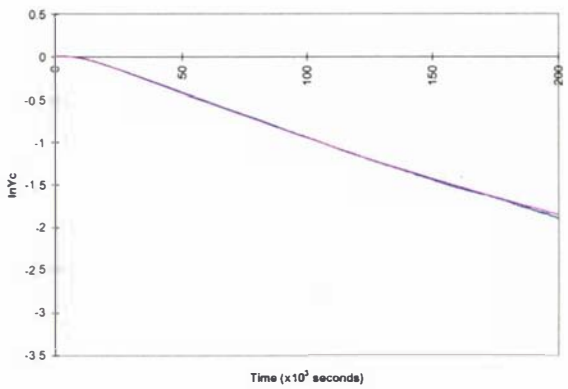

Figure 6.7 – 30mm void, high HTC (Run9)

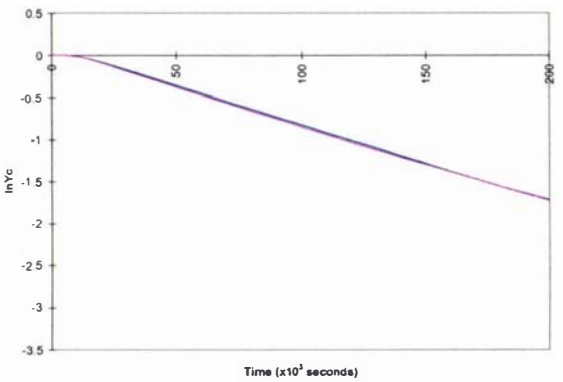

Figure 6.8 – 30mm void, low HTC (Run 10)

Table 6.5 Comparison of measured and predicted times for one $\ln Y_c$ reduction of blocks containing voids that had transparent or blackened walls

Run No.	Mean Measured Cooling Time (x 10^3 seconds)	Predicted Cooling Time (x 10^3 seconds)	% difference
7	98.5	98.8	+0.3
8	108.9	110.8	+1.7
9	97.6	101.4	+3.9
10	117.1	117.0	-0.1
		Mean % Diff.	+1.5
		St. Dev.	1.8

6.6 Conclusions

A model was developed to predict temperature-time profiles within two-dimensional solid blocks of food product that contain horizontal rectangular air voids. The model was solved using a customised two-dimensional finite element heat conduction program (called FINELX) that accounted for natural convection and radiation heat transfer effects by the use of effective thermal conductivity values within the voids.

Measured and predicted cooling rates for blocks with horizontal rectangular voids were very similar, and the percentage differences between measured and predicted times for one $\ln Y_c$ reduction were within the limits of expected experimental error and input data uncertainty. Therefore, although partly empirical, the model was validated as an accurate simulator of the overall heat transfer occurring in packages that contained a rectangular headspace void.

7. DEVELOPMENT AND TESTING OF A MODEL FOR PREDICTING HEAT TRANSFER DURING CHILLING OF PACKAGES CONTAINING COMBINED RECTANGULAR AND TRIANGULAR VOIDS

7.1 Development of the Physical Model

In chapter 6 an improved version of FINEL, called FINELX, was described. The improvements enabled rectangular air voids within a packaged food undergoing chilling to be modelled. However in the case of a meat carton there is often one large irregularly shaped air void occurring along the top of the carton (Figure 3.3a) that can be approximately described by combining several rectangular and triangular voids of various heights (as in Figure 3.3b for example). Hence FINELX required further modification to model such a void shape.

Goldstein *et al.* (1990) described flow characteristics within horizontal enclosures in detail. At *Ra* values below the critical value of 1708 (independent of *Pr*) the fluid within the horizontal enclosure is essentially motionless and heat transfer occurs by conduction and radiation only. At greater *Ra* values, a steady state flow ensues with two-dimensional roll-like structures of an aspect ratio close to 1 (Figure 7.1). For fluids with a *Pr* value of 0.7 (close to that of air) the steady state flow transforms to time-dependent unsteady state flow at $Ra > 5500$ (Krishnamurti, 1973).

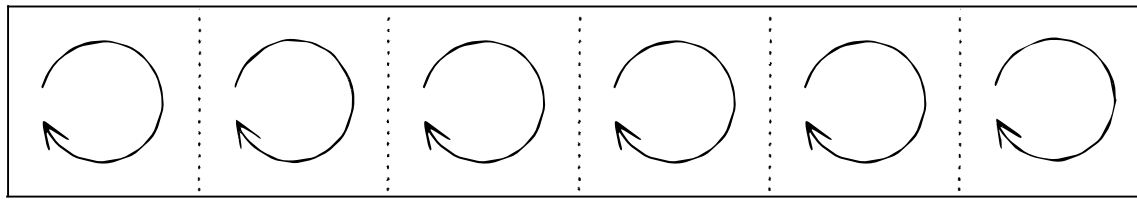

Figure 7.1 Two-dimensional roll-like flow in a rectangular void

Extending this concept, it was postulated that the flow in a combined rectangular/triangular void space might be as shown in Figure 7.2, thereby allowing the component rectangular and triangular void sections to be considered separately (although in reality the combined void sections are physically connected with no barriers between

them). It was assumed that there was little convective flow between the adjacent two-dimensional rolls (Figure 7.2).

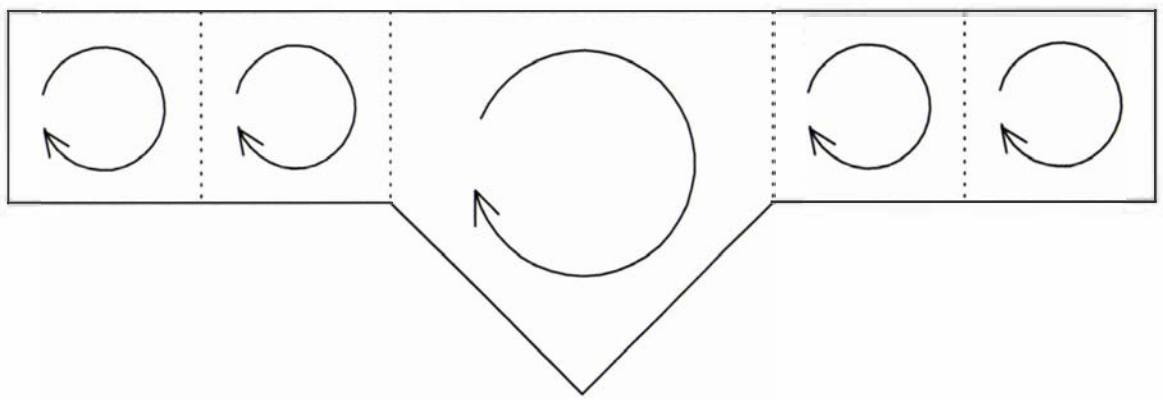

Figure 7.2 Expected two-dimensional roll-like flow in a combined void

In order to develop an unsteady state finite element conduction model for predicting heat transfer through packages that contain combined triangular and rectangular voids, a similar approach to that in chapter 6 was taken, i.e. a pseudo-steady state natural convection flow was assumed to occur within the voids, so that heat transfer due to natural convection and radiation was constant over the period of each time step of the finite element model. The model would use different Nu vs. Ra correlations for each different part of a combined void, just as it would have used for separate rectangular and triangular air voids. This resulted in the physical model shown in Figure 7.3.

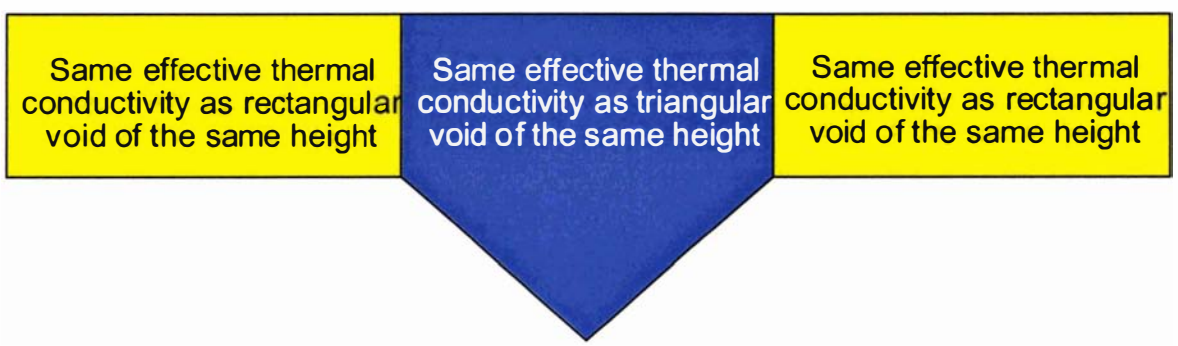

Figure 7.3 Simplified physical model for combined voids

In the model, the triangular void section of the physical model shown in Figure 7.3 has an effective thermal conductivity the same as a right-angled isosceles triangular void with the same height dimension Y (as shown in Figure 7.4). However the areas of overlap between the triangular and rectangular voids were considered as part of the rectangular

void sections in the physical model. The effective thermal conductivity must also consider radiation as well as natural convection.

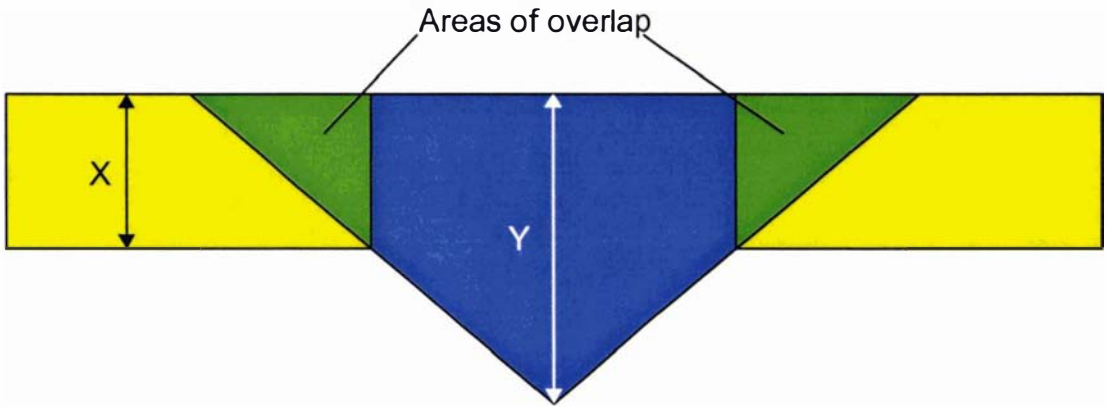

Figure 7.4 Areas of overlap in a combined void

Although the physical model accounted for intra-section natural convection and radiation within the sections of the void, it ignored inter-section radiation between the surfaces of the component sections. It was assumed that this inter-section radiation would be small compared to intra-section radiation, since each individual component section has very little surface area 'in view' of the other component sections. Therefore the physical model shown in Figure 7.3 was determined to be the simplest realistic physical model for packages containing combined void sections.

7.2 Incorporating the Physical Model into FINELX

In chapter 6, FINELX was altered to enable twenty different material types. The material types between one and five represented normal conducting solids - where the thermal conductivity of each element that contained this material could be dependent upon the temperature of the nodes at it's three vertices. The material types between sixteen and twenty represented rectangular void sections - where the thermal conductivity of each element within a given rectangular void section was the same, and the value was dependent upon the temperature of two transverse void section nodes specified by the user.

The ten remaining material types (from six to fifteen) were allocated to represent isosceles triangular void sections. FINELX was further altered to treat triangular void sections in a similar way to rectangular void sections - where the thermal conductivity of each element within a given triangular void section is the same, and that value is dependent upon the

temperatures of two transverse void nodes specified by the user. For consistency the transverse points for an isosceles triangular void section were kept the same as those used in the data analysis in chapter 5 (shown in Figure 5.22).

In the same way as for rectangular voids, FINELX used the positions and temperatures of the two selected nodes to calculate the characteristic dimension, transverse void temperature difference, mean void temperature, and the Rayleigh number (*Ra*) of the void at each time step (using equations 5.10 to 5.12). If the triangular void was cooled from below the *Nu* value was found by using the correlation reported in equation 5.14. If the triangular void was cooled from above the *Nu* value was found by using the correlation reported in equation 5.17. Since the results reported in chapter 5 included natural convection and radiation effects, the overall effective thermal conductivity of a triangular air void including natural convection and radiation effects was given by:

$$k_{overall} = Nu \times k_{air} \tag{7.1}$$

7.3 Experimental Methodology for Model Testing

The same experimental methodology as in chapter 6 was used to test the model for packages containing combined rectangular and triangular voids. The only difference was that the Tylose blocks were altered to contain different combinations of rectangular and triangular voids. A diagram of the sample holder is given in Figure 7.5.

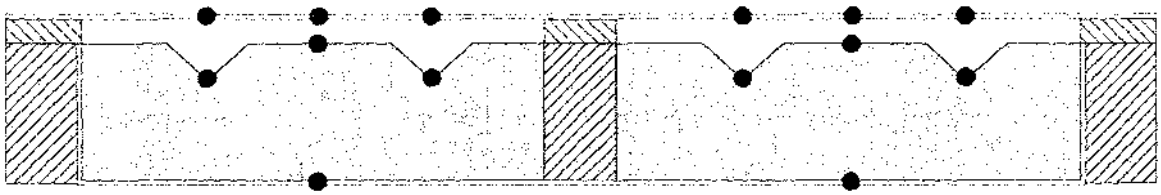

Figure 7.5 Side elevation of a sample holder containing combined rectangular and triangular voids

Each sample holder contained a horizontal rectangular headspace void between the polycarbonate lid and the Tylose block, created by using Styrodur walls of a known height. Appropriately sized right-angle isosceles triangular shaped voids were cut into the top surface of the Tylose blocks. To hold the triangular voids in shape and to eliminate any moisture loss, a 360mm long, 1mm thick L-shaped section of solid acrylic plastic was

placed along the surface of each triangular void, and a 0.03mm thick layer of polyethylene was tightly stretched along the top of the rectangular void sections of the Tylose block. The polyethylene was attached and sealed between the edges of the polycarbonate box and the L-shaped sections of solid acrylic to reduce moisture loss from the Tylose block. Tylose blocks that were not being used for an experimental run were kept in shape by placing a flat block of Styrodur on the top surface of the block with an evenly dispersed 20kg of weight on top. This ensured that the top surface of the Tylose block was flat and that the L-shaped sections of solid acrylic were pushed into the block until they were flush with the top surface of the Tylose block. Thermocouple positions are shown as dots in Figure 7.5.

Four different combinations of voids were used for the trials:

1) X = 25mm rectangular void & Y = 25mm triangular voids (see Figure 7.4),
2) X = 25mm rectangular void & Y = 50mm triangular voids,
3) X = 10mm rectangular void & Y = 30mm triangular voids,
4) X = 10mm rectangular void & Y = 50mm triangular voids.

The rectangular void heights of 25mm and 10mm were chosen to broadly align with those used by Wee and Pham (1990) and with those typically found in bulk-pack and primal cut meat cartons (as assessed from video footage of carton cross-sections from an unrelated study by MIRINZ Food Technology and Research, Ltd.).

Two separate sample holders were constructed to allow one to re-equilibrate to the initial temperature while the other was used for an experiment. The choice of the triangular void heights was important. They had to be larger than the rectangular void they were combined with, but were selected to be no higher than 50mm (the maximum height investigated in earlier chapters). For the block with a 25mm high rectangular void, a triangular void height of 50mm was chosen by elimination, because 40mm high triangular voids would have only given a 15mm high cut into the Tylose block, and the extra effect of this would be expected to be small when combined with a 25mm rectangular void.

As in chapter 6, the sample holders were cooled from the top surface only, using the same custom plate cooler. The bottom, sides, and ends of the sample holders were insulated using Styrodur polystyrene, and the insulation contacting the bottom of the sample was kept to within 0.1°C of the mean temperature at the bottom of the sample. This effectively created a zero heat flow or symmetry condition, allowing the bottom of the sample holder to be treated as the thermal centre. The runs were started before

construction of all sample holders was complete so the order in which the runs were performed could not be randomised. However random selection of runs within the available samples at any time was carried out.

Table 7.1 Treatment table for trials with combined voids

Run No.	Side	Rectangular void height (mm)	Triangular void height (mm)	Fibreboard sheets	Run Order
1	A	25	25*	1	5
	B	25	50		
2	A	25	25*	1	2
	B	25	50		
3	A	25	25*	3	6
	B	25	50		
4	A	25	25*	3	7
	B	25	50		
5	A	10	30	1	3
	B	10	50		
6	A	10	30	3	1
	B	10	50		
7	A	10	30	3	4
	B	10	50		

* effectively no triangular voids in these blocks.

All temperatures were measured with T-type copper/constantan thermocouples that were calibrated as explained in chapter 6. For all runs the initial temperature of the sample was approximately 30°C.

Sample holders were cooled at one of two different top surface heat transfer coefficients by placing the same thermal resistance as used in chapter 6 (either one or three sheets of fibreboard) between the sample holder and the top cooler plate. Contact integrity between the plate and the sample holder was maintained by placing an even load of 100 kg on top of the movable top plate. A total of 7 runs (with 2 blocks per run) were carried out for the trials giving a total of 14 experiments (shown in Table 7.1). Four runs without triangular voids used were to check that the measured temperature profiles agreed with predictions using the HTC's estimated in chapter 6, and the remaining ten were used to test the accuracy of the numerical model.

7.4 Evaluation of Input Data

7.4.1 Sample Dimensions

Sample dimensions were measured using vernier calipers. Three measurements of the sample length, width and height were taken. Void height was measured by six readings of the height of the Styrodur walls. The coordinates of the thermocouple positions were measured in relation to the closest end of the sample. These measurements were considered to represent mean values to an accuracy of ± 1mm.

7.4.2 Thermal Property Data

The thermal properties of all materials used in this chapter are given in Tables 5.2 and 5.6.

7.4.3 Initial and Boundary Conditions

The Tylose blocks were assumed to be initially at a uniform temperature equal to the measured centre temperature at the start of each run.

Boundary conditions were of the third kind and thus estimates of the mean cooling medium temperature and the surface heat transfer coefficients were required.

7.4.3.1 Cooling Medium Temperatures

For each run, the mean cooling medium temperature and the mean surrounding air temperature inside the plate cooler were measured and estimated in the same way as in section 6.4.3.1.

7.4.3.2 Heat Transfer Coefficients

The resistance to heat transfer between the sample holder and the cooler plates was kept exactly the same as the experimental trials conducted in chapter 6. Thus the heat transfer coefficients estimated in section 6.4.3.2 were also used for the trials with combined voids.

7.4.3.3 View Factors for Radiation Heat Transfer in Rectangular Voids

The view factor for radiation heat transfer occurring within the rectangular voids was estimated to be 0.9 in section 6.4.3.3. This value was again used when modelling the rectangular void parts of the combined voids.

7.5 Comparison of Measured and Predicted Data

Figure 7.6 shows a measured temperature-time profile near the thermal centre position for two otherwise identical Tylose blocks undergoing chilling (one block containing a 25mm high rectangular void combined with 50mm triangular voids, and the other block containing only a 25mm high rectangular void). The block containing the triangular voids cooled slightly faster than the block without. A similar result was observed for blocks with a 10mm headspace, the blocks with 50mm voids cooled faster than the blocks with 30mm voids. Presumably this increase in cooling rate was due to more natural convection and radiation heat transfer occurring within the larger sized triangular voids, and the reduced mass of material to be cooled.

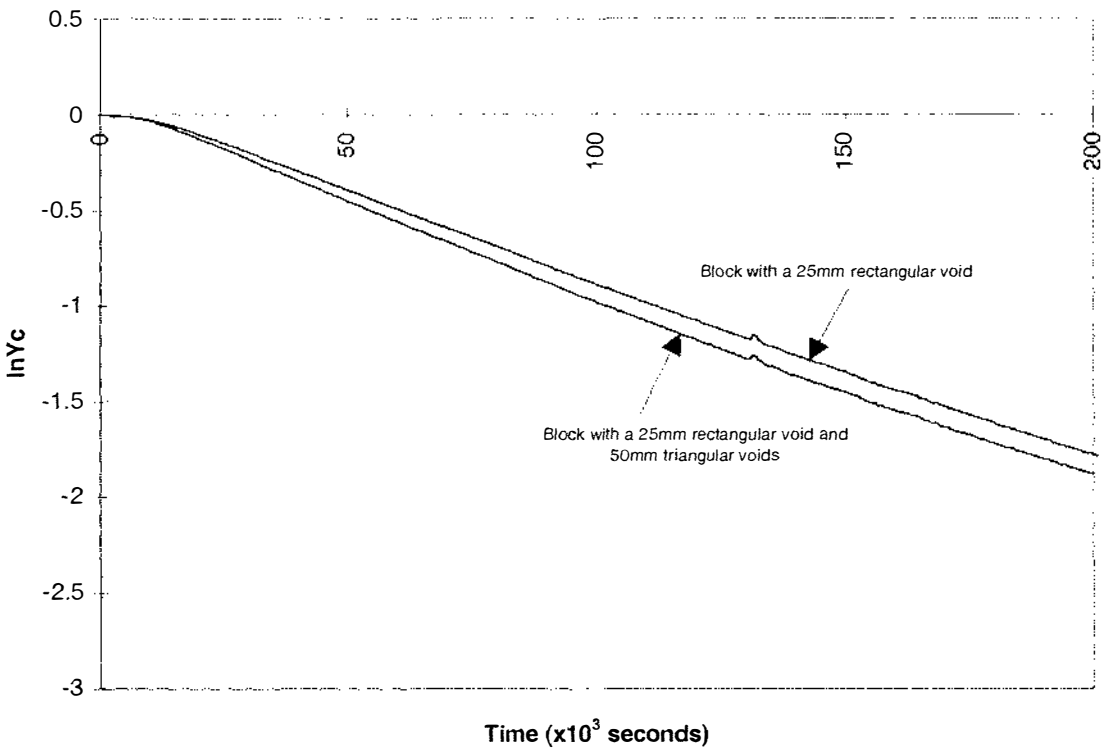

Figure 7.6 Plot showing an increase in the cooling rate of a block due to the presence of triangular voids (data taken from Runs 2A & 2B)

In order to check that the top surface HTC values in these experiments were effectively the same as those estimated in chapter 6, the measured and predicted times for one $\ln Y_c$ reduction for a block containing only a 25mm high rectangular void over four runs (two at 31.4 $Wm^{-2}K^{-1}$ and two at 13.6 $Wm^{-2}K^{-1}$) were compared. The measured and predicted cooling times are given in Table 7.2. The results were more spread than in Table 6.3 but they did indicate that the top surface HTC values occurring in the new experiments were the same as those estimated in chapter 6.

The standard deviations, expressed as a percentage, from the individual means of replicate runs 1A & 2A, and 3A & 4A, were used to estimate the percentage experimental uncertainty. There was 95% certainty that any measured value was within ±9% of the mean.

Table 7.2 Comparison of measured and predicted times for one $\ln Y_c$ reduction of blocks containing 25mm high rectangular voids (x 10^3 seconds)

Run No.	HTC ($Wm^{-2}K^{-1}$)	Measured Time	Predicted Time	% difference
1A	31.4	97.8	103.2	+5.5
2A	31.4	105.7	101.4	-4.1
3A	13.6	107.9	118.8	+10.1
4A	13.6	110.6	118.3	+7.0

Data files were constructed within FINELX using the model developed in sections 7.1 and 7.2 and the input data in section 7.4. The predicted temperature-time profiles were compared to those measured in ten experimental runs. Figures 7.7-7.16 show the $\ln Y_c$ vs. time plots for measured and predicted data of blocks containing various combined rectangular and triangular voids.

Figures 7.7 - 7.16 Plots of $\ln Y_c$ vs. time for measured and predicted data from blocks containing various combinations of rectangular and triangular voids at a high or low HTC *(measured = blue, predicted = pink)*:

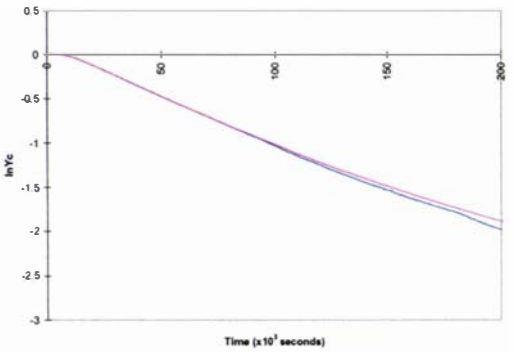

Figure 7.7 - 25mm rectangular and 50mm triangular voids, high HTC (Run 1B)

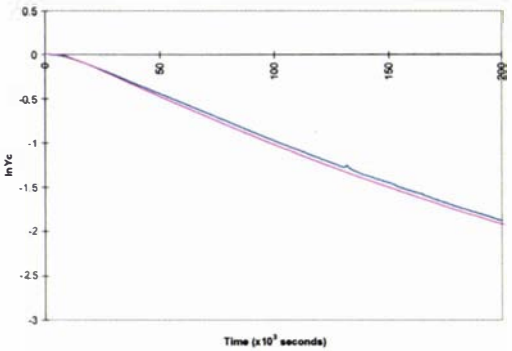

Figure 7.8 - 25mm rectangular and 50mm triangular voids, high HTC (Run 2B)

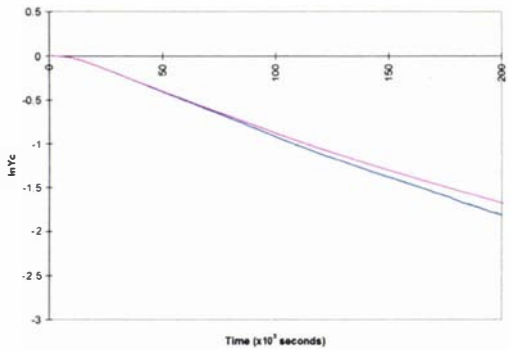

Figure 7.9 - 25mm rectangular and 50mm triangular voids, low HTC (Run 3B)

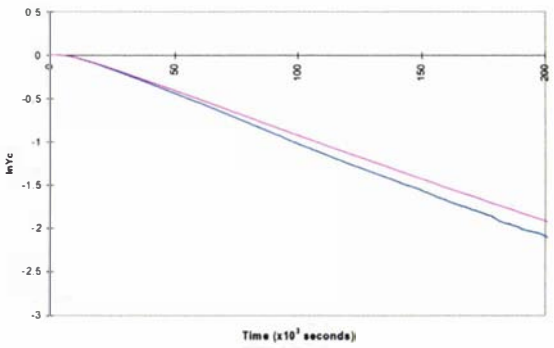

Figure 7.10 - 25mm rectangular and 50mm triangular voids, low HTC (Run 4B)

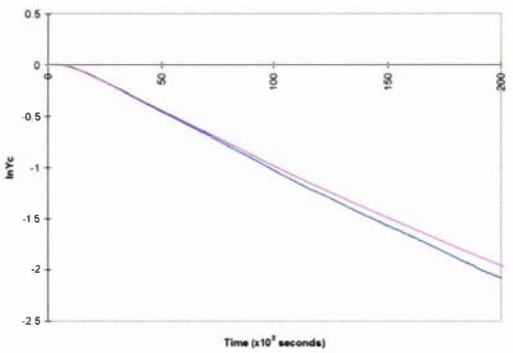

Figure 7.11 - 10mm rectangular and 30mm triangular voids, high HTC (Run 5A)

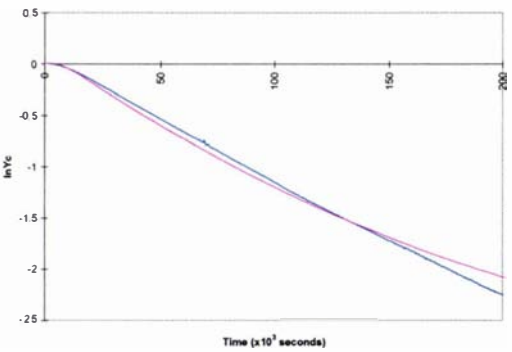

Figure 7.12 - 10mm rectangular and 50mm triangular voids, high HTC (Run 5B)

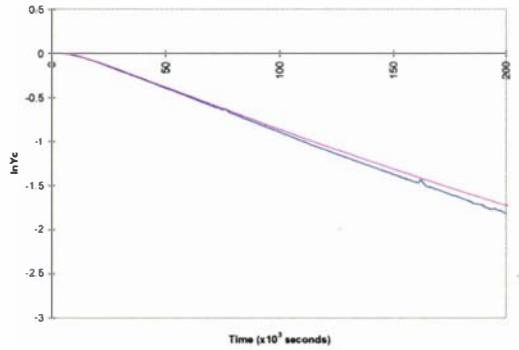

Figure 7.13 - 10mm rectangular and 30mm triangular voids, low HTC (Run 6A)

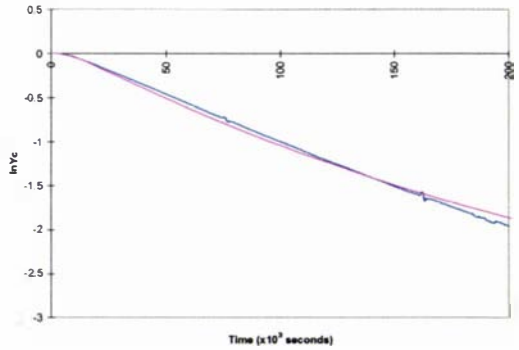

Figure 7.14 - 10mm rectangular and 50mm triangular voids, low HTC (Run 6B)

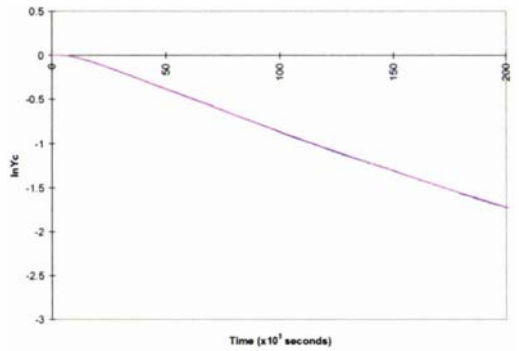

Figure 7.15 - 10mm rectangular and 30mm triangular voids, low HTC (Run 7A)

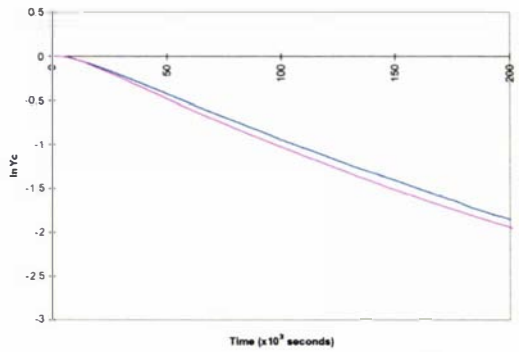

Figure 7.16 - 10mm rectangular and 50mm triangular voids, low HTC (Run 7B)

Table 7.3 Comparison of measured and predicted times for one $\ln Y_c$ reduction of blocks containing combined voids of various heights (x 10^3 seconds)

Run No.	Rectangular void height	Triangular void height	HTC ($Wm^{-2}K^{-1}$)	Measured Time	Predicted Time	% difference
1B	25mm	50mm	31.4	94.4	99.3	+5.1
2B	25mm	50mm	31.4	99.4	95.6	-3.8
3B	25mm	50mm	13.6	104.7	113.1	+8.0
4B	25mm	50mm	13.6	107.5	112.9	+5.0
5A	10mm	30mm	31.4	89.6	95.7	+6.8
5B	10mm	50mm	31.4	82.7	81.6	-1.3
6A	10mm	30mm	13.6	103.7	110.2	+6.3
6B	10mm	50mm	13.6	95.5	95.3	-0.2
7A	10mm	30mm	13.6	110.3	110.7	+0.4
7B	10mm	50mm	13.6	102.4	95.6	-6.6

Mean % Diff.	+2.0
St. Dev.	5.0

The measured and predicted times for one $\ln Y_c$ reduction are given in Table 7.3. The absolute percentage differences between measured and predicted times were all explainable by experimental uncertainty and input data uncertainty. The small systematic over-estimation of cooling time observed in Table 7.3 was consistent with the data analysis carried out in chapters 5 and 6, where it was postulated that the two-dimensional model did not fully account for third dimension edge effects, resulting in an under-predicted cooling rate, and subsequently a slightly over-estimated cooling time. The mean percentage difference between measured and predicted data was +2.0% with a standard deviation of 5.0%.

7.6 Conclusions

A model was developed to predict temperature-time profiles within two-dimensional solid blocks of food product that contained air voids defined by combining isosceles triangular and/or horizontal rectangular shapes. Any overlapping areas of these constituent void shapes was considered to be part of the rectangular void, and radiation heat transfer between the constituent voids was ignored. The model was solved using a customised two-dimensional finite element heat conduction program (called FINELX) that accounted for natural convection and radiation heat transfer effects by the use of effective thermal conductivity values within the voids.

Measured and predicted cooling rates were similar, and the percentage differences between measured and predicted times for one $\ln Y_c$ reduction were well within the combined limits of expected experimental and input data uncertainty.

Therefore, although partly empirical, the model was validated as an accurate simulator of the overall heat transfer occurring in packages that contained a void space that could be described by some combination of rectangular and right-angled isosceles triangular voids.

8. DEVELOPMENT OF A SIMPLE METHOD FOR PREDICTING HEAT TRANSFER DURING CHILLING OF PACKAGES CONTAINING RECTANGULAR AND TRIANGULAR VOIDS

8.1 Simplification of the Prediction Method

The model developed in chapters 6 and 7 predicted thermal centre chilling times that were within about ±7% and ±12% of those measured for food product packages containing rectangular voids and those containing combined rectangular and triangular shaped voids respectively. Computations using the customised FINELX finite element program typically took about 5 hours on a 350MHz Pentium II computer. Data file preparation, using BAMG (Bi-dimensional Anisotropic Mesh Generator) version 0.58 by Frederic Hocht, INRIA, France (free to download from the Internet) and several customised Perl programs, took up to 3 hours when creating a completely new file. Thus, assuming that the potential user understands finite element methods, the solution time for a new problem was in the order of eight hours, and this did not include the time that was necessary for the user to become familiar with the properties of the model and the customised programs. Overall, these factors represent a barrier that will severely limit the use of the method by engineers in industry. A simpler prediction method was therefore sought, which users with a reasonable knowledge of engineering heat transfer methods could apply to predict thermal centre chilling times of food product packages containing voids in a much shorter time and with less demand for access to software, hardware and technical support. It was postulated that the simple method would be expected to predict measured thermal centre chilling times with an accuracy of about ±10-15%. Any less accuracy may not be accepted in industry.

Simplification of the prediction method required a further simplification in the description of the geometry of the problem space. The cartons used in the New Zealand meat industry are rectangular in shape, and the majority of cooling from the carton is from the top and bottom surfaces. Thus the simplest realistic model shape was the one-dimensional infinite slab. The main advantages in assuming an infinite slab shape were that it has been widely used in heat transfer prediction methods and it has previously been successfully adapted by empirical means. For example, results predicted using an infinite slab shape can often be adapted to account for heat transfer in multiple dimensions by either superposing the Y values from the other dimensions (Carslaw & Jaeger, 1959, section 5.6) or by the use of shape factors (eg. Lin *et al.*, 1996).

It was assumed that the user would have access to some type of spreadsheet computer program, and either analytical or simple numerical solution methods to solve the simple model of chilling an infinite slab shape.

The temperature-time profile of a one-dimensional infinite slab shape is affected by several factors, but when converted to a system with four dimensionless variables, the dimensionless temperature (Y) at a given dimensionless position (r/R) and dimensionless time ($F\bullet$), depends only upon the Biot number (Bi). Therefore for any position in the slab, changes in Bi (according to the characteristics of the void space) could adjust the temperature-time profile of the infinite slab to match that of the food package.

Bi is defined as:

$$Bi = \frac{hR}{k} \tag{8.1}$$

To adjust Bi, a change in the external heat transfer coefficient (h), the half-thickness (R), or the thermal conductivity (k) of the slab would be required. However, it has already been established that the effect of a void space on the cooling rate of a package is often temporally and spatially variable. Thus the choice of which variable to adjust must consider:

1) The solution method that will be used to solve the simple model (ie. certain solution methods do not allow some of these variables to change with respect to time or space).

2) The responsiveness of the predictions from the simple model (ie. changes in the chosen variable should bring about changes in the cooling rate of the package that are physically representative of the effects of void spaces).

As stated, the simple model would ideally be solvable by using analytical or simple numerical solutions of one-dimensional heat transfer. However, analytical solutions of one-dimensional heat transfer do not easily allow for changes in any of these variables (h, R and k) with time, and certainly not with space. Thus adaptation of an analytical solution would probably involve both temporal and spatial averaging of the chosen variable and subsequent calculation of a mean Bi to ultimately estimate the slab cooling time. Simple numerical solution computer programs often allow k and/or h (but not R) to vary with time and space. In the author's experience, it is more common for simple numerical

solution programs to include the possibility for h to vary with time and space, whereas k is usually temperature dependent for a specific material type.

Physically, it also seemed sensible to vary h rather than k according to the characteristics of the void space because void space effects occur close to the package surface and k represents the full solid object. Thus choosing h as the changing variable ensures that the simple model is as physically representative of the actual effects of void spaces on package cooling times as possible.

8.2 Dealing With Asymmetric Heat Transfer Coefficients

Most food packages are cooled from above and below. In these cases, the effective lower surface heat transfer coefficient of the slab would account for the packaging material and any voids at the bottom of the package, and the effective upper surface heat transfer coefficient would account for the packaging material and any voids at the top of the package. However since most food packages contain more air voids nearer the top of the package, the simple infinite slab model would be likely to have different effective heat transfer coefficient values on the top and bottom surfaces.

Most numerical solvers of one-dimensional heat transfer allow the user to specify different heat transfer coefficients on the top and bottom surfaces. Therefore solution of the infinite slab model would be comparatively straightforward by these methods.

However in cases where the user does not have such a numerical solver, a different approach is required. Cleland (1990) stated a widely used iterative method for dealing with asymmetric heat transfer coefficients. The user must make an initial estimate of the thermal centre position, which will be closer to the surface with the lowest heat transfer coefficient. The respective distances from the estimated thermal centre position to the surfaces are called R_1 and R_2, where R_1 is the shorter of the two and $R_1 + R_2 = 2R$. Two chilling times can then be calculated using the analytical solution for an infinite slab, one with the higher heat transfer coefficient and R_2, and the other with the lower heat transfer coefficient and R_1. If the first chilling time is shorter than the second, R_2 must be increased (or decreased if the first chilling time is longer). This process must be iterated until the two chilling times match. The matching value identifies the position and chilling time of the thermal centre of the slab.

Alternatively, Uno & Hayakawa (1979) developed an approximate method for estimating chilling times by numerically solving the analytical formula for asymmetric heat transfer in an infinite slab (Carslaw & Jaeger, 1959). Charts were established for infinite slabs with some combination of top and bottom surface *Bi* numbers between 0.1 and 100. The location of the thermal centre and the parametric values of f and j for thermal centre, geometric centre, and mass average positions could be determined using the charts.

Either approach could be used in conjunction with the present work.

8.3 Food Packages Containing Rectangular Voids

8.3.1 Development of the Simple Physical Model

In food packages that contain only one rectangular void space at the top of the package (called a headspace) heat transfer is one-dimensional if end and edge effects are ignored. In this case, the appropriate simple physical model would be an infinite slab with the same thickness and thermal conductivity as the solid material contained within the package. However the upper surface and lower surface heat transfer coefficients on the slab would be different (h_{rect} and h_{surf} respectively in Figure 8.1). The value of h_{rect} would be time-variable and would account for the rectangular void space, the packaging material and the external heat transfer coefficient acting upon the packaging. The value of h_{surf} would be constant and would only account for the packaging material and the external heat transfer coefficient acting upon the packaging.

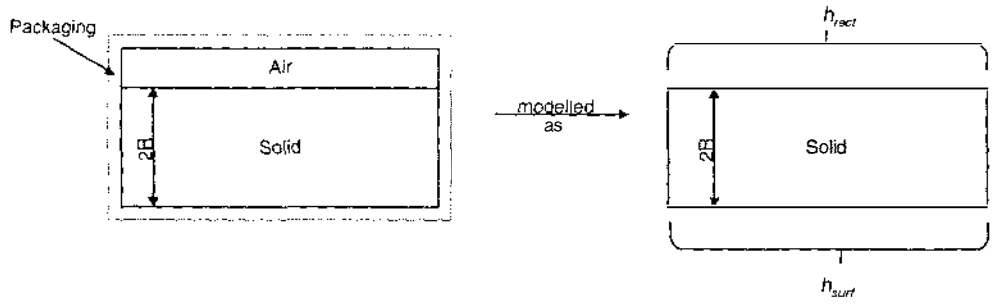

Figure 8.1 Simple physical model for food packages containing rectangular air voids

The work in chapter 6 showed that the appropriate value of h_{rect} for the infinite slab model shown in Figure 8.1 changed over time as the temperature difference across the void in the package changed (ie. the temperature difference between the top surface of the solid

and the underside of the packaging material). However, when using the infinite slab model the packaging is not included as a capacitive component and thus its temperature cannot be explicitly deduced. Nevertheless, the temperature of the underside surface of the packaging could be estimated by assuming a quasi-steady-state situation and using the steady-state sum of resistances theory. This method might slightly under-estimate the temperature of the underside of the packaging material, since the thermal mass of the packaging would be ignored and thus might lead to a slightly over-estimated h_{rect} value. In spite of this weakness, and in the absence of simple alternatives, this approach was adopted.

8.3.2 Calculation Method and Relevant Equations

The mean value of h_{surf} can be estimated by summing the resistances of the packaging material and the external heat transfer coefficient acting upon the packaging:

$$\frac{1}{h_{surf}} = \frac{1}{h_{packaging}} + \frac{x_{packaging}}{k_{packaging}} \tag{8.2}$$

where $h_{packaging}$ is the heat transfer coefficient between the packaging external surface and the external cooling medium(W $m^{-2} K^{-1}$)

$x_{packaging}$ is the thickness of the packaging (m)

$k_{packaging}$ is the thermal conductivity of the packaging (W $m^{-1} K^{-1}$)

The mean value of h_{rect} was estimated by summing the resistances of the rectangular void space, the packaging material, and the external heat transfer coefficient:

$$\frac{1}{h_{rect}} = \frac{1}{h_{packaging}} + \frac{x_{packaging}}{k_{packaging}} + \frac{x_{rect}}{k_{rect}} \tag{8.3}$$

where x_{rect} is the height of the rectangular air void (m)

k_{rect} is the effective thermal conductivity of the rectangular air void (W $m^{-1} K^{-1}$)

At this stage of a calculation the user would know the values of $h_{packaging}$, $k_{packaging}$, $x_{packaging}$, and x_{rect}. The value of k_{rect} at any time could be determined by using the previously developed equations 5.13, 6.1, 6.2, 6.7, and 6.8 in an iterative manner.

$$Ra = 10^6 \times \exp\left(5 - 0.016\frac{T_1 + T_2}{2}\right) \times (T_1 - T_2) \times (x_{rect})^3 \qquad (5.13)$$

for air voids at temperatures between –13°C and 47°C,

where T_1 is the upper surface temperature of the infinite slab (°C)

T_2 is the temperature of the underside of the packaging material (°C)

$$Nu = 1 + 1.44\left[1 - \frac{1708}{Ra}\right]^{\bullet} + \left[\left(\frac{Ra}{5830}\right)^{1/3} - 1\right]^{\bullet} \qquad (6.1)$$

Note that a bracket $[\ ]^{\bullet}$ indicates that if the argument inside the bracket was negative, the quantity is to be taken as zero.

$$k_{nat\ conv} = Nu \times k_{air} \qquad (6.2)$$

$$k_{rad} = F_{1\to 2}\sigma x\left(T_1^2 + T_2^2\right)\left(T_1 + T_2\right) \qquad (6.7)$$

where T_1 is the upper surface temperature of the infinite slab (K)

T_2 is the temperature of the underside of the packaging material (K)

$$k_{rect} = k_{rad} + k_{nat\ conv} \qquad (6.8)$$

At any time, the temperature at the underside of the packaging material (T_2) depends on the value of k_{rect} - because a quasi-steady-state situation was assumed and hence ($T_1 - T_a$) divides according to the individual resistances in equation 8.3. Therefore an initial estimate of T_2 must be made and the calculation process using equations 5.13, 6.1, 6.2, 6.7, and 6.8 must be iterated until the value of h_{rect} remains constant between iterations.

The simplest way to deal with the changing value of h_{rect} over time was to divide the simulation into time intervals that coincide with equally sized changes in the slab surface temperature. For example, if an infinite slab initially at a uniform temperature of 30°C was cooled from the top surface only in a cooling medium at 0°C, the user might choose two even step changes in slab surface temperature (ie. 30 to 15°C and 15 to 0°C). The mean slab surface temperature during each step (ie. 22.5°C and 7.5°C) would then be used to calculate the mean value of h_{rect} during that time period using equations 5.13, 6.1, 6.2, 6.7, and 6.8. The mean value of h_{rect} during the first interval would be used in a simulation until the slab surface temperature reached the minimum value for the first time

period (ie. 15°C). At this time, h_{rect} would change to the value calculated for the second interval. If the user required more accuracy, the number of surface temperature step changes could be increased above two. In this way, the user would have significant involvement in the trade-off decision between model accuracy and model complexity. Guidance on selection of the number of steps was seen as an important research outcome in the present work.

8.3.3 Averaging Temporal Variations – One Step Calculations

If the user does not have access to a numerical solver for one-dimensional heat transfer problems, or if the numerical solver does not allow the use of time-variable heat transfer coefficients, h_{rect} must be treated as constant implying a single time step approach. The best fit single value of h_{rect} might be determined by averaging over time.

As previously mentioned, the value of h_{rect} depends upon the temperature difference across the void. In most practical situations the packaging material approaches the cooling medium temperature relatively quickly, and the change in temperature difference across the void strongly reflects the temperature-time profile at the surface of the solid. In chilling processes, the difference between the surface temperature and the cooling medium temperature decreases approximately exponentially. This suggests that the value of h_{rect} might be more suitably determined from a logarithmic average of the maximum and minimum values over the length of the simulation than from an arithmetic mean. The maximum value of h_{rect} occurs at the start of cooling (assuming that the packaging immediately reaches the cooling medium temperature, the temperature difference across the void will be at a maximum) and the minimum value occurs at the end of cooling (when the temperature difference across the void approaches zero), so the calculation can be explicitly defined. Note that this method of averaging will not give the same result as using one step in the stepped procedure explained in section 8.3.2 because that method would calculate an arithmetic mean value of effective heat transfer coefficient, instead of a logarithmic mean value.

8.4 Food Packages Containing Triangular Voids

8.4.1 Development of a Simple Physical Model

Experience from previous chapters had shown that the presence of a void space that contained triangular shapes gave rise to heat transfer in more than one dimension and that

the extent of heat transfer in the void decreased over time as the temperature difference across the void approached zero.

The simple model could have been developed using either the principle of conservation of the package height (where the triangular voids would be assumed to be filled with solid material) or conservation of the packaged material volume (where the effective height of the slab would be altered according to the size and number of triangular voids in the package). Conserving packaged material volume would reduce the effective height of the slab as the size of the triangular voids increased, implying a decreasing predicted cooling time if no other variable was changed. This behaviour would be inconsistent with the measured data from chapter 5 that showed the cooling time of the package increased as void size increased. Thus, volume conservation was rejected and conservation of package height was used in the simple model.

The proposed simple physical model was thus an infinite slab with the same thickness and thermal conductivity as the solid material contained within the package, but the heat transfer coefficient could vary across the slab surface (Figure 8.2).

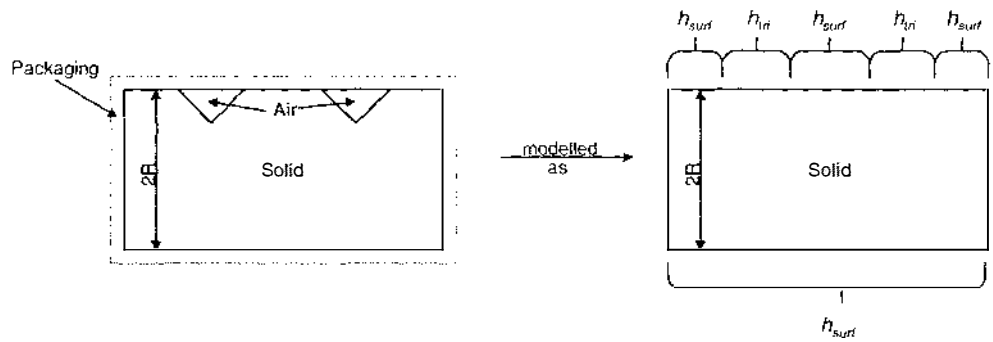

Figure 8.2 Simple physical model for food packages containing triangular air voids

In the simple model the concept chosen implies that the void space would effectively be filled with the solid material and thus it would not be possible to infer the true temperature difference across the void in order to estimate the effective thermal conductivity in the void. Hence at positions corresponding to the presence of a triangular void, the heat transfer coefficient (called h_{tri}) would have to be time-averaged and would take into account the effect of the triangular void space, the packaging material and the external heat transfer coefficient acting upon the packaging. At positions where no void was present on the upper surface, and for the whole lower surface, the heat transfer coefficient would be a constant value (h_{surf}) that accounted for the packaging material and the external heat transfer coefficient acting upon the packaging.

8.4.2 Averaging Temporal Variations

As discussed above, the use of an infinite slab model with solely one-dimensional heat transfer would make it impossible to infer the true temperature difference across the triangular void. Thus an average value of *Nu* must be estimated, and the specific value must be representative of the manner in which the *Nu* value changes over the time as the package cools.

The simplest possible model was chosen in which the packaging material was assumed to reach the cooling medium temperature immediately. The value of *Nu* would then change as the opposite apex of the void changed in temperature. The lag phase preceding the exponential cooling curve would be expected to be comparatively short due to the small thermal capacity of the air void. Hence, the most representative average value of *Nu* might be determined by a logarithmic average of the maximum *Nu* and minimum *Nu* values over the length of the simulation.

8.4.3 Averaging Spatial Variations

In order to implement the concept in Figure 8.2, a two-stage transformation was proposed. The first stage was to define heat transfer coefficients external to the solid, but within the void. The second stage was the geometric transformation to a one-dimensional slab.

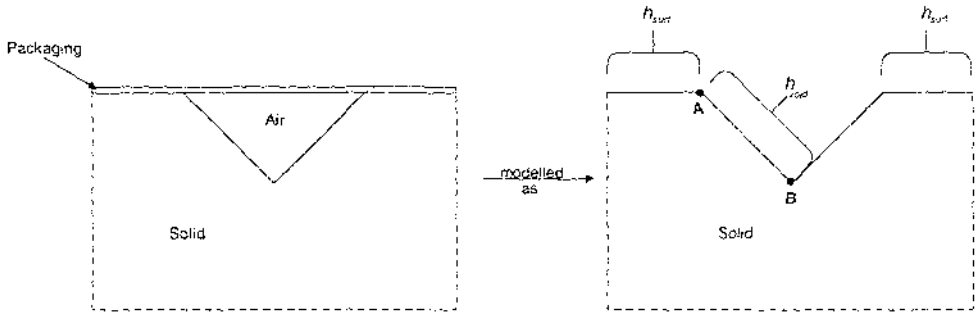

Figure 8.3 A physical model treating the triangular air void as an effective heat transfer coefficient

In the first stage, using the same approach as for rectangular voids, a triangular air void might be accounted for approximately by the use of an effective heat transfer coefficient (Figure 8.3). The value of h_{surf} would be constant and the value of h_{void} would vary in an approximately inverse manner with position along the surface of the void to take account of the linearly increasing air layer thickness above the solid material surface. The implied

assumption is that all heat transfer is uni-directional (perpendicular to the packaging), which may not be true in practice. For example, a sideways or lateral temperature gradient could occur in the packaging with resultant lateral heat transfer. The value of h_{void} at any position along the line AB would be given by:

$$\frac{1}{h_{void}} = \frac{1}{h_{surf}} + \frac{x_{air\ layer}}{k_{tri}} \tag{8.4}$$

where $x_{air\ layer}$ is the thickness of the air layer vertically above the position on line AB (m)
k_{tri} is the effective thermal conductivity of the triangular void (W m^{-1} K^{-1})

Thus at point A, h_{void} would be the same as h_{surf}, but at point B the value of h_{void} would be given by:

$$\frac{1}{h_{void}} = \frac{1}{h_{packaging}} + \frac{x_{packaging}}{k_{packaging}} + \frac{x_{tri}}{k_{tri}} \tag{8.5}$$

where x_{tri} is the height of the triangular void (m)

As stated above, it was assumed that the packaging material was always at the same temperature as the cooling medium, thereby allowing the value of k_{tri} to be estimated using the previously developed equations for natural convection and radiation effects in triangular voids.

$$Ra = 10^6 \times \exp\left(5 - 0.016\frac{T_1 + T_2}{2}\right) \times (T_1 - T_2) \times (x_{tri})^3 \tag{5.13}$$

for air voids at temperatures between –13°C and 47°C,

where T_1 is the solid material temperature at position B in Figure 8.3 (°C)
T_2 is the cooling medium temperature (°C)

Triangular voids cooled from below:

$$Nu = 1.12 \times 10^{-5} Ra + 2.31 \tag{5.14}$$

Triangular voids cooled from above:

$$Nu = 6.30 \times 10^{-4} Ra^{0.75} + 1.12 \times 10^{-5} Ra + 2.31 \tag{5.17}$$

$$k_{tri} = Nu \times k_{air} \tag{8.6}$$

Considering now the second stage of the transformation, the shape of the simple model (an infinite slab) was not as complex as the object in Figure 8.3. Assuming that the void was filled with the same solid material as the rest of the object, the model is illustrated in Figure 8.4.

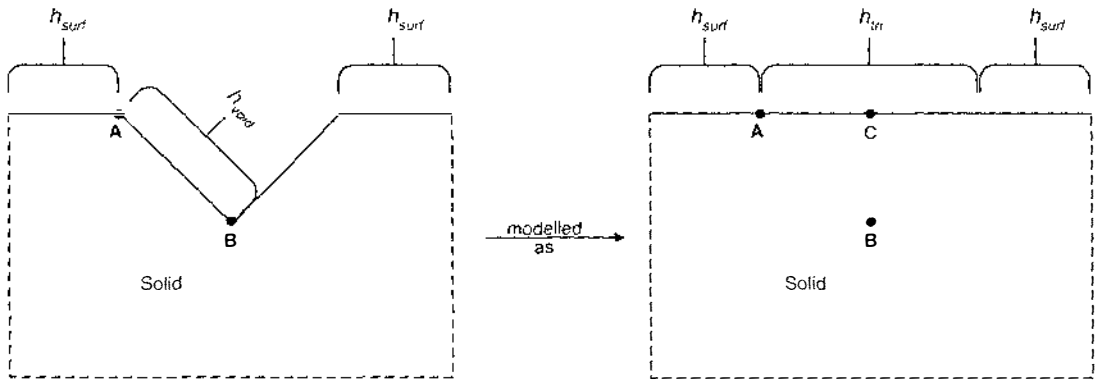

Figure 8.4 A physical model treating the triangular air void as part of the solid material with an effective heat transfer coefficient

The requirement was then to inter-relate h_{void} and h_{tri}. Extending the argument proposed above, along the section of the slab surface where the void was present, the effective heat transfer coefficient (h_{tri}) might vary approximately inversely with respect to position to represent the variation of h_{void} with position. The value of h_{tri} at point A would be the same as h_{surf}, but at point C, h_{tri} might be estimated by a quasi-steady-state approximation developed by subtracting the thermal resistance of the solid in the void from the sum of thermal resistances acting at point B:

$$\frac{1}{h_{tri}} = \frac{1}{h_{surf}} + \frac{x_{tri}}{k_{tri}} - \frac{x_{tri}}{k_{solid}} = \frac{1}{h_{surf}} + x_{tri}\left(\frac{1}{k_{tri}} - \frac{1}{k_{solid}}\right) \tag{8.7}$$

Several assumptions were implied by this quasi-steady-state approach. Firstly, the thermal capacity of the air in the void was ignored. Any invalidity in this assumption was likely to have little effect on cooling rates since the thermal capacity of most solid foods far outweighs the thermal capacity of air. Secondly, the void was assumed to be filled with solid material and the extra thermal capacity of this solid (which may have been significant) would tend to reduce the cooling rates predicted by the model. This was a methodological shortcoming that could not easily be avoided. Thirdly, the incorporation

of the thermal resistance of the packaging layer in the external heat transfer coefficient value meant that the thermal capacity of the packaging layer, and any heat transfer that occurred along the packaging layer rather than directly through it, was ignored. In most practical situations (where the packaging material is typically a 2 to 3mm thick layer of fibreboard or corrugated cardboard) the thermal capacity of the packaging layer and the lateral heat flow through the layer is likely to have little effect on the cooling rate of the package. However, the analogue package used to collect the measured data in chapter 5 had a 6mm thick layer of polycarbonate as packaging. In this case, the disregarded thermal capacity may lead to significant over-estimation of the cooling times predicted by the model and the exclusion of lateral heat flow along the packaging layer may differently affect the predicted cooling rates of analogue packages with different void sizes and different boundary conditions.

From equation 8.7 it can be seen that the value of h_{tri} varies with the depth of the void, and since in Figure 8.4 the depth of the void varies with position along the top surface, h_{tri} will vary in a hyperbolic fashion along the line AC. Thus for solution methods that do not allow h_{tri} to vary along the surface of the slab it was decided that a logarithmic mean of the maximum (at point A) and minimum (at point C) values would yield a more representative average value of h_{tri} than an arithmetic mean.

Furthermore, for solution methods that do not allow spatially different heat transfer coefficients an overall value that acts upon the whole slab surface is required (Figure 8.5).

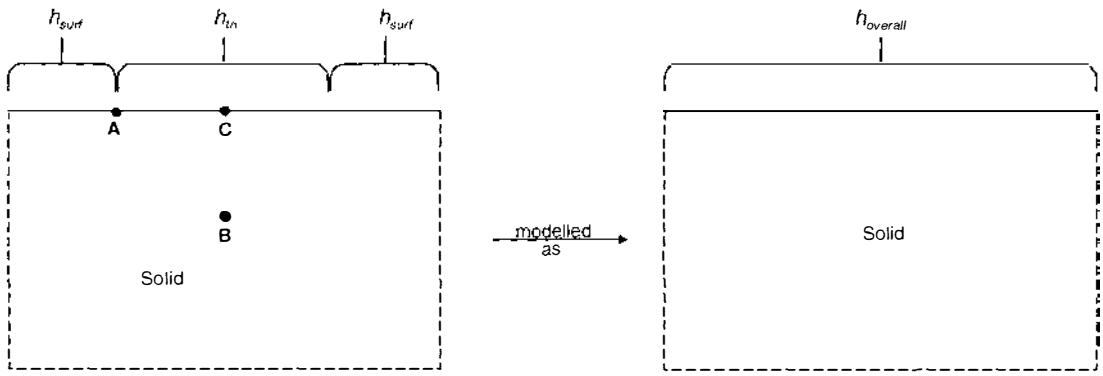

Figure 8.5 A physical model showing averaging of spatially varying heat transfer coefficients

Again, the overall heat transfer coefficient ($h_{overall}$) might be estimated as an average weighted by the proportion of the total surface area that each section with a different heat transfer coefficient occupies:

$$h_{overall} = \frac{A_1}{A_T} h_1 + \frac{A_2}{A_T} h_2 + \frac{A_3}{A_T} h_3 + \ldots\ldots + \frac{A_n}{A_T} h_n \qquad (8.8)$$

where $h_{overall}$ is the overall average heat transfer coefficient (W m^{-2} K^{-1})

n is the number of different sections along the surface

A_n is the surface area of section n (m^2)

A_T is the total top surface area of the slab (m^2)

h_n is the heat transfer coefficient of section n (W m^{-2} K^{-1})

Solution of this simple physical model would not predict a true thermal centre temperature-time profile. It would instead represent an 'averaged' temperature along the geometric centre-line of the package at any given time.

8.5 Food Packages Containing Combined Void Spaces

In chapter 7 it was shown that cooling rates of food packages containing void spaces described by some combination of triangular and rectangular shapes could be determined by treating the component voids separately, even when no physical barriers existed between the component voids. Any overlapping areas were assumed to be part of the rectangular void. The same approach was used in the development of a simple physical model for so called 'combined' void spaces.

Sections 8.3 and 8.4 outlined the development of simple physical models for individual triangular and rectangular void shapes. The simple physical model for packages containing combined void spaces was also an infinite slab with the same thickness and thermal conductivity as the solid material contained within the package. However, where solution methods allowed, the top surface heat transfer coefficient could vary spatially and temporally (Figure 8.6).

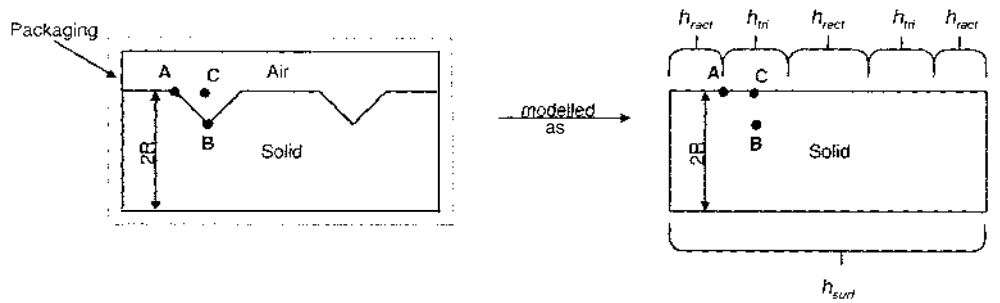

Figure 8.6 Simple physical model for food packages containing combined air spaces

At a position corresponding to the location of a rectangular void, the heat transfer coefficient (h_{rect}) could be determined in the same manner as for individual rectangular voids (section 8.3). At positions corresponding to the location of a triangular void, the heat transfer coefficient (h_{tri}) could be determined in a similar manner to individual triangular voids (section 8.4) but noting that the void height was the distance between the bottom apex of the void and the underside of the packaging material. However, in a combined void space the solid sides of the triangular void section did not touch the underside of the packaging material. Thus the effective heat transfer coefficient values at points A and C in Figure 8.6 had to be calculated in a slightly different way (the value at point B could be calculated in the same way). The value of h_{tri} at point A could be derived by summing the thermal resistances (equation 8.9). Note that the height of the rectangular void (x_{rect}) was used because this was the distance between point A and the underside of the packaging material.

$$\frac{1}{h_{tri}} = \frac{1}{h_{packaging}} + \frac{x_{packaging}}{k_{packaging}} + \frac{x_{rect}}{k_{tri}} \tag{8.9}$$

The value of h_{tri} at point C was estimated by subtracting the thermal resistance of the assumed solid in the void from the sum of thermal resistances acting at point B, which gave equation 8.10. Note that the solid in the void only filled the triangular void to the same height as the rectangular void, so at point C the height of added solid was equal to $(x_{tri} - x_{rect})$.

$$\frac{1}{h_{tri}} = \frac{1}{h_{packaging}} + \frac{x_{packaging}}{k_{packaging}} + \frac{x_{tri}}{k_{tri}} - \frac{(x_{tri} - x_{rect})}{k_{solid}} \tag{8.10}$$

Spatial and temporal averaging of the individual heat transfer coefficients (ie. h_{rect} and h_{tri}) may be required according to the solution method employed by the user. An overall

heat transfer coefficient weighted by the surface area taken up by each section may also be required (as shown in equation 8.8).

8.6 Accuracy of Predictions by the Simple Models

Chilling times for food packages containing various types of void space were predicted using the simple model postulated in sections 8.2 to 8.5. In order to determine the prediction accuracy associated with the simple model, comparisons against measured times and times predicted by the more sophisticated and complex models from chapters 5, 6 and 7 were carried out. If the manner in which the simple model failed to fit the measured data was similar to the complex model this would bring about further confidence in the simple model.

The analogue packages that were used to collect the measured data in chapters 5, 6 and 7 were of half normal carton height and were cooled from one surface only. Therefore the simple model only required a single surface heat transfer coefficient to be calculated and the effect of asymmetric heat transfer was not included.

Comparisons of the times taken for one $\ln Y_c$ reduction between the values of -0.5 and -1.5 were made. At $\ln Y_c$ values below this range, end and edge effects may have affected the measured data causing significant curving of $\ln Y_c$ vs. time plots (observed in the measured data reported in chapters 5, 6 and 7). The simple models were solved using a variety of solution methods to demonstrate the loss in accuracy that the user could expect by applying the assumptions associated with the different methods. A description of the different prediction methods that are compared in this section of the work is given in Table 8.1.

The solution method called FPM32 in Table 8.1, refers to Food Product Modeller version 2.00.842, which is a finite difference program developed by MIRINZ Food Technology and Research, New Zealand. For prediction methods B, C, F and H worked examples are given in Appendix A3. The other prediction methods utilised FINELX, which has been previously described in chapters 6 and 7.

Table 8.1 Description of prediction methods used in section 8.6

Method	Void type	Model	Time Averaged	Space Averaged	Solution Method
A*	Rectangular	2-D FE, fully described analogue package	-	-	FINELX
B	Rectangular	1-D FD, infinite slab	Effective HTC divided into steps	-	FPM32
C	Rectangular	1-D FD, infinite slab	Logarithmically averaged h_{rect}	-	FPM32
D**	Triangular	2-D FE, fully described analogue package	-	-	FINELX
E	Triangular	2-D FE, fully described analogue package	Logarithmically averaged k_{void}	-	FINELX
F	Triangular	1-D FD, infinite slab	Logarithmically averaged Nu	Logarithmically averaged h_{tri} and area-weighted average $h_{overall}$	FPM32
G***	Combined	2-D FE, fully described analogue package	-	-	FINELX
H	Combined	1-D FD, infinite slab	Logarithmically averaged Nu_{tri}	Logarithmically averaged h_{tri} and area-weighted average $h_{overall}$	FPM32

* model developed in chapter 6
** model developed in chapter 5
*** model developed in chapter 7
FE = finite elements
FD = finite differences

8.6.1 Food Packages Containing Rectangular Voids

In chapter 6, a relatively complex finite element conduction model was developed for packages containing rectangular void spaces up to 30mm high. The model was tested against results from six transient chilling trials using an analogue food package. The results from the complex model (called prediction method A hereafter - see Table 8.1) were reproduced in order to test the performance of the simple model.

Prediction method B (see Table 8.1) used the simple physical model from section 8.3. The effective heat transfer coefficient was evaluated over five consecutive time intervals as discussed in section 8.3.2, where the lengths of the time intervals varied because each interval corresponded to an equal change in the surface temperature of the slab (from the initial temperature to the cooling medium temperature).

Prediction method C (see Table 8.1) also used the simple physical model from section 8.3. However the effective heat transfer coefficient was logarithmically averaged over the time of cooling as discussed in section 8.3.3. Note that this is not the same as using prediction method B with one step, since prediction method B would calculate an arithmetic average value of effective heat transfer coefficient, instead of the logarithmic value used by prediction method C.

Table 8.2 Results from prediction method B (with 5 steps)

Run No.	Void Height (mm)	Step No.	Time to reach next step (sec x 10^3)	Cumulative Time (sec x 10^3)	Effective k_{void} ($Wm^{-1}K^{-1}$)	Effective HTC ($Wm^{-2}K^{-1}$)	One $\ln Y_c$ Reduction (sec x 10^3)
5	6	1	5.2	5.2	0.051	4.63	104.4
		2	22.3	27.4	0.050	4.61	
		3	41.3	68.7	0.050	4.58	
		4	71.7	140.5	0.049	4.56	
		5			0.049	4.54	
6	6	1	5.2	5.2	0.051	4.63	104.4
		2	22.3	27.4	0.050	4.61	
		3	41.3	68.7	0.050	4.58	
		4	71.7	140.5	0.049	4.56	
		5			0.049	4.54	
7	10	1	4.7	4.7	0.067	4.88	100.3
		2	20.6	25.3	0.067	4.85	
		3	39.5	64.8	0.066	4.83	
		4	68.9	133.7	0.066	4.81	
		5			0.066	4.78	
8	10	1	6.5	6.5	0.068	4.08	115.2
		2	26.7	33.2	0.067	4.06	
		3	45.7	78.9	0.067	4.04	
		4	79.4	158.3	0.066	4.01	
		5			0.066	3.99	
9	30	1	5.2	5.2	0.185	4.58	107.4
		2	22.8	28.0	0.183	4.54	
		3	42.0	70.0	0.181	4.50	
		4	73.7	143.7	0.177	4.43	
		5			0.160	4.10	
10	30	1	7.1	7.1	0.189	3.89	121.0
		2	28.6	35.7	0.186	3.86	
		3	47.8	83.5	0.184	3.83	
		4	83.3	166.9	0.180	3.78	
		5			0.169	3.63	

Prediction methods A, B, and C were used to predict the chilling times of the six transient chilling trials reported in chapter 6. The results of prediction method B with five steps are summarised in Table 8.2.

The measured data and predictions by methods A and B (with 5 steps) are compared in Table 8.3. Prediction method A gave good agreement with the measured times for one $\ln Y_c$ reduction (the mean percentage difference was +0.7% with a standard deviation of 3.1%, giving a 95% confidence interval of (-7, +8)%). Prediction method B (with 5 steps) agreed closely with method A (the mean percentage difference was +3.1% with a standard deviation of 1.7%), and also gave good agreement with the measured data (the mean percentage difference was +3.8% with a standard deviation of 4.3%, and the 95% confidence interval was (-7, +14)%). These results indicated that the simplifications employed by prediction method B (with 5 steps) led to a mean over-prediction of about 3% and slightly more spread of predictions than method A, although six results are unlikely to yield a robust estimate of the standard deviation. In section 6.4.3.3, an experimental uncertainty of ±5% was reported for the measured data, so while most of the lack of fit to prediction method A was explainable by measured uncertainty this was not true of prediction method B. However the uncertainty in prediction method B was not large.

Table 8.3 Comparison of measured data and results from prediction methods A and B (with 5 steps) - Times for one $\ln Y_c$ reduction (seconds x 10^3)

Run No.	Void Height (mm)	Measured Data	Prediction method A	% diff. from measured	Prediction method B	% diff. from method A	% diff. from measured
5	6	99.6	102.7	3.1	104.4	1.7	4.8
6	6	107.4	102.3	-4.7	104.4	2.1	-2.8
7	10	98.5	98.8	0.3	100.3	1.5	1.8
8	10	108.9	110.8	1.7	115.2	4.0	5.8
9	30	97.6	101.4	3.9	107.4	5.9	10.0
10	30	117.1	117.0	-0.1	121.0	3.4	3.3
			Mean	**+0.7**		**+3.1**	**+3.8**
			St. Dev.	**3.1**		**1.7**	**4.3**

In order to show how the number of steps in slab surface temperature over which the heat transfer coefficient was calculated affected the accuracy of method B, predictions using a different number of steps were carried out. The package that was most likely to have the largest change in heat flux occurring through the void over the course of the cooling trial was chosen. Run 9 had the largest change in effective HTC over the five steps (observed

in Table 8.3), and this run was also the package with the largest sized void and the highest heat transfer coefficient. The corresponding percentage differences from the measured result using 1, 2, 3, 4, 5, and 10 steps are shown in Table 8.4. No increase in accuracy was observed, suggesting that one step was adequate.

Table 8.4 Comparison of times for one $\ln Y_c$ reduction predicted by method B with a different number of steps (seconds x 10^3)

No. of steps, N	Measured Result	Prediction method B (with N steps)	% diff. from measured
1	97.6	105.5	+8.1
2	97.6	107.5	+10.2
3	97.6	107.9	+10.5
4	97.6	108.1	+10.7
5	97.6	107.4	+10.0
10	97.6	107.2	+9.9

The results of prediction method C are given in Table 8.5. A worked example is given in Appendix A3.

Table 8.5 Results from prediction method C

Run No.	Void Height (mm)	Maximum k_{void} ($Wm^{-1}K^{-1}$)	Minimum k_{void} ($Wm^{-1}K^{-1}$)	Maximum effective HTC ($Wm^{-2}K^{-1}$)	Minimum effective HTC ($Wm^{-2}K^{-1}$)	Logarithmic average effective HTC ($Wm^{-2}K^{-1}$)	Time for one $\ln Y_c$ reduction (sec x 10^3)
5	6	0.054	0.049	4.78	4.52	4.65	103.0
6	6	0.054	0.049	4.78	4.52	4.65	103.0
7	10	0.092	0.065	6.04	4.77	5.38	92.4
8	10	0.091	0.065	4.81	3.98	4.38	107.7
9	30	0.205	0.148	4.93	3.86	4.37	107.9
10	30	0.205	0.148	4.10	3.32	3.70	122.9

In Table 8.6 the measured data and the results from prediction method B (with one step) and prediction method C were compared. The data illustrated the difference between taking an arithmetic average or a logarithmic average of the effective heat transfer coefficient over time. The arithmetic average (method B) gave a 95% confidence interval of (-6, +12)% and the logarithmic average (method C) gave a 95% confidence interval of (-14, +17)%. Although six results were unlikely to yield a robust estimate of the standard deviation, the results indicate that prediction method B was more likely to give accurate predictions than method C.

Table 8.6 Comparison of measured data and results from prediction methods B (with one step) and C - Times for one $\ln Y_c$ reduction (seconds x 10^3)

Run No.	Void Height (mm)	Measured Data	Method B (with 1 step)	% diff. from measured	Method C	% diff. from measured
5	6	99.6	104.1	4.5	103.0	3.4
6	6	107.4	104.0	-3.1	103.0	-4.1
7	10	98.5	100.0	1.5	92.4	-6.2
8	10	108.9	114.7	5.3	107.7	-1.1
9	30	97.6	105.5	8.1	107.9	10.6
10	30	117.1	119.6	2.1	122.9	5.0
			Mean	**+3.1**		**+1.3**
			St. Dev.	**3.8**		**6.3**

The individual percentage differences between the measured data and prediction method A were plotted against the individual percentage differences between the measured data and prediction method B (with one step) in Figure 8.7. Only a small number of data points were available, but the plot displays a positive relationship between the percentage differences. The manner in which prediction method B failed to fit the measured data was similar to prediction method A, which provides further confidence in the validity of the simplifying assumptions employed by prediction method B. Figure 8.7 distinguishes between samples with high and low heat transfer coefficients. There was no apparent trend with heat transfer coefficient and, although not shown here, there was also no apparent trend with varying void size or with packages that were cooled from above or below.

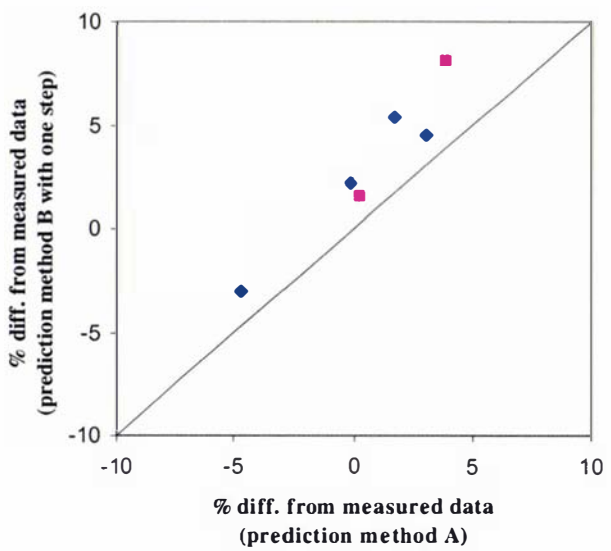

Figure 8.7 Plot of percentage differences from the measured data for prediction method A and prediction method B (with one step)
[KEY: pink squares = high HTC, blue diamonds = low HTC]

8.6.2 Food Packages Containing Triangular Voids

In chapter 5, the results of twenty-eight transient chilling trials with an analogue food package were reported. The measured data were used to establish the relationship between Ra and Nu for triangular voids up to 50mm high, enabling the effective thermal conductivities of the voids to be estimated. The complex finite element model developed in chapter 7 allowed the combined effects of natural convection and radiation in triangular air voids to be modelled in a food package undergoing transient chilling.

The level of agreement between the measured data and the results predicted by the complex finite element model had not been presented previously. This was because the measured data were used to determine the extent of natural convection and radiation in the air voids for the model, and thus the two data sets would be expected to broadly agree. However the data predicted by the model (called 'prediction method D' in this section - see Table 8.1) are presented to assist testing of the validity of the simple model that has been developed in this chapter.

Prediction method E (see Table 8.1) was the same as prediction method D except that the effective thermal conductivity of the air voids was not changed as the temperature difference across the void changed. Instead, the constant value of effective thermal conductivity was estimated by logarithmically averaging the maximum and minimum effective thermal conductivity values (assuming the maximum possible temperature difference across the void and no temperature difference across the void respectively).

In Table 8.7 the results from prediction methods D and E are compared to the measured data from chapter 5. Times for one $\ln Y_c$ reduction predicted by method D gave a mean percentage difference of -4.1% and a standard deviation of 3.8% from the measured results (excluding the measured results for 30mm high voids, which were considered invalid). The offset from zero difference can be explained as follows - the best-fit relationship to the experimental Nu and Ra data (equation 5.17 shown in Figure 5.23) tended to over-estimate values of Nu at lower Ra values. For the data sets here, during most of the cooling time of the food package the Nu number in the voids was lower than 5 (see Table 5.7). This may have led to over-estimation of the true effective thermal conductivity in the air voids for much of the time during cooling, which would in turn reduce the predicted cooling times.

For almost all runs where the air voids were cooled from above, prediction method E under-predicted the cooling times predicted by method D (with a mean percentage

difference of –1.7% and a standard deviation of 2.3% for all runs). This suggested that the logarithmic average employed by prediction method E gave slightly higher estimates of the effective thermal conductivity in the air voids than prediction method D. This led to further under-prediction of measured times for one $\ln Y_c$ reduction by method E (ie. a mean percentage difference of –6.1% and a standard deviation of 5.2% from the valid measured data). These results indicated that the simplification of logarithmically averaging the effective thermal conductivity of triangular air voids changed the quality of fit of the model from a 95% confidence interval of (-12, +4)% for method D, to a 95% confidence interval of about (-17, +4)% for method E.

Table 8.7 Comparison of measured data and results from prediction methods D and E - Times for one $\ln Y_c$ reduction (seconds x 10^3)

Run No.	Void Height (mm)	HTC ($Wm^{-2}K^{-1}$)	Measured Data	Prediction method D	% diff. from measured	Prediction method E	% diff. from method D	% diff. from measured
1	20	12.7	65.8	65.8	0	65.6	-0.3	-0.3
2	20	29.6	53.3	52.1	-2.3	52.2	0.2	-2.1
3	20	12.7	66.1	66.5	0.6	66.5	0	0.6
4	20	29.6	53.9	51.6	-4.3	51.6	0	-4.3
5	30	29.6	64.3*	54.1	-	53.2	-1.7	-
6	30	12.7	74.6*	68.1	-	68.1	0	-
7	30	29.6	64.3*	53.9	-	53.9	0	-
8	30	12.7	77.4*	68.0	-	68.0	0	-
9	30	29.6	67.2*	53.8	-	53.8	0	-
16	30	29.6	63.5*	53.4	-	53.4	0	-
11	40	12.7	74.9	72.4	-3.3	72.4	0	-3.3
12	40	12.7	71.9	68.9	-4.2	66.3	-3.8	-7.8
15	40	29.6	67.8	59.6	-12.1	59.6	0	-12.1
16	40	29.6	57.5	55.4	-3.7	53.5	-3.4	-6.9
5	50	29.6	66.4	66.9	0.8	66.9	0	0.8
6	50	12.7	76.4	79.4	3.9	79.4	0	3.9
7	50	29.6	58.8	55.7	-5.3	53.6	-3.8	-8.9
8	50	12.7	70.0	68.8	-1.7	65.1	-5.4	-7.0
9	50	29.6	59.2	55.2	-6.8	52.8	-4.3	-10.8
10	50	29.6	61.0	55.5	-9.0	53.0	-4.5	-13.1
10	50	29.6	68.5	64.4	-6.0	64.4	0	-6.0
11	50	12.7	72.1	67.8	-6.0	63.8	-5.9	-11.5
12	50	12.7	79.1	77.0	-2.7	77.0	0	-2.7
13	50	29.6	60.8	54.9	-9.7	52.7	-4.0	-13.3
13	50	29.6	66.7	64.4	-3.4	64.4	0	-3.4
14	50	12.7	73.6	68.5	-6.9	64.8	-5.4	-12.0
14	50	12.7	77.9	76.8	-1.4	76.8	0	-1.4
15	50	29.6	59.5	55.6	-6.6	52.6	-5.4	-11.6
				Mean	**-4.1**		**-1.7**	**-6.1**
				St. Dev.	**3.8**		**2.3**	**5.2**

* these measured results were affected by poor construction of the Tylose sample block.

Prediction method F (see Table 8.1) used the simple physical model described in section 8.4. Temporal and spatial variations were averaged as discussed in sections 8.4.2 and 8.4.3 respectively. An overall heat transfer coefficient (as in section 8.4.3) was determined since FPM32 did not allow spatially variable heat transfer coefficients. The results from prediction method F are given in Table 8.8 and a worked example is shown in Appendix A3.

Table 8.8 Results from prediction method F

Run No.	Void Height (mm)	Mean k_{void} value over time ($Wm^{-1}K^{-1}$)	Mean h_{tri} Value over time ($Wm^{-2}K^{-1}$)	Average Overall HTC ($Wm^{-2}K^{-1}$)	Time for one $\ln Y_c$ Reduction (sec x 10^3)
1	20	0.077	5.8	8.5	67.8
2	20	0.077	8.7	14.6	50.6
3	20	0.062	5.4	8.4	68.4
4	20	0.062	8.1	14.4	50.9
5	30	0.103	8.5	13.2	52.9
6	30	0.104	5.7	7.9	70.8
7	30	0.071	7.5	12.7	53.9
8	30	0.071	5.0	7.5	73.2
9	30	0.071	7.5	12.7	53.9
16	30	0.071	7.5	12.7	53.9
11	40	0.090	5.0	6.8	77.6
12	40	0.143	5.9	7.4	73.6
15	40	0.087	7.4	11.1	57.7
16	40	0.143	8.9	12.1	55.0
5	50	0.117	7.7	9.9	61.6
6	50	0.118	5.2	6.2	82.5
7	50	0.188	9.4	11.2	56.8
8	50	0.185	6.2	7.0	75.4
9	50	0.193	9.6	11.3	56.5
10	50	0.189	9.5	11.2	56.8
10	50	0.118	7.7	9.9	61.5
11	50	0.188	6.2	7.0	75.4
12	50	0.118	5.2	6.2	82.5
13	50	0.191	9.5	11.3	56.8
13	50	0.122	7.8	10.0	61.5
14	50	0.187	6.2	7.0	75.4
14	50	0.118	5.2	6.2	82.5
15	50	0.183	9.3	11.1	57.1

In Table 8.9, predictions by method F are compared to the measured data and results from prediction methods D and E. As expected, the substitution of solid material in the air void employed by prediction method F increased the amount of thermal mass within the slab, leading to predicted cooling times that generally got longer as the void size increased. Prediction method F also ignored any end or edge effects. Prediction method F broadly agreed with prediction method E (the mean percentage difference was +3.8%

with a standard deviation of 5.9%) and agreed similarly with prediction method D (the mean percentage difference was +2.1% with a standard deviation of 4.7%). Comparison of predictions by method F against the valid measured data gave a mean percentage difference of –2.0% with a standard deviation of 6.7%. The 95% confidence interval for prediction method F was (-15, +11)% indicating that the temporal and spatial averaging employed by the method gave predictions that were more spread than prediction method E. In section 5.3, an experimental uncertainty of ±5% was reported for the measured data, thus by subtracting the variances, prediction method F had a 95% confidence interval of (-14, +10)%, which was likely to be acceptable to industry.

Table 8.9 Percentage differences between prediction method F, the measured data, and prediction methods D and E

Run No.	Void Height (mm)	HTC ($Wm^{-2}K^{-1}$)	Measured Data	Prediction method F			
				Time for one $\ln Y_c$ reduction	% diff. from method E	% diff. from method D	% diff. from measured
1	20	12.7	65.8	67.8	3.2	2.9	2.9
2	20	29.6	53.3	50.6	-3.2	-3.0	-5.3
3	20	12.7	66.1	68.4	2.8	2.8	3.4
4	20	29.6	53.9	50.9	-1.4	-1.4	-5.9
5	30	29.6	-	52.9	-0.5	-2.3	-
6	30	12.7	-	70.8	3.8	3.8	-
7	30	29.6	-	53.9	0	0	-
8	30	12.7	-	73.2	7.1	7.1	-
9	30	29.6	-	53.9	0.2	0.2	-
16	30	29.6	-	53.9	0.9	0.9	-
11	40	12.7	74.9	77.6	6.7	6.7	3.5
12	40	12.7	71.9	73.6	9.9	6.4	2.3
15	40	29.6	67.8	57.7	-3.3	-3.3	-17.5
16	40	29.6	57.5	55.0	2.7	-0.7	-4.5
5	50	29.6	66.4	61.6	-8.6	-8.6	-7.8
6	50	12.7	76.4	82.5	3.8	3.8	7.4
7	50	29.6	58.8	56.8	5.7	1.9	-3.5
8	50	12.7	70.0	75.4	13.7	8.8	7.2
9	50	29.6	59.2	56.5	6.5	2.3	-4.8
10	50	29.6	61.0	56.8	6.7	2.3	-7.4
10	50	29.6	68.5	61.5	-4.7	-4.7	-11.4
11	50	12.7	72.1	75.4	15.4	10.1	4.4
12	50	12.7	79.1	82.5	6.7	6.7	4.1
13	50	29.6	60.8	56.8	7.2	3.3	-7.0
13	50	29.6	66.7	61.5	-4.7	-4.7	-8.5
14	50	12.7	73.6	75.4	14.1	9.2	2.4
14	50	12.7	77.9	82.5	6.9	6.9	5.6
15	50	29.6	59.5	57.1	7.9	2.6	-4.2
				Mean	**+3.8**	**+2.1**	**-2.0**
				St. Dev.	**5.9**	**4.7**	**6.7**

The individual percentage differences from the measured data for prediction method D were plotted against the individual percentage differences from the measured data for prediction method F in Figure 8.8. The plot shows that, compared to prediction method D, prediction method F over-estimated the cooling times of samples with a low heat transfer coefficient and slightly under-estimated the cooling times of samples with a high heat transfer coefficient. Although the equivalent plots are not shown here, there also appeared to be a possible trend whereby prediction method F over-estimated the cooling times of samples containing larger voids and samples that were cooled from below. It was considered probable that the observed differences were caused by sideways heat flow through the polycarbonate packaging layer, which prediction method F did not account for. Considering that the thermal conductivity of the air voids was much lower than that of solid Tylose, the section of polycarbonate packaging in contact with the solid Tylose would have been at a higher temperature than the section of polycarbonate in contact with the triangular air void. This would have given rise to sideways heat flow along the polycarbonate packaging layer (illustrated in Figure 8.9). The amount of sideways heat flow that was unaccounted for in prediction method F would be expected to be larger at lower heat transfer coefficients and in packages where the air voids had a lower thermal conductivity or were of a larger size. Therefore, the phenomenon of sideways heat flow could explain why the cooling times of packages with larger air voids, cooled from below with a low heat transfer coefficient were more over-estimated by prediction method F than prediction method D.

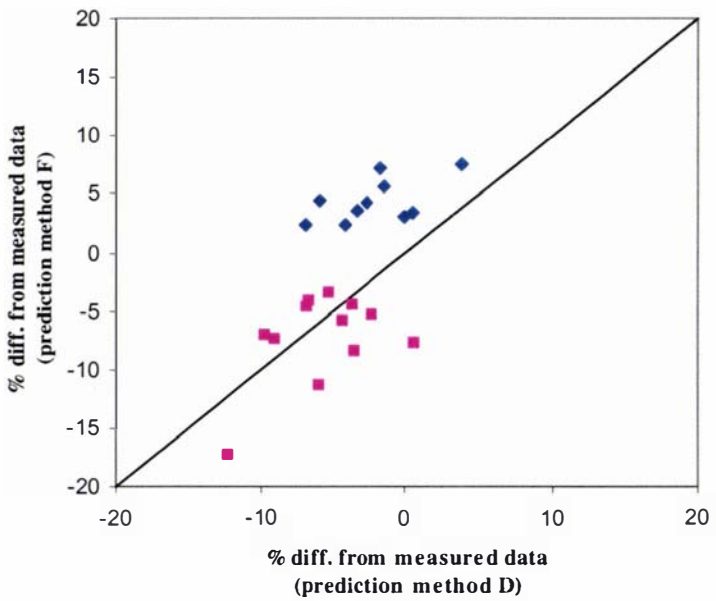

Figure 8.8 Plot of percentage differences from the measured data for prediction methods D and F

[KEY: pink squares = high HTC, blue diamonds = low HTC]

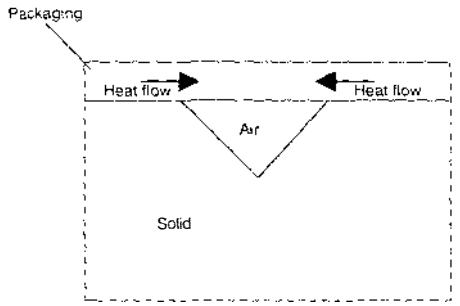

Figure 8.9 Sideways heat flow in the polycarbonate packaging layer

The potential amount of extra heat flow from the solid Tylose due to the sideways heat flow in the polycarbonate layer was illustrated by using steady-state finite element simulations. A 6mm thick polycarbonate layer with six different combinations of boundary conditions was simulated using FINELX (Figure 8.10). The details of the boundary conditions are given in Table 8.10. For each case, the average top surface temperature (T_s) was estimated by an arithmetic mean of temperatures calculated at one hundred evenly spaced intervals along the top surface, and the heat flow (ϕ) through the top surface of the polycarbonate layer was calculated using equation 8.11.

$$\phi = hA(T_s - T_a) \tag{8.11}$$

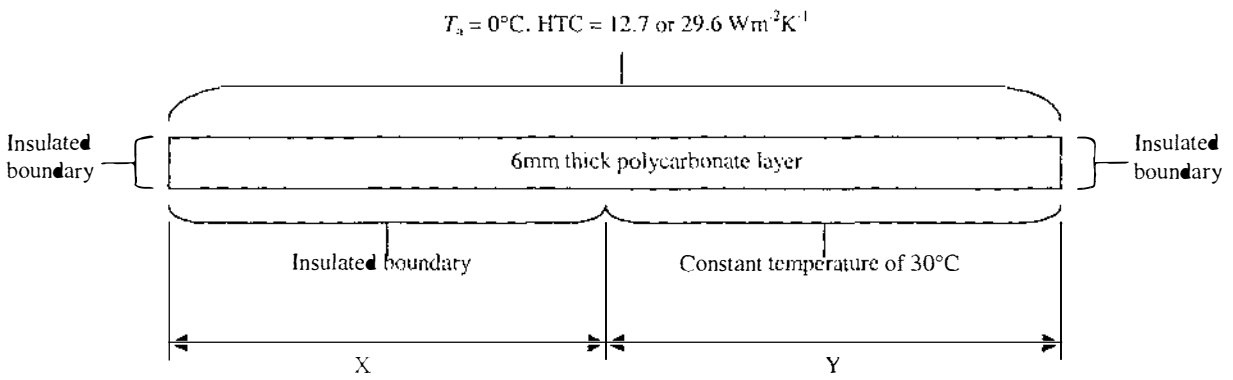

Figure 8.10 Diagram of the steady-state FINELX simulation to determine the effect of sideways heat flow (further details are given in Table 8.10)

Table 8.10 Combinations of boundary conditions for Figure 8.10

Void Size (mm)	Heat Transfer Coefficient ($Wm^{-2}K^{-1}$)	X (mm)	Y (mm)
20	12.7	20	45
20	29.6	20	45
40	12.7	40	25
40	29.6	40	25
50	12.7	50	15
50	29.6	50	15

The heat flow through the top surface of the polycarbonate layer was also estimated with no sideways heat flow, for each of the six different combinations of void size and heat transfer coefficient, by using analytical methods. For each combination, the total heat flows through the top surface with and without sideways heat flow were compared in order to observe the effect of sideways heat flow in the polycarbonate layer. These values are summarised in Table 8.11. Note that the values ignore any heat flow through the air void to the polycarbonate layer. However, since most of the heat in the package exited through the surface where the solid Tylose was in contact with the polycarbonate layer the estimated heat flow values illustrate the majority of the sideways heat flow effect.

Table 8.11 Estimated total heat flow values (with and without sideways heat flow)

Void Size (mm)	Heat Transfer Coefficient ($Wm^{-2}K^{-1}$)	Total Heat Flow with sideways heat flow (W)	Total Heat Flow without sideways heat flow (W)	Ratio of Heat Flows
20	12.7	15.48	13.08	1.18
20	29.6	26.05	23.16	1.12
40	12.7	9.82	7.27	1.35
40	29.6	15.87	12.87	1.23
50	12.7	6.94	4.36	1.59
50	29.6	10.76	7.72	1.39

The ratio of heat flows given in Table 8.11 could be used to account for the decrease in cooling time that was caused by sideways heat flow, since most of the heat in the package exited through the surface where the solid Tylose was in contact with the polycarbonate layer. A new effective area was calculated for these surfaces by multiplying the actual areas by the ratios of heat flows. For prediction method F, this yielded an increase in the effective area where the heat transfer coefficient h_{surf} acted (see Figure 8.4) and a corresponding decrease in the effective area where the heat transfer coefficient h_{tri} acted.

This increased the overall heat transfer coefficient, reducing the amount of cooling time over-estimation. The results of prediction method F (with the effective area adjustment included) are given in Table 8.12.

Table 8.12 Results from prediction method F (with effective area adjustment included)

Run No.	Void Height (mm)	Ratio of Heat Flows	New Overall HTC ($Wm^{-2}K^{-1}$)	Time for one $\ln Y_c$ Reduction (sec x 10^3)
1	20	1.18	9.0	65.5
2	20	1.12	15.3	49.5
3	20	1.18	8.9	65.9
4	20	1.12	15.1	49.6
5	30	-	-	-
6	30	-	-	-
7	30	-	-	-
8	30	-	-	-
9	30	-	-	-
16	30	-	-	-
11	40	1.35	7.4	73.6
12	40	1.35	7.9	70.5
15	40	1.23	12.0	55.5
16	40	1.23	12.8	53.5
5	50	1.39	10.7	58.7
6	50	1.59	6.8	77.6
7	50	1.39	11.9	55.2
8	50	1.59	7.5	73.2
9	50	1.39	12.0	55.0
10	50	1.39	11.9	55.2
10	50	1.39	10.8	58.7
11	50	1.59	7.5	72.6
12	50	1.59	6.8	77.6
13	50	1.39	12.0	55.0
13	50	1.39	10.8	58.4
14	50	1.59	7.5	72.6
14	50	1.59	6.8	77.6
15	50	1.39	11.8	55.5

The results from Table 8.12 were compared to the measured data and the results from prediction methods D and F. From Table 8.13 it can be seen that the inclusion of the effective area adjustment has not improved the agreement between prediction method F and the measured data - the new 95% confidence interval is (-17, +6)%. However, the inclusion of the effective area adjustment has made prediction method F agree much more closely with prediction method D – the new 95% confidence interval is (-10, +9)%.

Table 8.13 Percentage differences between prediction method F (with effective area adjustment included), the measured data, and prediction methods D and F

Run No.	Void Height (mm)	HTC ($Wm^{-2}K^{-1}$)	Measured Data	Prediction method F with effective area adjustment			
				Time for one $\ln Y_c$ reduction	% diff. from method D	% diff. from method F	% diff. from measured
1	20	12.7	65.8	65.5	-0.5	-3.4	-0.5
2	20	29.6	53.3	49.5	-5.0	-2.2	-7.1
3	20	12.7	66.1	65.9	-0.9	-3.7	-0.3
4	20	29.6	53.9	49.6	-3.9	-2.6	-8.0
5	30	29.6	-	-	-	-	-
6	30	12.7	-	-	-	-	-
7	30	29.6	-	-	-	-	-
8	30	12.7	-	-	-	-	-
9	30	29.6	-	-	-	-	-
16	30	29.6	-	-	-	-	-
11	40	12.7	74.9	73.6	1.7	-5.2	-1.7
12	40	12.7	71.9	70.5	2.3	-4.2	-1.9
15	40	29.6	67.8	55.5	-6.9	-3.8	-18.1
16	40	29.6	57.5	53.5	-3.4	-2.7	-7.0
5	50	29.6	66.4	58.7	-12.3	-4.7	-11.6
6	50	12.7	76.4	77.6	-2.3	-5.9	1.6
7	50	29.6	58.8	55.2	-0.9	-2.8	-6.1
8	50	12.7	70.0	73.2	6.4	-2.9	4.6
9	50	29.6	59.2	55.0	-0.4	-2.7	-7.1
10	50	29.6	61.0	55.2	-0.5	-2.8	-9.5
10	50	29.6	68.5	58.7	-8.9	-4.6	-14.3
11	50	12.7	72.1	72.6	7.1	-3.7	0.7
12	50	12.7	79.1	77.6	0.8	-5.9	-1.9
13	50	29.6	60.8	55.0	0.2	-3.2	-9.5
13	50	29.6	66.7	58.4	-9.3	-5.0	-12.4
14	50	12.7	73.6	72.6	6.0	-3.7	-1.4
14	50	12.7	77.9	77.6	1.0	-5.9	-0.4
15	50	29.6	59.5	55.5	-0.2	-2.8	-6.7
				Mean	**-0.7**	**-3.8**	**-5.4**
				St. Dev.	**4.8**	**1.2**	**5.8**

The individual percentage differences from the measured data for prediction method D were plotted against the individual percentage differences from the measured data for prediction method F with the effective area adjustment in Figure 8.11. The data sets with a high and low heat transfer coefficient were still distinctly separate, however, the bulk of the data were now much closer to the 45° line, which suggested that the inclusion of the effective area adjustment improved prediction method F so that the manner in which it failed to match the measured data was similar to prediction method D.

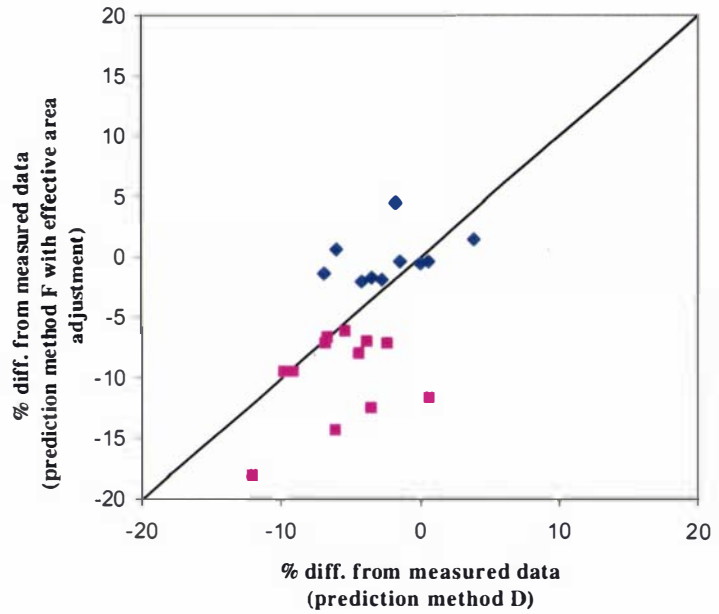

Figure 8.11 Plot of percentage differences from the measured data for prediction method D and prediction method F (with effective area adjustment included) [KEY: pink squares = high HTC, blue diamonds = low HTC]

In practical situations, where the packaging material is usually a 2 to 3mm thick layer of fibreboard or corrugated cardboard, the effective area adjustment would be expected to be closer to unity and thus its use would not be as important. This is because a thin packaging layer with a low thermal conductivity value would have a smaller amount of sideways heat flow when compared to these test cases.

8.6.3 Food Packages Containing Combined Voids

In chapter 7, a relatively complex finite element conduction model was developed for packages containing void spaces that could be described using some combination of rectangular and triangular void sections. The model was tested by the collection of measured data from fourteen transient chilling experiments using an analogue food package. These data were not used in model development and thus provided an independent test of the prediction accuracy of the model. The results from the complex model (called prediction method G hereafter - see Table 8.1) were reproduced in order to test the performance of the simple model.

Prediction method H (see Table 8.1) used the simple physical model explained in section 8.5. Since FPM32 did not allow spatially variable heat transfer coefficients, an average

overall heat transfer coefficient weighted by surface area was determined (as discussed in section 8.4.3).

Prediction methods G and H were used to predict the chilling times of the fourteen transient chilling trials reported in chapter 6. The results of prediction method H are summarised in Table 8.14 and a worked example is shown in Appendix A3.

Table 8.14 Results from prediction method H

Run No.	Rectangular Void Height (mm)	Triangular Void Height (mm)	Mean h_{tri} value over time ($Wm^{-2}K^{-1}$)	Mean h_{rect} value over time ($Wm^{-2}K^{-1}$)	Average Overall HTC ($Wm^{-2}K^{-1}$)	Time for one $\ln Y_c$ reduction (sec x 10^3)
1A	25	25	-*	4.54	4.54	104.8
1B	25	50	4.53	4.55	4.54	104.8
2A	25	25	-*	4.54	4.54	104.8
2B	25	50	4.46	4.55	4.52	105.1
3A	25	25	-*	3.81	3.81	120.1
3B	25	50	3.77	3.81	3.80	120.3
4A	25	25	-*	3.81	3.81	120.1
4B	25	50	3.76	3.81	3.79	120.5
5A	10	30	4.67	5.72	5.40	89.9
5B	10	50	6.26	5.73	6.06	82.5
6A	10	30	3.88	4.61	4.38	105.5
6B	10	50	4.96	4.62	4.83	97.4
7A	10	30	3.88	4.61	4.39	105.7
7B	10	50	4.96	4.61	4.83	97.4

* no triangular void present in these samples (ie. rectangular void height minus triangular void height = 0)

The measured data are compared to the results from prediction methods G and H in Table 8.15, and the lack of fit for each prediction method is compared in Figure 8.12. Prediction method G gave times for one $\ln Y_c$ reduction with a mean percentage difference of +1.7% and a standard deviation of 5.1% from the measured data, so the 95% confidence interval was (-9, +12)%. Prediction method H agreed closely with predictions from method G (a mean percentage difference of +2.9% with a standard deviation of 4.9%), and also with the measured results (a mean percentage difference of +4.6% with a standard deviation of 6.4%, giving a 95% confidence interval of (-9, +17)%). Figure 8.12 shows that the data are scattered in proximity to the 45° line, which suggested that the manner in which prediction method H failed to fit the measured data was similar to prediction method G. This provides further confidence in the validity of the simplifications employed when using prediction method H. There was no apparent trend with heat transfer coefficient, void size, or whether cooling was from above or below. In

section 7.5, an experimental uncertainty of ±9% was reported for the measured data, and thus by subtracting the variances the actual 95% confidence interval for prediction method H was about (0, +14)%, which was likely to be acceptable to industry.

Table 8.15 Comparison of measured data and results from prediction methods G and H - Times for one $\ln Y_c$ reduction (seconds x 10^3)

Run No.	Measured Data	Prediction method G	% diff. from measured	Prediction method H	% diff. from method G	% diff. from measured
1A	97.8	99.4	1.6	104.8	5.4	7.2
1B	94.4	99.3	5.2	104.8	5.5	11.0
2A	105.7	97.7	-7.6	104.8	7.3	-0.9
2B	99.4	95.6	-3.8	105.1	9.9	5.7
3A	107.9	114.9	6.5	120.1	4.5	11.3
3B	104.7	113.1	8.0	120.3	6.4	14.9
4A	110.6	114.4	3.4	120.1	5.0	8.6
4B	107.5	112.9	5.0	120.5	6.7	12.1
5A	89.6	95.7	6.8	89.9	-6.1	0.3
5B	82.7	81.6	-1.3	82.5	1.1	-0.2
6A	103.7	110.2	6.3	105.5	-4.3	1.7
6B	95.5	95.3	-0.2	97.4	2.2	2.0
7A	110.3	110.7	0.4	105.7	-4.5	-4.2
7B	102.4	95.6	-6.6	97.4	1.9	-4.9
		Mean	**+1.7**		**+2.9**	**+4.6**
		St. Dev.	**5.1**		**4.9**	**6.4**

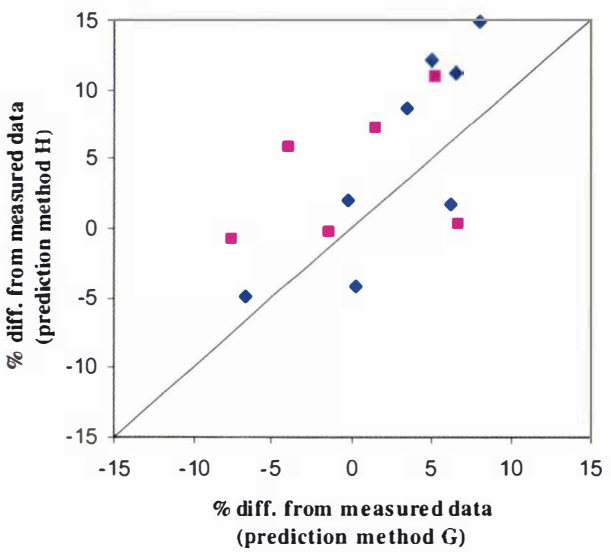

Figure 8.12 Plot of percentage differences from the measured data for prediction methods G and H
[pink squares = high HTC, blue diamonds = low HTC]

8.6.4 Cooling Times vs. Cooling Rates

In sections 8.6.1 to 8.6.3 the performance of the newly developed prediction methods was tested on the basis of matching measured times for one $\ln Y_c$ reduction during the period where the $\ln Y_c$ vs. time plot yielded a straight line (between the values of -0.5 and -1.5). This test effectively compared the rates of cooling at the centre of the package and ignored the lag phase at the centre position that exists during the initial part of all transient cooling processes with a Bi greater than zero.

To include this lag phase in the testing of the simple and complex methods, the measured and predicted times taken for one and a half $\ln Y_c$ reductions (from 0 to -1.5, where Y_c = 0.223) were compared for prediction methods A, B (with one step), D, F (with effective area adjustment included), G and H. At $\ln Y_c$ values below this range, end and edge effects may have affected the measured data causing significant curving of $\ln Y_c$ vs. time plots (observed in the measured data reported in chapters 5, 6 and 7).

For packages containing rectangular voids, Table 8.16 compared the measured times for 1.5 $\ln Y_c$ reductions with those predicted by methods A and B (with one step). The 95% confidence intervals were in a similar range to those calculated for one $\ln Y_c$ reduction. For prediction method A, the 95% confidence interval was (-6, +9)% and for prediction method B (with one step) it was (-4, +12)%.

Table 8.16 Comparison of measured data and results from prediction methods A and B (with one step) - Times for 1.5 $\ln Y_c$ reductions (seconds x 10^3)

Run No.	Void Height (mm)	Measured Data	Method A	% diff. from measured	Method B (with 1 step)	% diff. from measured
5	6	158.2	161.4	2.0	165.8	4.8
6	6	167.8	160.9	-4.1	165.8	-1.2
7	10	155.0	160.5	3.5	159.7	3.0
8	10	173.4	180.0	3.8	181.8	4.8
9	30	154.6	159.1	2.9	168.0	8.6
10	30	183.3	186.0	1.5	189.2	3.2
			Mean	**+1.6**		**+3.9**
			St. Dev.	**2.9**		**3.2**

For packages containing triangular voids, Table 8.17 compared the measured times for 1.5 $\ln Y_c$ reductions with those predicted by methods D and F (with the effective area adjustment included). The 95% confidence intervals were also in a similar range to those calculated for one $\ln Y_c$ reduction. For prediction method D, the 95% confidence interval

was (-11, +4)% and for prediction method F (with the effective area adjustment included) it was (-15, +8)%.

Table 8.17 Comparison of measured data and results from prediction methods D and F (with the effective area adjustment included) - Times for 1.5 $\ln Y_c$ reductions (seconds x 10^3)

Run No.	Void Height (mm)	Measured Data	Method D	% diff. from measured	Method F (with effective area adjustment)	% diff. from measured
1	20	105.1	104.9	-0.2	106.8	1.6
2	20	85.0	85.1	0.1	82.3	-3.2
3	20	106.6	105.4	-1.1	106.8	0.2
4	20	88.5	84.7	-4.3	82.4	-6.8
11	40	120.9	118.6	-1.9	119.3	-1.3
12	40	114.8	111.9	-2.5	113.2	-1.4
15	40	110.7	98.5	-11.0	92.1	-16.8
16	40	93.2	90.9	-2.5	87.6	-6.0
5	50	107.8	108.7	0.8	99.8	-7.4
6	50	122.2	128.4	5.1	130.6	6.8
7	50	93.9	90.0	-4.2	89.2	-5.0
8	50	112.3	109.9	-2.1	115.0	2.4
9	50	93.0	88.5	-4.8	88.8	-4.5
10	50	96.7	89.0	-8.0	89.2	-7.7
10	50	110.7	105.1	-5.1	99.8	-9.9
11	50	114.6	108.3	-5.5	115.0	0.3
12	50	126.3	124.6	-1.3	130.6	3.4
13	50	97.2	88.4	-9.1	89.2	-8.2
13	50	107.5	105.0	-2.3	99.8	-7.2
14	50	118.5	109.5	-7.6	115.0	-3.0
14	50	125.2	124.3	-0.7	130.6	4.3
15	50	95.6	89.2	-6.7	89.7	-6.2
			Mean	**-3.4**		**-3.4**
			St. Dev.	**3.7**		**5.5**

For packages containing combined rectangular and triangular voids, Table 8.18 compared the measured times for 1.5 $\ln Y_c$ reductions with those predicted by methods G and H. The 95% confidence intervals were also in a similar range to those calculated for one $\ln Y_c$ reduction. For prediction method G, the 95% confidence interval was (-10, +9)% and for prediction method H it was (-8, +16)%.

Table 8.18 Comparison of measured data and results from prediction methods G and H - Times for 1.5 $\ln Y_c$ reductions (seconds x 10^3)

Run No.	Measured Data	Prediction method G	% diff. from measured	Prediction method H	% diff. from measured
1A	154.3	154.9	0.4	166.7	8.1
1B	146.4	148.2	1.2	160.3	9.5
2A	166.7	153.0	-8.2	166.7	0.0
2B	154.3	146.9	-4.8	160.9	4.3
3A	170.9	177.5	3.9	189.8	11.1
3B	163.4	172.1	5.3	184.1	12.7
4A	174.9	176.9	1.1	189.9	8.6
4B	167.2	175.0	4.7	184.1	10.1
5A	143.3	147.5	2.9	144.0	0.5
5B	130.0	125.2	-3.7	129.8	-0.1
6A	164.2	168.7	2.7	167.3	1.9
6B	148.8	145.3	-2.4	152.5	2.5
7A	172.6	170.5	-1.2	167.3	-3.1
7B	159.7	146.6	-8.2	152.5	-4.5
		Mean	**-0.4**		**+4.4**
		St. Dev.	**4.5**		**5.6**

8.7 Comparison Against Other Existing Prediction Methods

To gauge the improvement in prediction accuracy that had been gained through the development of the models in chapters 5 to 8, the measured results were compared to prediction methods A, B (with one step), D, F (with the effective area adjustment included), G and H, and three other existing prediction methods that may currently be considered acceptable. The three existing methods chosen were:

1) A two-dimensional finite element model that accurately described the position and size of the air voids in a package, but assumed no natural convection and radiation heat transfer within the voids;

2) A one-dimensional finite difference model that used 'effective thermal properties' theory and treated the package as a homogeneous solid, implying that natural convection and radiation were also ignored.

3) A one-dimensional finite difference model that assumed the whole package was a solid slab where the voids had been filled with solid material (ie. the air voids had the same thermal properties as the solid material).

For the first existing method, FINELX was used to calculate the cooling rates. However, instead of treating air voids in the normal manner, the air voids were considered to be a solid material that had the same thermal properties as still air. The polycarbonate packaging layer, and edge and end effects were included in the same way as they were for the complex model developed in chapters 5 to 7.

For the second existing method, the package was considered to be a solid slab of homogeneous material. The effective thermal conductivity model by Levy (1981) was used to calculate the effective thermal properties of the homogeneous solid composed of air and Tylose (equations 8.12 to 8.15).

$$k_e = k_s\left(\frac{1-2U_1F}{1+U_1F}\right) \tag{8.12}$$

where $$U_1 = \frac{k_s - k_g}{2k_s + k_g} \tag{8.13}$$

and $$2F = \frac{2}{U_2} - 1 + 2\varepsilon - \left[\left(\frac{2}{U_2} - 1 + 2\varepsilon\right)^2 - \frac{8\varepsilon}{U_2}\right]^{1/2} \tag{8.14}$$

and $$U_2 = \frac{(k_g - k_s)^2}{(k_s - k_g)^2 + \frac{k_s k_g}{2}} \tag{8.15}$$

This model, based on the Maxwell-Eucken model (Eucken, 1940), was chosen because it did not require any curve fitting of parameters against measured data. Avoidance of curve fitting eliminated the possibility of matching predictions to the measured data by distorting the results of the effective thermal conductivity model. FPM32 was used to calculate the chilling rates using this method. The thermal resistance of the polycarbonate packaging layer was incorporated in the model as part of the top surface heat transfer coefficient by summing the resistances to heat transfer but the thermal capacity was ignored. The one-dimensionality of the model meant that end and edge effects were also ignored.

For the third existing method, the package was also considered to be a solid slab of homogeneous material. However, the thermal properties of the slab were assumed to be

the same as the solid material (Tylose). This simplification has been used in the expectation that the increase in effective thermal conductivity from ignoring the air voids might roughly balance the increase in thermal mass to give an approximation of the true cooling time. FPM32 was used to calculate the chilling rates by this method. Again, the thermal resistance of polycarbonate packaging layer was incorporated as part of the top surface heat transfer coefficient by summing the resistances to heat transfer but the thermal capacity was ignored. The one-dimensionality of the model meant that the end and edge effects were also ignored.

The results from prediction methods A, B (with one step), D, F (with the effective area adjustment included), G and H, and the three existing prediction methods are compared to the measured data in Tables 8.19 to 8.24.

For packages containing rectangular voids, the mean percentage difference and standard deviation for the existing method 1 (the two-dimensional finite element model with no natural convection or radiation) were not presented for all runs because the method was judged as very unacceptable after only two data points were collected. For existing methods 2 and 3, the mean percentage differences and standard deviations presented in Table 8.20 showed significantly lower accuracies than prediction methods A and B (with one step) for packages containing rectangular voids. The results highlighted the importance of accounting for natural convection and radiation effects when predicting heat transfer through packages that contain rectangular headspace voids, since all the energy lost through the top of the package must go through the headspace void. Existing methods 2 and 3 were not as inaccurate as existing method 1 because the methods assumed that the package contained an homogeneous solid, and since this solid material was in contact with the outer packaging material a larger amount of heat transfer could occur through the top surface than method 1 allowed.

Table 8.19 Comparison of times for one $\ln Y_c$ reduction by new and existing prediction methods for packages containing rectangular air voids (seconds x 10^3)

Run No.	Void Height (mm)	Measured Data	Prediction Method A	Prediction Method B (with 1 step)	Existing Method 1	Existing Method 2	Existing Method 3
5	6	99.6	102.7	104.1		66.5	65.5
6	6	107.4	102.3	104.0		66.5	65.5
7	10	98.5	98.8	100.0	185.1	57.6	53.5
8	10	108.9	110.8	114.7		71.9	69.5
9	30	97.6	101.4	105.5		65.3	71.8
10	30	117.1	117.0	119.6	496.4	109.3	90.9

The accuracy levels exhibited by all the three existing methods tested would not be accepted by industry. Therefore the two new methods (A and B) developed in this work have brought about a significant improvement in the accuracy of prediction methods for food packages containing rectangular voids.

Table 8.20 Percentage differences from measured data for new and existing prediction methods of packages containing rectangular air voids

Run No.	Void Height (mm)	Prediction Method A	Prediction Method B (with 1 step)	Existing Method 1	Existing Method 2	Existing Method 3
5	6	3.1	4.5		-33	-34
6	6	-4.7	-3.1		-38	-39
7	10	0.3	1.5	88	-42	-46
8	10	1.7	5.3		-34	-36
9	30	3.9	8.1		-33	-26
10	30	-0.1	2.1	324	-6.7	-22
	Mean	**+0.7**	**+3.1**	-	**-31**	**-34**
	St. Dev.	**3.1**	**3.8**	-	**12**	**8.5**

Table 8.21 Comparison of times for one $\ln Y_c$ reduction by new and existing prediction methods for packages containing triangular air voids (seconds x 10^3)

Run No.	Void Height (mm)	Measured Data	Prediction Method D	Prediction Method F	Existing Method 1	Existing Method 2	Existing Method 3
1	20	65.8	65.8	65.5	67.5	61.9	61.6
2	20	53.3	52.1	49.5	53.7	47.2	45.9
3	20	66.1	66.5	65.9	68.2	61.9	61.6
4	20	53.9	51.6	49.6	53.4	46.9	45.9
11	40	74.9	72.4	73.6	82.3	64.3	61.6
12	40	71.9	68.9	70.5	82.4	64.3	61.6
15	40	67.8	59.6	55.5	67.8	51.4	45.9
16	40	57.5	55.4	53.5	67.0	51.4	45.9
5	50	66.4	66.9	58.7	81.5	57.0	45.9
6	50	76.4	79.4	77.6	98.2	68.4	61.6
7	50	58.8	55.7	55.2	82.9	57.0	45.9
8	50	70.0	68.8	73.2	98.0	68.4	61.6
9	50	59.2	55.2	55.0	82.9	57.0	45.9
10	50	61.0	55.5	55.2	79.5	57.0	45.9
10	50	68.5	64.4	58.7	82.6	57.0	45.9
11	50	72.1	67.8	72.6	94.4	68.4	61.6
12	50	79.1	77	77.6	94.5	68.4	61.6
13	50	60.8	54.9	55.0	79.5	57.0	45.9
13	50	66.7	64.4	58.4	82.6	57.0	45.9
14	50	73.6	68.5	72.6	94.2	68.4	61.6
14	50	77.9	76.8	77.6	97.1	68.4	61.6
15	50	59.5	55.6	55.5	80.1	57.0	45.9

For packages that contained triangular voids, Table 8.22 shows that existing methods 1, 2, and 3 displayed significantly lower accuracies than prediction methods D and F (with the effective area adjustment included). The accuracy levels exhibited by the three existing methods tested were not likely to be accepted by industry. Therefore the two new methods (D and F) developed in this work have brought about a significant improvement in the accuracy of prediction methods for food packages containing triangular voids.

Table 8.22 Percentage differences from measured data for new and existing prediction methods of packages containing triangular air voids

Run No.	Void Height (mm)	Prediction Method D	Prediction Method F	Existing Method 1	Existing Method 2	Existing Method 3
1	20	0.0	-0.5	2.6	-5.9	-6.4
2	20	-2.3	-7.1	0.8	-11	-14
3	20	0.6	-0.3	3.2	-6.4	-6.8
4	20	-4.3	-8.0	-0.9	-13	-15
11	40	-3.3	-1.7	9.9	-14	-18
12	40	-4.2	-1.9	15	-11	-14
15	40	-12.1	-18.1	0.0	-24	-32
16	40	-3.7	-7.0	17	-11	-20
5	50	0.8	-11.6	23	-14	-31
6	50	3.9	1.6	29	-11	-19
7	50	-5.3	-6.1	41	-3.1	-22
8	50	-1.7	4.6	40	-2.3	-12
9	50	-6.8	-7.1	40	-3.7	-23
10	50	-9.0	-9.5	30	-6.6	-25
10	50	-6.0	-14.3	21	-17	-33
11	50	-6.0	0.7	31	-5.1	-15
12	50	-2.7	-1.9	20	-14	-22
13	50	-9.7	-9.5	31	-6.3	-25
13	50	-3.4	-12.4	24	-15	-31
14	50	-6.9	-1.4	28	-7.1	-16
14	50	-1.4	-0.4	25	-12	-21
15	50	-6.6	-6.7	35	-4.2	-23
	Mean	**-4.1**	**-5.4**	**+21**	**-9.8**	**-20**
	St. Dev.	**3.8**	**5.8**	**14**	**5.4**	**7.6**

For packages that contained combined triangular and rectangular voids, the mean percentage difference and standard deviation for the existing method 1 were not presented for all runs because the method was judged as very unacceptable after only two data points were collected. Table 8.24 shows that existing methods 2 and 3 had significantly lower accuracies than prediction methods G and H for packages containing combined voids. Again, the accuracy levels exhibited by all the three existing methods tested would not be accepted by industry. Therefore the two new methods (G and H) developed in this

work have brought about a significant improvement in the accuracy of prediction methods for food packages containing combined triangular and rectangular voids.

Table 8.23 Comparison of times for one $\ln Y_c$ reduction by new and existing prediction methods for packages containing combined air voids (seconds x 10^3)

Run No.	Measured Data	Prediction Method G	Prediction Method H	Existing Method 1	Existing Method 2	Existing Method 3
1A	97.8	99.4	104.8		84.0	67.0
1B	94.4	99.3	104.8		90.7	67.0
2A	105.7	97.7	104.8		84.0	67.0
2B	99.4	95.6	105.1	375.5	90.7	67.0
3A	107.9	114.9	120.1		97.8	85.3
3B	104.7	113.1	120.3		103.5	85.3
4A	110.6	114.4	120.1		97.8	85.3
4B	107.5	112.9	120.5		103.5	85.3
5A	89.6	95.7	89.9		59.6	53.4
5B	82.7	81.6	82.5		67.9	53.4
6A	103.7	110.2	105.5	219.8	73.1	69.5
6B	95.5	95.3	97.4		79.6	69.5
7A	110.3	110.7	105.7		73.1	69.5
7B	102.4	95.6	97.4		79.6	69.5

Table 8.24 Percentage differences from measured data for new and existing prediction methods of packages containing combined air voids

Run No.	Prediction Method G	Prediction Method H	Existing Method 1	Existing Method 2	Existing Method 3
1A	1.6	7.2		-14	-32
1B	5.2	11.0		-3.9	-29
2A	-7.6	-0.9		-21	-37
2B	-3.8	5.7	278	-8.7	-33
3A	6.5	11.3		-9.4	-21
3B	8.0	14.9		-1.1	-19
4A	3.4	8.6		-12	-23
4B	5.0	12.1		-3.7	-21
5A	6.8	0.3		-34	-40
5B	-1.3	-0.2		-18	-35
6A	6.3	1.7	112	-30	-33
6B	-0.2	2.0		-17	-27
7A	0.4	-4.2		-34	-37
7B	-6.6	-4.9		-22	-32
Mean	**+1.7**	**+4.6**	**-**	**-16**	**-30**
St. Dev.	**5.1**	**6.4**	**-**	**11**	**6.9**

8.8 Commercial Applications of the New Models

The new models developed in this work have been shown to more accurately predict the chilling rates of homogeneous solid packages containing some combination of rectangular and right-angled isosceles triangular voids than existing prediction methods. However, commercial application of these new models will not always be straightforward because meat cartons and many other food product packages contain non-homogeneous solids (e.g. meats cuts that include irregularly shaped fat layers).

Predicting heat transfer through non-homogeneous solids is a straightforward extension of the more complex numerical model developed in Chapter 7. However, due to long set-up and computation times, this model is probably currently more appropriate for use by researchers rather than engineers in industry. The simple model developed in this chapter, which is considered to be more suitable for commercial application than the numerical model, cannot account for packages that contain non-homogeneous solids other than by the use of mean thermal properties. It would be necessary for the user of the simple model to assume that the fat (or second solid phase component) was evenly distributed throughout the meat (or first solid phase component), and that the solid food possessed effective thermal properties defined by equations such as those proposed by Levy (1981) (equations 8.12 to 8.15).

The new models developed in this work were not tested against measurements from actual commercial chilling of primal cut meat cartons because the little amount of available data in the literature (e.g. Cain, 1986) did not include any description of the shape and size of the void spaces within the cartons tested, and because the resources for the present project had been exhausted.

8.9 Discussion and Conclusions

A simple conceptual physical model that endeavoured to account for the presence of rectangular or triangular voids, or some combination of the two, in food packages undergoing transient chilling was developed. This conceptual model could be implemented with several types of solution method (from simple analytical methods to more complicated numerical methods). The errors associated with the more relevant of these solution methods were investigated.

Compared to the complex numerical model of chapters 6 and 7, the simple model would save the user time and/or resources. Finite difference simulations using the simple method took a maximum of 10 minutes to set up, and less than 5 seconds to run on a typical modern personal computer. Furthermore, the simple method may be implemented using analytical solution methods, which eliminates the need for the user to have access to numerical heat transfer software (although a spreadsheet program is recommended to reduce computation time).

When the simplest solution methods were used (prediction method B with one step, and methods F and H) the 95% confidence intervals were (-6, +12)%, (-15, +11)%, and (-9, +17)% for packages containing rectangular voids, triangular voids, and combined voids respectively. After taking out the effect of experimental uncertainty by subtracting the variances, the 95% confidence intervals were (-3, +11)%, (-14, +10)%, and (0, +14)% for packages containing rectangular voids, triangular voids, and combined voids respectively. It is asserted that the assumptions on which the simple model was based did not worsen its prediction accuracy beyond a level that is likely to be acceptable in industry. In addition, the manner in which the new simple model failed to fit the measured data was similar to the accurate complex numerical model, which provides further confidence in the validity of its simplifying assumptions.

The prediction accuracies of the new methods developed in this work were tested against three existing methods that might previously have been considered acceptable. None of the existing methods tested gave accuracy levels that were likely to be accepted by industry. Therefore the new methods developed in this work have brought about a significant improvement in the accuracy of prediction methods for food packages containing air voids.

9. CONCLUSIONS

A two-dimensional finite element model was successfully developed for predicting the chilling rates of food packages that contained horizontal rectangular and right-angled isosceles triangular voids. For modeling the natural convection and radiation heat transfer in the voids suitable Nu vs. Ra correlations were available from the technical literature for rectangular voids, but for triangular voids correlations were developed by curve-fitting data that was measured experimentally during twenty-eight transient chilling trials. A customised heat conduction program called FINELX satisfactorily solved the model by using the correlations and representing the natural convection and radiation effects as a variable effective thermal conductivity in the air voids.

Measured and predicted cooling rates from six transient chilling trials using analogue food packages containing horizontal rectangular voids (up to 30mm high) were in close agreement (±7% at the 95% level of confidence). The percentage differences between the measured and predicted times for one $\ln Y_c$ reduction were close to the limits of expected experimental error and input data uncertainty, indicating that FINELX adequately simulated the overall heat transfer.

Measured and predicted cooling rates from fourteen transient chilling trials using analogue food packages containing combined rectangular and triangular voids were also in close agreement (±12% at the 95% level of confidence). Again, the percentage differences between the measured and predicted times for one $\ln Y_c$ reduction were close to the limits of expected experimental error and input data uncertainty, further validating FINELX.

A simplified model, based on the semi-infinite slab shape, that accounted for the presence of air voids by the use of effective heat transfer coefficients was successfully developed. The total preparation and computation time for implementation of the model on a typical modern personal computer was reduced from about 8 hours (when using FINELX) to about 30 minutes. Comparison of the cooling rates predicted by the simple model against measured data from forty-eight transient chilling trials gave 95% confidence intervals of (-6, +12)%, (-15, +11)%, and (-9, +17)% for packages containing rectangular voids, triangular voids, and combined voids respectively.

This quality of prediction indicated that the assumptions employed in the development of the simple model did not worsen its accuracy beyond a level that is likely to be acceptable

in industry. The manner in which the new simple model failed to fit the measured data was similar to the complex model, which provided further confidence in the validity of its simplifying assumptions.

Comparison of the prediction accuracies of the newly proposed methods against three existing methods that may have previously been considered acceptable showed that the new methods developed in this work have brought about a significant improvement in the accuracy of prediction methods for food packages containing air voids. The prediction accuracies of both the simple and complex models developed in this work are likely to be acceptable in industry.

Notation

0 is a vector containing all zeroes

a is a constant in equ. 5.13

A is the surface area of the object (m^2)

A_T is the total top surface area of an infinite slab (m^2)

b is a constant in equ. 5.13

Bi is the Biot number

c is specific heat capacity ($J\ kg^{-1}K^{-1}$)

C is the capacitance matrix

C is volumetric heat capacity ($Jm^{-3}K^{-1}$)

C_e is the effective volumetric heat capacity of a composite object ($J\ m^{-3}K^{-1}$)

C_s is the volumetric heat capacity of the solid component of a composite object ($J\ m^{-3}K^{-1}$)

E is the equivalent heat transfer dimensionality factor

f is the time for a 90% reduction in Y (s)

$F_{1\rightarrow 2}$ is the fraction of total net radiation emitted from surface 1 reaching surface 2

g is the force of gravity (N)

G is the geometry index

Gr is the Grashof number

H is the enthalpy of an object (J)

H is volumetric enthalpy (MJm^{-3})

h is the surface heat transfer coefficient ($Wm^{-2}K^{-1}$)

h_2 is the external heat transfer coefficient of the second dimension ($Wm^{-2}K^{-1}$)

h_e is the surface heat transfer coefficient ($Wm^{-2}K^{-1}$)

h_n is the heat transfer coefficient of section n ($Wm^{-2}K^{-1}$)

h_{new} is the heat transfer coefficient value excluding the heat transfer resistance of the oil bag ($Wm^{-2}K^{-1}$)

$h_{overall}$ is the mean overall heat transfer coefficient ($Wm^{-2}K^{-1}$)

$h_{packaging}$ is the heat transfer coefficient acting upon the packaging material ($Wm^{-2}K^{-1}$)

h_{rect} is the effective heat transfer coefficient for a rectangular void ($Wm^{-2}K^{-1}$)

h_{surf} is the effective heat transfer coefficient for a surface with no void ($Wm^{-2}K^{-1}$)

h_{tri} is the effective heat transfer coefficient for a triangular void ($Wm^{-2}K^{-1}$)

h_{void} is the effective heat transfer coefficient on the inner surface of a void ($Wm^{-2}K^{-1}$)

i is the current time step

j is the nodal position within a space step

J_0 is a zero- order Bessel's function

J_1 is a first-order Bessel's function

j_{av} is the lag factor for the mass average temperature of an object

j_c is the lag factor for the centre temperature of an object

K is the global conductance matrix

k is thermal conductivity ($Wm^{-1}K^{-1}$)

k_{air} is the thermal conductivity of still air ($Wm^{-1}K^{-1}$)

k_e is the effective thermal conductivity of a composite object ($Wm^{-1}K^{-1}$)

k_{eff} is the effective thermal conductivity of air within a void ($Wm^{-1}K^{-1}$)

k_g is the thermal conductivity of the gas component of a composite object ($Wm^{-1}K^{-1}$)

$k_{nat\ conv}$ is the air void effective thermal conductivity including natural convection effects ($Wm^{-1}K^{-1}$)

k_{oil} is the thermal conductivity of oil ($Wm^{-1}K^{-1}$)

$k_{overall}$ is the overall air void effective thermal conductivity ($Wm^{-1}K^{-1}$)

$k_{packaging}$ is the thermal conductivity of the packaging material ($Wm^{-1}K^{-1}$)

k_{rad} is the air void effective thermal conductivity including radiation effects ($Wm^{-1}K^{-1}$)

k_{rect} is the effective thermal conductivity of the air in a rectangular void ($Wm^{-1}K^{-1}$)

k_s is the thermal conductivity of the solid component of a composite object ($Wm^{-1}K^{-1}$)

k_{solid} is the thermal conductivity of the solid component of a composite object ($Wm^{-1}K^{-1}$)

k_{tri} is the effective thermal conductivity of the air in a triangular void ($Wm^{-1}K^{-1}$)

k_{void} is the effective thermal conductivity of an air void ($Wm^{-1}K^{-1}$)

L_2 is the half-thickness of the second dimension (m)

L_3 is the half-thickness of the third dimension (m)

L_x is the length of the objects shortest dimension or $2R$ (m)

L_y is the length of the first dimension orthogonal to L_x (m)

L_z is the length of the second dimension orthogonal to L_x (m)

n is the number of nodes between centre and surface axes

n is the number of different sections along a surface

n is a variable of equ. 5.13

Nu is the Nusselt number

P is the fluid pressure (Pa)

Pr is the Prandtl number

Q is the heat flux through the surface of an object ($W\ m^{-2}$)

R is the characteristic dimension or minimum half-thickness of the object (m)

Ra is the Rayleigh number

T is temperature (K or °C)

T is the vector of nodal temperatures

t is time (s)

$t_{0.5}$ is the half-life cooling time of an object (s)

t_{1D} is the chilling time of a one dimensional object (s)

t_{MD} is the chilling time of a multi-dimensional object (s)

T_1 is the hot wall temperature of an enclosure (K or °C)

T_2 is the cold wall temperature of an enclosure (K or °C)

T_a is the ambient or cooling medium temperature (K or °C)

T_c is the centre temperature of an object (°C)

T_{cold} is the cold wall temperature of an enclosure (°C)

$T_{\text{cooler plates}}$ is the temperature of the plates in the plate cooler (°C)

T_{hot} is the hot wall temperature of an enclosure (°C)

T_i is initial temperature of an object at $t = 0$ (K or °C)

$T_{\text{inside air}}$ is the temperature of the air inside the plate cooler (°C)

T_{mv} is the estimated mean air temperature in the void (°C)

$T_{oil\ bag}$ is the temperature of the oil bag surface nearest the sample (K or °C)

$T_{\text{outside air}}$ is the temperature of the air outside the plate cooler (°C)

T_s is the surface temperature of the object (K or °C)

v is the fluid velocity in the respective dimension (m s^{-1})

v is kinematic viscosity (m^2 s^{-1})

V is the volume of an object (m^3)

x is the displacement in the first dimension (m)

x is the characteristic dimension of an enclosure (m)

X is the height dimension of a rectangular void (mm)

$x_{air\ layer}$ is the thickness of the air layer (m)

$x_{oil\ bag}$ is the thickness of the oil bag (m)

$x_{packaging}$ is the thickness of the packaging material (m)

x_{rect} is the characteristic dimension of a rectangular air void (m)

x_{tri} is the characteristic dimension of a triangular air void (m)

x_{void} is the characteristic dimension of an air void (m)

y is the displacement in the second dimension (m)

Y is the height dimension of a triangular void (mm)

Y_c is fractional unaccomplished temperature change at the centre of an object

$Y_{edge\ effects}$ is the fractional unaccomplished temperature change of an object with only third dimensional edge effects

Y_{LS} is fractional unaccomplished temperature change at the lower surface of an object

Y_s is fractional unaccomplished temperature change at the surface of an object

Y_{US} is fractional unaccomplished temperature change at the upper surface of an object

$Y_{with\ edge\ effects}$ is the fractional unaccomplished temperature change of an object with third dimensional edge effects

$Y_{without\ edge\ effects}$ is the fractional unaccomplished temperature change of an object without third dimensional edge effects

z is the displacement in the third dimension (m)

α is thermal diffusivity ($m^2\ s^{-1}$)

β_1 is the ratio L_y/L_x

β_2 is the ratio L_z/L_x

δ_{ij} is the Kroneker delta (when $i = j$, $\delta_{ij} = 1$ and when $i \neq j$, $\delta_{ij} = 0$)

Δt is the time step (s)

Δx is the space step (m)

ε is the porosity (relative volume of an object taken up by air voids)

ε is the emissivity of a surface

ϕ is the heat flow to the surface (W)

ϕ_{in} is the heat flowing into the plate cooler from the outside air (W)

ϕ_{out} is the heat flowing out of the plate cooler through the cooler plates (W)

$(\phi_r)_{net}$ is the net rate of radiant-energy transfer from a surface (W)

κ is the bulk viscosity of the fluid (Pa s)

μ is the fluid viscosity (Pa s)

ρ is the density of a fluid or solid ($kg\ m^{-3}$)

ρ_e is effective density of the composite solid ($kg\ m^{-3}$)

ρ_s is density of the solid component without voids ($kg\ m^{-3}$)

σ is the Stefan-Boltzmann constant ($5.67 \times 10^{-8}\ W\ m^{-2}\ K^{-4}$)

τ is the viscous stress tensor (Pa)

ξ is the volumetric expansion coefficient (K^{-1})

References

Ahlers, G. (1980). Effect of departures from the Oberbeck-Boussinesq approximation on the heat transport of horizontal convecting fluid layers. J. Fluid Mech. 98(1): 137-148.

Akinsete, V.A., Coleman T.A. (1982). Heat transfer by steady laminar free convection in triangular enclosures. Int. J. Heat Mass Trans. 25(7): 991-998.

Amos, N.D. (1995). Mathematical modelling of heat and mass transfer and water vapour transport in apple coolstores. PhD Thesis, Massey University, Palmerston North, New Zealand.

Amos, N.D., Willix J., Chadderton T. (2000). A compilation of food thermophysical data. Int. J. Refrig. (in press).

Arpaci, V.S. (1986). Microscales of turbulence and heat transfer correlations. Int. J. Heat Mass Trans. 29: 1071-1078.

Baehr, H.D. (1953). Die berechnung der kuhldauer bei ein- und mehrdimensionalen warmefluss. Kaltetechnik. 5: 255-259.

Banerjee, P.K., Wilson, R.B. (1989). Industrial Applications of Boundary Element Methods. Elsevier Science Publishers, London.

Bonacina, C., Comini, G. (1972). Calculation of convective heat transfer coefficients from time-temperature curves. Refrig. Sci. Technol. 1972-1: 157-167.

Boyd, R.D. (1983). A correlation theory for steady natural convection heat transport in horizontal annuli. J. Heat Trans. 105(1): 139-150.

Busse, F.H. (1969). On Howard's upper bound for heat transport by turbulent convection. J. Fluid Mech. 33: 457-477.

Cain, B.P. (1986). Influence of carton type on chilling times for vacuum packaged meat. Aust. CSIRO Meat Research Lab., Meat Research Record No.A/86.

Canuto, V.M., Goldman, I. (1985). Analytical model for large-scale turbulence. Phys. Rev. Lett. 54: 430-433.

Carslaw, H.S., Jaeger, J.C. (1959). Conduction of Heat in Solids (2nd Edition). Claredon Press, Oxford.

Castrejon, A., Spalding, D.B. (1988). An experimental and theoretical study of transient free-convection flow between horizontal concentric cylinders. Int. J. Heat Mass Trans. 31(2): 273-284.

Catton, I., Ayyaswamy, P.S., Clever, R.M. (1974). Natural convection in a finite, rectangular slot arbitrarily orientated with respect to the gravity vector. Int. J. Heat Mass Trans. 17: 173-184.

Chan, S.K. (1971). Infinite Prandtl number turbulent convection. Stud. Appl. Maths 50: 13-49.

Charmchi, M., Sparrow, E.M. (1982). Analysis of natural convection in the space between concentric vertical cylinders of differing height and diameter. Num. Heat Trans. 5: 119-144.

Clary, B.L., Nelson, G.L., Smith, R.E. (1968). Heat transfer from hams during freezing by low-temperature air. Trans. ASAE, 11: 496-499.

Clary, B.L., Nelson, G.L., Smith, R.E. (1971). The application of geometry analysis techniques in determining the heat transfer rates from biological materials. Trans. ASAE, 14: 586-589.

Cleland, A.C. (1990). Food Refrigeration Processes - Analysis, Design and Simulation. Elsevier Science Publishers, London.

Cleland, A.C., Cleland, D.J., Earle, R.L., Serrallach, G.F., Paterson, A.H.J. (1987b). Cost-effective Refrigeration. Biotechnology Department, Massey University, Palmerston North, New Zealand.

Cleland, A.C., Earle, R.L. (1976). A new method for prediction of surface heat transfer coefficients in freezing. Refrig. Sci. Technol. 1976-1: 361-368.

Cleland, A.C., Earle, R.L. (1977). A comparison of analytical and numerical methods for predicting freezing times of foods. J. Food Sci. 42: 1390-1395.

Cleland, A.C., Earle, R.L. (1979a). A comparison of methods for predicting the freezing times of cylindrical and spherical foodstuffs. J. Food Sci. 44: 958-963.

Cleland, A.C., Earle, R.L. (1979b). Prediction of freezing times for foods in rectangular packages. J. Food Sci. 44: 964-970.

Cleland, A.C., Earle, R.L. (1982). A simple method for prediction of heating and cooling rates in solids of various shapes. Int. J. Refrig. 5: 98-106.

Cleland, A.C., Earle, R.L. (1984). Assessment of freezing time prediction methods. J. Food Sci. 49: 1034-1042.

Cleland, D.J. (1985). Prediction of freezing and thawing times for foods. PhD Thesis, Massey University, Palmerston North, New Zealand.

Cleland, D.J., Boyd, N.S., Cleland, A.C. (1982). A model for fish freezing and storage on board small New Zealand fishing vessels. Refrig. Sci. and Tech. 1982 - 1: 147-156.

Cleland, D.J., Cleland, A.C., Earle, R.L., Byrne, S.J. (1984). Prediction of rates of freezing, thawing or cooling in solids of arbitrary shape using the finite element method. Int. J. Refrig. 7: 6-13.

Cleland, D.J., Cleland, A.C., Earle, R.L., Byrne, S.J. (1987a). Prediction of freezing and thawing times for multi-dimensional shapes by numerical methods. Int. J. Refrig. 10: 32-39.

Cleland, D.J., Cleland, A.C., Jones, R.S. (1994). Collection of accurate experimental data for testing the performance of simple methods for food freezing time prediction. J. Food Proc. Eng. 17: 93-119.

Cleland, D.J., Davey, L.M. (1995). Prediction of food chilling rates with time-variable cooling medium temperature. Proc. 19th Int. Congr. Refrig. Vol 2: 392-399.

'Comparison of Materials' (1976), Anonymous, Materials Eng., Mid-November: 8-25.

Coulter, J.P., Guceri, S.I. (1987). Laminar and turbulent convection within irregularly shaped enclosures. Num. Heat Trans. 12(2): 211-227.

Crank, J., Nicolson, P. (1947). A practical method for numerical integration of solutions of partial differential equations of heat conduction type. Proc. Cam. Phil. Soc. 43: 50-67.

Crystall, B.B. (1989). Electrical stimulation, trends and developments in meat processing. In 'Meat production and Processing, publ. no. 11' (ed. R. Purchas, B. Butler-Hogg and A. Davies), 196-199. New Zealand Society of Animal Production.

Cuesta, J.F., Lamua, M., Moreno, J. (1990). Graphical calculation of half-cooling times. Int. J. Refrig. 13: 317-324.

del Campo, E.M., Mihir, S., Ramos, E. (1988). Analysis of laminar natural convection in a triangular enclosure. Num. Heat Trans. 13: 353-372.

Drummond, J.E., Korpela, S.A. (1987). Natural convection in a shallow cavity. J. Fluid Mech. 182: 543-564.

Earle, R.L., Fleming, A.K. (1967). Cooling and freezing of lamb and mutton carcasses - 1. Cooling and freezing rates in legs. Food Technol. 21(1): 79-84.

Eckert, E.R.G., Carlson, W.O. (1961). Natural convection in an air layer enclosed between two vertical plates at different temperatures. Int. J. Heat Mass Trans. 2: 106-129.

Edwards, D.K., Catton, I. (1969). Prediction of heat transfer by natural convection in closed cylinders heated from below. Int. J. Heat Mass Trans. 12: 23-30.

Elder, J.W. (1965). Laminar free convection in a vertical slot. J. Fluid Mech. 23: 77-111.

Eucken, A. (1940). Allgemeine gesetzmassig keiten fur das warmeleitvermogen versciediner stoffarten und aggregatzustande. Forsch. Gebiete Ingenieur (Ausgabe A).

Fikiin, A.G., Fikiina, I. (1971). Calculation de la durée de réfrigération des produits alimentaires et des corps solides. Proc. 13th Int. Congr. Refrig. 2: 411-414.

Flack, R.D. (1980). The experimental measurement of natural convective heat transfer in triangular enclosures. ASME J. Heat Trans. 102: 770-772.

Foust, A.S., Wenzel, L.A., Clump, C.W., Maus, L., Andersen, L.B. (1960). Principles of Unit Operations. John Wiley & Sons, Inc., New York.

Garon, A.M., Goldstein, R.J. (1973). Velocity and heat transfer measurements in thermal convection. Phys. Fluids 16(11): 1818-1825.

Goldstein, R.J., Chiang, H.D., See, D.L. (1990). High-Rayleigh-number convection in a horizontal enclosure. J. Fluid Mech. 213: 111-126.

Goldstein, R.J., Chu, T.Y. (1969). Thermal convection in a horizontal layer of air. Progress in Heat Mass Trans. 2: 55-75.

Goodman, T.R. (1964). Application of integral methods to transient nonlinear heat transfer. Adv. Heat Transfer, 1: 51-121.

Hellums, J.D., Churchill, S.W. (1962). Transient and steady state free and natural convection, Numerical Solutions : Part II - The region inside a horizontal cylinder. AIChE J. 8: 692-695, 719.

Herring, J.R. (1964). Investigation of problems in thermal convection: rigid boundaries. J. Atmos. Sci. 21: 277-290.

Hill, J.E., Leitman, J.D., Sunderland, J.E. (1967). Thermal conductivity of various meats. Food Technol. 21: 1143-1148.

Hollands, K.G.T. (1984). Multi-prantl number correlation equations for natural convection in layers and enclosures. Int. J. Heat Mass Transfer 27(3): 466-468.

Hollands, K.G.T., Konicek, L. (1973). Experimental study of the stability of differentially heated inclined air layers. Int. J. Heat Mass Transfer 16: 1467-1475.

Hollands, K.G.T., Raithby, G.D., Konicek, L. (1975). Correlation equations for free convection heat transfer in horizontal layers of air and water. Int. J. Heat Mass Transfer 18: 879-884.

Howard, L.N. (1963). Heat transport by turbulent convection. J. Fluid Mech. 17: 405-432.

Howard, L.N. (1966). Convection at high Rayleigh number. Proc. 11th int. Congr. On Apll. Mech. 1109-1115.

Iyican, L., Witte, L.C., Bayazitoglu, Y. (1980). An experimental study of natural convection in trapezoidal enclosures. J. Heat Transfer, 102(4): 648-653.

Kopelman, I.J. (1966). Transient heat transfer and thermal properties in food systems. PhD Thesis, Michigan State University, East Lansing, MI.

Kraichnan, R.H. (1962). Turbulent thermal convection at arbitrary Prandtl number. Phys. Fluids 5: 1374-1389.

Krischer, O. (1963). Die wissenschaftlichen Grundlagen der Trocknungstechnik (The Scientific Fundamentals of Drying Technology), 3rd Ed., Springer-Verlag, Berlin, 268-279.

Krishnamurti, R. (1973). Some further studies on the transition to turbulent convection. J. Fluid Mech. 60(2): 285-303.

Kuehn, T.H., Goldstein, R.J. (1976). An experimental and theoretical study of natural convection in the annulus between horizontal concentric cylinders. J. Fluid Mech. 74: 695-724.

Lees, M. (1966). A linear three level difference scheme for quasi-linear parabolic equations. Maths Comput. 20: 516-522.

Levy, F.L. (1981). A modified Maxwell-Eucken equation for calculating the thermal conductivity of two-component solutions or mixtures. Int. J. Refrig. 4: 223-225.

Lin, Z. (1994). Prediction of chilling times of foods. PhD Thesis, Massey University, Palmerston North, New Zealand.

Lin, Z., Cleland, A.C., Cleland, D.J., Serrallach, G.F. (1996). A simple method for prediction of chilling times for objects of two-dimensional irregular shape. Int. J. Refrig. 19(2): 95-106.

Lin, Z., Cleland, A.C., Cleland, D.J., Serrallach, G.F. (1997). Models of the thermal conductivity of a food (cheese) with voids during chilling. In 'Engineering and Food at ICEF 7' (Proc. 7thInt. Congr. Engng. Food), (ed. R. Jowitt), Section F: 13-16. Sheffield Academic Press, U.K.

Lindsay, D.T., Lovatt, S.J. (1994). Further enthalpy values of foods measured by an adiabatic calorimeter. J. Food Eng. 23: 609-620.

Locker, R.H., Hagyard, C.J. (1963). A cold shortening effect in beef muscles. Journal of Science and Food Agriculture. 14: 787-793.

Long, R.R. (1976). Relation between Nusselt number and Rayleigh number in turbulent thermal convection. J. Fluid Mech. 73: 445-451.

Martini, W.R., Churchill, S.W. (1960). Natural convection inside a horizontal cylinder. AIChE J. 6: 251-257.

Mattea, M., Urbicain, M.J., Rotstein, E. (1986). Prediction of thermal conductivity of vegetable foods by the Effective Medium Theory. J. Food Sci. 51: 113-115, 134.

Mull, W., Reiher, H. (1930). Der Warmeschutz van Luftschichten. Beihefte zum Gesundheits-Ingenieur 1: 28. Munich & Berlin.

Murikami, E.G., Okos, M.R. (1989). Measurement and prediction of thermal properties of foods. Food Properties and Computer-Aided Engineering of Food Processing Systems, Kluwer Academic Publishers, 3-48.

Nguyen, A.V., Pham, Q.T. (1999). A computational fluid dynamic model of beef chilling. Proc. 20th Int. Congr. Refrig. (in press).

Nithiarasu, P., Sundararajan, T., Seetharamu, K.N. (1998). Finite element analysis of transient natural convection in an odd-shaped enclosure. Int. J. Num. Methods for Heat & Fluid Flow. 8(2): 199-216.

Norrie, D.H., de Vries, G. (1978). An introduction to finite element analysis. Academic Press, New York.

Ostrach, S. (1950). A boundary layer problem in the theory of free convection. PhD Thesis, Graduate Division of Applied Mathematics, Brown University, Providence, RI.

Ostrach, S. (1964). Laminar flows with body forces. In 'High Speed Aerodynamics and Jet Propulsion' Vol.4, Theory of Laminar Flows (ed. F.K. Moore), 528-718. Princeton University Press.

Ostrach, S. (1968). Completely confined natural convection. Development in Mechanics, 4: 53-81. Proc. 10th Midwestern Mechanics Conf., Johnson Publ. Co., Fort Collins, CO.

Ostrach, S. (1988). Natural convection in enclosures. J. Heat Trans. 110: 1175-1190.

Ozoe, H., Salmun, H., Churchill, S.W. (1974a). Natural convection in an inclined square channel. Int. J. Heat Mass Trans. 17: 401-406.

Ozoe, H., Salmun, H., Churchill, S.W. (1974b) . Natural circulation in an inclined rectangular channel heated on one side and cooled on the opposing side. Int. J. Heat Mass Trans. 17: 1209-1217.

Perry, R.H., Green, D. (1984). Perry's Chemical Engineers' Handbook, 6th Edition, McGraw-Hill Book Company, New York.

Pham, Q.T. (1989). Prediction of thermal conductivity of meats and other products from composition data. Proc. 5th Int. Congr. Engng. & Food, Cologne. 2: 408-423.

Poulikakos, D., Bejan, A. (1983a). The fluid dynamics of an attic space. J. Fluid Mech. 131: 251-269.

Poulikakos, D., Bejan, A. (1983b). Natural convection experiments in a triangular enclosure. J. Heat Trans. 105(3): 652-655.

Priestly, C.H.B. (1959). Turbulent Transfer in the Lower Atmosphere. University of Chicago Press.

Riedel, L. (1960). Eine Prufsubstanz für Gefrierversuche. Kaltetechnik. 12: 222-226.

Roberts, P.H. (1966). On non-linear Benard convection. In 'Non-Equilibrium Thermodynamics, Variational Techniques, and Stability' (ed. R. Donnelly, R. Hermann and I. Prigogine), 125-162. University of Chicago Press.

Rutov, D.G. (1958). Calculation of the time of cooling of food products. Refrigeration Science and Technology, 1958-1: 415-421.

Salmun, H. (1995). Convection patterns in a triangular domain. Int. J. Heat Mass Trans. 38(2): 351-362.

Sanz, P.D., Mascheroni, R.H., Domniguez, M., Garcia de Vinuesa, S. (1986). Time-temperature prediction curves of food stuffs by means of the z-transfer function method. Int. J. Refrig. 9: 89-92.

Segerlind, L.J. (1984). Applied Finite Element Analysis, 2nd Edition. John Wiley & Sons, New York.

Smith, R.E., Nelson, G.L. (1969). Transient heat transfer in solids: theory versus experiment. Trans. ASAE, 12: 833-836 & 844.

Smith, R.E., Nelson, G.L., Henrickson, R.L. (1967). Analyses on transient heat transfer from anomalous shapes. Trans ASAE, 10: 236-245.

Smith, R.E., Nelson, G.L., Henrickson, R.L. (1968). Applications of geometry analysis of anomalous shapes to problems in transient heat transfer. Trans. ASAE, 11: 296-302.

Srinivasa Murthy, S., Krishna Murthy, M.V., Ramachandran, A. (1974). Heat transfer during air cooling and storing of moist food products. Trans. ASAE, 17: 769-773.

Tanner, D.J. (1998). Mathematical modelling for design of horticultural packaging. PhD thesis, Massey University, Palmerston North, New Zealand.

Tanner, D.J., Cleland, D.J., Wake, G.C. (1995). Prediction of food chilling rates with time-variable surface heat transfer coefficient. Proc. 19th Int. Congr. Refrig. Vol 2: 455-462.

Uno, J., Hayakawa, K. (1979). Non-symmetric heat conduction in an infinite slab. J. Food Sci. 44(2): 396-403.

Van de Sande, E., Hamer, B.J.G. (1979). Steady and transient natural convection in enclosures between horizontal and circular cylinders (constant heat flux). Int. J. Heat Mass Trans. 22: 361-370.

Van Dyke, M. (1964). Perturbation Methods in Fluid Mechanics. Academic Press, New York.

Wade, N.L. (1984). Estimation of the refrigeration capacity required to cool horticultural produce. Int. J. Refrig. 7: 358-366.

Wee, H.K., Pham, Q.T. (1990). Numerical model of unsteady-state heat transfer with convection and phase-change in a carton of meat, Proc. 18th Aust. Chem. Eng. Conf., Auckland, NZ, 93-100.

Weinbaum, S. (1964). Natural convection in a horizontal cylinder. J. Fluid Mech. 18: 409.

Willix, J., Lovatt, S.J., Amos, N.D. (1998). Additional thermal conductivity values of foods measured by a guarded hot plate. J. Food Eng. 37, 159-174.

Wrobel, L.C., Brebbia, C.A. (1979). The boundary element method for steady state and transient heat conduction. In: Numerical Methods in Thermal Problems, p.58-73 (ed. R.W. Lewis and K. Morgan), Pineridge Press, Swansea.

APPENDIX A1

DETERMINATION OF THERMAL CONDUCTIVITY FOR TEST MATERIALS

Note: references used in this appendix are listed in the 'References' section of this thesis.

A1.1 Polycarbonate Sheeting

The thermal conductivity was estimated by measuring the centre temperature-time profile of a given sample of regular shape cooling under known conditions. If the $\ln Y_c$ vs. time profile of the sample can be accurately determined, and all the initial and boundary conditions are known, then the thermal diffusivity of the sample can be calculated using analytical solutions. If the specific heat capacity and density of the material are also known, the thermal conductivity can then be estimated.

The polycarbonate sheets were available at a maximum thickness of 12mm. A preliminary calculation using estimated thermal properties showed that, even at low heat transfer coefficients, the cooling time of a polycarbonate infinite cylinder of radius 6mm was too short for sample transfer and set up time to be ignored. This eliminated the possibility of using semi-infinite cylinders or sphere shapes, so a semi-infinite slab shape was chosen.

The two main issues of importance were considered to be accurately measuring the $\ln Y_c$ vs. time profile and accurately positioning the thermocouples. A semi-infinite slab shape was constructed by using two polycarbonate sheets of the maximum available thickness (12mm). This gave the maximum possible overall slab thickness (which lead to longer cooling times, and hence a more accurate measurement of the $\ln Y_c$ vs. time profile). Accuracy of thermocouple placement was also improved by this construction method because the thermocouple in the thermal centre could be positioned where the top and bottom sheets were brought together. Movement after placement between the solid sheets was considered negligible. Calculations using analytical methods at two different heat transfer coefficients (20 W/m^2K and 400 W/m^2K) were carried out using preliminary estimates of the thermal properties of polycarbonate. A thermocouple placement error of 1mm (the maximum expected error) gave a change in half cooling time of 0.23% and 0.6% respectively, which in

both cases amounted to an error of 1.0% in the estimates of thermal diffusivity. This was considered acceptable.

To minimise edge effects in such experiments Cleland *et al.* (1994) recommended that the ratio of surface area exposed to the cooling medium to surface area contacting the edge insulation be greater than 2.0. A value of 250mm was chosen for the exposed surface diameter, resulting in a ratio of 2.5.

The maximum heat loss from the sample through the thermocouple wires (of diameter 0.254mm) was estimated to constitute only 0.001% of the total heat lost from the sample.

A straight shallow channel was scratched on the top and bottom surfaces of both polycarbonate cylinders (each 250mm in diameter and 12mm high) from the edge to the centre. T-type thermocouples of 0.254mm diameter, that had been calibrated to 0°C using an ice reference, were placed into three of these channels and held in place by small drops of epoxy adhesive. The two sheets were then carefully joined together so that the channel that contained no thermocouple was matched up to a channel that did. This created a 24mm high cylinder-shaped sample with two thermocouples on the surface and one thermocouple in the centre. The edges were insulated with 'Styrodur' polystyrene to minimise unwanted heat transfer through the edges. The sample was warmed in a 25°C room until a uniform temperature of 25°C was reached (uniformity was confirmed by agreement between thermocouples placed upon each surface of the sample, within the sample centre, and in the surrounding air at 25°C).

A plate cooler containing alcohol that was circulated by a Julabo FPW65-MS controlled temperature bath running on an internal set point of 0°C was used for the trials. The temperature of the plates was measured in four places using T-type thermocouples that were calibrated to 0°C using an ice reference.

The semi-infinite polycarbonate slab was insulated during transport to the cooler. Thermocouples from the sample and from the cooler plates were attached to a Squirrel data logger where temperature readings were collected every ten seconds. The insulation was then removed and the sample was placed between the cooler plates. Weights totalling 100kg were evenly distributed onto the movable top cooler plate to ensure that contact integrity between

the sample and the plates was maintained. Three replicate trials were carried out using the same polycarbonate sample.

The external surface heat transfer coefficient on the sample was independently estimated by carrying out exactly the same experiment but instead using an aluminium cylinder (250mm in diameter and 25mm high) as the sample. During the cooling phase of the experiment the entire aluminium sample maintained a uniform temperature (i.e. there was no difference between the readings of the thermocouples on the surface and in the centre). Thus a simple analytical solution was derived (equations A3.1-A3.3) to determine the surface heat transfer coefficient using the measured temperature-time data of the aluminium slab, the mass of the aluminium slab, and the specific heat capacity of aluminium (Perry & Green, 1984).

$$hA(T - T_a) = Mc\frac{dT}{dt} \tag{A3.1}$$

where h is the external heat transfer coefficient (W m^{-2} K^{-1})
A is the exposed surface area of the aluminium slab (m^2)
T is the temperature of the aluminium slab (°C)
T_a is the mean cooling medium temperature (°C)
M is the mass of the aluminium slab (kg)
c is the specific heat capacity of the aluminium slab (J kg^{-1} K^{-1})

$$\int_0^t dt = \int_{T_i}^{T} \frac{Mc}{hA(T - T_a)}.dT \tag{A3.2}$$

$$h = -\frac{Mc}{tA}\ln(T - T_a) \tag{A3.3}$$

Three replicate trials using the same aluminium slab gave heat transfer coefficient estimates of 137, 125 and 132 W m^{-2} K^{-1}. The true mean heat transfer coefficient was 131 $\pm$ 11 W m^{-2} K^{-1} to 95% confidence.

Cleland (1990) outlined the analytical solution for Y_c of an infinite slab (equation A3.4) with a third kind of boundary condition (originally from Carslaw & Jaeger, 1959).

$$Y_c = \sum_{i=1}^{\infty} \frac{2\,Bi\,\sec(\beta_i)}{Bi(Bi+1)+\beta_i^{\,2}} \exp\left(-\beta_i^{\,2} Fo\right) \qquad \text{(A3.4)}$$

Converting Y_c to $\ln Y_c$ and substituting for Fo, gives equation A3.5. From this equation the slope of the straight line section of a $\ln Y_c$ vs. time plot (where only the first term of the infinite series is significant) is proportional to the thermal diffusivity (k/C) of the slab material (analytical methods assume the thermal diffusivity is constant with temperature).

$$\ln Y_c = \ln\left(\frac{2\,Bi\,\sec(\beta_i)}{Bi(Bi+1)+\beta_i^{\,2}}\right) - \left(\frac{\beta_i^{\,2}}{R^2} \times \frac{k}{C}\right) t \qquad \text{(A3.5)}$$

The specific heat capacity of polycarbonate was given in 'Comparison of Materials' (1976) as 1255 J kg^{-1} K^{-1} and the density of the polycarbonate sheets was measured by the author to be 1170 kg m^{-3}. The slopes of the $\ln Y_c$ vs. time plots from the three replicate runs were used to determine thermal conductivity estimates of 0.257, 0.222 and 0.256 W m^{-1} K^{-1}. The true mean thermal conductivity was 0.245 $\pm$ 0.036 W m^{-1} K^{-1} to 95% confidence.

A1.2 'Styrodur' Polystyrene Insulation

The thermal conductivity of 'Styrodur' was determined in the same way as the polycarbonate sheeting. A 380mm x 380mm square sample of half thickness 40mm was constructed. The sample was considered to have 40mm of insulation around the outer edges, within this insulation the minimum ratio of exposed area and edge area was calculated to be 2.0 (as recommended by Cleland *et al.*, 1994). Due to the insulating properties of 'Styrodur' no separate edge insulation was required. Three replicate runs were carried out.

The specific heat capacity of polystyrene was given in 'Comparison of Materials' (1976) as 1255 J kg^{-1} K^{-1} and the density of Styrodur was measured by the author to be 30.8 kg m^{-3}. The slopes of the $\ln Y_c$ vs. time plots from the three replicate runs were then used to determine thermal conductivity estimates of 0.030, 0.031 and 0.031 W m^{-1} K^{-1}. The true mean thermal conductivity was 0.031 $\pm$ 0.001 W m^{-1} K^{-1} to 95% confidence.

APPENDIX A2

USER'S GUIDE TO FINELX PROGRAM

Mike North (Jul-2000)

Adapted from 'USER'S GUIDE TO FINEL PROGRAM' by Q.T.Pham (Nov-1989)

1. SCOPE

In FINELX the object must be divided into (triangular) elements, the vertices of these elements are called "nodes". The program calculates and writes out the nodal temperatures at various times (for transient problems), or the equilibrium nodal temperatures (for steady-state problems).

FINELX uses the finite-element method to solve heat conduction problems. It can solve:

- Two-dimensional or axisymmetric problems.
- Cooling/heating, sharp or gradual phase change.
- Up to 5 different constituent solid materials.
- Up to 5 boundaries, of type 1 (prescribed temperature), 2 (prescribed flux) or 3 (convection).
- Variable environment at each boundary is allowed.
- Temperature-dependent thermal properties is allowed.
- Steady-state or transient problems.
- Temperature-dependent chemical reaction or microbial growth.
- Accounts for natural convection and radiation effects in isosceles triangular and horizontal rectangular air voids.
- Up to 10 separate triangular air voids, a maximum of 50mm high.
- Up to 5 separate rectangular air voids, a maximum of 30mm high.

There are several programs recommended for use with FINELX. They are described below:

(a) BAMG (bi-dimensional anisotropic mesh generator) by Frederic Hocht, INRIA, France (Oct. 1998) is freely available from the Internet. It creates triangular grids in a similar format to that accepted by FINELX (see part 3.2).

(b) mkfinel.pl by Simon Lovatt, AgResearch, Hamilton, NZ (1999) is a PERL based program that combines grids created by BAMG with skeleton FINELX data files, to create full data files in a format acceptable to FINELX (see 3.3).

(c) FINELVIEW by Simon Lovatt, AgResearch, Hamilton, NZ (1999) allows the finite element grid, the element numbers, the node numbers and the element materials of FINELX data files to be viewed (see 3.5).

(d) GRIDEDITX by Simon Lovatt, AgResearch, Hamilton, NZ (1999), based on GRIDEDIT by Pham (1989), edits finite element grids (see 3.6):

- Allows merging of nodes

- Re-orders the nodes to reduce bandwidth

- Renames the nodes and elements to restore numerical order

- Automatically reduces the bandwidth by the use of GPS/GK algorithms

- Shows what node pairs are causing high bandwidth.

2. DATA OUTPUT FROM FINELX

The program writes out the nodal temperatures at various times (for transient problems), or the equilibrium nodal temperatures (for steady-state problems).

At the end of the calculation, the heat balance (for transient problems) or net heat flow (for steady-state problem) is given. The heat balance discrepancy should be less than 1%, the net heat flow should be much smaller than the heat flows through individual boundaries. If that's not the case, re-run with a smaller time step.

3. INPUT DATA PREPARATION PROCEDURE

3.1 Setting up the grid manually

(a) Divide the object into triangle or "elements". Element vertices are called "nodes". One element's vertices must not lie on another element's side. For composite objects, each element must be made up of one type of material only.

(b) Number the nodes.

(c) See if you can rearrange the order of the nodes to minimise the bandwidth. The bandwidth is maximum difference between the nodal orders of any one element's vertices, plus 1. Nodes should be ordered in such a way that the bandwidth is as small as possible, to speed up computation. You can use GRIDEDITX to do this (see part 3.6).

(d) Find the x & y coordinates for each node. In axisymmetric problems, you can specify either x or y as the distance from the symmetry axis (see SYMM in example input file).

(e) Number the elements. Any way will do.

(f) Identify the points on the (non-adiabatic) boundaries. (In finite elements, boundaries are assumed to be adiabatic unless otherwise specified.)

3.2 Setting up the grid using BAMG

(a) Create an input text file (.msh) that contains a list of the vertices, edges, subdomains (for composite objects) and desired grid resolution (see example 1).

Example 1. A BAMG .msh file:

```
Dimension 2

Vertices 12
0 0 1
0.326 0 2
0.326 0.102 3
0 0.102 4
0 0.006 5
0.32 0.006 6
0.32 0.096 7
0 0.096 8
0.02 0.006 9
0.02 0.096 10
0.28 0.006 11
0.28 0.096 12

Edges 15
1 2 1
2 3 1
3 4 1
4 8 1
8 5 1
5 1 1
5 9 2
9 10 2
10 8 2
9 11 3
11 12 3
12 10 3
11 6 4
6 7 4
7 12 4

SubDomain 4
2 2 1 1
2 14 1 4
2 11 1 2
2 8 1 4

hVertices
0.003 0.003 0.001 0.001 0.006 0.003 0.003 0.003 0.006 0.003 0.006 0.003
```

(b) The list of vertices states the total number of vertices and then lists the x and y coordinates of each of these.

(c) The list of edges states the total number of edges in the object and then lists the two vertices at the end of each edge and the boundary number that the particular edge belongs to.

(d) The subdomain section allows the object to be split into different material types. The list states the total number of subdomains, then lists them. The fourth number in each listing refers to the material number. The second number denotes the edge number that the subdomain lies against, and the third number identifies whether the subdomain is on the left or the right of that edge (-1 means the subdomain is to the right of the edge, 1 means it's to the left).

(e) The hVertices section allows the user to choose the resolution of the grid by stating the mesh size at each vertex.

(f) Run the .msh file through BAMG using the MS-DOS command line with the appropriate file names: bamg –g *inputname*.msh –o *outputname*.msh

3.3 Constructing and combining skeleton FINELX data files

The format and organisation of full FINELX data files is explained in part 4. When constructing a skeleton data file (to be later merged together with a BAMG .msh file using mkfinel.pl) only part of the full file is required. The only missing parts from the skeleton file are the NODE and ELEMent sections. Once a skeleton data file has been constructed it may be combined with a BAMG .msh file by using the following MS-DOS command with the appropriate skeleton, grid and full data file names included:

perl mkfinel.pl *skeletonfilename*.dat *gridfilename*.msh >*fulldatafilename*.dat

3.4 Constructing tables of thermal property data.

The skeleton file must include tables for thermal property data. The thermal conductivity k (in $Wm^{-1}K^{-1}$), and, for transient problems, either the volumetric specific heat c (in $MJm^{-3}K^{-1}$) or preferably, the volumetric enthalpy H (in MJm^{-3}) must be known as a function of temperature for each constituent material, and approximated by broken lines. When phase change is very sharp, assume that the latent heat is released over a range of about 0.01 to 0.1 °C.

For each thermal property, values must be specified at a common set of temperatures for all materials. For example, if -40, 0 and +40°C are used to specify the k-T curves, then values of k for each of the materials must be given at all three temperatures, even if k is constant for some material.

For air voids, instead of thermal conductivity the user must enter the value of $Pr*(g\beta\rho^2/\mu^2)x10^{-6}$ [K^{-1} m^{-3}] for air as a function of temperature. A list of these is given below (from Perry and Green, 1984):

T (K)	$Pr*(g\beta\rho^2/\mu^2)\times10^{-6}$
250	334.9
260	185.0
280	129.4
300	94.0
320	69.9

The volumetric heat capacity or volumetric enthalpy of air must still be used for air voids in the second thermal property table.

3.5 Viewing the grid

Once a FINELX data file is complete the grid may be viewed in FINELVIEW. The viewer allows element numbers, node numbers, element material numbers or just the plain grid to be displayed. It also has a zooming function in order to check very fine grids.

3.6 Reducing the bandwidth of the problem

Once a FINELX data file is complete the bandwidth of the problem may be reduced by using GRIDEDITX. The simplest way is to select the 'automatic node re-sequencing using the GPS/GK algorithms' function. This will minimise the bandwidth of the matrices and allow the fastest simulation time.

4. FINELX DATA FILE FORMAT

4.1 Organisation

The input file consists of different "paragraphs", each headed by a codeword which indicates what kind of data follow. The computer reads only the first 4 letters of each codeword. Numerical data are in free format.

Codewords can be in any order. Codewords (only the first 4 letters are required) and their meanings are:

BNODes	Nodes on non-adiabatic boundaries
BOUNdaries	Number of non-adiabatic boundaries (a boundary is a set of connected nodes) and boundary conditions
CONDuctivity	Data on thermal conductivity vs temperature for each material
ELEMents	Element vertices (in anticlockwise order) & element material
ENTHalpy	Data on volumetric enthalpy vs temperature for each material
MATL	Data on no. of voids, material number for each void and the transverse void node numbers for each void
VIEW	Data on radiation view factor within each rectangular void
INITialcondition	Initial temperature
NMATerials	No. of different constituent materials
NODEs	Nodal coordinates
PNODes	Nodes whose temperatures are to be printed (Optional)

PPOSitions	Positions whose temperatures are to be printed (Optional) (only one of PNOD or PPOS should be present; if neither is present, temperatures at all nodes are printed)
SPECificheat	Data on volumetric specific heat vs temp. for each material
STEP	Time steps (Transient problems)
SYMMetry	Whether geometry is plane or axisymmetric (1: plane; 2: axisymmetric with x as radius; 3: y as radius)
TEST	When to end calculations

For transient problems, either ENTH or SPEC but not both must be present.

For steady-state problems, ENTH, INIT, SPEC & STEP are not required.

Ensure codewords are in CAPITALS and are the first characters on their line.

4.2 Units

All numerical data must be in SI units, except that volumetric heats must be in $MJm^{-3}K^{-1}$, volumetric enthalpies in MJm^{-3} and for air voids $Pr*(g\beta\rho^2/\mu^2)$ must be in $x\,10^{-6}\ K^{-1}\ m^{-3}$. Temperature can be in °C.

4.3 Options

In addition, for transient problems, FINELX may ask you interactively to choose between several calculation methods. To be safe, just take the default options by pressing RETURN in answer to all questions.

4.4 Example One

The following FINELX data file, with explanations on RHS in blue, illustrates how to input data (file does not include air voids).

```
SAMPLE INPUT FILE:        EXPLANATIONS:
-------------------------------------------------------------------------
BOUNDARIES                Non-adiabatic boundaries:
3                         3 bndaries.  For each interpolate bw following values:
0    3    15.0   -25.0      At time=0, type=3, Htc=15 Wm-2K-1, Amb.T=-25°C
99   3    18.0   -40.0      At time=99, type=3, Htc=18 Wm-2K-1, Amb.T=-40°C

0    1     0.0   -30.0      Type 1, specified T=-30°C (Htc=0 is a dummy
                            value)
0    2    20.0     0.0      Type 2, specified flux=20 Wm-2 (T=0 is a dummy
                            value)
(Leave line space between data for separate boundaries. Zero-value of
time indicates going to next boundary)

NMATERIALS                No. of different constituent materials:
2                         2 materials

CONDUCTIVITIES            Thermal conductivity (k) data:
```

```
2                   2 points on k-T curve will be given
-40.0  1.0  1.5     At -40°C, k=1.0 & 1.5 Wm-1K-1 for the 2 materials
 40.0  1.0  2.0     At  40°C, k=1.0 & 2.0 Wm-1K-1 for the 2 materials

ENTHALPIES          Volumetric enthalpy (H) data
4                   4 points on H-T curve will be given
-40.0   2.0 -15     At -40°C, H=2 MJm-3 & -15 MJm-3 for the 2 materials
 -1.0  78.0  -2     Etc...
  0.0 280.0   0
 40.0 320.0  20

INITIALCONDITIONS   Initial condition:
3.5                 Initial temperature is 3.5°C

PPOS
2                   Print temperatures at following 2 points:
0.00  0.01          (X,Y) = (0.00,0,01)
0.01  0.02          (X,Y) = (0.01,0,02)

STEP                Time steps (Transient problems):
5.0   100.0         5s steps, print temperatures every 100s

TEST                When to stop calculations:
4                   Criterion 4 (see Note)
-10.0 3             Stop when node 3 reaches -10°C

SYMMETRY            Plane or axisymmetric geometry:
1                   1=Plane, 2=Axisymmetric (x=radius),
                    3=Axisymmetric (y=radius).  Plane in this case.

BNODES              Nodes on each boundary (in connected order):
2                   there are 2 nodes on 1st boundary
1,2                 they are nodes 1 & 2
4                   there are 4 nodes on 2nd boundary
3,7,8,6             they are nodes 3,7,8,6 (note order)
2                   there are 2 nodes on 2nd boundary
4,6                 they are nodes 4,6

NODES               Nodal coordinates:
8                   There are 8 nodes (see Figure 1)
1    0.00   0.00    1st node: x = 0.00m, y = 0.00m
2    0.00   0.02    2nd node: x = 0.00m, y = 0.02m
3    0.01   0.00    etc...
4    0.01   0.02
5    0.02   0.00
6    0.02   0.02
7    0.03   0.00
8    0.03   0.02

ELEMENTS            Element vertices (anticlockwise) & material:
6                   there are 6 elements (see Figure 1)
1    1 3 4    2          Element 1: defined by nodes 1,3,4, made of mtl 2
2    1 4 2    1          Element 2: defined by nodes 1,4,2, made of mtl 1
3    3 5 6    1          etc...
4    3 6 4    1
5    5 7 8    1
6    5 8 6    1
```

Note: Alternatives for TEST:

```
TEST
1           Criterion 1: Steady state problem.
0.01  20    Stop when max.  T change is 0.01°C, or after 20 iterations

TEST
2           Criterion 2: Transient problem.  Stop at a given time.
2500        Stop at 2500s

TEST
3           Criterion 3: Transient problem.  Stop when ANY node reaches
-10.0       -10.0°C

TEST
4           Criterion 4: Transient problem.  Stop when a given node
-10  3      reaches a given T.  In this case, when node 3 reaches -10°C.
```

Figure 1: Grid described in sample input file.

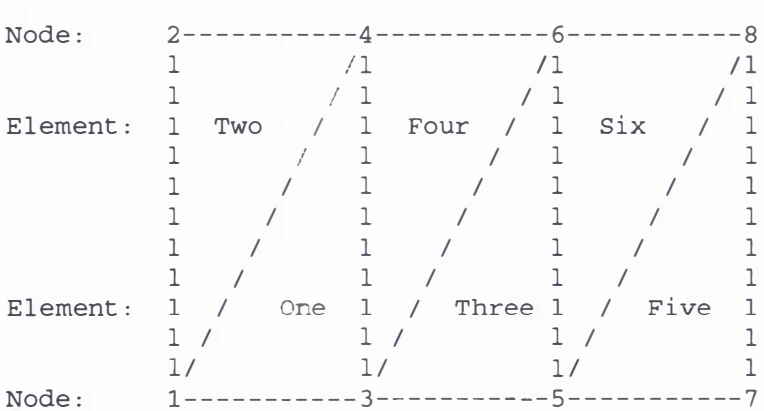

4.5 Example Two

The following FINELX data file includes air voids. Explanations are given on RHS in blue for MATL and VIEW sections.

SAMPLE INPUT FILE:				EXPLANATIONS:
NMAT				
20				
COND				
5				
-23.0000	0.245	0.4326	0.031	etc.
-13.0000	0.245	0.4326	0.031	etc
7.0000	0.245	0.4788	0.031	etc.
27.0000	0.245	0.5096	0.031	etc.
47.0000	0.245	0.5404	0.031	etc.
SPEC				
5				

```
-23.0000  1.4680   4.0650   0.0387  etc.
-13.0000  1.4680   4.0650   0.0387  etc.
  7.0000  1.4680   4.0650   0.0387  etc.
 27.0000  1.4680   4.0650   0.0387  etc.
 47.0000  1.4680   4.0650   0.0387  etc.

MATL                No. of voids in the object
5                   5 voids in total
11    672   592     first void contains material 11 (a rectangular void)
12    1774  1620    and its transverse node numbers are 672 and 592, etc…
16    374   345
17    1152  1068
18    2169  2077

VIEW                Radiation view factor within rectangular void
3                   3 rectangular voids in total
16    0.9           void with material number 16 has a view factor of 0.9
17    0.7           void with material number 17 has a view factor of 0.7
18    0.5           void with material number 18 has a view factor of 0.5

BOUN
2
0     3     13.6  -0.27

0     3     5.0   14.24

INIT
29.84

PPOS
1
0.085 0.006

STEP
10    3600

TEST
2
216000

SYMM
1

NODE
2738
1     0     0.112
2     0.001 0.112
3     0.00200001  0.112
4     0.00148784  0.11117
5     0.00300001  0.112
etc.

ELEM
4829
1     2531  2535  2555  1
2     2532  2531  2555  1
3     2530  2553  2529  1
4     2508  2530  2529  1
5     2554  2553  2530  1
etc.
```

```
BNOD
327
1,2,3,5,9,14,15,etc.
113
2738,2736,2732,2729,etc.
```

5. SYMBOLS USED IN PROGRAM FINELX

Relating to nodes:

CNODE(I)	Specific heat at each node (lumped capacitance versions)
COMP(J,I)	Fraction of node I's thermal volume being made of stuff J (Lumped capacitance version)
NRAD	1 for plane geometry, 2 for axisymmetric geometry with radius x, 3 for axisymmetric geometry with radius y.
NN	No. of nodes
T(I),TO(I)	Nodal temperatures at new & old time levels
X(I),Y(I)	Node coordinates
ZM(I)	Control volume associated with each node (lumped capacitance versions)

Relating to elements:

AE(L)	Element area
IV(J,L)	Node corresponding to J-th vertex of L-th element
MAT(L)	Stuff of which element L is made(1 to 20)
NE	No. of elements

Relating to initial & boundary conditions:

HTC(J)	Heat transfer coefficient, or specified flux, for boundary J
IBC(J)	Type of boundary condition (1,2 or 3) for boundary J
NBC	No. of boundaries (max. 5)
NNBD(J)	No. of nodes on J-th boundary
NODEBD(J,I)	I-th node on J-th boundary
SE(J,I)	Distance between I-th and (I+1)th nodes on J-th boundary
TA(J)	Environment temp. for boundary J
TI	Initial temp. of body

Relating to finite element procedure:

NB	Bandwidth
ZC	Global capacitance matrix (banded notation)
ZF	Global forcing vector
ZK	Global conductance matrix (banded notation)

Relating to material properties:

CONDT(I,J)	J-th thermal conductivity value on thermal conductivity curve of I-th material

ENTHALT(I,J)	J-th enthalpy value on enthalpy curve of I-th material
NCOND	No. of temp.s at which thermal conductivity are specified
NMAT	No. of different materials (1 to 5 normal solids, 6 to 15 triangular voids, 16 to 20 rectangular voids)
NSPEC	No. of temp. at which specific heats or enthalpies are specified
SPECT(I,J)	J-th specific heat value on specific heat curve of I-th material
TCOND(J)	J-th temp. value on thermal conductivity curves
TSPEC(J)	J-th temp. value on specific heat or enthalpy curves

Relating to air voids:

MATL (I,vn1,vn2)	Transverse void nodes (vn1 and vn2) for each void material I
DSTN	Height displacement between vn2 and vn1
DPTN	Absolute height difference between vn2 and vn1
TVTD	Transverse void temperature difference between vn2 and vn1
tempDiff	Absolute value of transverse void temperature difference
meanTemperature	Mean temperature of transverse void nodes
Nu	Calculated Nusselt number for void at a given time step
Ra	Calculated Rayleigh number for void at a given time step
CC	value of $Pr*(g\beta\rho^2/\mu^2)x10^{-6}$ for air voids
F_12	view factor value for rectangular voids
krad	effective thermal conductivity for radiation in rectangular voids

Relating to stepping procedure:

CRIT	Max. T.change for convergence (in steady-state problems)
DT	Length of time step, s
DTPRINT	Time interval for printing, s
ITEMAX	Max. no. of iteration (in steady-state problems)
ITEST	Node used to test for end point (if =0, test all nodes)
IEND	See below
TFINAL	Final time (if IEND=-1), or final temp.criterion (if IEND>1)

Relating to computational method:

IOPT	Method for calc. capacitances in transient problems: -3.Direct calcn -2.Morgan eqn -1.Comini(1974) eqn 0.Constant specific heat 1.Comini(1976) eqn 2.Lumped capacitances
INVERT	Time stepping method: 1:Galerkin 2: Crank-Nicolson 3:Backward
ICOR	If =1, carry out QTP's enthalpy-temperature correction

SPECIAL NOTES: NODE ORDER AND NODE NAME.

Each node can be referred to in one of 2 ways:

a. Within program, node is referred to by its node order "NORD". Thus, the node numbers in the arrays IV(I,J) (I-th vertex of J-th element), or the node

numbers in the array BNODE(I,J) (J-th node of I-th boundary), are NORD-numbers; X(I),Y(I) are the coordinates of the node NORD = I

b. Outside program, ie. in input/output files, each node is referred to by its node name NNAME. Thus, the first number in the section "NODE" or the 2nd to 4th numbers in the section "ELEM", or the numbers in the section BNOD or TEST are NNAME's.

The relationship between NORD and NNAME is established in the NODE section of the input file. The n-th line of that section contains details of the node NORD = n, while the 1st number of that line contains NNAME(n).

You could say that NORD is the node's "true" name. The bandwidth of the finite element node depends thus not on how you name the nodes, but on how you order it in the input file.

While the section NODE of the input file is read, the names NNAME are put in appropriate cells of the array NORD and the order numbers NORD are put in appropriate cells of the array NNAME. This way, there is a 1-to-1 relationship between NORD and NNAME so that NORD(NNAME(I)) = I and NNAME(NORD(I)) = I.

A similar relationship exists between LORD (element order) and LNAME (element name)

---

6. RUNNING FINELX PROBLEMS

Once construction of the input data file is complete FINELX can be run using the following MS-DOS command and the appropriate file names:

finelx *inputfilename*.dat >*outputfilename*.dat

APPENDIX A3

WORKED EXAMPLES USING THE SIMPLE PREDICTION METHOD DEVELOPED IN CHAPTER 8

1) Prediction method B (with 5 steps) - a package with a horizontal rectangular headspace void modelled as a slab with a time-variable heat transfer coefficient.

The following is an example of the working carried out for Run 7 from section 8.6.1. The actual calculations were carried out using a spreadsheet – data for all runs with rectangular voids were summarised in Table 8.2. The simple model used was taken from section 8.3 and was shown in Figure 8.1. This package was half-normal height and cooled from the top surface only.

The known data were:

Height of the solid material in the package, R = 90mm
Height of the rectangular void, x_{rect} = 10mm
Thermal conductivity of still air, k_{air} = (0.0241 + 0.0000788T)Wm^{-1}K^{-1}, where T is the mean temperature of the air (°C)
Thickness of the packaging (polycarbonate layer), $x_{packaging}$ = 6mm
Thermal conductivity of the packaging (polycarbonate layer), $k_{packaging}$ = 0.245 Wm^{-1}K^{-1}
Heat transfer coefficient acting upon the packaging, $h_{packaging}$ = 31.4 Wm^{-2}K^{-1}
Radiation view factor inside the void, F_{12} = 0.9
Initial temperature of the material, T_{in} = 27.99°C
Mean cooling medium temperature, T_a = -0.63°C
Number of steps used for calculation, N = 5

1. Calculate the change in surface temperature (T_s) for each step:

$$\Delta T_s = \frac{T_{in} - T_a}{N} = \frac{27.99 - (-0.63)}{5} = \frac{28.62}{5} = 5.724°C \qquad \text{(A3.1)}$$

2. Calculate the surface temperature at the start and end of each step, and then the mean surface temperature during that step:

ie. (T_s at start of period) – (ΔT_s) = (T_s at end of period)
for the first time step, T_s at end of period = 27.99 - 5.724 = 22.266°C

Time Step	T_s at start of period (°C)	T_s at end of period (°C)	Mean T_s (°C)
1	27.99	22.266	25.128
2	22.266	16.542	19.404
3	16.542	10.818	13.68
4	10.818	5.094	7.956
5	5.094	-0.63	2.232

3. For each time step calculate the first estimate of the effective thermal conductivity due to natural convection in the void using equations 8.4 to 8.6 (restated below), where T_1 = mean surface temperature and T_2 = estimated temperature of the underside of the packaging material (for first estimate assume temperature of packaging material = cooling medium temperature):

$$Ra = 10^6 \times \exp\left(5 - 0.016\frac{T_1 + T_2}{2}\right) \times (T_1 - T_2) \times (x_{vert})^3 \qquad (5.13)$$

$$Nu = 1 + 1.44\left[1 - \frac{1708}{Ra}\right]^* + \left[\left(\frac{Ra}{5830}\right)^{1/3} - 1\right]^* \qquad (6.1)$$

$$k_{nat\ conv} = Nu \times k_{air} \qquad (6.2)$$

Time Step	T_1 (°C)	T_2 (°C)	Ra	Nu	$k_{nat\ conv}$ ($Wm^{-1}K^{-1}$)
1	25.128	-0.63	3142	1.66	0.0416
2	19.404	-0.63	2559	1.48	0.0368
3	13.68	-0.63	1913	1.15	0.0284
4	7.956	-0.63	1202	1.00	0.0244
5	2.232	-0.63	419	1.00	0.0242

4. For each time step calculate the first estimate of the effective thermal conductivity due to radiation in the void using equation 6.7:

$$k_{rad} = F_{1\to 2}\sigma x\left(T_1^2 + T_2^2\right)\left(T_1 + T_2\right) \tag{6.7}$$

Time Step	T_1 (K)	T_2 (K)	k_{rad} ($Wm^{-1}K^{-1}$)
1	298.13	272.37	0.0475
2	292.40	272.37	0.0460
3	286.68	272.37	0.0446
4	280.96	272.37	0.0432
5	275.23	272.37	0.0419

5. For each time step calculate the first estimate of the combined effective thermal conductivity due to natural convection and radiation in the void using equation 6.8:

$$k_{rect} = k_{rad} + k_{nat\ conv} \tag{6.8}$$

Time Step	$k_{nat\ conv}$ ($Wm^{-1}K^{-1}$)	k_{rad} ($Wm^{-1}K^{-1}$)	k_{rect} ($Wm^{-1}K^{-1}$)
1	0.0416	0.0475	0.0891
2	0.0368	0.0460	0.0828
3	0.0284	0.0446	0.0731
4	0.0244	0.0432	0.0676
5	0.0242	0.0419	0.0661

6. For each time step calculate the first estimate the effective heat transfer coefficient (h_{rect}) using equation 8.3:

$$\frac{1}{h_{rect}} = \frac{1}{h_{packaging}} + \frac{x_{packaging}}{k_{packaging}} + \frac{x_{rect}}{k_{rect}} \qquad (8.3)$$

Time Step	$h_{packaging}$ ($Wm^{-2}K^{-1}$)	k_{rect} ($Wm^{-1}K^{-1}$)	x_{rect} (m)	$k_{packaging}$ ($Wm^{-1}K^{-1}$)	$x_{packaging}$ (m)	h_{rect} ($Wm^{-2}K^{-1}$)
1	31.4	0.0891	0.01	0.0245	0.006	5.93
2	31.4	0.0828	0.01	0.0245	0.006	5.65
3	31.4	0.0731	0.01	0.0245	0.006	5.18
4	31.4	0.0676	0.01	0.0245	0.006	4.90
5	31.4	0.0661	0.01	0.0245	0.006	4.82

7. For time each step re-estimate T_2 (the temperature of the underside of the packaging material) assuming a steady state situation and using the sum of resistances theory:

$$T_2 = T_s - \left[\frac{x_{rect} h_{rect}}{k_{rect}}(T_s - T_a)\right] = 25.128 - \left[\frac{0.01 \times 5.93}{0.0891}(25.128 + 0.63)\right] = 7.98^{\bullet}C \qquad (A3.2)$$

and recalculate k_{rect} by repeating steps 3 to 6.

Time Step	T_s (°C)	2nd estimate of T_2 (°C)	2nd estimate of k_{rect} ($Wm^{-1}K^{-1}$)
1	25.128	7.98	0.0676
2	19.404	5.74	0.0670
3	13.68	3.54	0.0664
4	7.956	1.74	0.0659
5	2.232	0.15	0.0655

8. Iterate step 7 until k_{rect} does not change by more than 1%:

Time Step	T_s (°C)	T_2 (°C) (3rd estimate)	k_{rect} ($Wm^{-1}K^{-1}$) (3rd estimate)	Percentage change in k_{rect}	h_{rect} ($Wm^{-2}K^{-1}$)
1	25.128	6.48	0.0672	-0.6 %	4.88
2	19.404	4.86	0.0668	-0.3 %	4.85
3	13.68	3.27	0.0663	-0.15 %	4.83
4	7.956	1.70	0.0659	0 %	4.81
5	2.232	0.14	0.0655	0 %	4.78

9. Set up a numerical solver of one-dimensional heat transfer with a 0.09m thick slab initially at 27.99°C, cooled from the top surface with a heat transfer coefficient of 4.88 $Wm^{-2}K^{-1}$ and a cooling medium temperature of –0.63°C. Run the simulation until the surface of the slab reaches the temperature at the end of the first step (ie. 22.266°C). Note the time taken to reach this surface temperature (in this case it was 78.05 minutes). This is the time taken to reach the second step.

10. Alter the data file so that the heat transfer coefficient changes to the appropriate value for the second step, at the appropriate time (ie. it changes from 4.88 to 4.85 $Wm^{-2}K^{-1}$ after 78.05 minutes).

11. Iterate this process until the start for each step are known:

Time Step	h_{rect} ($Wm^{-2}K^{-1}$)	Time at start of step (minutes)
1	4.88	0
2	4.85	78.05
3	4.83	421.4
4	4.81	1080
5	4.78	2228

12. Run the numerical simulation using the heat transfer coefficient values during the appropriate time period. Calculate the time for one $\ln Y_c$ reduction (from –0.5 to –1.5). In the case of Run 7 this was (100.3×10^3) seconds.

2) Prediction method C - a package with a horizontal rectangular headspace void modelled as a slab with a time-averaged heat transfer coefficient.

The following is an example of the calculations carried out for Run 7 from 8.6.1 – data for all runs with rectangular voids were summarised in Table 8.5. The simple model used was taken from section 8.3 (shown in Figure 8.1), and the heat transfer coefficient was time-averaged as discussed in section 8.3.3. This package was half-normal height and cooled from the top surface only.

The known data were:

Height of the solid material in the package, $R = 90$mm
Height of the rectangular void, $x_{rect} = 10$mm
Thermal conductivity of still air, $k_{air} = (0.0241 + 0.0000788T)\text{Wm}^{-1}\text{K}^{-1}$, where T is the mean temperature of the air (°C)
Thickness of the packaging (polycarbonate layer), $x_{packaging} = 6$mm
Thermal conductivity of the packaging (polycarbonate layer), $k_{packaging} = 0.245\ \text{Wm}^{-1}\text{K}^{-1}$
Heat transfer coefficient acting upon the packaging, $h_{packaging} = 31.4\ \text{Wm}^{-2}\text{K}^{-1}$
Radiation view factor inside the void, $F_{12} = 0.9$
Initial temperature of the material, $T_{in} = 27.99$°C
Mean cooling medium temperature, $T_a = -0.63$°C

1. Calculate the maximum temperature difference across the void:

$$T_{in} - T_a = 27.99 - (-0.63) = 28.62°\text{C}$$

2. Assume the minimum temperature difference across the void is equal to zero.

3. Calculate the maximum and minimum effective thermal conductivities due to natural convection in the void using equations 5.13, 6.1 and 6.2 (ie. for maximum value T_1 = initial temperature and T_2 = cooling medium temperature, for minimum value $T_1 = T_2$ = cooling medium temperature):

	T_1 (°C)	T_2 (°C)	Ra	Nu	$k_{nat\ conv}$ ($Wm^{-1}K^{-1}$)
Maximum	27.99	-0.63	3413	1.72	0.0433
Minimum	-0.63	-0.63	0	1.00	0.0241

4. Calculate the maximum and minimum effective thermal conductivities due to radiation in the void using equation 6.7 (for maximum value T_1 = initial temperature and T_2 = cooling medium temperature, for minimum value $T_1 = T_2$ = cooling medium temperature):

	T_1 (K)	T_2 (K)	k_{rad} ($Wm^{-1}K^{-1}$)
Maximum	300.99	272.37	0.0482
Minimum	272.37	272.37	0.0412

5. Calculate the maximum and minimum combined effective thermal conductivity due to natural convection and radiation in the void using equation 6.8 (for maximum value T_1 = initial temperature and T_2 = cooling medium temperature, for minimum value $T_1 = T_2$ = cooling medium temperature):

	$k_{nat\ conv}$ ($Wm^{-1}K^{-1}$)	k_{rad} ($Wm^{-1}K^{-1}$)	k_{rect} ($Wm^{-1}K^{-1}$)
Maximum	0.0433	0.0482	0.0915
Minimum	0.0241	0.0412	0.0653

6. Calculate the maximum and minimum values of effective heat transfer coefficient (h_{rect}) using equation 8.3:

	$h_{packaging}$ ($Wm^{-2}K^{-1}$)	k_{rect} ($Wm^{-1}K^{-1}$)	x_{rect} (m)	$k_{packaging}$ ($Wm^{-1}K^{-1}$)	$x_{packaging}$ (m)	h_{rect} ($Wm^{-2}K^{-1}$)
Maximum	31.4	0.0915	0.01	0.0245	0.006	6.04
Minimum	31.4	0.0653	0.01	0.0245	0.006	4.77

7. Calculate the logarithmic average effective heat transfer coefficient (h_{rect}) using the maximum and minimum values calculated above:

$$h_{\log average} = \frac{h_{rect\,\max} - h_{rect\,\min}}{\ln\left[\frac{h_{rect\,\max}}{h_{rect\,\min}}\right]} = \frac{6.04 - 4.77}{\ln\left[\frac{6.04}{4.77}\right]} = 5.38\ \mathrm{Wm^{-2}K^{-1}}$$

8. Run a numerical solver or an analytical solver of one-dimensional heat transfer with a 0.09m thick slab initially at 27.99°C, cooled from the top surface with a heat transfer coefficient of 5.38 $\mathrm{Wm^{-2}K^{-1}}$ and a cooling medium temperature of –0.63°C. Calculate the time for one $\ln Y_c$ reduction (from -0.5 to –1.5). In the case of Run 7 this was (92.4×10^3) seconds.

3) Prediction method F - a package with triangular voids modelled as a slab with a time- and spatially- averaged heat transfer coefficient.

The following is an example of the calculations carried out for Run 7 (from section 8.6.2) with 50mm high triangular voids – the data for these predictions was summarised in Table 8.8. The simple model used was taken from section 8.4 (shown in Figure 8.2), and the heat transfer coefficient was time-averaged and spatially-averaged as discussed in sections 8.4.2 and 8.4.3 respectively. This package was half-normal height and cooled from the top surface only.

The known data were:

Height of the solid material in the package, R = 90mm
Width of the package, A_T = 260mm
Height of the triangular voids, x_{tri} = 50mm (cooled from above)
Width of triangular voids = 2 × 50 = 100mm
Number of triangular voids = 2
Total combined width of triangular voids, A_{tri} = 100 × 2 = 200mm
Thermal conductivity of still air, k_{air} = (0.0241 + 0.0000788T)$\mathrm{Wm^{-1}K^{-1}}$, where T is the mean temperature of the air (°C)
Thickness of the packaging (polycarbonate layer), $x_{packaging}$ = 6mm

Thermal conductivity of the packaging (polycarbonate layer), $k_{packaging} = 0.245\ Wm^{-1}K^{-1}$
Heat transfer coefficient acting upon the packaging, $h_{packaging} = 29.6\ Wm^{-2}K^{-1}$
Initial temperature of the material, $T_{in} = 28.5°C$
Mean cooling medium temperature, $T_a = 0.4°C$

1. Calculate the maximum temperature difference across the void:

$$T_{in} - T_a = 28.8 - 0.4 = 28.4°C$$

2. Assume the minimum temperature difference across the void is equal to zero.

3. Calculate the maximum and minimum value of *Nu* using equations 5.13, 5.14 and 5.17 (ie. for maximum value T_1 = initial temperature and T_2 = cooling medium temperature, for minimum value $T_1 = T_2$ = cooling medium temperature):

$$Ra = 10^6 \times \exp\left(5 - 0.016\frac{T_1 + T_2}{2}\right) \times (T_1 - T_2) \times (x_{tri})^3 \qquad (5.13)$$

Triangular voids cooled from below:

$$Nu = 1.12 \times 10^{-5} Ra + 2.31 \qquad (5.14)$$

Triangular voids cooled from above:

$$Nu = 6.30 \times 10^{-4} Ra^{0.75} + 1.12 \times 10^{-5} Ra + 2.31 \qquad (5.17)$$

	T_1 (°C)	T_2 (°C)	*Ra*	*Nu*
Maximum	28.8	0.4	417110	17.32
Minimum	0.4	0.4	0	2.31

4. Calculate the logarithmic average value of *Nu* using the maximum and minimum values calculated above:

$$Nu_{\log average} = \frac{Nu_{\max} - Nu_{\min}}{\ln\left[\frac{Nu_{\max}}{Nu_{\min}}\right]} = \frac{17.32 - 2.31}{\ln\left[\frac{17.32}{2.31}\right]} = 7.45$$

5. Use the logarithmic average value of Nu and the mean value of k_{air} to calculate the log average value of k_{tri} (equation 8.6):

$$k_{tri} = Nu \times k_{air} = 7.45 \times 0.0252 = 0.188 \text{ Wm}^{-1}\text{K}^{-1}$$

6. Calculate the maximum and minimum effective heat transfer coefficient over the void section:

Maximum effective heat transfer coefficient -

$$\frac{1}{h_{tri}} = \frac{1}{h_{surf}} = \frac{1}{29.6} + \frac{0.006}{0.245} = 0.0583 \text{ W}^{-1}\text{m}^2\text{K}$$

Therefore, maximum $h_{tri} = h_{surf} = 17.16 \text{ Wm}^{-2}\text{K}^{-1}$

Minimum effective heat transfer coefficient (using equation 8.7) -

$$\frac{1}{h_{tri}} = \frac{1}{h_{surf}} + \frac{x_{void}}{k_{void}} - \frac{x_{void}}{k_{solid}} = \frac{1}{17.16} + \frac{0.05}{0.188} - \frac{0.05}{0.498} = 0.224 \text{ W}^{-1}\text{m}^2\text{K}$$

Therefore, minimum $h_{tri} = 4.47 \text{ Wm}^{-2}\text{K}^{-1}$

7. Calculate the logarithmic average effective heat transfer coefficient (h_{tri}) using the maximum and minimum values calculated above:

$$h_{\log average} = \frac{h_{tri\max} - h_{tri\min}}{\ln\left[\frac{h_{tri\max}}{h_{tri\min}}\right]} = \frac{17.16 - 4.47}{\ln\left[\frac{17.16}{4.47}\right]} = 9.43 \text{ Wm}^{-2}\text{K}^{-1}$$

8. Calculate the spatially-averaged overall effective heat transfer coefficient ($h_{overall}$) using an area weighted average (equation 8.8):

$$h_{overall} = \frac{A_1}{A_T} h_1 + \frac{A_2}{A_T} h_2 + \frac{A_3}{A_T} h_3 + ... + \frac{A_n}{A_T} h_n$$

$$h_{overall} = \frac{A_{tri}}{A_T} h_{tri} + \frac{A_{surf}}{A_T} h_{surf} = \frac{200}{260} \times 9.43 + \frac{(260-200)}{260} \times 17.16 = 11.2 \text{ Wm}^{-2}\text{K}^{-1}$$

9. Run a numerical solver or an analytical solver of one-dimensional heat transfer with a 0.09m thick slab initially at 28.8°C, cooled from the top surface with a heat transfer coefficient of 11.2 $\text{Wm}^{-2}\text{K}^{-1}$ and a cooling medium temperature of 0.4°C. Calculate the time for one $\ln Y_c$ reduction (from –0.5 to –1.5). In the case of Run 7 this was (56.8 x 10^3) seconds.

4) Prediction method H - a package with combined triangular and rectangular voids modelled as a slab with a time- and spatially- averaged heat transfer coefficient.

The following is an example of the calculations carried out for Run 5A (from section 8.6.3) with a 10mm high rectangular void and 30mm high triangular voids – data for all combined void runs were summarised in Table 8.14. The simple model used was taken from section 8.4 and was shown in Figure 8.6, the overall heat transfer coefficient was time-averaged and spatially-averaged as discussed in sections 8.3.3, 8.4.2 and 8.4.3. This package was half-normal height and cooled from the top surface only.

The known data were:

Height of the solid material in the package, R = 90mm
Width of the package, A_T = 260mm
Height of the rectangular voids, x_{rect} = 10mm
Height of the triangular voids, x_{tri} = 30mm (cooled from above)
Width of triangular slice = 2 × 20 = 40mm
Number of triangular voids = 2

Total combined width of triangular voids, $A_{tri} = 40 \times 2 = 80$mm

Total combined width of rectangular voids, $A_{rect} = 260 - 80 = 180$mm

Thermal conductivity of still air, $k_{air} = (0.0241 + 0.0000788T)\text{Wm}^{-1}\text{K}^{-1}$, where T is the mean temperature of the air (°C)

Thickness of the packaging (polycarbonate layer), $x_{packaging} = 6$mm

Thermal conductivity of the packaging (polycarbonate layer), $k_{packaging} = 0.245\ \text{Wm}^{-1}\text{K}^{-1}$

Heat transfer coefficient acting upon the packaging, $h_{packaging} = 31.4\ \text{Wm}^{-2}\text{K}^{-1}$

Radiation view factor inside the void, $F_{12} = 0.9$

Initial temperature of the material, $T_{in} = 29.15$°C

Mean cooling medium temperature, $T_a = -0.17$°C

1. Calculate the maximum temperature difference across the voids:

$$T_{in} - T_a = 29.15 - (-0.17) = 29.32\text{°C}$$

2. Assume the minimum temperature difference across the voids is equal to zero.

3. For both triangular and rectangular voids, calculate the maximum and minimum value of *Nu* using equations 5.13, 5.14, 5.17 and 6.1:

Note - for maximum value T_1 = initial temperature and T_2 = cooling medium temperature, for minimum value $T_1 = T_2$ = cooling medium temperature.

Void Type	Max/Min	T_1 (°C)	T_2 (°C)	*Ra*	*Nu*
Triangular	Maximum	29.15	-0.17	93180	6.71
	Minimum	-0.17	-0.17	0	2.31
Rectangular	Maximum	29.15	-0.17	3450	2.35
	Minimum	-0.17	-0.17	0	1.0

4. For both triangular and rectangular voids, calculate the maximum and minimum value of k_{tri} and $k_{nat\ conv}$, using equations 8.6 and 6.2 respectively (ie. for maximum value T_1 = initial temperature and T_2 = cooling medium temperature, for minimum value $T_1 = T_2$ = cooling medium temperature):

Void Type	Max/Min	*Nu*	k_{air} ($Wm^{-1}K^{-1}$)	k_{tri} ($Wm^{-1}K^{-1}$)	$k_{nat\ conv}$ ($Wm^{-1}K^{-1}$)
Triangular	Maximum	4.45	0.0253	0.169	
	Minimum	3.5	0.0241	0.056	
Rectangular	Maximum	2.41	0.0253		0.0610
	Minimum	1.0	0.0241		0.0241

5. Calculate the logarithmic average value of k_{tri} using the maximum and minimum values calculated above:

$$k_{tri\,\log average} = \frac{k_{tri\,max} - k_{tri\,min}}{\ln\left[\frac{k_{tri\,max}}{k_{tri\,min}}\right]} = \frac{0.169 - 0.056}{\ln\left[\frac{0.169}{0.056}\right]} = 0.102\ Wm^{-1}K^{-1}$$

6. Calculate the maximum and minimum effective thermal conductivity due to radiation in the rectangular void using equation 6.7 (for maximum value T_1 = initial temperature and T_2 = cooling medium temperature, for minimum value $T_1 = T_2$ = cooling medium temperature):

	T_1 (K)	T_2 (K)	k_{rad} ($Wm^{-1}K^{-1}$)
Maximum	302.32	272.83	0.0486
Minimum	272.83	272.83	0.0415

7. Calculate the maximum and minimum effective thermal conductivity due to natural convection and radiation in the rectangular void using equation 6.8:

	$k_{nat\ conv}$ ($Wm^{-1}K^{-1}$)	k_{rad} ($Wm^{-1}K^{-1}$)	k_{rect} ($Wm^{-1}K^{-1}$)
Maximum	0.0610	0.0486	0.1096
Minimum	0.0241	0.0415	0.0656

8. Calculate the maximum and minimum effective heat transfer coefficient over the rectangular void section using equation 8.3:

Void Type	Max/Min	k_{rect} ($Wm^{-1}K^{-1}$)	h_{rect} ($Wm^{-2}K^{-1}$)
Rectangular	Maximum	0.1096	6.77
	Minimum	0.0656	4.79

9. Calculate the logarithmic average effective heat transfer coefficient (h_{rect}) using the maximum and minimum values calculated above:

$$h_{log\ average} = \frac{h_{rect\ max} - h_{rect\ min}}{\ln\left[\frac{h_{rect\ max}}{h_{rect\ min}}\right]} = \frac{6.77 - 4.79}{\ln\left[\frac{6.77}{4.79}\right]} = 5.72\ Wm^{-2}K^{-1}$$

10. Calculate the maximum and minimum effective heat transfer coefficient over the triangular void section using equations 8.9 and 8.10 respectively:

Maximum effective heat transfer coefficient -

$$\frac{1}{h_{tri}} = \frac{1}{h_{packaging}} + \frac{x_{packaging}}{k_{packaging}} + \frac{x_{rect}}{k_{tri}} = \frac{1}{31.4} + \frac{0.006}{0.245} + \frac{0.01}{0.102} = 0.154\ W^{-1}m^2K$$

$$h_{tri\ max} = 6.48\ Wm^{-2}K^{-1}$$

Minimum effective heat transfer coefficient –

$$\frac{1}{h_{tri}} = \frac{1}{h_{packaging}} + \frac{x_{packaging}}{k_{packaging}} + \frac{x_{tri}}{k_{tri}} - \frac{(x_{tri} - x_{rect})}{k_{solid}} = \frac{1}{31.4} + \frac{0.006}{0.245} + \frac{0.03}{0.102} - \frac{0.02}{0.498}$$

$= 0.310\ \mathrm{W^{-1}m^2K}$, therefore, $h_{tri\,min} = 3.22\ \mathrm{Wm^{-2}K^{-1}}$

11. Calculate the logarithmic average effective heat transfer coefficient for the triangular void section (h_{tri}) using the maximum and minimum values calculated above:

$$h_{log\,average} = \frac{h_{tri\,max} - h_{tri\,min}}{\ln\left[\frac{h_{tri\,max}}{h_{tri\,min}}\right]} = \frac{6.48 - 3.22}{\ln\left[\frac{6.48}{3.22}\right]} = 4.67\ \mathrm{Wm^{-2}K^{-1}}$$

12. Calculate the spatially-averaged overall effective heat transfer coefficient ($h_{overall}$) using an area weighted average (equation 8.8):

$$h_{overall} = \frac{A_1}{A_T}h_1 + \frac{A_2}{A_T}h_2 + \frac{A_3}{A_T}h_3 + \ldots\ldots + \frac{A_n}{A_T}h_n$$

$$h_{overall} = \frac{A_{tri}}{A_T}h_{tri} + \frac{A_{rect}}{A_T}h_{rect} = \frac{80}{260} \times 4.67 + \frac{180}{260} \times 5.72 = 5.40\ \mathrm{Wm^{-2}K^{-1}}$$

13. Run a numerical solver or an analytical solver of one-dimensional heat transfer with a 0.09m thick slab initially at 29.15°C, cooled from the top surface with a heat transfer coefficient of 5.40 $\mathrm{Wm^{-2}K^{-1}}$ and a cooling medium temperature of -0.17°C. Calculate the time for one $\ln Y_c$ reduction (from –0.5 to –1.5). In the case of Run 5A this was (89.9 x 10^3) seconds.

APPENDIX A4 – Published Work

Copies of the following published work are included as appendices:

Pages A4-2 to A4-3:

1) North, M.F., Cleland, A.C. and Lovatt, S.J. (1996). Prediction of Chilling and Freezing Rates of Cartoned Meat (a technical note). Proc. 3rd NZ Conf. of Postgraduate Students in Engng and Tech., University of Canterbury, Christchurch: 493-494.

Pages A4-4 to A4-12:

2) North, M.F., Lovatt, S.J. and Cleland, A.C. (1998). Methods for Evaluating the Effect of Large Voids on Food Package Cooling Times. Proc. Int. Symp. 'Model-It', Acta Horticulturae, ISHS, No. 476: 95-103.

Pages A4-13 to A4-19:

3) North, M.F., Lovatt, S.J. and Cleland, A.C. (1999). The Effect of Void Space on Chilling Times for Food Product Packages. Proc. 20th Int. Congr. Refrig. (in press).